



**Regulation of PKP1's function in intercellular adhesion,
proliferation and barrier formation**

Dissertation

zur Erlangung des
Doktorgrades der Naturwissenschaften (Dr. rer. nat.)

der

Naturwissenschaftlichen Fakultät I – Biowissenschaften –

der Martin-Luther-Universität
Halle-Wittenberg,

vorgelegt

von Frau Katrin Rietscher

geb. am 18.06.1985 in Räckelwitz

Gutachter:

Prof. Dr. M. Hatzfeld

Prof. Dr. S. Hüttelmaier

Prof. Dr. C. Niessen

Verteidigungsdatum: 19.04.2018

Meinen Eltern.

*„Die Endlosigkeit des wissenschaftlichen Ringens sorgt unablässig dafür,
daß dem forschenden Menschengest seine beiden edelsten Antriebe erhalten bleiben und
immer wieder von neuem angefacht werden:
Die Begeisterung und die Ehrfurcht.“*

- Max Planck -

CONTENTS

1	ABSTRACT.....	1
2	INTRODUCTION	3
2.1.	The epidermis: a network of cytoskeletal elements and cellular junctions.....	3
	The function and structure of the epidermis	3
	Epithelial cell-cell junctions.....	3
	Epidermal differentiation	6
2.2.	The multifunctional protein PKP1.....	9
	The structure and expression of PKP1.....	9
	The PKP1-associated disease Ectodermal dysplasia-skin fragility syndrome (EDSFS)	11
	Function of PKP1 in regulating desmosomal adhesion	12
	Function of PKP1 in the cytoplasm.....	13
	Function of PKP1 in the nucleus	15
	Post-translational regulation of PKP1.....	17
2.3.	Epidermal homeostasis: regulation by growth factors	18
	Growth factor signaling pathways	18
	Regulation of protein synthesis by growth factors	21
2.4.	The 14-3-3 proteins	22
	The 14-3-3 protein family: an overview	22
	14-3-3 proteins as regulators of PKP functions.....	24
2.5.	The aim of the study.....	26
3	RESULTS	27
3.1.	Generation and characterization of PKP1 knockout mice.....	27
	Generation and validation of PKP1-KO mice.....	27
	PKP1-KO mice reveal growth retardation and die postnatally.....	30
	Desmosome formation and mechanical integrity are disturbed in PKP1-KO epidermis.....	30
	PKP1-KO mice suffer from a defect in the epidermal barrier	34
	Desmosomal proteins are compensatorily upregulated in PKP1-KO skin	37

Keratin expression is increased in the PKP1-KO skin.....	39
Differentiation is mildly altered in PKP1-KO skin	40
The localization of AJs is not affected in PKP1-null skin.....	42
PKP1-KO keratinocytes recapitulate the effects observed in the epidermis	43
3.2. Insulin signaling via Akt2 influences PKP1’s subcellular localization and function	49
Generation and characterization of PKP1 phospho-site mutants.....	49
PKP1 localization is regulated by insulin signaling via Akt2	53
PKP1 phospho-mimetic mutant reduces intercellular adhesion and promotes wound healing	55
PKP1 phosphorylation promotes proliferation and confers the capacity for anchorage-independent growth.....	57
3.3. 14-3-3 proteins regulate desmosomal adhesion via PKPs	61
14-3-3 γ and 14-3-3 σ affect intercellular adhesion of keratinocytes.....	61
14-3-3 proteins affect desmosomal protein localization.....	64
14-3-3 proteins interact with PKPs in a phosphorylation-dependent manner	68
14-3-3 γ and 14-3-3 σ differentially regulate adhesion via PKP1 and PKP3	70
Insulin/Akt2-dependent phosphorylation is required for the PKP1–14-3-3 γ association.....	72
14-3-3 γ interferes with desmosomal adhesion by sequestering PKP1 in the cytoplasm.....	73
14-3-3 proteins differentially modulate PKP dynamics at the desmosome.....	75
4 DISCUSSION.....	78
4.1. The role of PKP1 in skin homeostasis	78
4.2. Post-translational regulation of PKP1 by insulin signaling	82
4.3. Isoform-specific PKP-14-3-3-interactions regulate desmosomal adhesion in keratinocytes.....	88
4.4. PKP1 and β-catenin: comparison of two multifunctional proteins	93
5 MATERIAL & METHODS	98
5.1. Chemicals and general lab material.....	98
5.2. Phenotypic analysis of PKP1 knockout mice	98
5.2.1. Animals	98
5.2.2. Documentation of weight development.....	99
5.2.3. Transepidermal water loss (TEWL) assay	99

5.2.4. Detection of TJ barrier function <i>in vitro</i> by biotin diffusion assay	99
5.2.5. Toluidine blue dye penetration assay	99
5.2.6. Preparation and analysis of corneocytes.....	100
5.2.7. Ultrastructural analysis of skin samples.....	100
5.2.8. Preparation of paraffin sections	101
5.2.9. Preparation of cryosections	101
5.2.10. Hematoxylin & Eosin (H&E) staining	101
5.2.11. Connective tissue stain	102
5.2.12. Immunohistochemistry (IHC) of paraffin sections.....	102
5.2.13. Immunofluorescence (IF) of cryosections.....	103
5.3. Cell culture methods.....	104
5.3.1. Cultivation of eukaryote cell lines	104
5.3.2. Isolation, culture and differentiation of mouse keratinocytes.....	104
5.3.3. Generation of stable cell lines.....	106
5.3.4. Transfection of eukaryote cell lines	108
5.3.5. Indirect immunofluorescence	110
5.3.6. Bimolecular fluorescence complementation (BiFC).....	112
5.3.7. Dispase/epithelial sheet assay.....	112
5.3.8. Measurement of transepithelial electrical resistance (TER)	112
5.3.9. Fluorescence recovery after photobleaching (FRAP).....	113
5.3.10. Cell migration assay	114
5.3.11. Soft agar assay for colony formation	114
5.3.12. Cell count analysis.....	116
5.3.13. Cell proliferation assay (BrdU).....	116
5.3.14. Cell viability assay (crystal violet)	117
5.4. Biochemical methods	117
5.4.1. Preparation of protein lysates.....	117
5.4.2. Solubility assay.....	118
5.4.3. Determination of protein concentration by BCA assay.....	119
5.4.4. Sodium dodecyl sulfate polyacrylamide gel electrophoresis (SDS-PAGE)	120
5.4.5. Coomassie staining of polyacrylamide gels	120
5.4.6. Western blot.....	121
5.4.7. Expression of GST-fusion proteins	122
5.4.8. Glutathione S-transferase (GST) pulldown.....	123
5.4.9. Immunoprecipitation (IP)	124

5.5.	Molecular biological methods	125
5.5.1.	Reverse transcription (cDNA synthesis)	125
5.5.2.	Polymerase chain reaction (PCR)	126
5.5.3.	Site-directed mutagenesis.....	127
5.5.4.	Agarose gel electrophoresis	128
5.5.5.	Purification of nucleic acids.....	129
5.5.6.	Cloning of PCR products by use of TA system	129
5.5.7.	Restriction endonuclease digestion of nucleic acids	129
5.5.8.	Ligation.....	130
5.5.9.	Preparation and transformation of competent <i>E. coli</i>	131
5.5.10.	Preparation of plasmid DNA.....	132
5.5.11.	Preparation of genomic DNA from mouse tails for PCR genotyping	132
5.5.12.	Sequencing	133
5.5.13.	Southern blot.....	133
5.6.	Image processing, quantification and statistical analysis.....	135
6	REFERENCES	137
7	APPENDIX	I
7.1.	Supplementary materials	I
7.1.1.	Lab equipment.....	I
7.1.2.	Kits and ready-to-use reagents	III
7.1.3.	DNA and protein standards	IV
7.1.4.	Solutions.....	IV
7.1.5.	Oligonucleotides	VI
7.1.6.	Antibodies.....	VIII
7.1.7.	Cell lines	X
7.1.8.	Plasmids	XI
7.1.9.	siRNAs	XII
7.1.10.	<i>E. coli</i> strains.....	XII
7.2.	Supplementary tables and figures	XIII
7.3.	Abbreviations	XXII
7.4.	List of figures	XXVII
7.5.	List of tables.....	XXIX

1 ABSTRACT

Desmosomes are adhesive intercellular junctions essential for tissue integrity such as of the epidermis and the heart. These structures contain a set of desmosomal cadherins, which are connected to intermediate filaments by densely clustered cytoplasmic plaque proteins comprising members of the armadillo gene family, including plakophilins (PKPs) and members of the plakin family of cytolinkers such as desmoplakin. PKPs reveal overlapping but distinct expression patterns in the epidermis. So far, the functional significance of differentially composed desmosomes for their formation, stability, or dynamic is still not completely understood.

Loss of function mutations in the *PKP1* gene in humans lead to Ectodermal dysplasia-skin fragility syndrome (EDSFS), a skin disease with reduced epithelial stability. Other symptoms of this disease include for example abnormalities of the ectodermal development with growth delay, hypotrichosis, or alopecia. These pathological features point to an important role of PKP1 in promoting desmosomal strength on the one hand and in controlling growth on the other hand. However, the mechanisms regulating PKP1's multiple functions had not been addressed in full at the beginning of this doctoral study.

To resolve the contribution of PKP1 in desmosome stability, tissue differentiation, and homeostasis, PKP1 knockout mice were generated and characterized. *Pkp1*^{-/-} mice were born with reduced birth weight and died postnatally, developing fragile skin with lesions in the absence of obvious mechanical trauma. Despite the upregulation of most desmosomal proteins, desmosome number and size were significantly decreased. Interestingly, the inside-out epidermal barrier was impaired caused by disturbed tight junction (TJ) function in PKP1 knockout mice. Keratinocytes isolated from these mice revealed strongly reduced intercellular cohesion, delayed TJ formation, reduced transepithelial resistance, and proliferation rates.

Besides a structural function of PKP1 in desmosomes, a role in signaling has been postulated in analogy to other armadillo proteins such as β -catenin, but regulatory mechanisms were unknown. In this doctoral thesis it was investigated that PKP1 is regulated by insulin/IGF1 signaling. Upon activation of the PI3K/Akt pathway, PKP1 is phosphorylated by Akt2 resulting in its predominant cytoplasmic accumulation correlated with reduced in-

tercellular adhesion, enhanced proliferation, wound healing, and anchorage-independent growth suggesting that PKP1 may contribute to tumorigenesis in a context-dependent way.

Moreover, growth factor signaling regulates the association of PKP1 with 14-3-3 proteins uncovering partially antagonistic functions of two members of the 14-3-3 family in the regulation of desmosomal adhesion. While 14-3-3 σ promotes strong intercellular adhesion mediated by PKP1 by an indirect mechanism that targets PKP3, 14-3-3 γ has an opposite effect. 14-3-3 γ acts by retaining PKP1 in the cytoplasm, thereby reducing its exchange rates at the desmosome and increasing its soluble pool. As a consequence, intercellular adhesion is severely compromised.

The results of this doctoral thesis identify PKP1 as a key regulator of tissue homeostasis controlling intercellular adhesion as well as growth control, a function that is crucial in wound healing and epidermal carcinogenesis. This study further clearly demonstrates that mechanisms such as phosphorylation and 14-3-3 binding are essential features to ensure the precise regulation of PKP1 within the cell. In addition, these findings may provide insights into understanding the complex pathobiology of EDSFS syndrome.

2 INTRODUCTION

2.1. The epidermis: a network of cytoskeletal elements and cellular junctions

The function and structure of the epidermis

The mammalian skin consists of the epidermis, its underlying dermis and the subcutis. Numerous essential protective functions have to be fulfilled by the epidermis: e.g. protecting from dehydration, resisting mechanical stress or participating in immune responses. The epidermis encompasses also different appendages such as sweat and sebaceous glands, hair follicles, and the touch dome, essential for thermoregulation, sensing the environment, and influencing social behavior (Sotiropoulou and Blanpain, 2012). Keratinocytes – the main cell type of the epidermis – build an adhesive network organized into multiple layers to establish a barrier between the organism and its environment (Candi et al., 2005, Fuchs and Raghavan, 2002). This stratified epithelium contains a single basal layer (*stratum basale*) of proliferative cells continuously regenerating the overlaying layers, termed *stratum spinosum*, *granulosum*, and *corneum* (Fig. 1A). Most cells within the basal layer are transit amplifying cells, rapidly dividing progeny of stem cells. These cells undergo a limited number of cell divisions before withdrawing from the cell cycle and committing to terminal differentiation, which is accompanied by detachment from the basement membrane and movement towards the surface of the skin [reviewed in (Fuchs and Raghavan, 2002, Watt, 1998)]. Thus, the epidermis is an epithelium in a constant state of dynamic equilibrium, renewing itself every two weeks throughout life.

Epithelial cell-cell junctions

To fulfill the protective functions, tight mechanical cohesion between the cells of the same as well as different epidermal layers is required. Therefore, keratinocytes have to be connected to each other by intercellular junctions that link the cytoskeleton of adjacent cells, such as tight junctions (TJs), adherens junctions (AJs), and desmosomes (Fig. 1B-D).

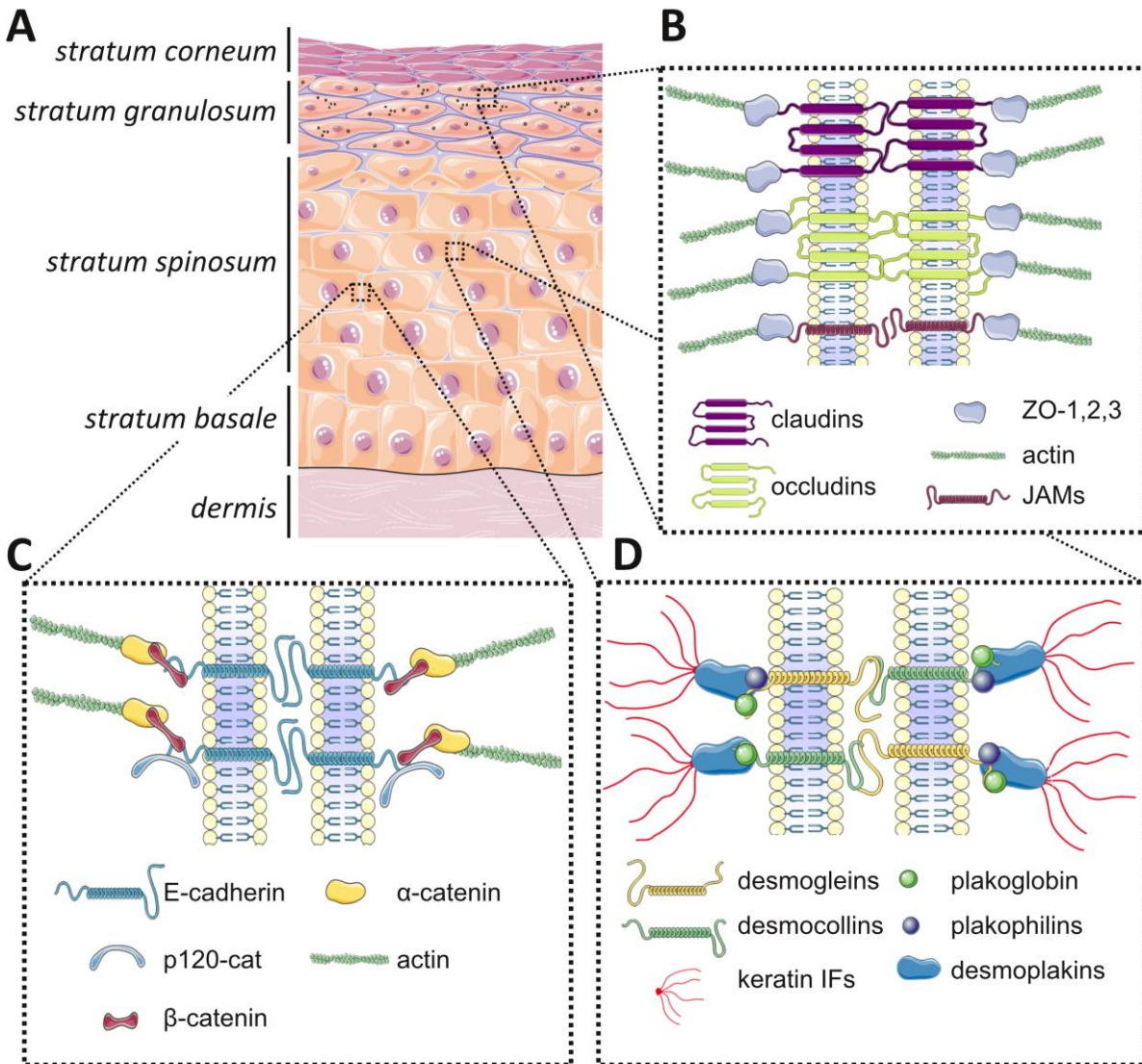


Fig. 1| Intercellular junctions of the epidermis.

(A) Simplified model of the epidermis modified after (Simpson et al., 2011) illustrates the stratified epithelium comprising four layers: *stratum corneum*, *stratum granulosum*, *stratum spinosum*, and *stratum basale*. TJs are located in the *stratum granulosum*. AJs and desmosomes are found in all layers of the epidermis, except the cornified layer. (B) The main barrier function of the epidermis is ensured by TJs [structure modified after (Aktories and Barbieri, 2005)]. TJs comprise claudins, occludins, and JAMs, connected to adaptor proteins like ZO-1, 2, 3. (C) Simplified model of an AJ modified after (Fuchs and Raghavan, 2002). Cadherin adhesion molecules like E-cadherin are AJ core components. p120-catenins and β -catenin bind the cytoplasmic tail of E-cadherin connecting them with the actin filament cytoskeleton. (D) Simplified structure of a desmosome modified after (Fuchs and Raghavan, 2002). Desmosomes are composed of clustered transmembrane cadherins: desmogleins and desmocollins. These bind to plakoglobin and plakophilins recruiting the cytolinker desmoplakin, which binds keratins. AJ, adherens junction; IF, intermediate filament; JAMs, junctional adhesion molecules; p120-cat, p120-catenins; TJ, tight junction; ZO, zonula occludens.

TJs are localized in the outermost viable layer – the *stratum granulosum* – and in hair follicles (Brandner et al., 2003). The essential transmembrane proteins of the TJs are claudins (CLDNs), occludins (OCLNs), and junctional adhesion molecules (JAMs, Fig. 1B). Zonula occludens (ZO-1, -2 and -3) proteins are highly enriched at the cytoplasmic sites of the integral membrane proteins and may be important for junction formation (Hernandez et al., 2007) as well as for the connection to the actin cytoskeleton via α -actinin [(Fanning et al., 1998) and reviewed in (Chiba et al., 2008, Gonzalez-Mariscal et al., 2008, Guillemot et al., 2008, Paris et al., 2008)]. TJs have been proposed to ensure a barrier function by forming a paracellular size- and ion-specific barrier. This selectivity is mainly based on which members of the claudin family of transmembrane proteins are located in the TJs. For instance, loss of CLDN1 in mice revealed a neonatal lethality attributable to dehydration (Furuse et al., 2002). Furthermore, TJs ensure the maintenance of cell polarity and prevent the mixing of proteins in the apical membrane with those in the lateral membrane (Hartsock and Nelson, 2008, Sawada et al., 2003, Steed et al., 2010).

AJs (Fig. 1C) fulfill multiple functions including initiation and stabilization of cell-cell adhesion, regulation of the actin cytoskeleton, intracellular signaling, and transcriptional regulation (Hartsock and Nelson, 2008, Perez-Moreno and Fuchs, 2006). The transmembrane glycoproteins of the classical cadherin superfamily, such as E- or P-cadherin, build up the core of the AJs associating with catenin family members including p120-catenins (e.g. p120ctn, p0071), α -catenin, and β -catenin (Pokutta and Weis, 2007).

Desmosomes (Fig. 1D) are intercellular junctional complexes that confer strong cell-cell adhesion and thereby provide mechanical stability especially in tissues that have to resist large amounts of strain such as the heart and the skin (Green and Simpson, 2007). The transmembrane glycoproteins desmogleins (DSGs) 1-4 (Amagai et al., 1991, Koch et al., 1990, Schafer et al., 1994, Whittock and Bower, 2003) and desmocollins (DSCs) 1-3 (Collins et al., 1991, Mechanic et al., 1991, Parker et al., 1991, Wheeler et al., 1991) belong to the cadherin superfamily of calcium-dependent adhesion molecules (Garrod and Chidgey, 2008). Their extracellular domains mediate cohesion, whereas the cytoplasmic tails associate with desmosomal plaque proteins, such as plakoglobin [PG, also known as γ -catenin (Cowin et al., 1986)] and the three plakophilins 1, 2 and 3 [PKPs (Bonne et al., 1999, Hatzfeld et al., 1994, Mertens et al., 1996, Schmidt et al., 1999)]. Desmoplakin [DSP, (Green

et al., 1990)] links the desmosome to keratin intermediate filaments (Garrod, 2010, Kowalczyk et al., 1994, Stappenbeck et al., 1993).

Epidermal differentiation

Keratinocytes undergo a transformation as they differentiate and migrate outwards to replace the cells that are shed from the body surface (Fuchs and Raghavan, 2002). The basal cells of the *stratum basale* remain attached to the underlying extracellular matrix and proliferate, whereas their daughter cells enter the spinous layer through asymmetric mitoses, where they exit the cell cycle, grow larger and establish stable intercellular connections (Simpson et al., 2011). As keratinocytes differentiate and stratify, they completely reorganize their adhesive junctions and the cytoskeleton. Although desmosomes are present in basal keratinocytes, stratification induces a marked increase in the concentration of these adhesive structures (White and Gohari, 1984) and also reorganizes their associated cytoskeletal elements (Fuchs, 1993). The basal, proliferative layer of the epidermis predominantly expresses the keratins 5, 14, and 15, which upon terminal differentiation in the upper layers of the epidermis, are replaced by keratins 1 and 10 (Fig. 2). During processes such as wounding, tissue regeneration or barrier disruption, this distinct pattern is altered. In this setting, keratins 6, 16, and 17 are rapidly and transiently expressed at the expense of keratins 1 and 10, ensuring transiently decreased intercellular stability, enhanced proliferation, and migration of keratinocytes (Homberg and Magin, 2014, Loschke et al., 2015).

Like keratins 5, 14 and 15, DSG2 and 3 are concentrated in the basal layer, whereas DSG1/DSC1 expression is turned on gradually as cells undergo the transition to a highly differentiated state. Additionally, the levels of DSG2/DSC2 decrease from basal to suprabasal layers, whereas DSG4 reveals high expression in the granular and cornified layers (Dusek et al., 2007, Garrod et al., 2002, Mahoney et al., 2006, North et al., 1996). In addition to the desmosomal cadherins, the desmosomal plaque proteins are differentially expressed to adjust desmosomes to their altered environment during differentiation (Green and Simpson, 2007). For instance, PKP1, originally described as band 6 protein (Hatzfeld et al., 1994), localizes primarily to desmosomes in the suprabasal layers of the epidermis. PKP2 reveals a decreasing expression from basal to suprabasal layers, whereas for PKP3 no differentiation-associated changes in its distribution have been noted (Fig. 2).

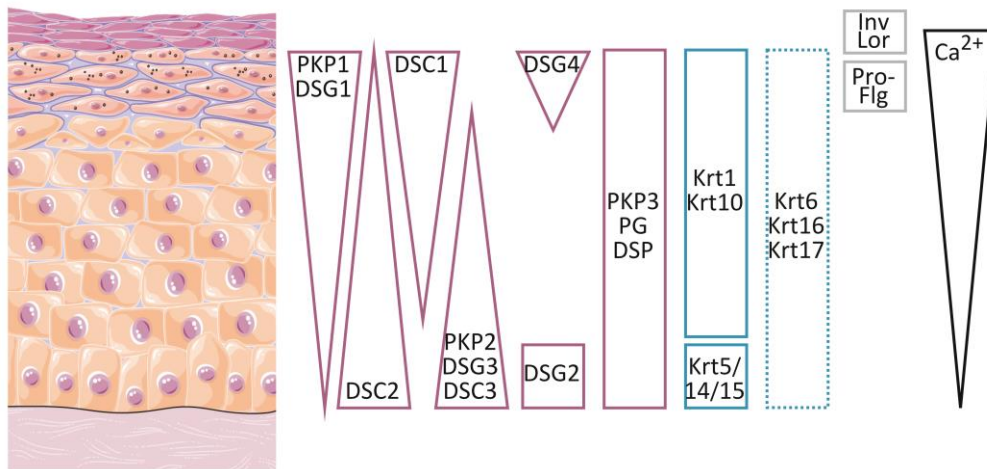


Fig. 2| Heterogeneous expression of desmosomal proteins, keratins, and differentiation markers in the epidermis.

The scheme of the epidermis modified after (Dubash and Green, 2011, Sandilands et al., 2009) shows that desmosomal proteins (in violet) are expressed in a differentiation-dependent manner. E.g., PKP1 localizes primarily to desmosomes in suprabasal layers, whereas PKP3 shows no differentiation-associated changes in its distribution. The expression of keratins (Krt) is shown in blue. Transiently expressed keratins 6, 16, and 17 are shown blue-dotted. The cornified envelope composed of involucrin, loricrin, filaggrin (in grey) and others reflects fully differentiated keratinocytes and corneocytes. For the regeneration of the skin, in particular to maintain the integrity of skin barrier, a characteristic calcium gradient (in black) - with low calcium levels in the basal layers and progressively increasing levels towards the upper layers - is essential. Ca, calcium; DSC, desmocollin; DSG, desmoglein; DSP, desmoplakin; Inv, involucrin; Krt, keratin; Lor, loricrin; PG, plakoglobin; PKP, plakophilin; Pro-Flg, profilaggrin.

These overlapping but distinct expression patterns of the desmosomal proteins suggest on the one hand tissue-specific functions and on the other hand guarantees cell cohesion based on redundancy (Bass-Zubek et al., 2009). However, isotype-specific functions and differentiation-specific expression of desmosomal proteins remain incompletely understood. Gene ablation in mice has been used to establish the role of desmosomal proteins *in vivo*. For example, knockout (KO) of the three *Dsc* genes differs dramatically in the severity of phenotypes: whereas a *Dsc2* KO did not result in any obvious phenotype (Rimpler, 2014), ablation of *Dsc1* led to epidermal fragility with hyperproliferation and dermatitis, but mice were viable and fertile (Chidgey et al., 2001). *Dsc3* ablation resulted in preimplantation lethality suggesting a desmosome-independent role during early development (Den et al., 2006).

An additional major regulator of keratinocyte differentiation is calcium, which forms a steep gradient within the epidermis, with the highest concentration in the *stratum corneum* [(Menon et al., 1985), Fig. 2]. A number of signaling pathways involved in differen-

tiation are regulated by calcium, which in turn play an important role in the activation of various kinases and phospholipases, such as for protein kinase C (PKC) activity [reviewed in (Bikle et al., 2012)]. Besides the formation of cell-cell contacts [e.g. desmosomes (Hennings and Holbrook, 1983)], a stabilization of adhesion molecules (Demlehner et al., 1995, Kolly et al., 2005) and morphological change from angular to flat and polygonal (Kolly et al., 2005) as well as the formation of the cornified envelope, the final product of epidermal differentiation, is mainly driven by calcium (Kasturi et al., 1993, Rinnerthaler et al., 2015).

The cornified envelope (*stratum corneum*) ensures the formation of the epidermal barrier in the skin besides the TJs barrier and consists of involucrin (Inv), loricrin (Lor), filaggrin (Flg), and additional proteins [(Steinert and Marekov, 1995), Fig. 2]. Profilaggrin (Pro-Flg), precursor of filaggrin, is found in *stratum granulosum* and may play a role in maintaining the water content of the epidermis, as it is degraded into smaller peptides revealing osmotic properties (Dale et al., 1985). The terminally differentiated keratinocytes are termed as corneocytes, which mostly consist of keratins embedded in Flg matrix and surrounded by a complex series of insoluble lipids such as ceramides (Candi et al., 2005). Corneocytes are tightly connected to each other by corneodesmosomes – modified desmosomal structures, which are proteolytically degraded in the uppermost layers of the cornified layer to allow desquamation (Serre et al., 1991). Transglutaminases modify desmosomes by crosslinking DSG1, DSC1, and corneodesmosin during terminal keratinocyte differentiation.

In summary, epidermal keratinocytes are highly specialized epithelial cells with distinct cell-cell junctions, whose composition, assembly, and dynamics have to be coordinated throughout multiple cell layers of the epidermis. In diverse multicellular processes, including tissue morphogenesis during development, collective cell migration during wound healing, epithelial barrier formation, and cancer progression, the spatio-temporal regulation of cell-cell contact proteins is essential for the maintenance of tissue integrity as well as for communication and coordination between cells. How the assembly and remodeling of junctions occurs and is controlled at the molecular level is a challenge for today's and future studies. The next paragraph focuses on the desmosomal plaque protein PKP1 and will provide some insight into how this protein can modulate intercellular cohesion.

2.2. The multifunctional protein PKP1

The structure and expression of PKP1

The desmosomal plaque proteins PKP1-3 are members of the p120ctn family of armadillo (arm)-related proteins. This family comprises seven members, four of which are primarily found in AJ [p120ctn, NPRAP (Neural Plakophilin-Related Armadillo Protein)/ δ -catenin, ARVCF (Armadillo-Repeat gene deleted in Velo-Cardio-Facial syndrome) and p0071/PKP4], whereas PKPs localize primarily at desmosomes (Hatzfeld, 2005). The proteins of this family contain nine copies of a ~42 amino acid residue repeat motif (Andrade et al., 2001), each consisting of three short α -helices (Huber et al., 1997) and packed together to form an elongated superhelical structure (Choi and Weis, 2005). PKPs consist of a central domain of nine arm repeats flanked by rather long N- and short C-terminal domains, respectively (Fig. 3A). The arm repeat structure of PKP1 is sickle-shaped due to a long, flexible insert between the fifth and sixth arm repeats (Fig. 3B). Although this region does not disrupt the packing of the arm repeats, it causes a major bend in the arm domain (Choi and Weis, 2005). Binding partners for PKP1 identified to date preferentially interact with the N-terminal head domain. With the exception of a short conserved α -helical stretch close to the N-terminus, the head domain reveals no known secondary structures (Hatzfeld et al., 2014).

The genes of the p120ctn family reveal a widespread distribution throughout the human genome, although the sequences are highly related (Hatzfeld, 2005), e.g. *PKP1* is located on 1q32, *PKP2* on 12p13, and *PKP3* on 11p15, respectively (Bonne et al., 1998). Isolation of the human genomic sequence of *PKP1* allowed the determination of its gene structure covering about 50 kb and composed of 15 exons of which exon 7 is alternatively used (Schmidt et al., 1997b). Thus, PKP1 exists in two alternative splice variants, a shorter isoform a lacking exon 7 and a longer isoform b, which differ by an insertion of 21 amino acids. Both variants reveal a distinct intracellular localization with the smaller 1a isoform being more common at desmosomes and the 1b isoform found in the nucleus (Schmidt et al., 1997a).

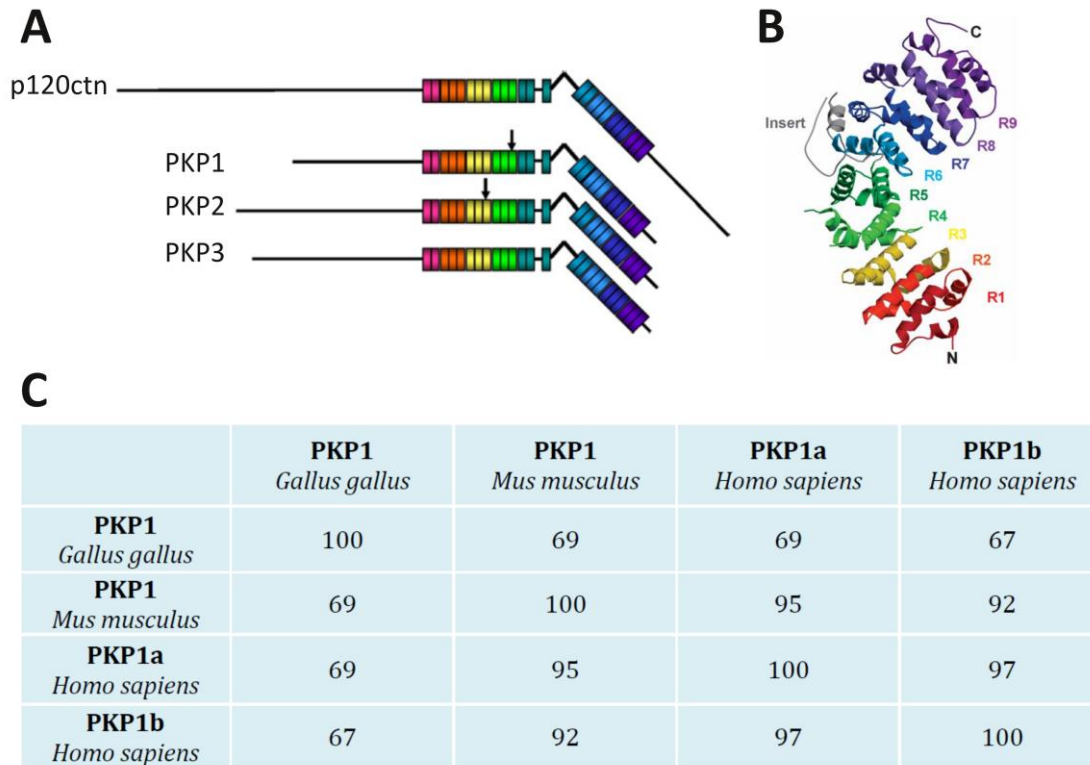


Fig. 3I Structural details of PKP1.

(A) Domain structure of PKPs compared to p120ctn (Hatzfeld, 2007). The members of the p120ctn family contain a central arm repeat domain. PKPs consist of nine tandemly linked imperfect 42 amino acid repeats. PKP1b and PKP2b (alternative splice isoforms) contain inserts in the H3 region of arm repeats 3 and 4 (black arrow). (B) Ribbon diagram of the PKP1 arm repeat domain crystal structure (Choi and Weis, 2005) illustrates a single sickle-shaped structure due to a long, flexible insert containing residues 464-524 between the fifth and sixth arm repeats. Each repeat (R1-9) is composed of three α -helices. (C) Sequence conservation between PKP1 para- and orthologues from chicken (*Gallus gallus*), mouse (*Mus musculus*), and human (*Homo sapiens*) determined by protein-protein BLAST alignment (<https://blast.ncbi.nlm.nih.gov/Blast.cgi>; 02.11.2017). Numbers indicate amino acid sequence identity (%). Human PKP1a shows very high homology with its orthologue from mouse. C/N, C/N-terminus; PKP, plakophilin; p120ctn, p120-catenin; R1-9, arm repeats 1-9.

Protein sequence alignments of PKP1 para- and orthologues from chicken (*Gallus gallus*), mouse (*Mus musculus*), and human (*Homo sapiens*) reveal high sequence conservation with 95% amino acid identity between human PKP1a and its orthologue from mouse (Fig. 3C). The PKPs show tissue-specific expression patterns, with PKP1 being predominantly expressed in the suprabasal layers of stratified epithelia (Bass-Zubek et al., 2009, Hatzfeld, 2007, Neuber et al., 2010).

The PKP1-associated disease Ectodermal dysplasia-skin fragility syndrome (EDSFS)

Pathogenic mutations have been described in many different desmosomal proteins such as PKP1 and PKP2, DSP, PG, DSG1, 2 and 4, DSC2 and 3, and corneodesmosin (McGrath and Mellerio, 2010). However, the first human disease of the desmosomes was detected in 1997 in a family with a compound mutation in *PKP1* (McGrath et al., 1997) revealing a rare autosomal recessive disorder termed Ectodermal dysplasia-skin fragility syndrome (OMIM 604536, see <http://www.omim.org/>). Since then, several cases of this syndrome have been reported from different parts of the world (overview in Table 21 in appendix).

This genodermatosis is classified as a suprabasal form of epidermolysis bullosa simplex and characterized by skin fragility, chronic cheilitis, and palmoplantar hyperkeratosis with painful cracking of the skin. Additional more variable features include abnormalities of ectodermal development combined with growth retardation (McGrath et al., 1999, McGrath et al., 1997), hypotrichosis or alopecia (Ersoy-Evans et al., 2006), hypohidrosis and nail dystrophy (Vazquez-Osorio et al., 2017). Uncommon manifestations such as pruritus (Whitlock et al., 2000), dental caries (Boyce et al., 2012, Hamada et al., 2002), recurrent systemic infections, follicular hyperkeratosis (Steijlen et al., 2004), or perianal erythema (Boyce et al., 2012) have also been reported. Skin biopsies revealed acanthosis, acantholysis, and a reduced number of small, poorly formed desmosomes. The integral weakness within the desmosomal plaque leading to desmosomal detachment and cell-cell separation is caused by the loss of PKP1. Notably, most reported *PKP1* mutations are splice-site mutations resulting in exon skipping or cryptic splicing rather than complete ablation of PKP1 (Ersoy-Evans et al., 2006) as well as nonsense (Tanaka et al., 2009) or frameshift mutations (Boyce et al., 2012, Ersoy-Evans et al., 2006, Hernandez-Martin et al., 2013) being located within the N-terminus as well as in the arm repeat domain of PKP1. Most of the reported mutations have been homozygous (McGrath and Mellerio, 2010). However, patients, who are a compound heterozygote for functional knockout mutations in *PKP1*, have also been identified (McGrath et al., 1999, McGrath et al., 1997, Zheng et al., 2005). In summary, these clinical and diverse features indicate the essential role of PKP1 in the stabilization of desmosomal structure and function, predominantly in the spinous layer of the epidermis (McGrath and Mellerio, 2010). However, the rarity of cases of EDSFS impedes to establish accurate genotype-phenotype correlations.

Function of PKP1 in regulating desmosomal adhesion

It has been shown that PKPs play a key role in the clustering of desmosomal proteins that promotes the formation of this highly ordered structure. This function is particularly evident in PKP1 (Delva et al., 2009). Only PKP1 considerably enhances the number and size of desmosomes, when overexpressed in cultured cells (Hatzfeld et al., 2000, Kowalczyk et al., 1999, South, 2004, South et al., 2003). The N-terminal head domain of PKP1 interacts with DSG1, DSC1, DSP, and keratins (Bornslaeger et al., 2001, Hatzfeld et al., 2000, Smith and Fuchs, 1998). Although an *in vitro* association of PKP1 with keratins was detected (Hatzfeld et al., 2000, Kapprell et al., 1988, Smith and Fuchs, 1998), the relevance of this finding for keratin anchorage at the desmosomal plaque has been disputed due to the location of PKP1 in the outer desmosomal plaque, while keratins contact the inner plaque (North et al., 1999). The binding of PKP1 to DSP, which bridges the distance between the inner and the outer desmosomal plaque, appears particularly robust and enhances DSP's recruitment to sites of cell-cell junctions (Kowalczyk et al., 1999). Thus, PKP1 is considered to anchor keratins at the desmosome indirectly via DSP (Fig. 4B).

PKP1 overexpression not only increased desmosomes, but in addition transformed desmosomal adhesion from a calcium-dependent to a calcium-independent state. These two functionally distinct adhesive states are distinguished by their reaction to calcium-depletion: in normal tissues, desmosomes adopt a calcium-independent state, also termed hyperadhesion (Garrod et al., 2005, Kimura et al., 2007, Wallis et al., 2000), whereas during wound healing and regeneration, desmosomes become calcium-dependent leading to weaker intercellular adhesion that allows for tissue remodeling (Kimura et al., 2012, Wallis et al., 2000). In cultured keratinocytes the capacity to impart calcium-independent intercellular cohesion is unique to PKP1, whereas PKP3 not only fails to confer calcium-independence and strong adhesion, but directly contributes to destabilization and dynamic desmosomes (Keil et al., 2016). These data indicate that PKP1 is well suited to impart strong intercellular cohesion and protect the epidermis from mechanical stress.

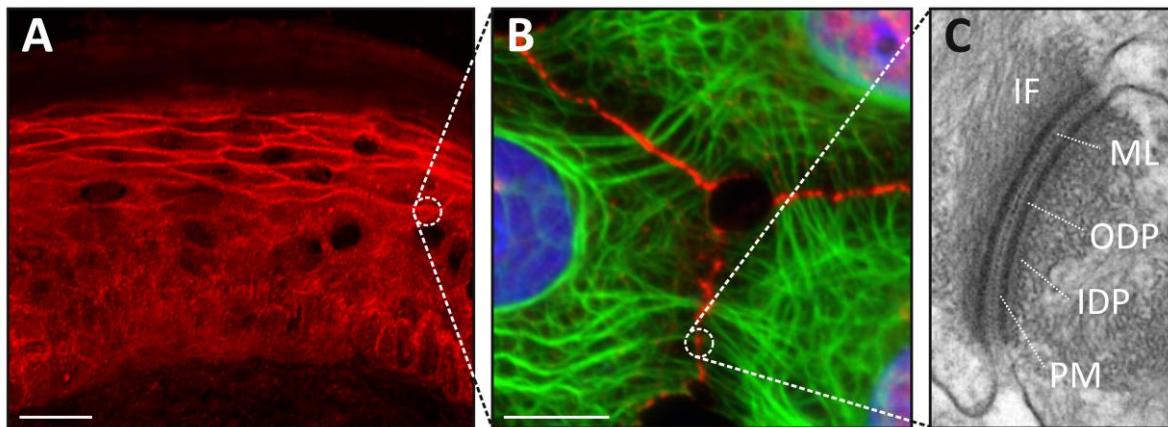


Fig. 4| PKP1: an important stabilizer of desmosomes.

(A) PKP1 (in red) is found in stratified epithelia such as the epidermis and localizes primarily to desmosomes in suprabasal layers, though it reveals also a cytoplasmic localization increasing from suprabasal to basal epidermal layers. Cryosections from back skin of neonatal mice were stained with an antibody directed against PKP1. Scale bar: 25 μm . (B) At cellular level, the immunofluorescence image illustrates the anchorage of keratins (in green) to desmosomal junctions, which are highlighted by PKP1 (in red), thereby creating a transcellular cytoplasmic network. DNA is shown in blue. Scale bar: 5 μm . (C) Appearance of a highly organized desmosome between two adjacent epithelial cells at ultrastructural level taken from (Green and Gaudry, 2000) and modified. The electron dense plaques (ODP and IDP) flank the two opposing plasma membranes (PM) and serve to anchor keratins (IF) to the desmosome. The central dense stratum (electron-dense midline) is composed of the extracellular domains of DSGs and DSCs. DSC, desmocollin; DSG, desmoglein; IDP, inner dense plaque; IF, intermediate filaments; ML, midline; ODP, outer dense plaque; PM, plasma membrane.

Function of PKP1 in the cytoplasm

The cytoplasmic localization of PKP1 and PKP3 suggested an additional role of these proteins beside their involvement in cell-cell adhesive interactions. Several cytoplasmic RBPs (RNA-binding proteins) such as PABPC1 (cytoplasmic poly(A)-binding protein 1), FXR1 (Fragile X mental retardation syndrome-related protein 1), UPF1 (up-frameshift factor 1) or G3BP (Ras-GTPase activating protein SH3 domain binding protein) have been shown to partially co-distribute with PKP1 and PKP3 after sucrose gradient centrifugation (Fischer-Keso et al., 2014, Hofmann et al., 2006, Yang et al., 2013). When cells were exposed to environmental stress (i.e. heat shock or oxidative stress), FXR1, G3B, and PABPC1 were found together with PKP1 or PKP3 in stress granules [SGs, (Hofmann et al., 2006)]. SGs are transient, dynamic cytoplasmic sites containing aggregates of mRNA bound to 48S preinitiation factors (Anderson and Kedersha, 2008). SGs are proposed to play a role in mRNA triage in stressed cells by sorting sequestered mRNAs for re-initiation, storage, or degradation (Anderson and Kedersha, 2008, Kedersha et al., 2005). RBPs in general control the pro-

cessing, translation, stability, transport, and localization of mRNAs (Collins et al., 2009, Glisovic et al., 2008). Due to the fact that all three RBPs associating with PKP1 affect the turnover and translation of mRNAs in the cytoplasm, it is conceivable that PKP1 as well as PKP3 play a role in post-transcriptional gene regulation (Wolf et al., 2010). In agreement, it was shown that PKP1/3 containing messenger ribonucleoproteins (mRNPs) comprise PKP2 and DSP mRNAs. Knockdown experiments suggest that PKP1/3 enhances the mRNA stability of desmosomal proteins (Fischer-Keso et al., 2014). Taken together, these studies reveal that the mRNA level of desmosomal components can be regulated by PKP1 (Fischer-Keso et al., 2014, Whitman et al., 2011).

In addition, PKPs may also associate with actin, actin regulating proteins, and microtubules [MTs, (Hatzfeld et al., 2000)]. However, although the function of p120ctn and its direct homologs in regulating the actin cytoskeleton via small Rho-GTPases is well established (Anastasiadis, 2007, Dohn et al., 2009, Ghose et al., 2015, Keil et al., 2007, Schackmann et al., 2013, Wolf et al., 2006), the role of PKP1 in organizing actin filaments and regulating Rho-GTPases is unknown. Ectopically expressed in cells with little or no desmosomes such as NIH3T3 or HeLa cells, PKP1 associated with actin filaments (Hatzfeld et al., 2000). In filopodia of keratinocytes not connected to neighboring cells, an association of PKP1 with actin was also observed. It was further shown that *pemphigus vulgaris* autoantibodies induced skin blistering by interference with RhoA signaling, a reduction in RhoA activity, and a loss of desmosomal adhesion indicating that Rho A is involved in the regulation of desmosomal adhesion, at least in part by maintaining the cytoskeletal anchorage of desmosomal proteins (Waschke et al., 2006). However, the impact of PKP1 on actin organization and its role in regulating Rho-GTPases remains to be determined.

Moreover, PKP1 has been shown to stimulate translation *in vitro* as well as in cells (Wolf et al., 2010). PKP1 associated with the mRNA-cap-binding complex consisting of eukaryotic translation initiation factors (eIFs) 4A, 4B, 4G, 4E, and PABPC. Via its N-terminal head domain PKP1 specifically interacted with the ATP-dependent RNA helicase eIF4A1 and stimulated its enzymatic activity. The helicase has been implicated in the unwinding of secondary structures in the 5'-UTRs of mRNAs to facilitate scanning for the start codon and translation initiation. PKP1-overexpressing cells revealed an overall upregulation of translation, whereas the knockdown of PKP1 reduced protein synthesis. These findings on the

stimulation of translation correlated with the capacity of PKP1 to increase proliferation and cell size (Wolf and Hatzfeld, 2010, Wolf et al., 2010).

Function of PKP1 in the nucleus

All three PKPs have been observed in the nucleus (Bonne et al., 1999, Heid et al., 1994, Mertens et al., 1996, Schmidt and Jager, 2005, Schmidt et al., 1997b). The nuclear localization of PKP1 is most abundant and both, endogenous and overexpressed PKP1 have been detected in the nucleus. Post-transcriptional processing via alternative splicing may be involved in the regulation of PKP1's localization to the nucleus as the two splice variants reveal distinct subcellular localizations, as mentioned above (Schmidt et al., 1997b). Transfection of PKP1 fragments suggested that the N-terminal domain of PKP1 contains a nuclear localization sequence [NLS, (Hatzfeld et al., 2000, Kowalczyk et al., 1999)]. However, analysis of the amino acid sequence of PKP1 revealed no canonical NLS or DNA-binding motifs. Due to the fact that the head domain (1-235aa) of PKP1 as well as its arm repeats (235-726aa) each localize to the nucleus, one can suggest that there are at least two NLSs in PKP1. Moreover, a region in the N-terminal head domain of PKP1 (55-125aa) appears important for directing the protein to the nucleus (Sobolik-Delmaire et al., 2010).

DNase I digestion of chromatin revealed a decreased pool of nuclear PKP1 suggesting that PKP1 specifically associates with nuclear components. Furthermore, DNA damage resulted in partial displacement of PKP1 from the nucleoplasm to the nucleolus resulting in increased cell survival. In agreement, an association of PKP1 with ssDNA was investigated *in vitro* (Sobolik-Delmaire et al., 2010). Protein binding partners of PKP1 linking it to DNA damage response and providing some mechanistic insight have not been reported. However, the role of PKP1 in the nucleus requires further studies to validate the examined findings and to address the functional relevance.

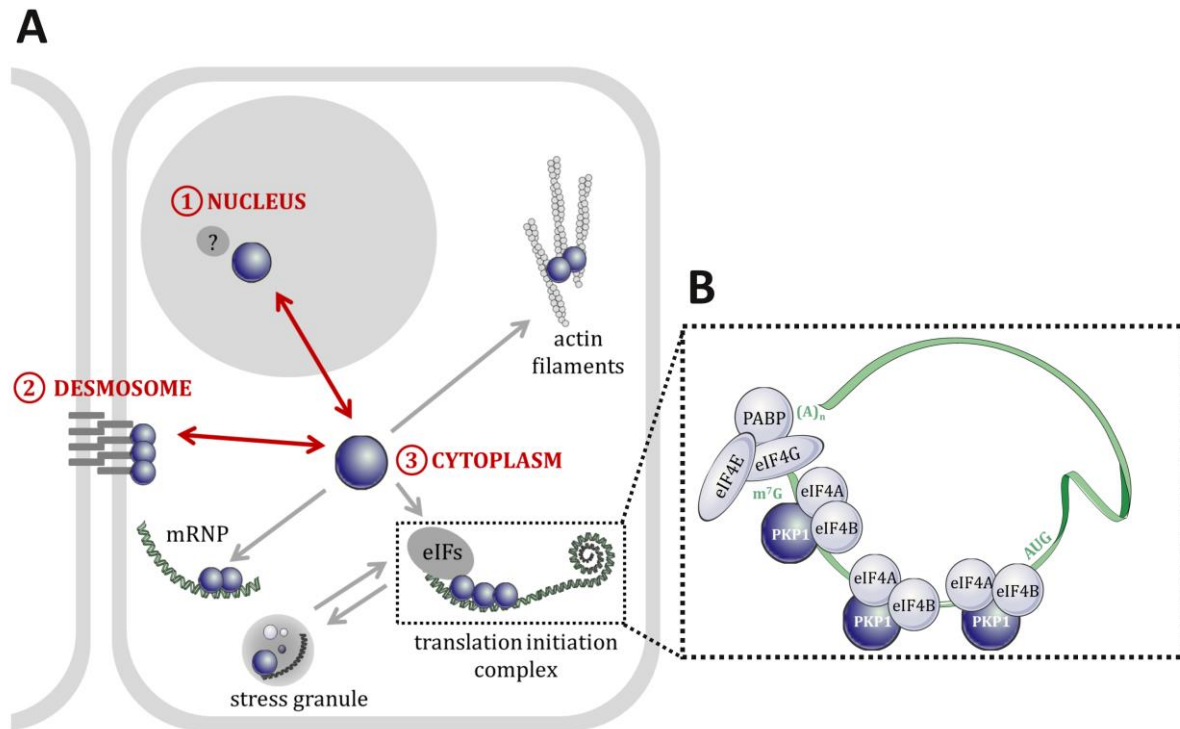


Fig. 5I Model of PKP1's subcellular localization and function.

Schematic model of nuclear, desmosomal, and cytoplasmic PKP1. ① The role of PKP1 in the nucleus remains unclear. *In vitro* analysis revealed an interaction of PKP1 with ssDNA suggesting that PKP1 may protect cells from DNA damage (Sobolik-Delmaire et al., 2010). ② At the desmosome, PKP1 acts as scaffold, interacting with both desmosomal cadherins and desmoplakin and promotes desmosome assembly, maturation and linkage to the cytoskeleton (Hatzfeld, 2007). ③ In the cytoplasm, PKP1 is found in stress granules, when cells were exposed to environmental stress [e.g. heat shock or oxidative stress, (Hofmann et al., 2006)]. Additionally, PKP1 was described as a component of mRNA ribonucleoprotein particles and acts as posttranscriptional regulator of gene expression (Fischer-Keso et al., 2014). Ectopically expressed in cells with little or no desmosomes like HeLa or NIH3T3 cells, PKP1 associates with actin filaments (Hatzfeld et al., 2000) suggesting a role of PKP1 in actin organization. By interacting with components of the translation initiation complex, PKP1 promotes translation (Wolf and Hatzfeld, 2010, Wolf et al., 2010). (B) Model of the cap-binding translation initiation complex in the presence of PKP1 modified after (Wolf and Hatzfeld, 2010). eIF4E binds to the cap and recruits eIF4G, eIF4A and eIF4B into the complex. In the presence of PKP1 more eIF4A and eIF4B are recruited into the complex facilitating scanning of the 5'-UTR and start codon (AUG) recognition. AUG, start codon; eIF, eukaryotic initiation factor; m⁷G, 7-methylguanosine cap; mRNP, messenger ribonucleoprotein; PABP, poly(A)-binding protein; PKP, plakophilin.

In summary, PKP1 combines multiple functions in different subcellular compartments. In the desmosomal plaque, PKP1 reveals an essential function in regulating desmosome number, size, and stability as well as strengthening desmosomal adhesion. Cytoplasmic PKP1 plays a role in promoting translation and proliferation. However, this is not consistent with its function in increasing adhesion, but strongly suggests that PKP1 has additional functions, presumably in growth control. The dual localization at desmosomes and in

the cytoplasm places PKP1 in a prime position to coordinate alterations in cell adhesion, with changes in signaling during processes such as the formation and development of the epidermis. Under certain pathological conditions, this equilibrium may be disturbed, leading to tumorigenesis, impaired wound healing, or other skin pathologies. Interestingly, several studies addressed the role of PKP1 in carcinogenesis. However, the results are contradictory with upregulation, downregulation, or maintenance of PKP1 being reported [reviewed in (Hatzfeld et al., 2014)]. The contribution of PKP1 in cancer might be context-dependent and determined by the status of distinct signaling pathways. Therefore, it was of great interest at the beginning of this study to elucidate, how the equilibrium between these distinct roles of PKP1 is regulated.

One of the most commonly used mechanisms for changing the properties of a protein is the covalent modification of its structure. Post-translational modifications (PTMs) can range from the addition of small chemical groups as in phosphorylation and methylation, to more substantial additions such as lipid groups or entire polypeptides. The functional consequence of PTMs is to change the physical structure of the protein (generally the shape, charge, or hydrophobicity of the surface) which, in turn, affects how the protein behaves and associates with other molecules within the cell (Lim et al., 2015). The next paragraph briefly addresses PTMs related to PKP1.

Post-translational regulation of PKP1

Over 200 types of PTMs have been identified (Jensen, 2006). The variety of PTMs as well as the large number of different sites on a protein that can be modified, dramatically expand the possible states for each protein (Lim et al., 2015). During processes such as epidermal development or wound healing, cell adhesion junction components are tightly regulated at the gene expression level. However, PTMs of junction components also contribute to their proper function. Several PTMs have been identified for PKPs, e.g. palmitoylation (Roberts et al., 2014, Roberts et al., 2016), methylation (PhosphoSitePlus®), acetylation (PhosphoSitePlus®) or ubiquitination (Kim et al., 2011, Wagner et al., 2012). The consequences with respect to PKP's localization and functions as well as the physiological relevance of these findings need to be determined (Hatzfeld et al., 2014). However, one of the most prevalent modifications is phosphorylation, the transfer of the terminal phosphate group from ATP to proteins, most commonly to the hydroxyl groups of serine, threonine, or

tyrosine side chains (Prabakaran et al., 2012). PKP1 contains numerous putative phosphorylation sites highly clustered in its N-terminal domain (Hatzfeld et al., 2014). Large-scale mass spectrometry detected many of these sites, e.g. PKP1 contains 52 serine/threonine and 15 tyrosine residues that were found to be phosphorylated (<http://www.phosphosite.org/>). In agreement with this, a yeast two-hybrid (Y2H) screen revealed a putative interaction of PKP1 with Akt2 (data from Prof. Hatzfeld) suggesting that PKP1 can be phosphorylated by this kinase and that PI3K-dependent signaling may be involved in modulating its functions. The next chapter will briefly describe the PI3K/Akt signaling pathway.

2.3. Epidermal homeostasis: regulation by growth factors

Growth factor signaling pathways

The equilibrium between cellular proliferation and differentiation plays a vital role in several physiological processes. In the epidermis, the homeostasis of the balance, i.e. between the proliferation of mitotically active keratinocytes and the differentiation of post-mitotic cells is essential for skin formation and development (Fuchs and Raghavan, 2002). Keratinocyte differentiation begins in the basal layer and involves cross-talk between cells of the dermis and epidermis via growth factors including epidermal growth factors [EGFs, (Piepkorn et al., 1998)] and transforming growth factors [TGFs, (Letterio and Bottinger, 1998)], the vitamin-D receptor system (Bikle, 1997), ECM (extracellular matrix) proteins such as integrins (Cotsarelis et al., 1999, Levy et al., 2000) and others. Furthermore, insulin-like growth factors (IGFs) and their relative insulin have important roles in homeostasis and physiology of the skin.

Activation of growth factor receptor protein tyrosine kinases results in autophosphorylation on tyrosine residues. Phosphatidylinositol-3-kinase (PI3K) is then recruited to the membrane by directly binding to phospho-tyrosine consensus residues of growth factor receptors or adaptors through one of the two SH2 domains in the adaptor subunit. Activated PI3K converts phosphatidylinositol-4,5-bisphosphate (PIP₂) to phosphatidylinositol-3,4,5-triphosphate (PIP₃). PIP₃ then recruits a subset of signaling proteins with pleckstrin homology (PH) domains to the membrane, including protein serine/threonine kinase 3'-phosphoinositide-dependent kinase 1 (PDK1) and Akt/protein kinase B [PKB, (Cantley,

2002, Vivanco and Sawyers, 2002)]. PDK1 and Akt induce a kinase cascade that plays a central role in the regulation of glucose transport, protein synthesis, cell proliferation, and survival (Fresno Vara et al., 2004). Akt occurs in three isoforms, of which Akt1 (PKB α) is the dominant form, whereas Akt2 (PKB β) is predominantly expressed in insulin-responsive tissues. Akt3 (PKB γ) is highly expressed in testis and brain (Altomare et al., 1998, Nakatani et al., 1999).

Additionally, growth factors like EGF can activate the Ras-Raf-MEK-Erk mitogen activated protein kinase (MAPK) pathway. Activated Raf induces a signal transduction cascade, which includes the Mitogen-activated protein kinase/Erk kinase (MEK) and extracellular-signal-regulated kinase (Erk). Activated Erk phosphorylates cytoplasmic signaling proteins, including RSK (p90 ribosomal S6 kinase) and end-point effectors such as transcription factors. RSK similarly phosphorylates several cytoplasmic targets and transcriptional regulators (Mendoza et al., 2011). Insulin and IGF1 are weaker activators of the MAPK pathway, but strong PI3K/Akt activators (Clerk et al., 2006, Weng et al., 2001).

Stachelscheid et al. identified insulin- and IGF1 receptor signaling in keratinocytes as key regulators of epidermal morphogenesis and proliferative potential as epidermal loss of IR, IGF1R, or both increasingly impaired stratification (Stachelscheid et al., 2008). In addition, it was reported that insulin/IGF1 signaling plays a role in the control of p63, a key determinant of epidermal cell fate, to regulate asymmetric divisions and progression of mitosis during epidermal morphogenesis (Gunschmann et al., 2013). However, signaling pathways regulating the role of desmosomal proteins in adhesion or cell signaling are not well characterized. Inhibitors that block the EGF receptor (EGFR) promoted desmosome assembly along with a change in morphology from a mesenchymal to an epithelial appearance suggesting that growth factor signaling counteracts desmosomal adhesion (Lorch et al., 2004). Furthermore, EGFR activation resulted in tyrosine phosphorylation of PG, which was accompanied by a loss of DSP from desmosomes and decreased cell adhesion (Yin et al., 2005).

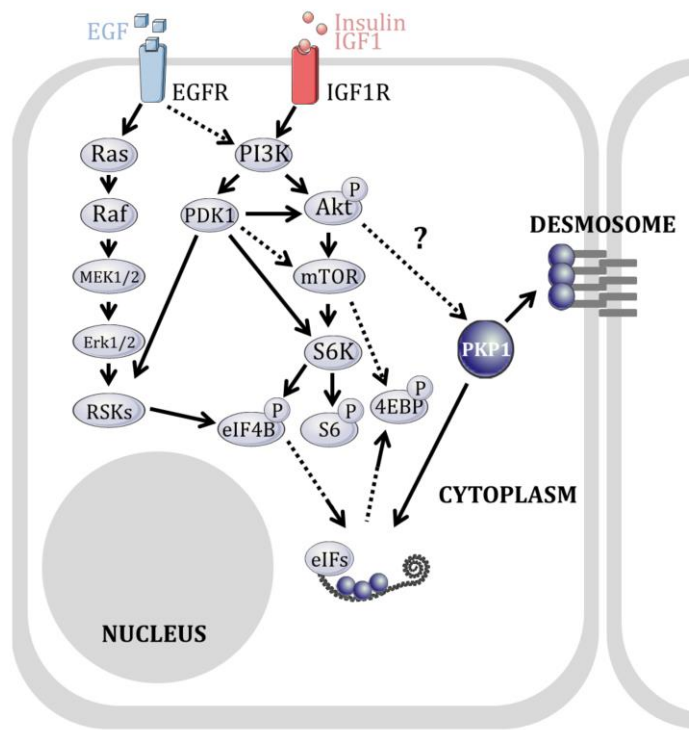


Fig. 6| Regulation of translation initiation by growth factors and PKP1.

(A) Schematic overview of the regulation of translation initiation based on (Kong and Lasko, 2012). Growth factors such as insulin, IGF1 or EGF stimulate cellular translation by triggering mTOR signaling via the PI3K/Akt or the MEK/Erk pathway. Activated mTOR phosphorylates multiple sites on 4E-BP, which causes its dissociation from eIF4E (not shown in detail), allowing binding of eIF4E to eIF4G, assembly of an active cap-binding complex and recruitment of mRNA to the 40S ribosomal subunit. Additionally, activated mTOR promotes phosphorylation of eIF4B and ribosomal protein S6 by p70S6K. Phosphorylated eIF4B enhances the enzymatic activity of eIF4A and thereby promotes the scanning step of translational initiation. EGF(R), epidermal growth factor (receptor); eIF, eukaryotic initiation factor; Erk, extracellular signal-regulated kinase; IGF1(R), insulin-like growth factor 1 (receptor); MEK, mitogen-activated protein kinase kinase; mTOR, mammalian target of rapamycin; PDK1, phosphoinositide-dependent kinase-1; PI3K, phosphatidylinositol-4,5-bisphosphate 3-kinase; PKP, plakophilin; RSK, p90 ribosomal S6 kinase; S6, ribosomal protein S6; S6K, p70 ribosomal S6 kinase; 4E-BP, eIF4E-binding protein.

As mentioned before, studies conducted by Wolf et al. provide evidence that PKP1 plays a direct role in growth control by stimulating translational initiation and thus protein synthesis (Wolf and Hatzfeld, 2010, Wolf et al., 2010), although the responsible signaling pathway(s) by growth factors remained unknown. Because of the involvement of PKP1 in the regulation of protein synthesis as well as the identification of eIF4A1 as a PKP1 interacting partner, the next chapter will concisely summarize the control of translational initiation.

Regulation of protein synthesis by growth factors

Translation initiation is the rate limiting step in translation and accordingly, protein synthesis is regulated primarily at the level of initiation rather than at elongation, or termination steps. In eukaryotic cells, several initiation factors (eIFs) are important for the assembly of the initiation complex on the mRNA. The initiation factor eIF4E is a key component that binds to the 7-methylguanosine cap at the 5' end of mRNAs, interacting with either eIF4E-binding proteins (4E-BPs) or with the eIF4F complex. The eIF4F complex includes the ATP-dependent helicase eIF4A, eIF4G that bridges the mRNA to the ribosome through its interaction with eIF3, which binds directly to the ribosome, and eIF4E itself (Goodfellow and Roberts, 2008, Hinton et al., 2007, Prevot et al., 2003, Svitkin et al., 2001). Finally, the eIF4F complex scans the mRNA in a 5' to 3' direction and unwinds secondary structures in the 5' untranslated region (UTR) to reveal the initiation codon and allow for ribosome loading (Goodfellow and Roberts, 2008, Hinton et al., 2007, Prevot et al., 2003, Svitkin et al., 2001).

Several translation factors are regulated in response to growth factors and nutrients via the MEK/Erk cascade or PI3K/Akt pathway (Fig. 6A). These processes are precisely regulated by phosphorylation (Hara et al., 1997). For example, the assembly of the eIF4F complex depends on the availability of eIF4E, which is regulated by 4E-BPs and is present just in limiting amounts compared to other eIFs (Graff et al., 2008). eIF4G competes with members of the 4E-BP family for a shared binding site on eIF4E (Haghighat et al., 1995). Their binding to eIF4E prevents the formation of the eIF4F complex, ribosomal subunit formation and thus translation initiation. Insulin or other growth factors can promote the binding of 4E-BPs to the Ser/Thr kinase mTORC1 (mammalian target of rapamycin complex 1), which is a key sensor of nutrient status (Hay and Sonenberg, 2004, Rapley et al., 2011) and phosphorylates 4E-BPs. Increased phosphorylation of 4E-BPs promotes their dissociation from eIF4E and thus increases translational activity. Furthermore, mTORC1 is directly or indirectly responsible for the phosphorylation of additional substrates, which are important for controlling translation rates, e.g. p70S6K, which in turn phosphorylates eIF4B and thereby facilitates the recruitment of the 40S ribosomal subunit to the mRNA (Holz et al., 2005, Proud and Denton, 1997).

2.4. The 14-3-3 proteins

Protein phosphorylation often depends on PI3K/Akt signaling in response to insulin/IGF1. The first signaling molecules identified as phospho-serine/-threonine binding proteins were 14-3-3 proteins (Yaffe, 2002). The next chapter will give a brief overview of this protein family as well as reported PKP-14-3-3 interactions.

The 14-3-3 protein family: an overview

The 14-3-3 proteins are abundant 28-33 kDa, conserved regulatory molecules expressed in all eukaryotic cells and participate in a wide range of cellular processes through interactions with numerous proteins (Aitken, 1996, 2006, Morrison, 2009). Members of this protein family were first identified by Moore and Perez in 1967 during a systematic classification of brain proteins (Dougherty and Morrison, 2004, Moore and Perez, 1967). The name “14-3-3” describes the elution fraction containing these proteins following DEAE-cellulose chromatography and their migration position after starch gel electrophoresis (Dougherty and Morrison, 2004). In mammals, there are at least seven isoforms: γ , σ , η , ϵ , β , ζ and τ , of these the phosphorylated forms of β and ζ were initially described as α , and δ , respectively (Aitken et al., 1995), each encoded by a distinct gene. Among the seven mammalian 14-3-3 members, differences in their expression pattern between cell-types and tissues have been reported (Kilani et al., 2008, Moreira et al., 2008). All seven isoforms have been found in human cultured keratinocytes as well as, with the exception of 14-3-3 τ , in the human epidermis. Within the whole skin, only 14-3-3 γ is also present in the dermal layer of the skin (Kilani et al., 2008).

Studies by Kilani et al. showed that immunohistochemical staining of human skin sections revealed variable levels of 14-3-3 γ , σ , η , β , and ζ expressed by suprabasal keratinocytes and that the intensity of this expression increased as keratinocytes become more differentiated. The highest expression levels of these proteins were detected in keratinocytes located within the *stratum lucidum*, an epidermal layer found under the *stratum corneum* of the skin of the palms and soles. However, the expression of 14-3-3 ϵ seemed to be limited to terminally differentiated keratinocytes located within *stratum lucidum*. In contrast, 14-3-3 β is equally expressed within keratinocytes of all suprabasal layers. No immunohistochemical staining was detected for 14-3-3 τ in human skin sections. Neither of the 14-3-3 isoforms was detectable in basal keratinocytes and fibroblasts [(Kilani et al., 2008), Fig. 7].

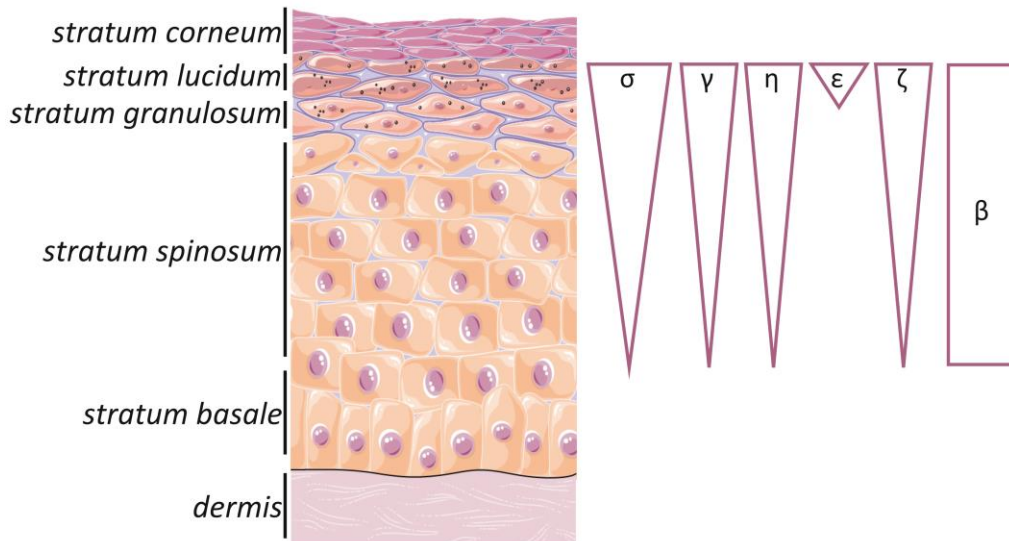


Fig. 7| Expression patterns of 14-3-3 proteins in human epidermis.

The scheme of the epidermis [based on (Kilani et al., 2008)] illustrates the expression levels of the 14-3-3 isoforms (σ , γ , η , ϵ , ζ and β) in human epidermis. Most 14-3-3 isoforms showed the highest expression in highly differentiated keratinocytes. Note, that no immunohistochemical staining was detected for 14-3-3 τ .

14-3-3 proteins exist as dimers and form homo- as well as heterodimers (Jones et al., 1995). Due to their specific phospho-serine/-threonine binding activity, 14-3-3 proteins are able to bind many different proteins (Muslin et al., 1996). Two high-affinity phosphorylation-dependent 14-3-3 binding motifs, that are recognized by all 14-3-3 isotypes, have been described in target proteins: RSXpSXP (mode 1) and RXXXpSXP (mode 2), whereas pS represents phospho-serine (Rittinger et al., 1999, Yaffe et al., 1997). Though, phosphorylation-dependent sites diverging significantly from these motifs have also been reported (Aitken, 2002). Moreover, some examined 14-3-3 interactions are independent of target phosphorylation such as binding of 14-3-3 to exoenzyme S or p190RhoGEF (Henriksson et al., 2002, Masters et al., 1999, Zhai et al., 2001). In a survey of defined 14-3-3-binding sites in mammalian proteins, mode 1 motifs dominated, although the +2 proline residue occurs in less than half (Chen et al., 2011, Johnson et al., 2010). Interestingly, these 14-3-3 binding sequences showed an overlap with the specificities of the protein kinase A/protein kinase G/protein kinase C (AGC) and Ca²⁺/calmodulin protein kinase (CAMK) group of protein kinases (Johnson et al., 2010). These basophilic kinases include e.g. PKC isoforms, Akt, p70S6K, and RSKs [reviewed in (Pearce et al., 2010)].

Crystal structures of 14-3-3 ζ and 14-3-3 τ revealed that they are highly helical, dimeric proteins (Liu et al., 1995, Xiao et al., 1995). Each monomer is composed of nine anti-parallel α -helices, organized into an N- and C-terminal domain and contains an amphipathic groove acting as a ligand binding channel (Liu et al., 1995, Obsil et al., 2001, Rittinger et al., 1999, Xiao et al., 1995, Yaffe et al., 1997). Due to two binding pockets within each dimer, two motifs can be associated simultaneously, either a single target or separate binding partners (Obsil et al., 2001, Rittinger et al., 1999, Yaffe et al., 1997). The regions, which are conserved throughout all 14-3-3 isoforms, are mainly found in the interior of the binding channel, whereas the variable residues are located on the surface of the proteins (Aitken et al., 2002) determining the specificity of the association of 14-3-3 isoforms with diverse target proteins. The variable N-terminal residues of all 14-3-3 homologues are important for dimer formation and may be a limit to the number of possible homo- or heterodimer combinations (Aitken, 2002).

14-3-3 proteins reveal distinct features like acting as adaptor molecules, facilitating or inhibiting protein-protein interactions, modulating the subcellular localization of proteins, regulating enzymatic activities, protecting against proteolytic degradation or dephosphorylation, and stabilizing multiprotein complexes, respectively (Obsil and Obsilova, 2011). Thus, the family of 14-3-3 proteins is being implicated in a growing number of cellular processes such as signal transduction, apoptosis, cell cycle regulation, or stress response indicating the multifunctionality of these ubiquitous adaptor proteins [reviewed in (Aghazadeh and Papadopoulos, 2016, Morrison, 2009, van Hemert et al., 2001)].

14-3-3 proteins as regulators of PKP functions

Two reports reveal that 14-3-3 proteins are involved in the modulation of PKP's localizations and functions, respectively. Müller and colleagues identified a molecular pathway that explains the trafficking of PKP2 from cytoplasm to nucleus [(Müller et al., 2003), Fig. 8]. The Cdc25C-associated kinase 1 (C-TAK1), involved in cell-cycle regulation and Ras-signaling, phosphorylates PKP2 at S82, which promotes the binding of 14-3-3. PKP2 mutated at this site (S82A) and transfected in SCC-9 keratinocytes exhibited an increased nuclear accumulation suggesting that C-TAK1 phosphorylation and subsequent interaction with 14-3-3 proteins prevents PKP2's nuclear localization (Müller et al., 2003). However, it remained unknown, which specific 14-3-3 isoform interacts with PKP2, although PKP2 ap-

pears to be able to associate with more than one isoform, since 14-3-3 σ , ϵ , β , and τ were identified as interaction partners in large-scale interaction screens (<https://thebiogrid.org/111335>).

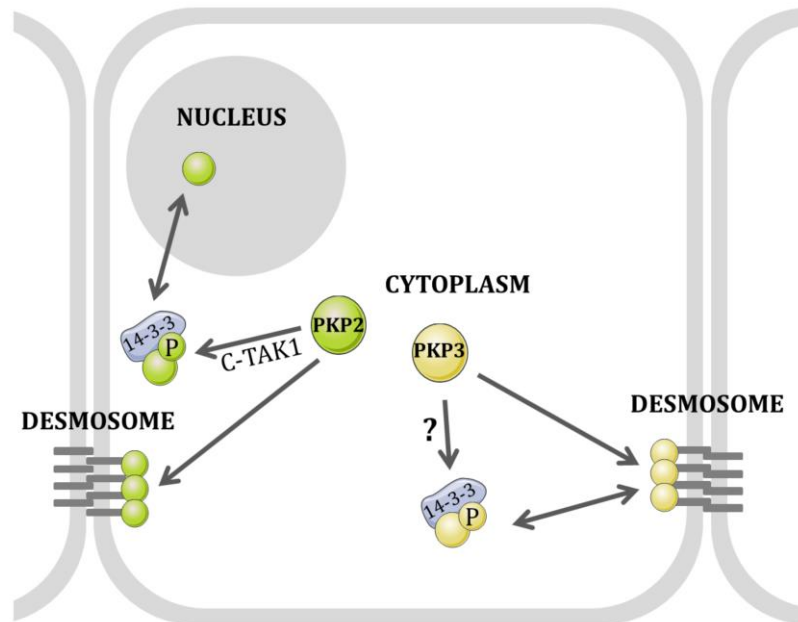


Fig. 8| Regulation of PKP2 and PKP3 by 14-3-3 proteins.

The role of 14-3-3 proteins in the regulation of PKPs is shown in this scheme modified after (Hatzfeld et al., 2014) and based on (Müller et al., 2003, Roberts et al., 2013). PKP2 (in green) is phosphorylated at serine 82 by C-TAK1 leading to 14-3-3 binding and preventing its accumulation in the nucleus. Thus, 14-3-3 binding modulates the balance between the cytoplasmic and nuclear distribution of PKP2, respectively. PKP3 (in yellow) is phosphorylated at serine 285 by an unknown kinase. The further 14-3-3 σ (stratiferin) association with PKP3 in the cytosol sequesters and restricts its exchange with the desmosomal plaque. In conclusion, here 14-3-3 binding regulates the cytoplasmic versus desmosomal PKP3 localization. C-TAK1, Cdc25C-associated protein kinase; PKP, plakophilin.

A proteomic screen conducted by Roberts et al. identified 14-3-3 σ , also called stratiferin, as a PKP3-associated protein (Fig. 8). This interaction was specific for PKP3 and not detected for PKP1 or PKP2 in a Y2H approach. Mutation analyses showed that the binding site includes S285 in the N-terminal head domain of PKP3. Moreover, 14-3-3 σ preferentially interacted with cytoplasmic PKP3 and limited the exchange of cytoplasmic PKP3 with its desmosomal pool shown by fluorescence recovery after photobleaching (FRAP) analysis. Thus, decreased 14-3-3 σ expression results in weakened desmosomal adhesion and increased cell migration (Roberts et al., 2013). The kinase(s) or signaling pathway(s) involved in this PKP3-14-3-3 mechanism has not been reported. However, these findings point to a conserved biochemical mechanism, whereby desmosomal protein phosphorylation and fol-

lowing 14-3-3 binding contributes to the subcellular partitioning of these proteins and presumably affecting desmosome dynamic.

2.5. The aim of the study

Desmosomes are adhesive cell-cell contacts essential for mediating strong intercellular cohesion. They are especially abundant in tissues prone to mechanical strain such as the skin or the heart. The strong cell-cell adhesion is mediated by desmosomal cadherins that interact with intracellular linker proteins including PKPs 1-3. How the individual PKPs differentially regulate desmosome function is not well understood.

One of the main aims of this work was to investigate the *in vivo* function of PKP1 in desmosome stability, tissue differentiation, and homeostasis. For this purpose, PKP1-null mice were generated and characterized. Keratinocytes isolated from these mice were examined to get further insight into molecular mechanisms.

Besides providing mechanical stability, desmosomes are thought to function in cell-cell communication and signal transduction processes. Notably, PKP1 is a multifunctional protein: at desmosomes it can increase intercellular adhesion by recruiting desmosomal proteins to the plasma membrane (Hatzfeld et al., 2000, Kowalczyk et al., 1999), whereas in the cytoplasm PKP1 can stimulate translation and proliferation by interacting with components of the translation initiation complex (Wolf and Hatzfeld, 2010, Wolf et al., 2010). Therefore, the second major aim was to elucidate, how the equilibrium between these two antagonistic roles of PKP1 is regulated.

14-3-3 proteins are suggested to contribute to the regulation of PKPs 2 and 3 (Müller et al., 2003, Roberts et al., 2013) by modulating their subcellular localization, whereas a potential role of this protein family in regulating PKP1 was unknown. Thus, the third aim of the study was to analyze the impact of 14-3-3 proteins on intercellular cohesion in mouse keratinocytes in general as well as in the regulation of PKP1.

While perturbation of PKP1's functions contribute to epidermal carcinogenesis and inherited diseases, elucidation of all three aspects will help to understand the physiological significance of this multifunctional protein and by which its behaviors are regulated.

3 RESULTS

3.1. Generation and characterization of PKP1 knockout mice

Generation and validation of PKP1-KO mice

The targeting vector, ES cells and mouse strain *Pkp1*-tm2a(KOMP)Wtsi were generated by the trans-NIH Knock-out Mouse Project (KOMP) and obtained from the KOMP Repository (www.komp.org).

The resulting chimeric offspring were bred with C57BL/6N mice to obtain germline transmission of the mutated *Pkp1* allele and obtain *Pkp1*-*fl*-*neo* mice. Mice carrying the floxed allele in the germline revealed no phenotypic abnormalities, verifying that the genetic manipulations had no effect on the functionality of the *Pkp1* gene. Due to possible interference with the splicing process, the neomycin cassette can lead to an alteration of gene expression. Thus, it was desirable to remove the neomycin cassette by mating mice transgenic for FLP1 recombinase under the control of an actin promoter. Therefore, *Pkp1*-*fl*-*neo* mice were crossed with B6;SJL-Tg(ACTFLPe)9205Dym/J mice to remove the floxed neomycin selection marker from the *Pkp1* mutated allele. To generate *Pkp1*^{+/-} mice, *Pkp1*-*fl* mice were further bred with B6.C-Tg(CMV-cre)1Cgn/J mice transgenic for Cre recombinase under the control of the CMV promoter active in all tissues to remove exon 2 from the germline. Mice homozygous for the deleted allele were generated by inbreeding the *Pkp1*^{+/-} mice (Fig. 9A). The resulting *Pkp1*^{-/-} (KO, knockout) mice were analyzed in comparison to their *Pkp1*^{+/+} (WT, wildtype) littermates. All breeding steps were monitored by PCR performed by Dr. Annika Wolf (Fig. 9B).

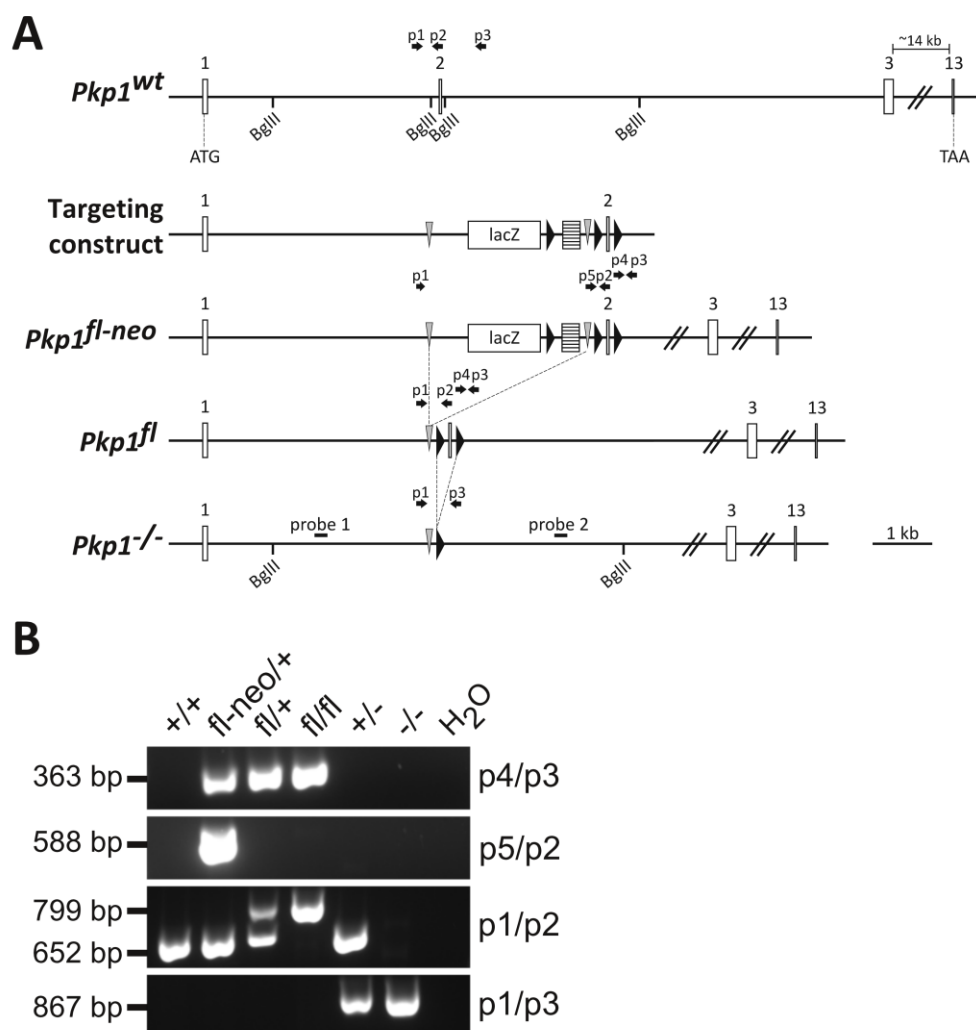


Fig. 9| Generation of the PKP1 knockout.

(A) Scheme of the *Pkp1* WT allele, *Pkp1* targeting construct and mutated *Pkp1* alleles. Exons are indicated as numbered white boxes, *Frt* sites as grey triangles, *loxP* sites as black triangles and neomycin resistance cassette as striped box. The targeted region of the *Pkp1* gene is located between *Bgl*II restriction sites. PCR oligonucleotides p1-p5 are indicated by black arrows. (B) PCR analysis of genomic DNA derived from mouse tails were performed by Dr. Annika Wolf. ATG, start codon; *Bgl*II, restriction site; fl, floxed; lacZ, lacZ reporter gene; neo, neomycin resistance; p1-p5, PCR primer; PKP, plakophilin; TAA, stop codon; wt/(+/+), wildtype; (+/-), heterozygous; (-/-), homozygous.

The removal of exon 2 was verified by Southern blot using *Bgl*II digested genomic DNA and two internal probes (Fig. 10A). On the protein level, no PKP1 was detectable (Fig. 10B). Since exons 3-6 have a different reading frame, deletion of exon 2 is predicted to result in a protein fragment comprising amino acids 1-68 encoded by exon 1 plus additional 18 amino acids of an unrelated sequence resulting from a different reading frame of exon 3 (Fig. 10C).

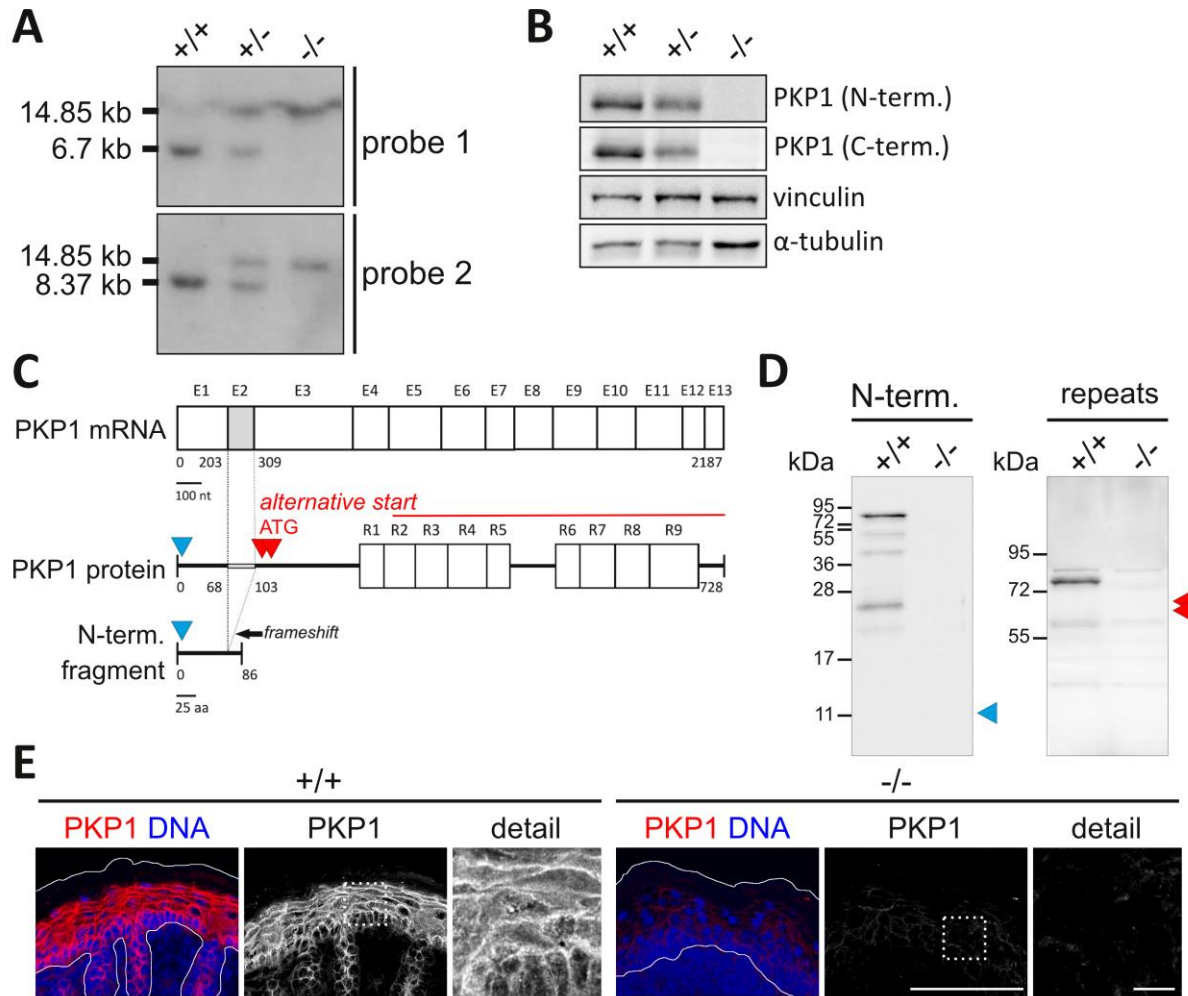


Fig. 10| Validation of the PKP1 knockout.

(A) Southern blot of BglII-digested genomic DNA. Probe 1 detects restriction fragments of 6.7 kb (WT allele) and 14.85 kb (targeted allele) and probe 2 of 8.37 kb (WT allele) and 14.85 kb (targeted allele). (B) Western blot analysis of total protein from *Pkp1*^{+/+}, *+/−* and *−/−* dorsal skin. PKP1 was probed with antibodies against N- and C-terminal domains. Vinculin and α -tubulin were used as loading controls. (C) Schematic representation of PKP1 mRNA and protein sequences. Exon 2 and the corresponding protein sequence in the PKP1 head domain are shown in grey. The blue triangle indicates the binding site for PKP1 antibody clone 10B2 directed against the N-terminus of PKP1 (aa 1-27). The red line indicates the antigen used for the production of antibody PKP1 #670. Putative PKP1 fragments resulting from the translation of exon 1 fused to exon 3 and from translation starting at putative initiation codons in exon 3 are shown below. Red triangles denote the position of hypothetical alternative start codons. (D) Western blot analysis of *Pkp1*^{+/+} and *Pkp1*^{−/−} keratinocytes using antibodies directed against different protein domains. The blue triangle indicates the position of a putative truncated protein of ~ 10 kDa resulting from translation of exon 1 fused to exon 3 (in a different reading frame). Red triangles denote the position of putative truncated PKP1 protein products resulting from alternative start codon usage in exon 3. (E) Immunofluorescence images show the presence of PKP1 (in red) in the epidermis of control mice (+/+) and the loss of PKP1 in PKP1-KO mice (-/-). To compare fluorescence intensities, images were collected with equal hardware settings. Hoechst 33342 staining served as nuclear marker (in blue). White lines mark the SC and basement membrane. Scale bar: 100 μ m, detail: 10 μ m. aa, amino acid; ATG, start codon; E1-13, exons; mRNA, messenger RNA; PKP, plakophilin; R1-9, arm repeats; SC, *stratum corneum*; term., terminal; (+/+), wildtype; (+/-), heterozygous; (-/-), homozygous.

Since this short amino acid sequence is sufficient for DSP binding *in vitro* (Hatzfeld et al., 2000), the putative expression of such a PKP1 fragment was examined by using a PKP1 antibody that binds to amino acids 1-27 by Western blot analysis. No fragment of the expected or larger size, which could result from alternative splicing, was detected. To exclude usage of an alternative start codon, an antibody against the C-terminal domain of PKP1 was used to confirm the complete absence of PKP1 protein (Fig. 10D). In addition, immunofluorescence staining of PKP1 confirmed the complete absence of PKP1 in PKP1-KO mouse epidermis (Fig. 10E).

PKP1-KO mice reveal growth retardation and die postnatally

PKP1-null mice were born at the expected Mendelian ratio of approximately 25%. Macroscopic examination of newborn animals did not show any skin blistering. With the exception of absent whiskers, the skin of mutant mice appeared unaffected. However, during the following hours, PKP1-KO mice developed skin lesions without obvious mechanical trauma (Fig. 11A, detail). Surprisingly, during the first day PKP1-null mice died, with an average lifetime of approximately 12 hours. Additionally, PKP1-null mice showed significantly lower birth weight than WT mice (Fig. 11B). This observation suggests a role of PKP1 in growth control *in vivo*.

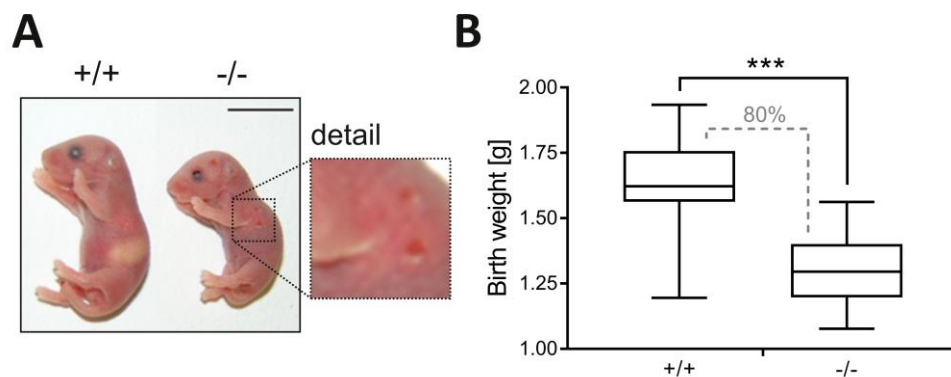


Fig. 11| PKP1-KO mice suffer from skin fragility and reduced birth weight.

(A) Depicted are representative images of *Pkp1*^{+/+} and *Pkp1*^{-/-} pups. Note that the PKP1-KO mouse shows wounds and fragile skin. Scale bar: 1 cm. (B) Measurement of birth weight of PKP1-KO mice (n=23) compared with WT littermates (n=18) depicted by boxplots. The whiskers indicate the minimum and maximum values. Statistical significance was determined by a two-tailed Student's *t*-test. ****P* ≤ 0.0005. (+/+), wildtype; (-/-), homozygous.

Desmosome formation and mechanical integrity are disturbed in PKP1-KO epidermis

PKP1 is predominantly expressed in the suprabasal layers of complex and stratified epithelia (Bass-Zubek et al., 2009, Hatzfeld, 2007, Neuber et al., 2010). Loss-of-function mutations in PKP1 result in EDSFS with defects in skin integrity, hair development, sweating, and inflammation (Lai-Cheong et al., 2007, McGrath et al., 1997, Tanaka et al., 2009).

Thus, to resolve the *in vivo* function of PKP1 in epithelial homeostasis, the skin of PKP1-KO versus WT mice was examined.

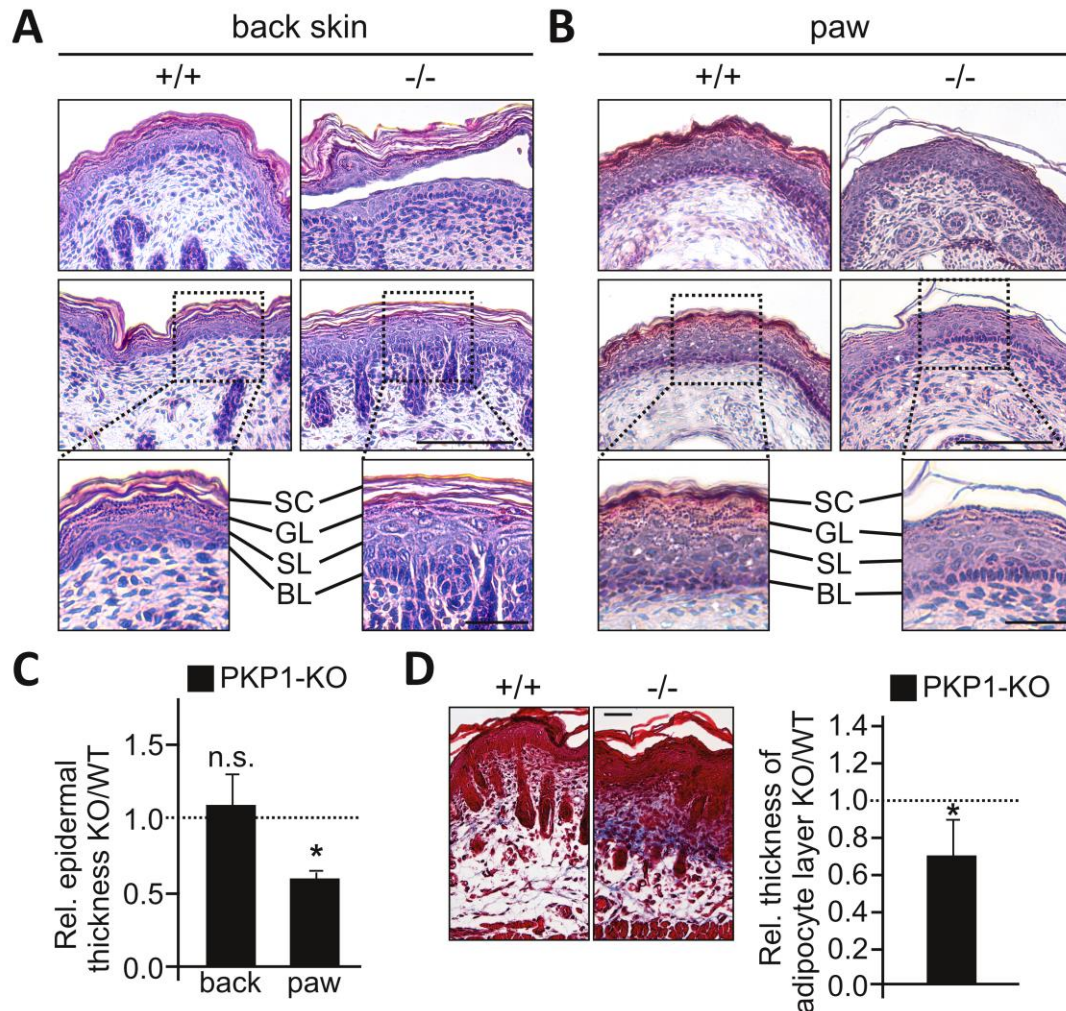


Fig. 12| PKP1-KO skin shows cell separation and a reduced adipocyte layer.

Paraffin sections of (A) dorsal and (B) paw skin from WT and PKP1-KO pups were stained with hematoxylin and eosin. Higher-magnification images illustrate the morphology of skin layers. Scale bar: 100 μ m; detail: 25 μ m. (C) Epidermal thickness of back and paw skin was determined using ImageJ by measuring the length from basement membrane to SC of 35 individual images. The diagram depicts the epidermal thickness relative to the thickness of WT epidermis (mean \pm SD, n=35 images of three independent mice). Statistical significance was determined by a two-tailed Student's *t*-test. * $P \leq 0.05$. n.s. = not significant. (D) Paraffin-embedded dorsal skin sections from WT and PKP1-KO mice were stained with Trichrome III stain to visualize collagenous connective tissue fibers (collagen in blue, muscle fibers in red, and nuclei in black/blue, adipose tissue remains white). Scale bar: 25 μ m. The diagram on the right depicts the thickness of subcutaneous adipocyte layer of PKP1-KO skin relative to WT (mean \pm SD, n=40 images of three independent mice). Statistical significance was determined by a two-tailed Student's *t*-test. * $P \leq 0.05$. BL, basal layer; GL, granular layer; KO/(-/-), knockout; n.s., not significant; Rel., relative; SC, *stratum corneum*; SL, spinous layer; WT/(+/+), wildtype.

PKP1-null mice epidermis exhibited all stages of terminal differentiation, including the flattened squames of the *stratum corneum* (Fig. 12A, B). Notably, widening of intercellular spaces was observed predominantly in the suprabasal layers, whereas epidermal adhesion in the basal layer and adhesion to the underlying basement membrane appeared normal. Cell separation started in the granular layer and this layer appeared considerably reduced in thickness in paw skin (Fig. 12B, detail). Complete detachment typically occurred between the granular and the spinous layer (Fig. 12A). The *stratum corneum* was often loose and flaky, with diminished cohesion between corneocyte layers and was reduced in paw skin. Whereas thickness of back skin was unaltered, paw skin was slightly thinner in PKP1-null mice (Fig. 12C). Interestingly, the subcutaneous adipocyte layer was considerably reduced (Fig. 12D), which may account for the reduced birth weight.

Because the *stratum corneum* appeared impaired, components of this layer - the corneocytes - were isolated and the morphology was assessed. No gross alterations were detected in the structure or stability of corneocytes (Fig. 13A), although these terminally differentiated keratinocytes were somewhat smaller in PKP1-KO mice compared to their littermates (Fig. 13B).

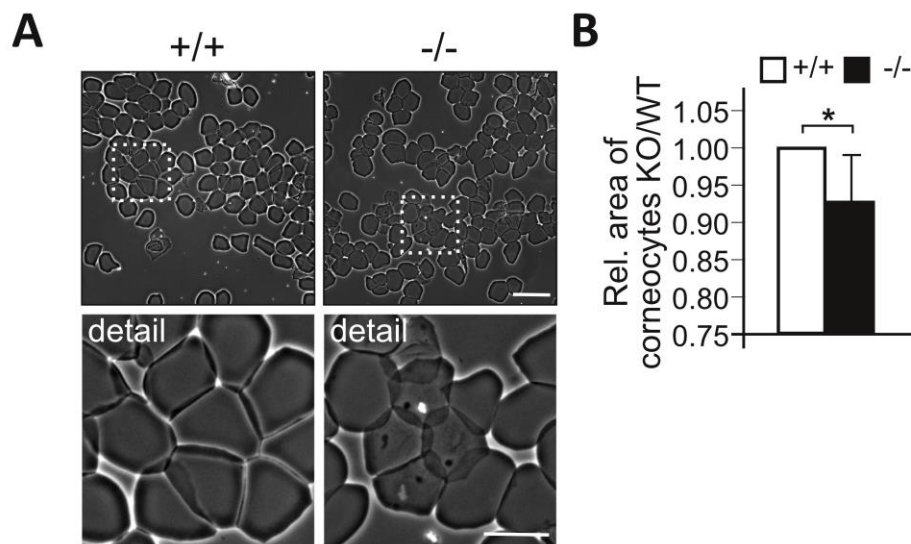


Fig. 13| Analysis of corneocytes in WT and PKP1-KO dorsal skin.

(A) Isolated corneocytes from WT and PKP1-KO skin were applied on glass slides and representative images are shown. Scale bar: 100 μm ; detail: 50 μm . (B) Quantification reveals a slightly smaller area of PKP1-KO corneocytes. The area of corneocytes was quantified using the MiToBo plugin for ImageJ (mean \pm SD, $n > 300$ corneocytes of three independent mice). Statistical significance was determined by a two-tailed Student's t -test. $*P \leq 0.05$. KO/(-/-), knockout; Rel., relative; WT/(+/+), wildtype.

Due to the observation, that PKP1 promotes cell proliferation (Wolf and Hatzfeld, 2010, Wolf et al., 2010), proliferation was examined in WT and PKP1-KO epidermis by the use of Ki-67, which labels the nucleus of cells in the active phases of the cell cycle [G_1 , S, G_2 , and M, (de Azambuja et al., 2007)]. In agreement with unaltered epidermal thickness of neonatal dorsal skin (Fig. 12C), no significant changes in proliferation rates were observed as indicated by Ki-67 staining (Fig. 14).

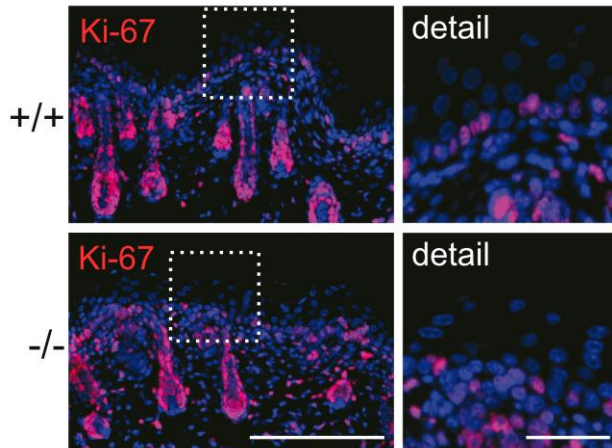


Fig. 14| Analysis of proliferation in WT and PKP1-KO dorsal skin.

Immunofluorescence microscopy of the proliferation marker Ki-67 on dorsal skin reveals unaltered proliferation in PKP1-KO skin compared to WT. Formaldehyde-fixed cryosections were labeled with Ki-67 (shown in red). Hoechst 33342 staining served as nuclear marker (shown in blue). To compare fluorescence intensities, all images were collected with equal hardware settings. Scale bar: 100 μm ; detail: 25 μm . (-/-), knockout; (+/+), wildtype.

Overexpression of PKP1 increased desmosome number and size in cultured cells (Hatzfeld et al., 2000, Kowalczyk et al., 1999), and the loss of PKP1 in EDSFS patients correlated with reduced desmosome number and size (McGrath et al., 1997, McGrath and Mellerio, 2010). To resolve the ultrastructure of desmosomes in PKP1-KO and WT mouse skin, electron microscopy was conducted. In general, desmosomes have a highly characteristic ultrastructure (remember Fig. 4C). The desmosomal plaque is composed of two dense structures with a less dense intervening region. Adjacent to the plasma membrane is the outer dense plaque (ODP), an extremely electron-dense structure, whereas at the inner edge is the inner dense plaque (IDP), which is less dense than the ODP (Al-Amoudi et al., 2011, Garrod and Kimura, 2008). The intercellular space of the desmosome also reveals a characteristic appearance including an electron-dense midline. Ultrastructural analysis revealed sparse and smaller desmosomes in PKP1-KO mice skin compared with WT mice (Fig. 15A). A quantitative assessment confirmed a significant reduction in desmosome number ($\sim 91\%$ reduction) and size ($\sim 44\%$

reduction) in the suprabasal layers (Fig. 15B). Moreover, the ultrastructure appeared altered, with a lack of the inner plaque structure. Nevertheless, keratin filaments remained anchored at the residual desmosomes (Fig. 15A).

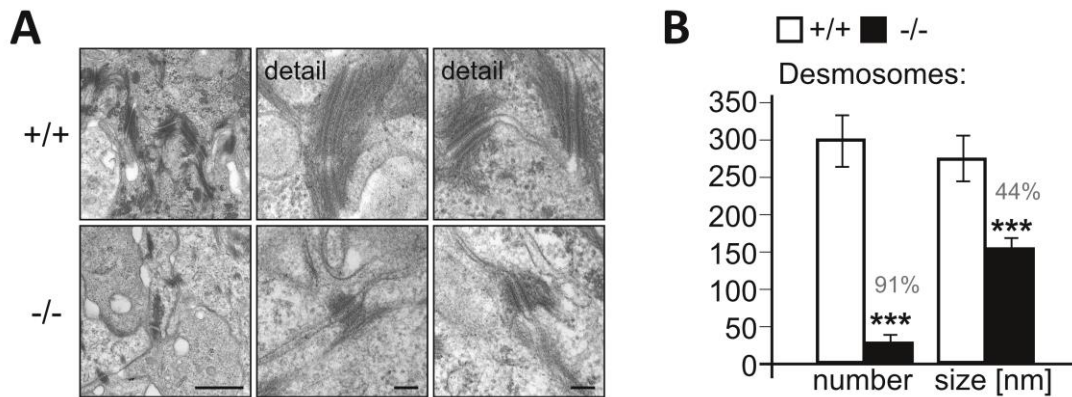


Fig. 15| Ultrastructure reveals sparse and smaller desmosomes in PKP1-null mice skin.

(A) Ultrastructural analysis of WT and PKP1-KO desmosomes. Scale bar: 500 nm; details: 100 nm. (B) The diagram depicts the number and size of desmosomes in WT and PKP1-KO dorsal skin. To quantify the number of desmosomes, 14 electron microscopy images were counted for desmosomes (mean \pm SD, n=14 images of three independent mice). To quantify the size of desmosomes, the desmosomal length was measured (mean \pm SD, n=50 desmosomes of three independent mice). All morphometric measurements were kindly done by Annkatrin Rother with the use of iTEM software from Olympus SIS. Statistical significance was determined by a two-tailed student's *t*-test. *** $P \leq 0.0005$. (-/-), knockout; (+/+), wildtype.

PKP1-KO mice suffer from a defect in the epidermal barrier

Given the reduced birth weight (Fig. 11B) and short life span of PKP1-KO mice, it raised the question, if water loss due to an impaired epidermal barrier could be responsible for the appearance. Weighting experiments revealed that PKP1 mutant mice lost around 8% more weight than WT mice during a period of 7 hours (Fig. 16A). However, water loss during time could be also caused by skin lesions in PKP1-null mice (Fig. 11A). To exclude this, transepidermal water loss (TEWL) was directly measured in nonlesional regions by estimating the flux density of evaporated water from the skin surface (Gardien et al., 2016). This analysis confirmed an approximately 3-fold increase of water loss in the PKP1-KO mice compared with WT mice (Fig. 16B), in agreement with the weight measurements. Because TJs are considered to contribute to the inside-out liquid barrier in the epidermis (Matsui and Amagai, 2015), the expression and localization of TJ components was examined next (Fig. 16C, D). A slight increase in protein expression of TJs was observed. Moreover, several TJ proteins showed altered localization with discontinuous (ZO-1), diffuse (OCLN), or extended (CLDN-1) distribution, further supporting a role of PKP1 in the development of the epidermal barrier.

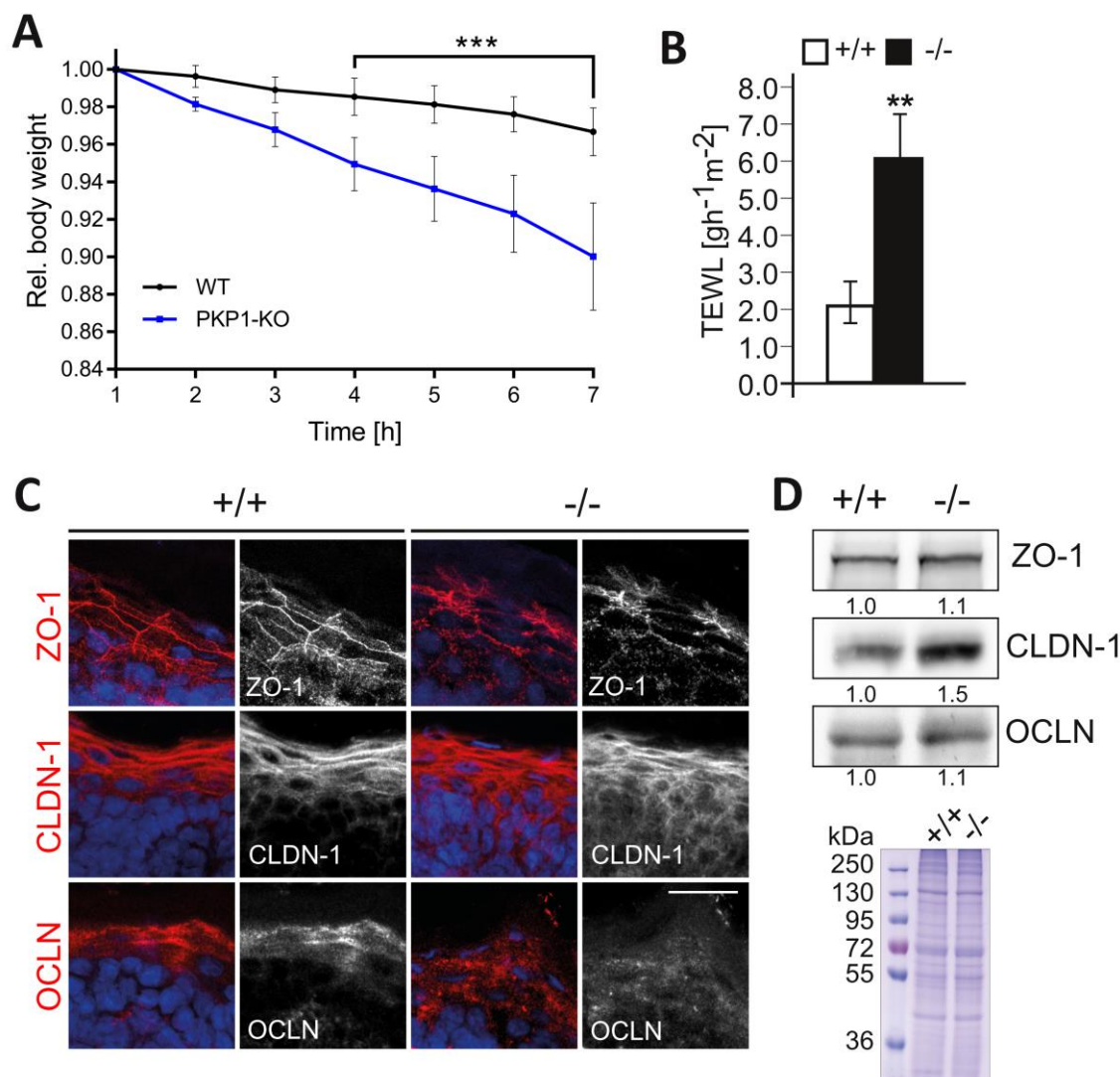


Fig. 16| PKP1-KO mice reveal a defective epidermal barrier.

(A) Weight time-course analysis of newborn WT and PKP1-KO mice (mean \pm SD, $n=8$ WT & $n=5$ KO mice). Statistical significance was determined by a 2-way ANOVA. $***P \leq 0.0005$. (B) The graph depicts the transepidermal water loss (TEWL) measurements of WT and PKP1-KO mice (mean \pm SD, $n=3$ WT & $n=5$ KO mice). Statistical significance was determined by a two-tailed Student's t -test. $**P \leq 0.005$. (C) Immunofluorescence microscopy analysis of newborn WT and PKP1-KO skin stained for TJs proteins (in red) as indicated. Hoechst 33342 staining served as nuclear marker (in blue). Depicted are representative confocal images of maximum intensity projections of at least 45 optical sections. To compare fluorescence intensities, all images were collected with equal hardware settings. Scale bar: 25 μ m. (D) Western blot analysis from total skin lysates ($n=3$ pooled WT and PKP1-KO mice) showing expression levels of TJs proteins. Relative expression levels normalized to WT are given below the lanes. A Coomassie-stained gel run in parallel shows equal loading (below). CLDN, claudin; KO/(-/-), knockout; OCLN, occludin; Rel., relative; TEWL, transepidermal water loss; WT/(+/+), wildtype; ZO, zonula occludens.

To assess the epidermal barrier function more directly, different dye penetration assays have been developed to determine a potential defect in the *stratum corneum* or TJ barrier [dye penetration assays are reviewed in (Schmitz et al., 2015), Fig. 17A].

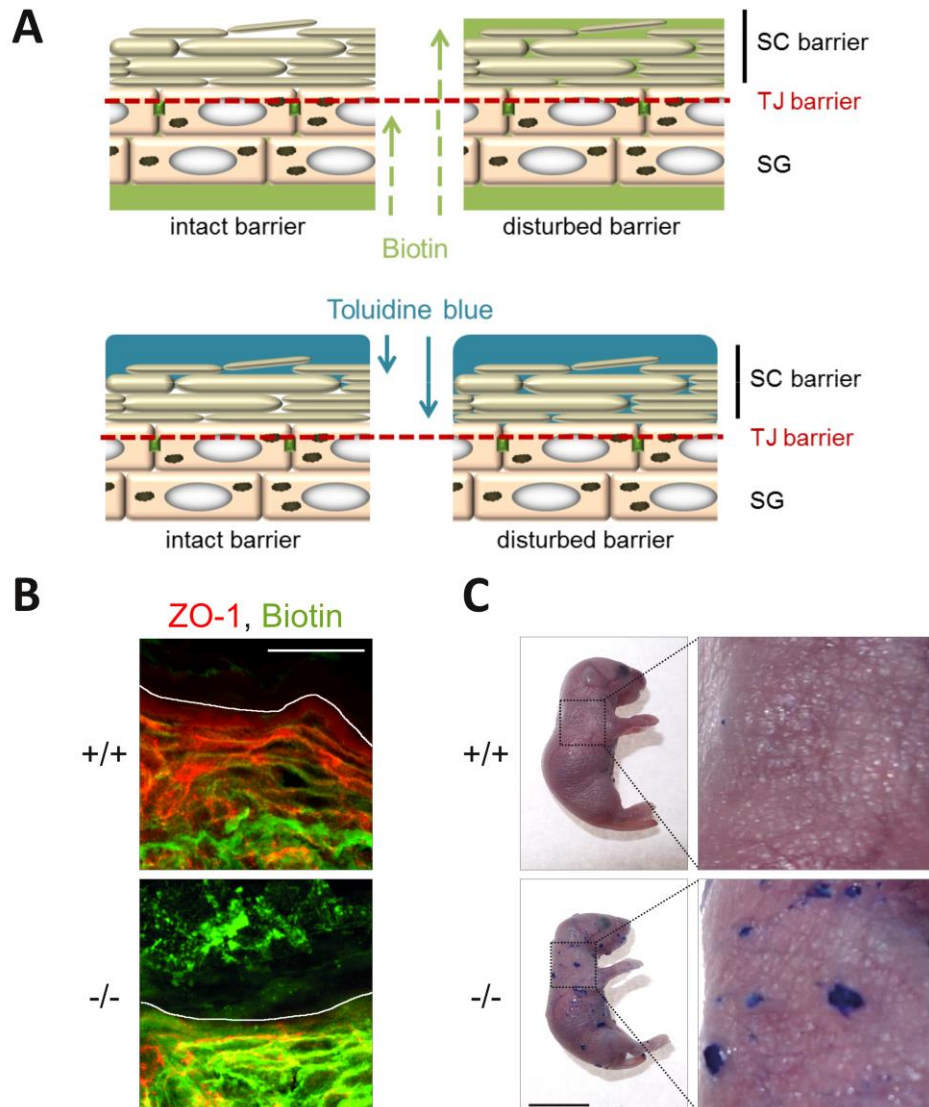


Fig. 17| The inside-out liquid barrier is impaired in the epidermis of PKP1-KO mice.

(A) Schematic representation of biotin diffusion assay (inside-out barrier, above) and toluidine blue penetration assay (outside-in barrier, below) in healthy and disturbed skin barrier modified after (Koch et al., 2000). In intact skin, the diffusion of subcutaneously injected biotin (in green) is restricted by TJs of the *stratum granulosum* (SG). Disturbed epidermal TJ function leads to penetration of biotin through the TJ layer. A functional *stratum corneum* (SC) barrier blocks the diffusion of toluidine blue through the epidermis. Toluidine blue penetrance into the epidermis uncovers a skin barrier dysfunction by disturbed SC barrier. (B) Inside-out permeability assay of WT and PKP1-KO mice subcutaneously injected with biotin. Skin cryosections were stained with streptavidin to examine the penetration of biotin (in green) and counterstained with ZO-1 (in red) to mark TJs. White lines mark the upper end of TJs. Scale bar: 25 μ m. (C) A toluidine blue penetration assay of newborn WT and PKP1-KO mice revealed a properly developed outside-in barrier. Scale bar: 1 cm. SC, *stratum corneum*; SG, *stratum granulosum*; TJ, tight junction; ZO, zonula occludens; (+/+), wildtype; (-/-), knockout.

The functionality of the TJ barrier can be tested using tracer molecules, which cannot pass a properly functioning TJ barrier. Therefore, EZ-link sulfo-NHS-LC-biotin was injected into the dermis and its diffusion through the granular layer of the epidermis was analyzed by immunofluorescence staining (Fig. 17B). The diffusion of subcutaneously injected biotin was restricted by the TJs in PKP1-WT mice as shown by ZO-1 labeling (white line in Fig. 17B), whereas biotin penetrated through the TJ barrier in the PKP1-null mice. Taken together, these data show a defect in the inside-out TJ barrier leading to dehydration and probably contributing to lethality. In contrast, the outside-in barrier provided by the *stratum corneum* appeared properly developed as indicated by a toluidine blue penetration assay (Hardman et al., 1998). Only at skin lesions blue staining was observed, whereas the barrier was intact in non-lesional regions of PKP1-null mice (Fig. 17C).

Desmosomal proteins are compensatorily upregulated in PKP1-KO skin

Given the aberrant number and ultrastructure of desmosomes in the PKP1-null epidermis (Fig. 15), desmosomal proteins were analyzed. To examine the localization and expression of desmosomal proteins in WT and PKP1-KO mice, immunofluorescence staining on skin cryosections as well as Western blot analyses of total protein extracts from WT and PKP1-KO mouse skin was performed. Despite a strong reduction in desmosomes (Fig. 15B), most desmosomal proteins, including PKP3, were expressed at elevated levels in PKP1-null skin, although the extent of upregulation varied between individual animals (Fig. 18B, C). Additionally, PKP3 localization at cell borders was more prominent (Fig. 18A). In contrast, DSP was partially displaced from the plasma membrane showing an increased cytoplasmic localization. The localization of PG was not affected, whereas DSG1/2 revealed a slightly extended localization towards basal layers in PKP1 mutant skin (Fig. 18A). Both proteins, PG and DSG1/2 show a not significant upregulation (Fig. 18B, C), probably due to high variance between individual mice. However, only DSC2 was consistently reduced in PKP1-KO skin (Fig. 18). PKP2 was not detected, either in WT or in PKP1-null skin (Fig. 18D). These data suggest, PKP1 regulates the expression and localization of desmosomal proteins. Interestingly, the observed compensatory increased expression of PKP3 is not sufficient to fully recover for the loss of PKP1.

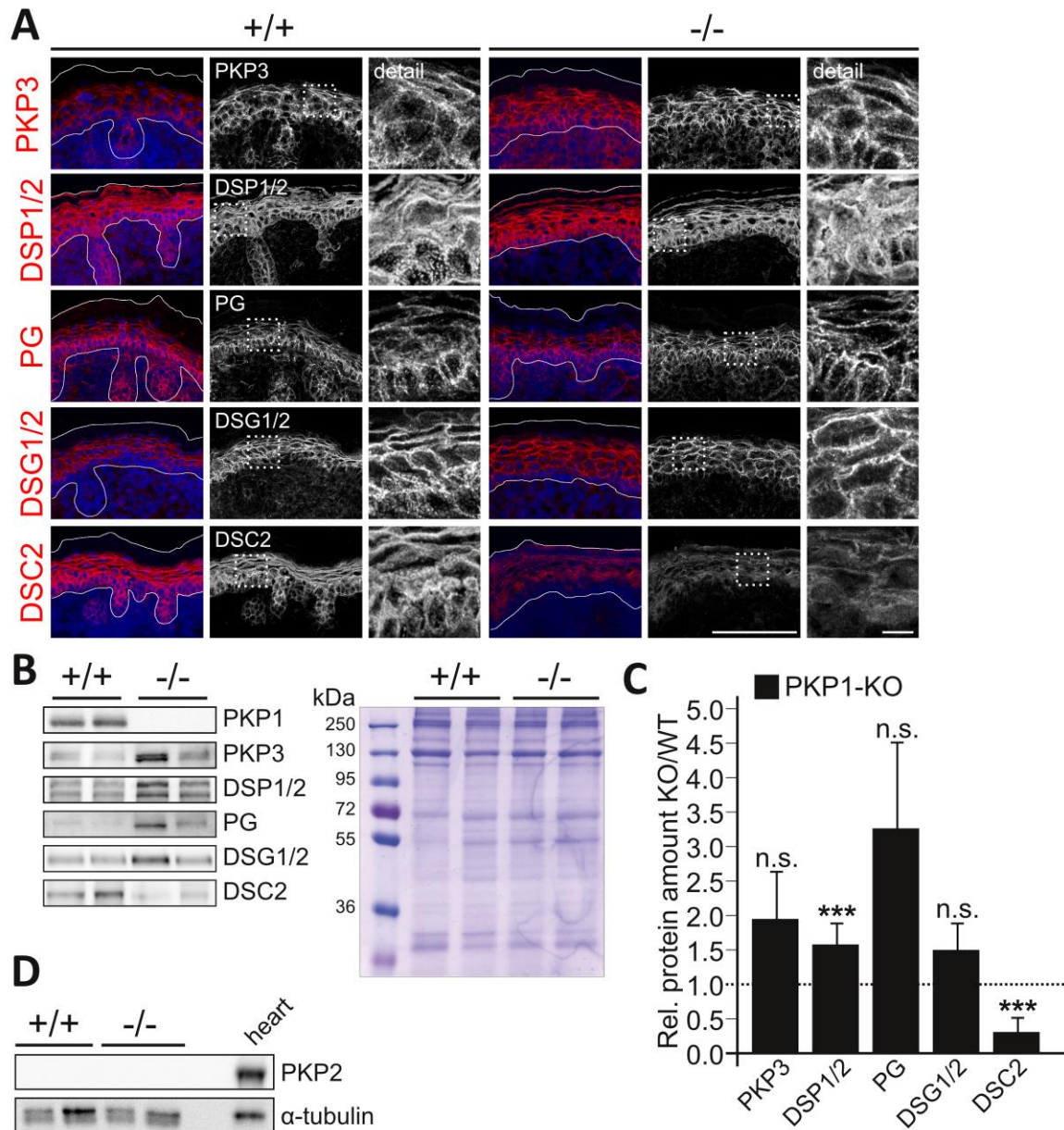


Fig. 18| PKP1 is essential for the localization of desmosomal proteins.

(A) Immunofluorescence microscopy analysis of WT and PKP1-KO skin cryosections. Depicted are confocal images of maximum intensity projections of at least 45 optical sections. To compare fluorescence intensities, all images were collected with equal hardware settings. The left column shows desmosomal proteins in red and DNA (Hoechst 33342 staining) in blue, the second column shows the proteins alone. A detail is depicted in the third column. White lines mark the SC and basement membrane. Scale bar: 100 μ m, detail: 10 μ m. (B) Total proteins were isolated from WT and PKP1-KO mice skin and depicted desmosomal proteins were analyzed by Western blot. Equal loading was assessed by Coomassie staining. (C) Western blot based quantification of desmosomal protein expression in PKP1-KO skin relative to WT (mean \pm SD, n=3-11 mice). Statistical significance was determined by a two-tailed Student's *t*-test. *** $P \leq 0.0005$, n.s. = not significant. (D) Western blot analysis of PKP2 expression in WT & PKP1-KO skin. Mouse heart is shown as positive control for PKP2. α -tubulin was used as loading control. DSC, desmocollin; DSG, desmoglein; DSP, desmoplakin; KO/(-/-), knockout; PG, plakoglobin; PKP, plakophilin; Rel., relative; SC, *stratum corneum*; WT/(+/+), wildtype.

Keratin expression is increased in the PKP1-KO skin

Given the importance of desmosomes to epidermal keratin organization [(Bornslaeger et al., 1996, Kröger et al., 2013, Loschke et al., 2016), remember chapter 2.1.], the localization and expression of epidermal keratins was examined by immunofluorescence microscopy and Western blot analysis. Keratins 5 and 14 were used as marker for the basal, proliferative compartment of the epidermis.

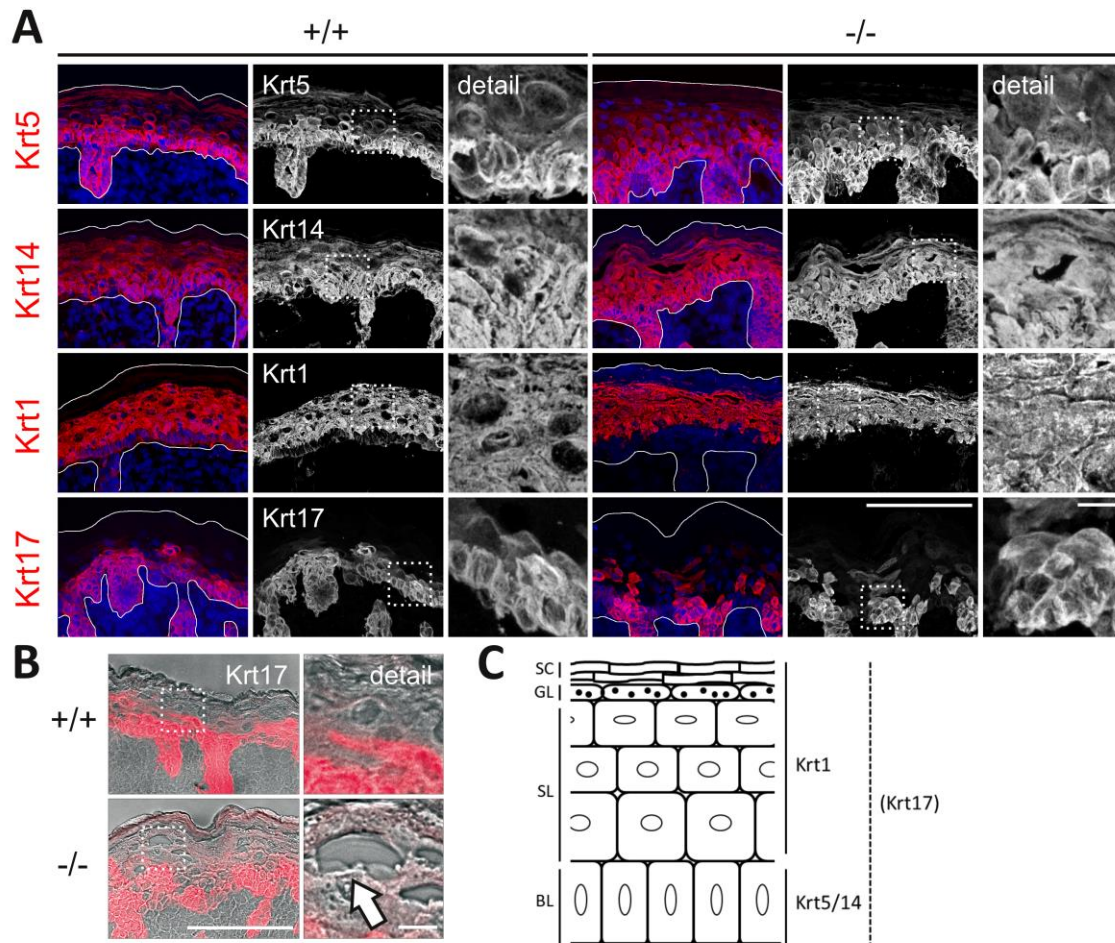


Fig. 19| Keratin localization in WT and PKP1-KO epidermis.

(A) Cryosections of dorsal skin from WT and PKP1-KO mice were analyzed by immunofluorescence microscopy. Depicted are confocal images of maximum intensity projections of at least 45 optical sections. To compare fluorescence intensities, all images were collected with equal hardware settings. Hoechst 33342 staining served as nuclear marker (blue). Keratins are shown in red. White lines mark the SC and basement membrane. Scale bar: 100 μ m, detail: 10 μ m. (B) Overlay of Krt17 immunofluorescence (red) and phase contrast images. White arrows indicate microlesions in the PKP1-KO skin. Scale bar: 100 μ m, detail: 10 μ m. (C) Scheme depicting the expression of epidermal keratins used in this study. BL, basal layer; GL, granular layer; Krt, keratin; SC, stratum corneum; SL, spinous layer; (+/+), wildtype; (-/-), knockout.

Keratin 1 staining served as marker for the upper layers of the epidermis. Keratin 17 is expressed in hair follicles (McGowan and Coulombe, 1998) and also transiently expressed during enhanced proliferation (Depianto et al., 2010) and migration of keratinocytes such as in cases of wounding or tissue regeneration (Fig. 19C). Keratins 5 and 14 were expressed in the basal layers in WT as well as mutant epidermis, although their expression was somewhat more extended towards suprabasal layers in mutant skin. Keratin 1 was restricted to the suprabasal layers (Fig. 19A). Keratin 17 was increased in PKP1-KO epidermis in the basal and the suprabasal compartments (Fig. 19A). However, no direct correlation between microlesions and keratin 17 upregulation was detected (Fig. 19B). Total expression of all keratins tested was increased (Fig. 20). Although slightly altered, this again suggests that the general process of epidermal differentiation is not grossly disturbed in the PKP1-null epidermis.

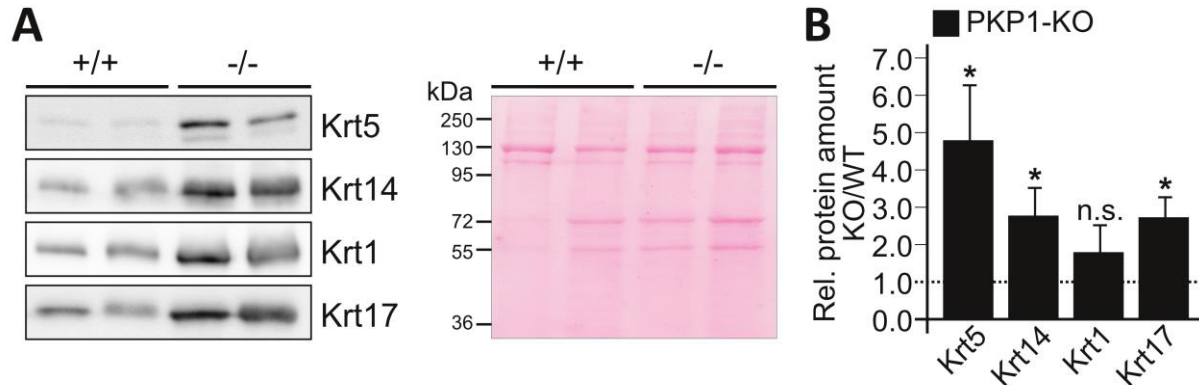


Fig. 20| Analysis of keratin expression in WT and PKP1-KO epidermis.

(A) Total proteins were isolated from WT and PKP1-KO mice skin and depicted keratins were analyzed by Western blot. Equal loading was assessed by Ponceau staining (right). (B) Western blot based quantification of keratin expression in PKP1-KO skin relative to WT (mean \pm SD, n=3-4 mice). Statistical significance was determined by a two-tailed Student's *t*-test. * $P \leq 0.05$, n.s. = not significant. Krt, keratin; (-/-)/KO, knockout; Rel., relative; (+/+)/WT, wildtype.

Differentiation is mildly altered in PKP1-KO skin

In addition to keratins, the expression and distribution of differentiation markers was analyzed to unveil defects in differentiation that might be caused by PKP1 deficiency. In agreement with the minor changes in keratin expression, staining with antibodies against involucrin, loricrin and filaggrin (Fig. 21E) revealed that epidermal-specific gene expression was retained, thus indicating that the overall differentiation process of the epidermis was not severely affected.

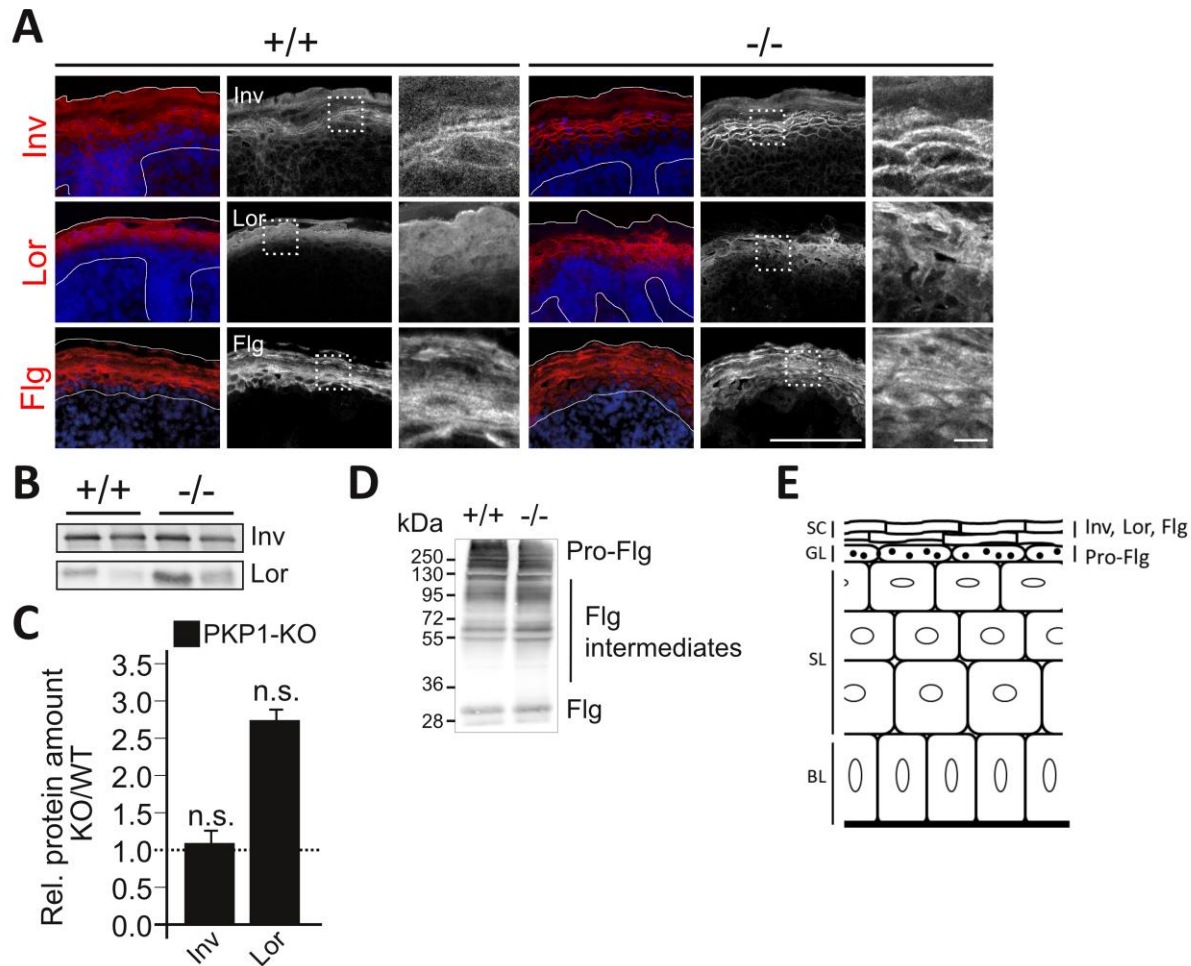


Fig. 21| Differentiation is mildly altered in the PKP1-null epidermis.

(A) Cryosections of dorsal skin from newborn WT and PKP1-KO mice were analyzed by immunofluorescence microscopy. Depicted are confocal images of maximum intensity projections of at least 45 optical sections. To compare fluorescence intensities, all images were collected with equal hardware settings. The left column shows epidermal differentiation marker in red and DNA (Hoechst 33342 staining) in blue, the second column shows the proteins alone. A detail is depicted in the third column. White lines mark the SC and basement membrane. Scale bar: 100 μ m, detail: 10 μ m. (B) Total proteins were isolated from WT and PKP1-KO mice skin and depicted proteins were analyzed by Western blot. Equal loading was assessed by Coomassie staining (not shown). (C) Western blot based quantification of protein expression in PKP1-KO skin relative to WT (mean \pm SD, n=3-7 mice). Statistical significance was determined by a two-tailed Student's *t*-test. n.s. = not significant. (D) Western blot analysis of filaggrin (Flg) and its processing products in WT and PKP1-KO skin. (E) Scheme depicting the expression of epidermal differentiation marker used in this study. BL, basal layer; Flg, filaggrin; GL, granular layer; Inv, involucrin; KO/(-/-), knockout; Lor, loricrin; Rel., relative; SC, *stratum corneum*; SL, spinous layer; WT/(+/+), wildtype.

The expression level of involucrin was similar in WT and PKP1 mutant mice (Fig. 21B, C), but its membrane association was increased in the PKP1-KO epidermis (Fig. 21A). In contrast, total expression of loricrin was upregulated in some but not all newborn mutant mice (Fig. 21B, C) with essentially unaltered localization in the suprabasal layers of the epidermis (Fig. 21A).

Filaggrin localization appeared extended (Fig. 21A), but Western blot analysis revealed a similar pro-filaggrin to filaggrin processing pattern in WT and PKP1-KO epidermis (Fig. 21D). Taken together, these data indicate that the overall differentiation in the PKP1-null epidermis was not considerably perturbed.

The localization of AJs is not affected in PKP1-null skin

Since desmosomes and AJs are interdependent, the localization and expression of AJ proteins was analyzed. Whereas E- and P-cadherin localization and expression levels were unaltered, p120-catenin and β -catenin were increased (Fig. 22 and 23), but retained their localization at AJs (Fig. 22).

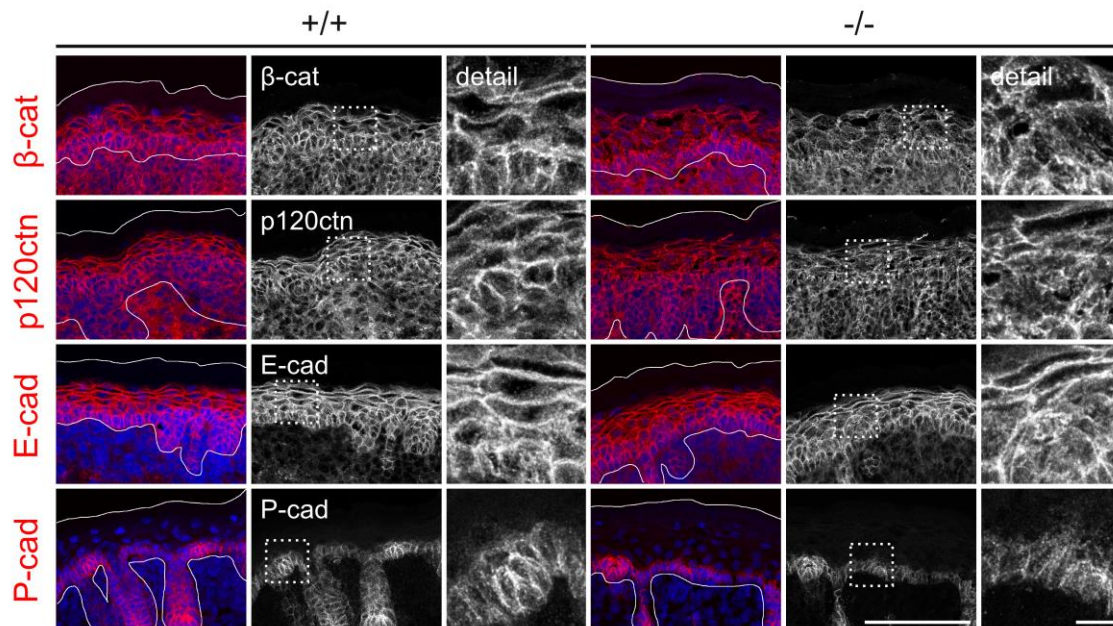


Fig. 22| Localization of AJ proteins in WT and PKP1-KO epidermis.

Cryosections of dorsal skin from newborn WT and PKP1-KO mice were analyzed by immunofluorescence microscopy. Depicted are confocal images of maximum intensity projections of at least 45 optical sections. To compare fluorescence intensities, all images were collected with equal hardware settings. The left column shows AJ proteins in red and DNA (Hoechst 33342 staining) in blue, the second column shows the proteins alone. A detail is depicted in the third column. White lines mark the SC and basement membrane. Scale bar: 100 μ m, detail: 10 μ m. cad, cadherin; cat, catenin; p120ctn, p120-catenin; SC, *stratum corneum*; (+/+), wildtype; (-/-), knockout.

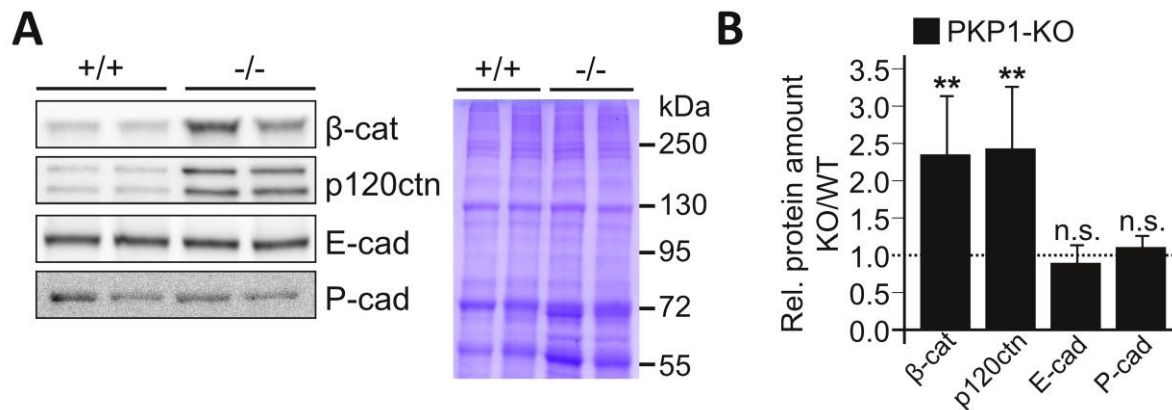


Fig. 23| Expression of AJ proteins in WT and PKP1-KO epidermis.

(A) Total proteins were isolated from WT and PKP1-KO mice skin and depicted proteins were analyzed by Western blot. Equal loading was assessed by Coomassie staining (right). (B) Western blot based quantification of AJs expression in PKP1-KO skin relative to WT (mean \pm SD, $n=3-11$ mice). Statistical significance was determined by a two-tailed Student's *t*-test. ** $P \leq 0.005$, n.s. = not significant. cad, cadherin; cat, catenin; KO/(-/-), knockout; p120ctn, p120-catenin; Rel., relative; WT/(+/+), wildtype.

PKP1-KO keratinocytes recapitulate the effects observed in the epidermis

To analyze the underlying mechanisms, how PKP1 is involved in desmosome adhesion and TJ function, keratinocytes were isolated from newborn WT and PKP1-KO pups [described in (Kashiwagi and Huh, 2005)] and cell lines were established. Upon isolation of epidermal keratinocytes, the cells were long-term cultured on collagen-coated dishes in growth factor-containing medium. With several rounds of subculture, the keratinocytes adapted to culture conditions, maintained an epithelial morphology and were apparently immortal. The immortalized keratinocytes retained the ability to differentiate with increased calcium concentration by switching the low calcium medium (LCM, 50 μM Ca^{2+}) to high calcium medium (HCM, 1.2 mM Ca^{2+}). Before using these cell lines, keratinocytes were characterized with respect to keratin 15 expression, since several authors have described keratin 15 as a putative epidermal stem cell marker primarily expressed in stem cells residing in the bulge region of hair follicles [(Bose et al., 2013), not shown]. The mesenchymal marker vimentin was analyzed to exclude putative contaminations with dermal fibroblasts or melanocytes. Based on keratin 15 and vimentin (low), equal keratinocytes were used for further analyses.

Western blot analysis confirmed the complete absence of PKP1 and a nonsignificant upregulation of PKP3 (Fig. 24A, B), whereas PKP2 was not detected (not shown). Although the amount of DSP remained unchanged, DSG1/2, DSC2, and PG were reduced (Fig. 24A, B).

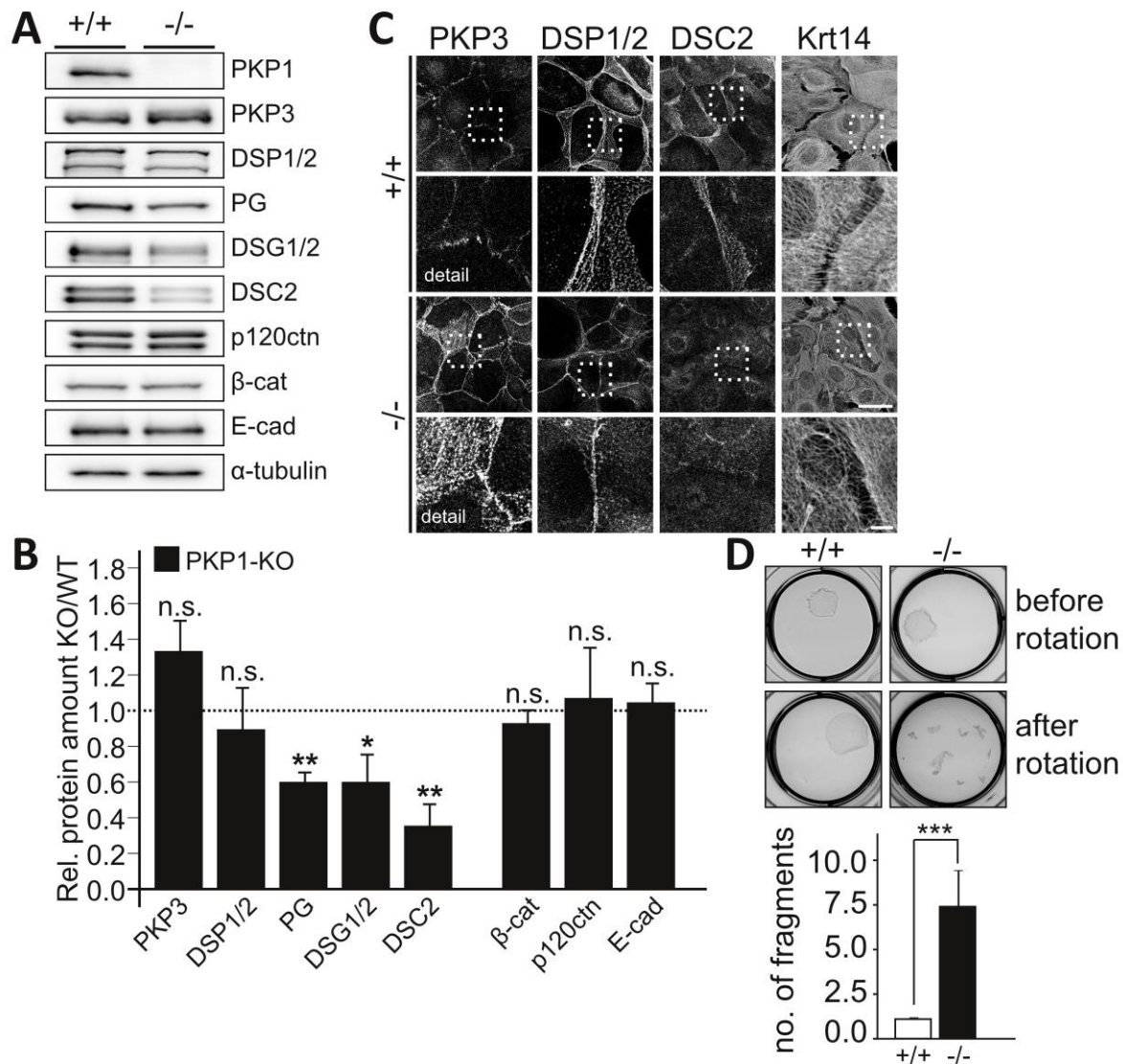


Fig. 24| PKP1-KO keratinocytes recapitulate the defects observed in PKP1-KO epidermis.

(A) Representative Western blots of WT and PKP1-KO mouse keratinocytes grown for 24 hours in HCM. α -tubulin was used as loading control. (B) Western blot based quantification of indicated protein expression in PKP1-KO keratinocytes relative to WT and normalized to α -tubulin (mean \pm SD, $n=3$). Statistical significance was determined by a two-tailed Student's *t*-test. * $P\leq 0.05$, ** $P\leq 0.005$, n.s. = not significant. (C) WT and PKP1-KO keratinocytes grown for 24 hours in HCM were immunostained for the indicated proteins. Depicted are confocal images of single optical sections. To compare fluorescence intensities, all images were collected with equal hardware settings. Scale bar: 50 μ m, detail: 10 μ m. (D) The strength of intercellular cohesion of WT versus PKP1-KO keratinocytes was assessed by disperse assays. Representative images show the integrity of the detached cell monolayer before and after application of mechanical stress (rotation). Diagram depicts the quantification of counted fragments after rotation (below, mean \pm SD, $n=5$). Statistical significance was determined by a two-tailed Student's *t*-test. *** $P\leq 0.0005$. cad, cadherin; cat, catenin; DSC, desmocollin; DSG, desmoglein; DSP, desmoplakin; HCM, high calcium medium; KO/(-/-), knockout; Krt, keratin; no., number; p120ctn, p120-catenin; PG, plakoglobin; PKP, plakophilin; Rel., relative; WT/(+/+), wildtype.

Immunofluorescence staining of desmosomal proteins and intermediate filaments revealed a partially displaced localization of DSP1/2 and DSC2 from the plasma membrane (Fig. 24C). Furthermore, the preferential accumulation of PKP3 at tricellular contacts sites was abolished in PKP1-KO keratinocytes. These cells revealed an increased lateral localization of PKP3 (Fig. 24C). In further support, this implies that the upregulation of desmosomal proteins as observed in the epidermis might be indeed a compensatory response and depends on the context. Keratin 14 staining showed that keratin filaments were anchored at the plasma membrane in the PKP1-KO cells. However, membrane anchorage appears considerably less abundant and filament bundling was reduced (Fig. 24C). In contrast to desmosomal proteins, the expression of AJ proteins such as E-cadherin, β -catenin, and p120ctn was unchanged (Fig. 24, B).

PKP1-KO mice showed widening of intercellular spaces in suprabasal layers (Fig. 12A, B), pointing to a decreased intercellular cohesion of keratinocytes. To further validate and directly address the role of PKP1 in intercellular cohesion, dispase was used to detach confluent keratinocyte monolayers from the cell dish. After mild rotational stress, PKP1-null epithelial sheets immediately disintegrated into small fragments, whereas the epithelial sheet of WT keratinocytes remained intact under the same conditions (Fig. 24D). Thus, stable intercellular cohesion of keratinocytes *in vitro* critically depends on PKP1. This supports the hypothesis that epidermal PKP1 is crucial for the maintenance of desmosomal adhesion *in vivo*.

The biotin penetration assay (Fig. 17B) pointed to a defect in the TJ barrier of the PKP1-null epidermis. To exclude an indirect effect caused by microlesions in the area of injection and to analyze the molecular requirement for PKP1 in *de novo* TJ formation, a system was required, where intercellular junction formation can be controlled. Therefore, the TJ barrier was characterized *in vitro* in PKP1-KO keratinocytes in comparison with WT cells. TJ proteins ZO-1 and CLDN were expressed at similar levels in both cell lines at 24 hours after high calcium addition, whereas OCLN was significantly reduced (Fig. 25A, B).

To test whether PKP1 is required for proper incorporation of TJ components, immunofluorescence staining was performed using WT and PKP1-null keratinocytes differentiated for 2, 6, and 24 hours in HCM. Interestingly, membrane recruitment of all TJ proteins was strongly delayed and remained irregular and partially discontinuous at 24 hours after Ca^{2+} addition (Fig. 25C). To directly test TJ function *in vitro*, the capacity of PKP1-null keratinocytes to form a TJ barrier was assessed by transepithelial electrical resistance (TER) measurements. In this

assay para-cellular diffusion of ions is measured, which is shown as electrical resistance and corresponds to the barrier properties of the TJ.

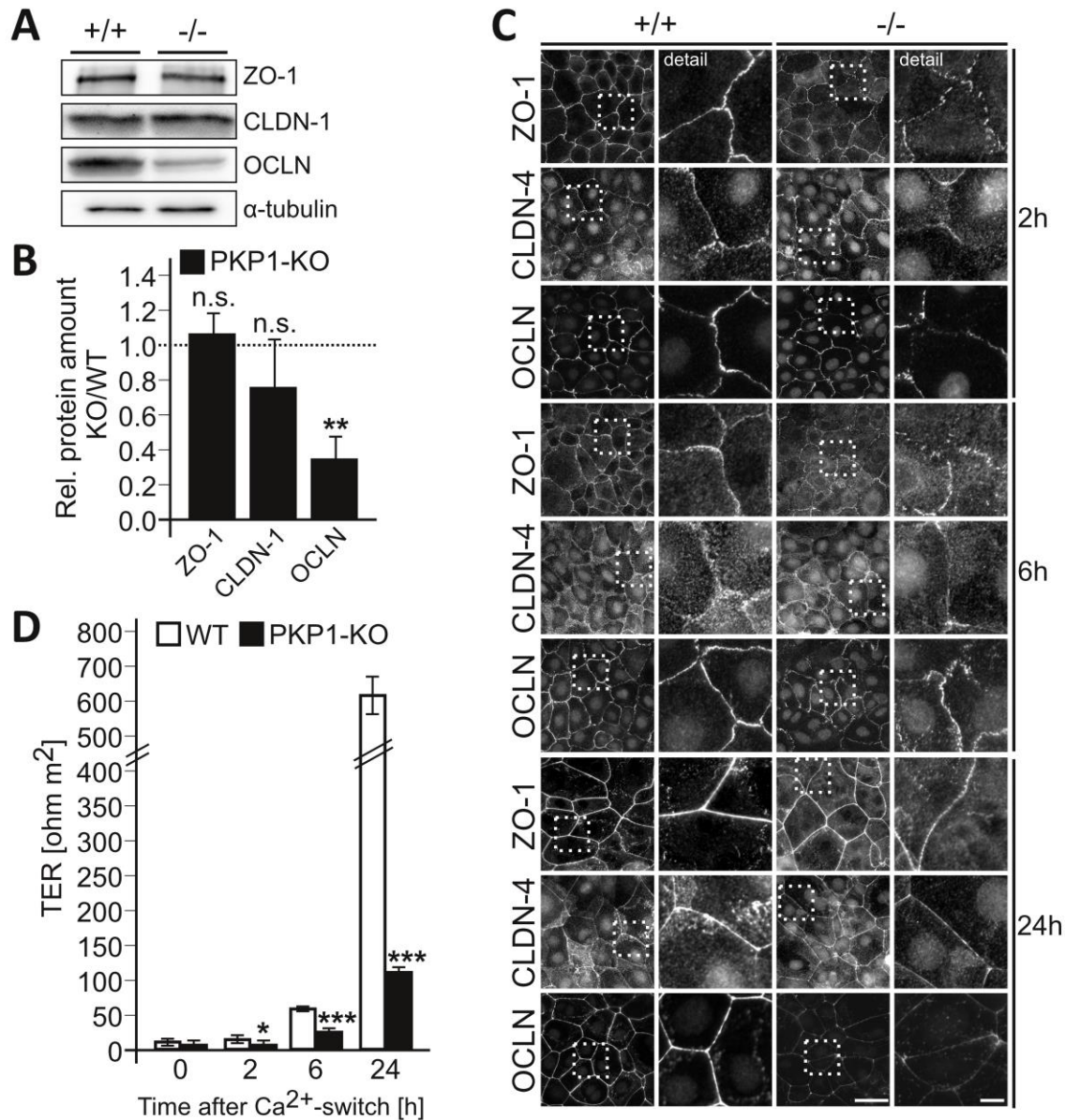


Fig. 25I TJ function and recruitment to the plasma membrane is disturbed in PKP1 deficient keratinocytes.

(A) Representative Western blot images of TJ proteins from WT and PKP1-KO keratinocytes grown for 24 hours in HCM. α -tubulin was used as loading control. (B) Western blot based quantification of TJ proteins in PKP1-KO keratinocytes relative to WT and normalized to α -tubulin (mean \pm SD, n=3). Statistical significance was determined by a two-tailed Student's *t*-test. ** $P \leq 0.005$, n.s. = not significant. (C) Transepithelial electrical resistance (TER) measurements of WT versus PKP1-KO keratinocytes at the indicated time points after Ca²⁺-switch (mean \pm SD, n=3). Statistical significance was determined by a two-tailed Student's *t*-test. * $P \leq 0.05$, *** $P \leq 0.0005$. (D) WT and PKP1-KO keratinocytes were immunostained for the indicated TJ proteins at 2, 6 and 24 hours after Ca²⁺-switch. Scale bar: 50 μ m, detail: 10 μ m. CLDN, claudin; HCM, high calcium medium; KO/(-/-), knockout; OCLN, occludin; Rel., relative; TER, transepithelial electrical resistant; WT/(+/+), wildtype; ZO, zonula occludens.

Therefore, WT and PKP1-KO keratinocytes were grown to confluency on filter inserts. Keratinocytes establish no measureable TER in LCM indicating that keratinocytes without intercellular contacts are unable to form electrical resistance. When intercellular junction formation was induced by culturing the cells in HCM, WT keratinocytes established a TER over the time period of 24 hours, whereas PKP1 deficient keratinocytes showed a strong delay and reduced efficiency in establishing TER (Fig. 25D).

The reduced birth weight of PKP1-KO mice (Fig. 11B) raised the question, if PKP1 controls cell growth in a keratinocyte-intrinsic manner. Cell counts of WT compared with PKP1-KO keratinocytes revealed a reduced proliferation of KO cells (Fig. 26). To confirm PKP1-dependence of this phenotype, two additional cell lines, either re-expressing human PKP1-GFP or cells expressing a GFP construct as control, were generated by lentiviral transduction (provided by Dr. René Keil). Expression of PKP1-GFP in PKP1-null keratinocytes rescued proliferation compared with GFP-expressing cells (Fig. 26), verifying that PKP1 promotes cell proliferation.

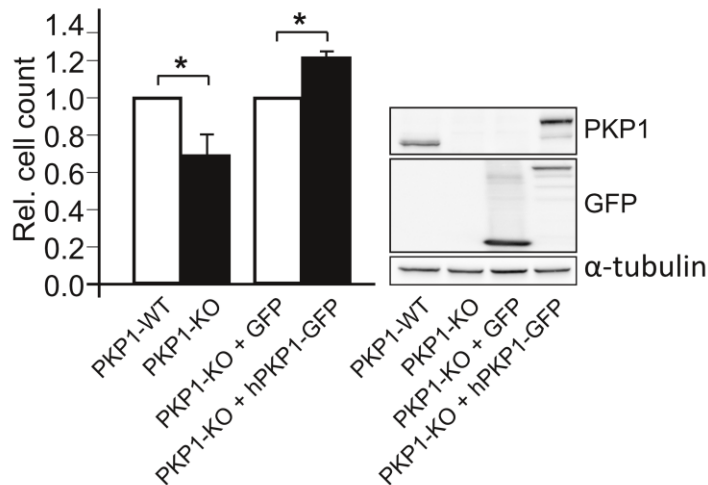


Fig. 26| PKP1 controls cell growth in a keratinocyte-intrinsic manner.

Analysis of cell counts of WT versus PKP1-KO keratinocytes and rescue cell lines PKP1-KO + GFP versus PKP1-KO + hPKP1-GFP performed by Dr. René Keil (mean \pm SD, n=3). Statistical significance was determined by a Student's *t*-test. * $P \leq 0.05$. Expression of hPKP1-GFP and GFP was validated by Western blotting with anti-PKP1 antibody (against C-terminus) and anti-GFP antibody. GFP, green fluorescent protein; KO, knockout; PKP, plakophilin; Rel., relative; WT, wildtype.

In summary of this chapter, PKP1-null mice were generated and analyzed to address the function of this protein *in vivo*. The homozygous mutant mice died postnatally and showed fragile skin with lesions strongly resembling the phenotype observed in human patients with EDSFS (Table 21). Desmosome number and size were significantly decreased, despite the up-

regulation of most desmosomal proteins. Interestingly, PKP1-null mice showed an impaired inside-out barrier caused by disturbed TJ function. Furthermore PKP1-KO mice revealed a reduced birth weight. Taken together, this study identifies PKP1 as a protein essential for the integrity of the epidermis by regulating desmosomal adhesion, TJ function, and growth control.

3.2. Insulin signaling via Akt2 influences PKP1's subcellular localization and function

Desmosomes, AJ, and TJ are sites of intercellular anchoring and signaling, which comprise a network of proteins and associated molecules that contribute to the maintenance and integrity of functional cell-cell cohesion (chapter 2.1.). The molecular mechanisms that underlie cell-cell connections are precisely controlled. Dysregulation of cellular adhesion plays a key role in the process of cellular transformation and metastasis (Morris et al., 2008). How desmosomal proteins contribute to malignant transformation and carcinogenesis is poorly understood. The desmosomal plaque protein PKP1 can increase intercellular adhesion by recruiting desmosomal proteins to the plasma membrane (Hatzfeld et al., 2000, Sobolik-Delmaire et al., 2006). However, the protein can stimulate proliferation by enhancing translation rates as well (Wolf and Hatzfeld, 2010, Wolf et al., 2010). Thus, PKP1 combines a function in strengthening desmosomal adhesion with a complementary role in stimulating translation and thereby promoting tumorigenesis. Therefore, it is of great interest and the subject of the following chapter to examine how the equilibrium between these two distinct roles of PKP1 is regulated.

As described in chapter 2.2., phosphorylation of proteins is the most prevalent PTM (Prabakaran et al., 2012) and PKP1 contains numerous putative phosphorylation sites highly clustered in the N-terminal head domain (Hatzfeld et al., 2014). Preliminary experiments elucidated that PKP1 interacts with the serine/threonine protein kinase Akt2 in an activation-dependent manner. Moreover, Akt2 phosphorylates PKP1 at four motifs in its N-terminal head domain, with 9, 2, 4, and 9 serine or threonine residues in the particular motif (Fig. 27A and 53A in appendix). Based on these observations, the aim of this study was to investigate how phosphorylation of these motifs correlates with PKP1's function.

Generation and characterization of PKP1 phospho-site mutants

The introduction of a very large, strongly charged group by phosphorylation often has a dramatic effect on the characteristics of the target protein, such as alterations in the localization (Stulke, 2010). To analyze the impact of the distinct phosphorylation motifs on the subcellular localization of PKP1, site-directed PKP1 mutants were generated and immunofluorescence studies were examined. For this approach, non-phosphorylatable variants of PKP1 (A-mutants by exchanging Ser/Thr to Ala) as well as phospho-mimetic mutants of PKP1 (E-mutants by exchanging Ser/Thr to Glu) were generated to analyze the impact of PKP1 phos-

phorylation more directly. Fig. 27B illustrates the nomenclature and sequence of the generated PKP1 mutants. On the one hand single-motif mutants were prepared to determine the influence of each phosphorylation motif and on the other hand PKP1 mutants with all four motifs being mutated were analyzed.

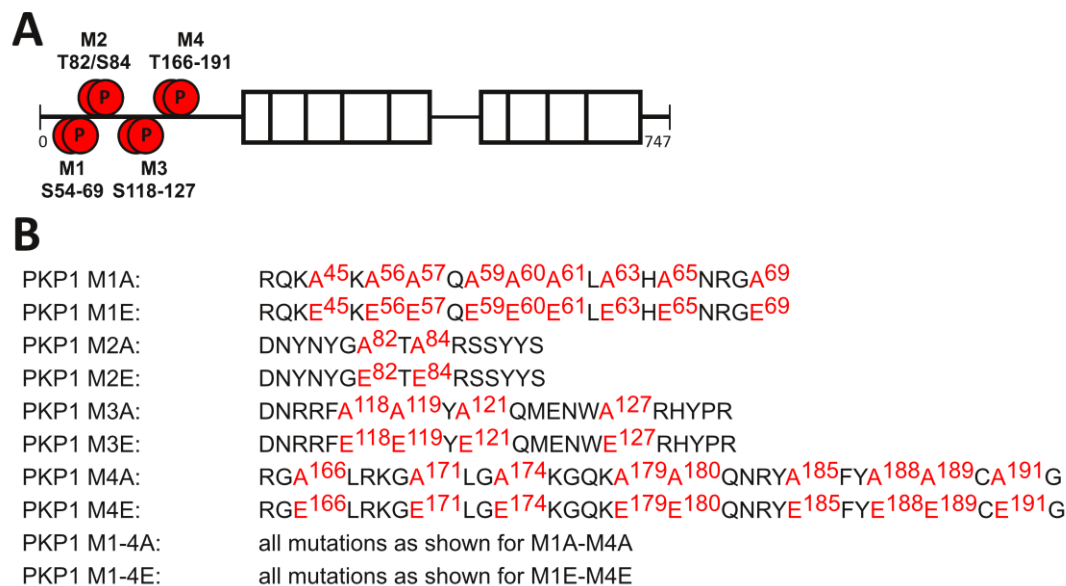


Fig. 27I Schematic view, nomenclature, and amino acid sequence of PKP1 phosphosite mutants.

(A) Schematic protein structure of PKP1 showing the four phosphorylation motifs (M1-4). (B) Single-motif phosphorylation mutants of PKP1 as well as mutants in which all four motifs were mutated were prepared to analyze the effects of PKP1 phosphorylation more directly. Site-directed mutagenesis was used to construct non-phosphorylatable variants of PKP1 (A-mutant) and phospho-mimetic mutants (E-mutant). A, alanine; E, glutamate; M1-4, phosphorylation motif 1-4; PKP, plakophilin; S, serine; T, threonine.

The localization of the PKP1 mutants was analyzed by immunofluorescence microscopy in MCF-7 cells as they contain numerous desmosomes, but express virtually no PKP1 excluding bias by interference of endogenous PKP1. It has been shown that PKP1 can bind desmosomal proteins via its N-terminal head domain (Hatzfeld et al., 2000). However, in MCF-7 cells, all PKP1 mutants localized at desmosomes in a similar manner as PKP1-WT indicating that no major folding defects were caused by the mutations (Fig. 28). A-mutants showed an almost exclusive localization at desmosomes. In contrast, E-mutants of the 1st and 4th motif (PKP1M1E and PKP1M4E) as well as PKP1M1-4E revealed considerably elevated cytoplasmic pools. Notably, MCF-7 cells expressing PKP1M4E and PKP1M1-4E showed lamellipodia and long protrusions. The 2nd phosphorylation motif had no and the 3rd motif only a weak effect on the subcellular localization of this protein (Fig. 28).

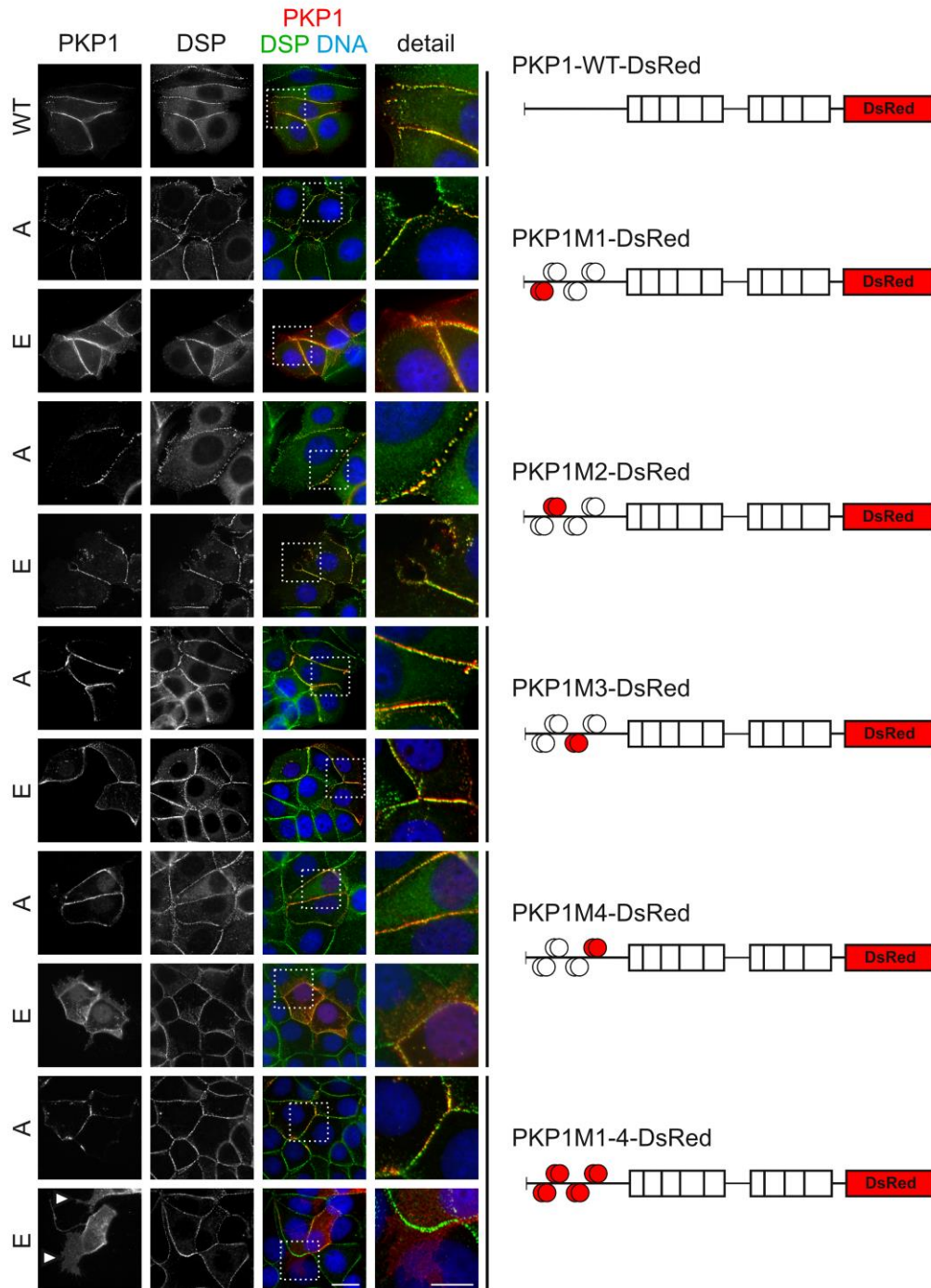


Fig. 28| Intracellular localization of PKP1 depends on its phosphorylation.

PKP1 phosphosite mutants reveal distinct intracellular localization patterns. MCF-7 cells transfected with the indicated PKP1-DsRed constructs were labeled with DSP antibody as a marker for desmosomes (in green). Nuclei were stained with Hoechst 33342 (in blue). Arrowheads indicate transfected cells with extensive lamellipodia and long protrusions. Scale bar: 20 μm , detail: 10 μm . A, alanine; DSP, desmoplakin; E, glutamate; M1-4, phosphorylation motif 1-4; PKP, plakophilin; WT, wildtype.

In addition to the immunofluorescence studies in MCF-7 cells, the effect on the subcellular localization was confirmed in HaCaT keratinocytes, which express endogenous PKP1. In agreement with the results in MCF-7 cells, an elevated cytoplasmic pool was observed for PKP1M1E and -M4E as well as for PKP1M1-4E mutants, whereas the non-phosphorylatable A-mutants associated exclusively with desmosomes (Fig. 54 in appendix). Again, extensive lamellipodia and long protrusions were observed in PKP1M1-4E-expressing cells (Fig. 54, arrowheads). Many of these cells detached from the monolayer and formed protrusions on the top of their neighboring cells. In regions of lamellipodia formation, desmosomes seemed reduced indicated by DSP staining. In summary, these experiments support the hypothesis that non-phosphorylatable PKP1 is mainly found in desmosomes, whereas phosphorylated PKP1 as mimicked by the negative charge of the E-mutants showed an increased, accumulated pool in the cytosol. Thus, phosphorylation of PKP1 modulates its subcellular localization.

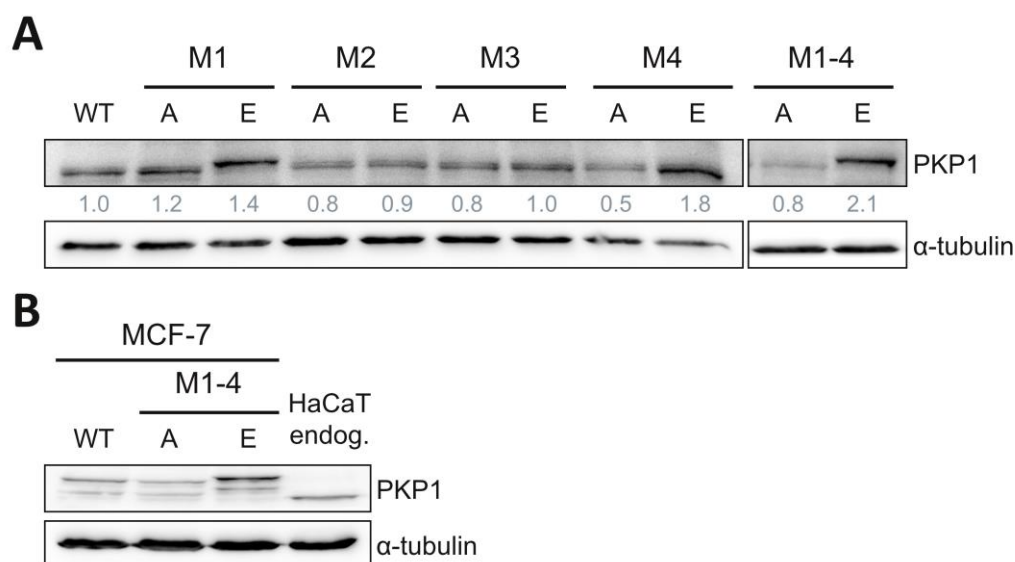


Fig. 29| Phospho-mimetic mutations cause PKP1 to accumulate in the cytoplasm.

(A) Western blot analysis of total protein extracts from MCF-7 cells transfected with the indicated PKP1-DsRed constructs. α -tubulin was used as loading control. The fold change of PKP1 mutants abundance (indicated below the lanes) was determined relative to PKP1-WT. (B) Western blot analysis of total protein extracts showing expression levels of PKP1-WT, M1-4A and M1-4E mutants in MCF-7 cells compared with the expression of endogenous PKP1 in HaCaT cells. α -tubulin was used as loading control. A, alanine; E, glutamate; endog., endogenous; M1-4, phosphorylation motif 1-4; PKP, plakophilin; WT, wildtype.

To exclude bias caused by varying levels of the individual mutant, expression levels were compared by Western blot analysis. This revealed increased protein amounts for PKP1M1E, M4E, and M1-4E mutants, respectively (Fig. 29A). Thus, PKP1M1E and PKP1M4E became stabilized in MCF-7 cells, whereas PKP1M2E and PKP1M3E were not. All other mu-

tants showed very similar expression levels, which were similar to the amount of endogenous PKP1 observed in HaCaT cells (Fig. 29B). Moreover, accumulation of the phospho-mimetic mutant PKP1M1-4E at protein level was also observed in HEK293 cells, although mRNA levels were similar for all PKP1 mutants (experiment conducted by Dr. Annika Wolf, not shown).

The immunofluorescence studies and Western blot analyses of total protein lysates supported the view that phosphorylated PKP1 accumulates in the cytoplasm. In addition, mild detergent extraction of transfected MCF-7 cells was used to evaluate the solubility of PKP1 mutants. As expected, PKP1-WT and the M1-4A mutant were essentially insoluble, whereas abundance of the M1-4E mutant was considerably elevated in the soluble fraction. The solubility of keratins was not affected (Fig. 55A in appendix). To test whether the modification of PKP1 by Akt2 enhances its stability, PKP1 protein degradation was determined after inhibiting protein synthesis using cycloheximide. The protein level of the PKP1M1-4A mutant was reduced to 50% after ~5 hours, whereas the PKP1M1-4E mutant was very slowly degraded with >70% remaining at 9 hours (Fig. 55B in appendix). Thus, it can be suggested that phosphorylation of PKP1 retarded its degradation and promoted its cytoplasmic accumulation.

PKP1 localization is regulated by insulin signaling via Akt2

The Akt kinases (Akt1-3) can be activated through receptor tyrosine kinase pathways, such as those of insulin, EGF, IGF1 amongst others [remember Fig. 6, (Blume-Jensen and Hunter, 2001, Chan et al., 1999, Coffey et al., 1998, Schlessinger, 2000)]. In the absence of growth factor stimulation in quiescent cells, the Akt kinases are catalytically inactive (Liao and Hung, 2010). Stimulation by growth factors activates the kinases through a PI3K-dependent process (Chan et al., 1999, Coffey et al., 1998). Experiments by Dr. Annika Wolf indicated that PKP1 associates preferentially with activated Akt2 (Fig. 53B in appendix). In transiently transfected HEK293 cells, PKP1 co-immunopurified with Akt2 upon insulin stimulation, whereas hardly any association was observed in unstimulated cells. In contrast, Akt1 was not co-immunoprecipitated with PKP1 (Fig. 53B).

To characterize, how phosphorylation of PKP1 by Akt2 modulates its cellular functions, the subcellular localization of the protein was investigated. For this approach a constitutively active myristoylated Akt2 (myr-Akt2) as well as a kinase-inactive Akt2 (K181M/T309A/S474A) was used. Immunofluorescence staining revealed that PKP1 preferentially localized in the cytoplasm in MCF-7 cells overexpressing activated myr-Akt2. In contrast, co-expression of kinase-inactive Akt2 resulted in a punctate staining pattern of PKP1 at

the plasma membrane characteristic for its desmosomal localization. In these cells, PKP1 was essentially depleted from the cytoplasm (Fig. 30A). These data indicate that the subcellular localization of PKP1 was regulated by Akt2-dependent signaling and suggest that phosphorylation of PKP1 by Akt2 enhances its cytoplasmic accumulation.

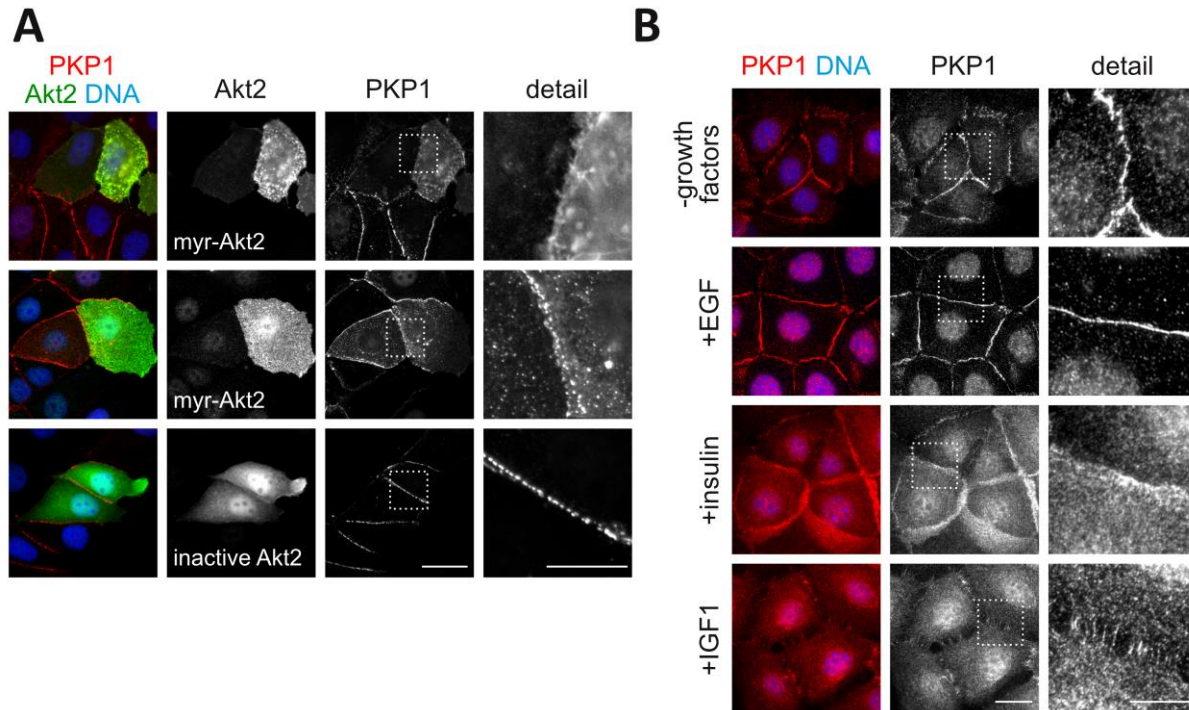


Fig. 30| Growth factor signaling regulates the localization of PKP1.

(A) PKP1 localization is regulated by Akt2. MCF-7 cells stably expressing PKP1-DsRed were transfected with myr-Akt2 or kinase inactive Akt2 (in green) and analyzed by immunofluorescence microscopy at 24 hours post transfection. Nuclei were stained with Hoechst 33342 (in blue). Scale bar: 20 μm , detail: 10 μm . (B) Mouse keratinocytes were serum-starved for 24 hours (+1.2 mM CaCl_2) and stimulated with EGF, insulin or IGF1 for 24 hours as indicated. Endogenous PKP1 was visualized using rabbit serum antibody (in red). Nuclei were stained with Hoechst 33342 (in blue). Scale bar: 20 μm , detail: 10 μm . EGF, epidermal growth factor; IGF1, insulin-like growth factor-1; myr, myristoyl; PKP, plakophilin.

To validate whether the shift from desmosomal to cytoplasmic PKP1 is also induced by physiological stimuli such as growth factor signaling, mouse keratinocytes were stimulated with EGF, insulin, or IGF1 and analyzed by immunofluorescence microscopy. As expected, cells stimulated with insulin and IGF1 revealed an increased cytoplasmic pool of endogenous PKP1 in comparison to serum-starved keratinocytes (Fig. 30B). EGF treatment showed no obvious change in the subcellular localization of PKP1, in agreement with the observation that EGF signaling did not result in PKP1 phosphorylation (personal communication by Dr. Annika Wolf). Thus, insulin/IGF1 signaling induces an Akt2-dependent redistribution of PKP1 from the desmosomes to the cytosol.

PKP1 phospho-mimetic mutant reduces intercellular adhesion and promotes wound healing

The formation of protrusions and lamellipodia with reduced desmosomes at sites of neighboring cells expressing PKP1M1-4E suggested a hitherto unrecognized dependence of the phosphorylation state of PKP1 on cell-cell adhesion, prompting the question whether modification of PKP1 affects the adhesive strength of cells.

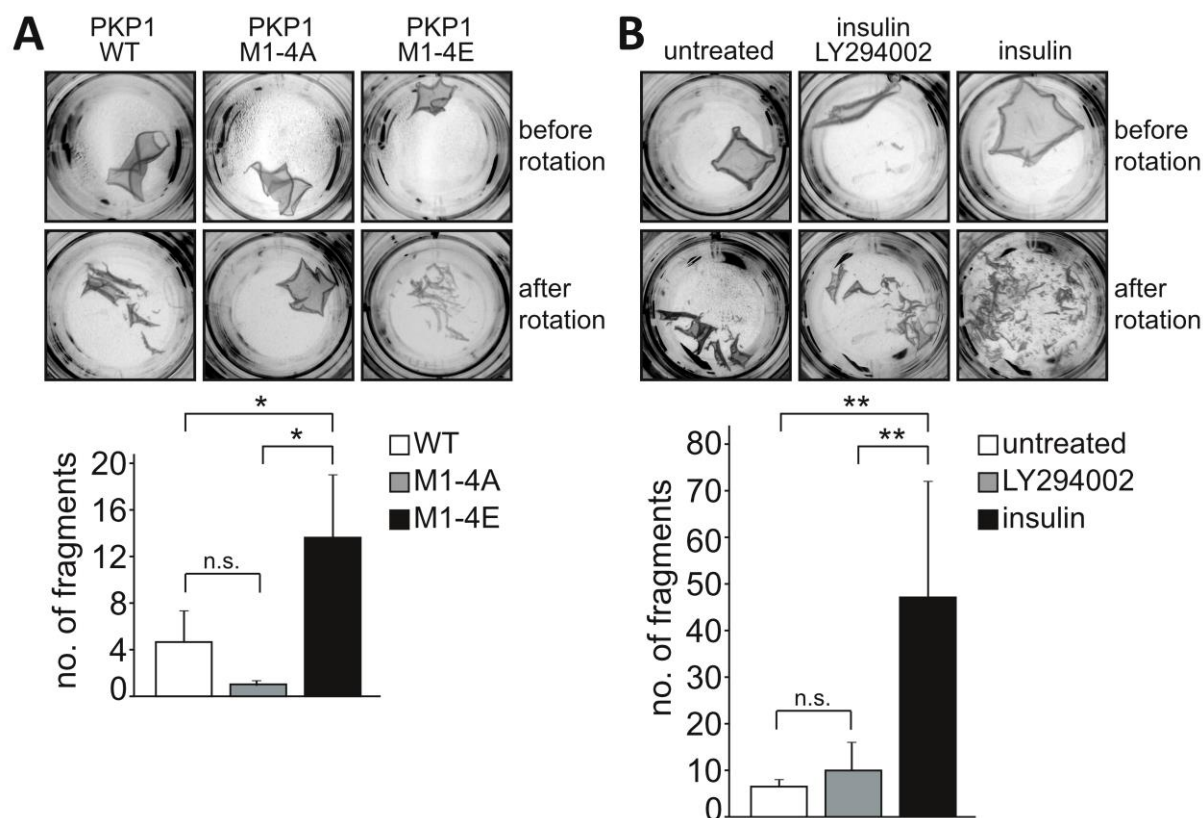


Fig. 31| PKP1 phospho-mimetic mutant reduces intercellular adhesion.

(A) Intercellular adhesion of PKP1M1-4E-expressing MCF-7 cells is reduced. The strength of intercellular cohesion of MCF-7 cells stably expressing PKP1-WT or M1-4A/E was assessed by dispase assays. Representative images show the integrity of the detached cell monolayer before and after application of mechanical stress (rotation). Diagram depicts the quantification of counted fragments after rotation (below, mean \pm SD, $n=3$). Statistical significance was determined by 1-way ANOVA testing (Tukey's multiple comparison test). * $P \leq 0.05$. n.s. = not significant. (B) Insulin stimulation reduced the intercellular adhesion of PKP1-WT-expressing cells. The monolayer of MCF-7 cells stably expressing PKP1-WT treated with insulin dissociated into noticeable smaller fragments than the monolayer of the cells treated with insulin together with LY294002. Diagram depicts the quantification of counted fragments after rotation (below, mean \pm SD, $n=3$). Statistical significance was determined by 1-way ANOVA testing (Tukey's multiple comparison test). ** $P \leq 0.005$. n.s. = not significant. A, alanine; E, glutamate; LY294002, PI3K inhibitor; M1-4, phosphorylation motif 1-4; no., number; PKP, plakophilin; WT, wildtype.

To analyze this, dispase was used to detach confluent monolayers of MCF-7 cells stably expressing PKP1-WT, M1-4A, or M1-4E before probing intercellular adhesion by applying mechanical stress via rotation. Whereas the monolayer of PKP1M1-4A-expressing cells remained essentially intact under the experimental conditions, the PKP1M1-4E-expressing cell layers dissociated into numerous fragments indicating a reduced intercellular cohesion. MCF-7 cells expressing PKP1-WT dissociated into fewer fragments in comparison to cells expressing the phospho-mimetic mutant (Fig. 31A). Additionally, PKP1-WT-expressing cells were stimulated with insulin, which strongly reduced intercellular adhesion. Inhibition of PI3K upstream of Akt by LY294002 rescued this phenotype (Fig. 31B).

To further elucidate the mechanism by which phosphorylation of PKP1 influences desmosome stability, the dynamics of nuclear, cytoplasmic, and desmosomal PKP1-GFP mutants were analyzed by FRAP. Therefore, comparable regions of nuclear, cytoplasmic, and desmosomal PKP1-WT or mutants were bleached and then the recovery was monitored over time. In agreement with the stable desmosomal association of non-phosphorylatable PKP1 (PKP1M1-4A), its desmosomal pool revealed a low dynamic, with a half-life of ~ 12.5 s and a large immobile fraction ($I_f=0.63$) compared to PKP1-WT with a half-life of ~ 6.6 s and a considerably smaller immobile fraction ($I_f=0.4$). In contrast, PKP1M1-4E showed a significantly reduced half-life of only ~ 2.4 s with a small immobile fraction ($I_f=0.26$) in desmosomes indicating an elevated exchange rate and a considerably reduced stability of its desmosomal association (Fig. 32A). In the nucleoplasm and cytoplasm, PKP1 mutants revealed no significantly altered diffusion rates compared to WT (not shown). These studies suggest that un-phosphorylated PKP1 is stabilized in the desmosome, thereby promoting intercellular adhesion. Since intercellular adhesion and cell migration are interdependent, the migratory capacity of MCF-7 cells stably expressing PKP1-WT or mutants was examined. To mimic cell migration during wound healing, a scratch wound assay was performed. After creating a “wound” (scratch) in the MCF-7 cell monolayer, images were captured at the beginning and at regular intervals during cell migration to close the wound. Whereas PKP1-WT- and PKP1M1-4E-expressing cells were able to close the ~ 500 μm gap within 18 hours, a gap of ~ 150 - 200 μm remained in the PKP1M1-4A-expressing cells suggesting that migration into the cell-free area was reduced (Fig. 32B, left). Quantitative assessment of wound closure over time confirmed that PKP1-WT and PKP1M1-4E revealed significantly elevated migratory capacity (Fig. 32B, right).

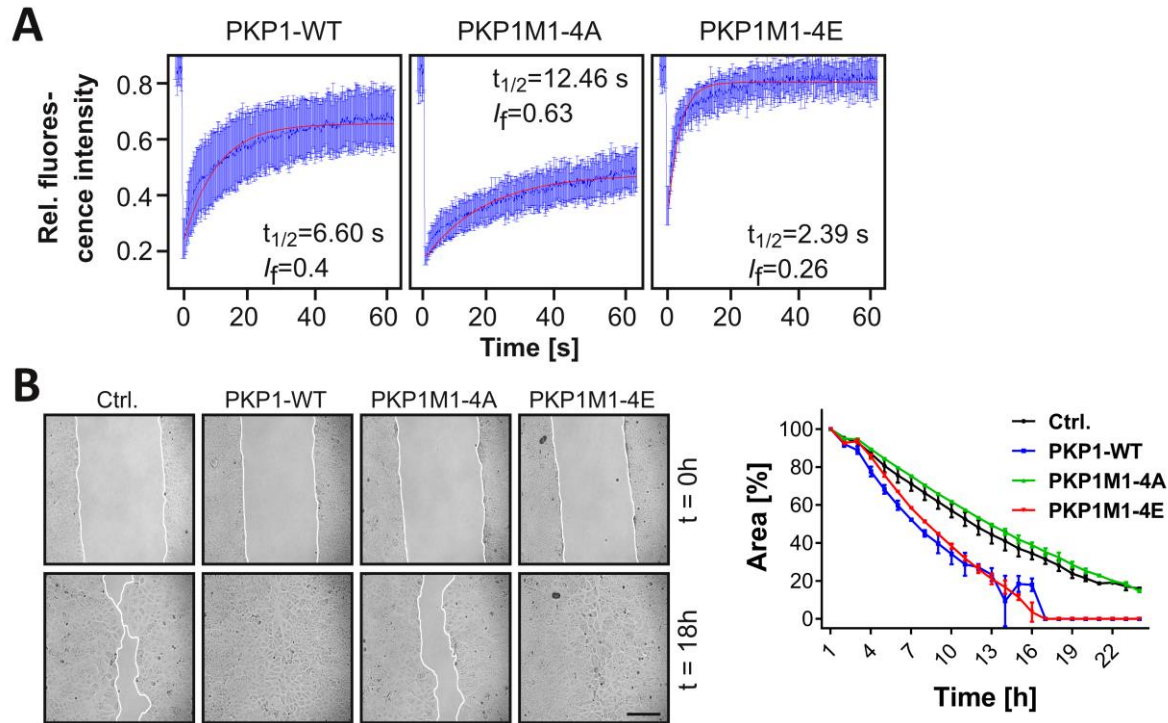


Fig. 32| PKP1 phospho-mimetic mutant promotes wound healing of MCF-7 cells.

(A) Desmosomal fluorescence recovery intensities over the time were measured in MCF-7 cells transfected with PKP1-WT, PKP1M1-4A, or PKP1M1-4E. Red lines show the fitted single exponential recovery curves (mean \pm SD, $n=11$). The $t_{1/2}$ (half-time) and I_f (immobile fraction) are indicated. FRAP measurements were done by Dr. Markus Glaß. (B) Phosphorylation of PKP1 affects wound healing. The capacity of MCF-7 cells stably expressing PKP1 mutants to migrate into a gap between two confluent regions was analyzed by live cell imaging. The gap area was quantified using the MiToBo plugin for ImageJ (mean \pm SD, $n=3$). Scale bar: 100 μm . A, alanine; Ctrl., control; E, glutamate; FRAP, fluorescence recovery after photobleaching; I_f , immobile fraction; M1-4, phosphorylation motif 1-4; PKP, plakophilin; Rel., relative; $t_{1/2}$, half-time; WT, wildtype.

In summary, these observations provide strong evidence that Akt2-directed phosphorylation of PKP1 interferes with intercellular adhesion and enhances the migratory capacity, presumably by inducing the cytoplasmic localization of PKP1.

PKP1 phosphorylation promotes proliferation and confers the capacity for anchorage-independent growth

Previous studies revealed that the cytoplasmic pool of PKP1 stimulates translation (Wolf et al., 2010). Additionally, cap-dependent luciferase reporter assays (performed by Dr. Annika Wolf) showed that mRNA translation was increased by the overexpression of PKP1 phospho-mimetic mutant, the co-expression of PKP1 with active Akt2 as well as by insulin stimulation (not shown) indicating that the phosphorylation of PKP1 enhances protein synthesis. As translation and proliferation are tightly coupled processes and previous data indicated that depletion of PKP1 reduced translation as well as cell proliferation [(Wolf and

Hatzfeld, 2010, Wolf et al., 2010), Fig. 26], it was examined whether the stimulation of translation by the PKP1 phospho-mimetic mutant directly correlated with their capacity to stimulate proliferation. To analyze this, MCF-7 cells transfected with PKP1-WT, M1-4A, or M1-4E were cultured with 5-bromo-2'-deoxyuridine (BrdU) treated medium for 1 hour. This pyrimidine analog is incorporated in place of thymidine into newly synthesized DNA of proliferating cells. Quantification of BrdU-incorporation revealed slightly increased proliferation rates in PKP1-WT- and M1-4A-expressing cells compared to control transfected cells (1.6- and 1.4-fold, respectively, Fig. 33A), in agreement with the elevated wound closure (Fig. 32B). In contrast, BrdU-incorporation was severely (2.4-fold) upregulated in cells expressing the PKP1M1-4E mutant. In addition to the BrdU incorporation assay, a colorimetric growth assay based on crystal violet uptake (Gillies et al., 1986) was used to quantify cell numbers. As expected, proliferation was slightly reduced in PKP1M1-4A-expressing cells, whereas it was considerably upregulated by the PKP1M1-4E mutant (Fig. 33B). These results correlated well with the predominant desmosomal association of PKP1-WT and A-mutants and an enhanced cytoplasmic pool of PKP1 E-mutants.

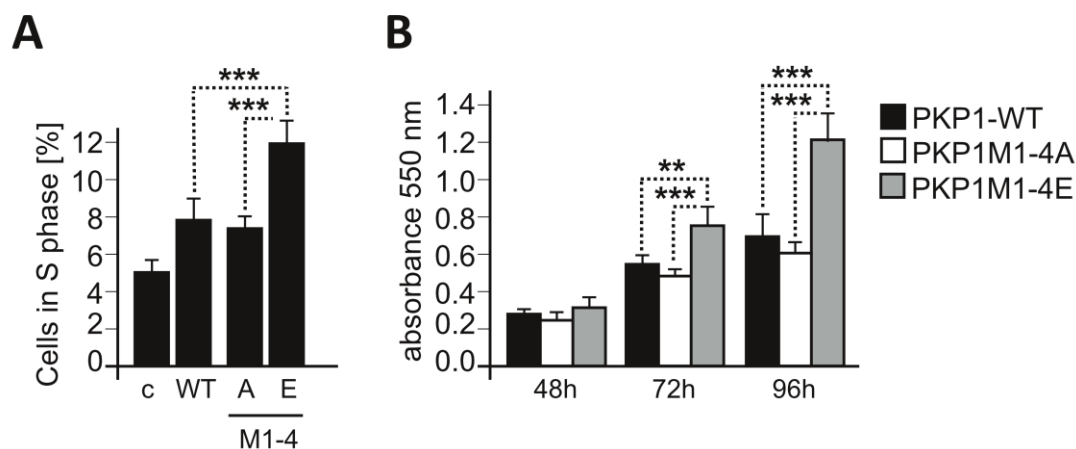


Fig. 33| PKP1 phospho-mimetic mutant increases proliferation.

Phospho-mimetic mutant of PKP1 stimulates proliferation more efficiently than PKP1-WT or non-phosphorylatable PKP1. (A) At 48 hours after transfection with the indicated plasmids, MCF-7 cells were incubated with BrdU and harvested for quantification of BrdU-incorporation (mean \pm SD). At least 200 transfected cells were counted for each of three independent experiments. Statistical significance was determined by 1-way ANOVA testing (Tukey's multiple comparison test). $***P \leq 0.0005$. (B) Quantification of cell count by measuring crystal violet incorporation. MCF-7 cells stably expressing the indicated constructs were cultured in 96-well plates, stained with crystal violet and quantified by measuring the OD₅₅₀ and normalizing to values determined at 24 hours (mean \pm SD, n=3). Statistical significance was determined by 1-way ANOVA testing (Tukey's multiple comparison test). $**P \leq 0.005$, $***P \leq 0.0005$. A, alanine; BrdU, 5-bromo-2'-deoxyuridine; c, control; E, glutamate; M1-4, phosphorylation motif 1-4; OD, optical density; PKP, plakophilin; WT, wildtype.

Multiple phenotypic changes correlate with the transition of a normal cell to a transformed one. The ability of a transformed cell to grow unattached to a solid substrate is one characteristic feature, a property that has been termed anchorage-independent growth. Since anchorage independence and tumorigenic properties of cells positively correlate (Freedman and Shin, 1974, Shin et al., 1975) and increased proliferation rates as well as increased migratory capacity are hallmarks of cellular transformation, MCF-7 cells stably expressing the PKP1 mutants were examined for colony formation in soft agar. Most importantly, the expression of PKP1M1-4E revealed a significant increase in the number and size of colonies formed, whereas PKP1M1-4A-expressing cells formed very little colonies in soft agar (Fig. 34A).

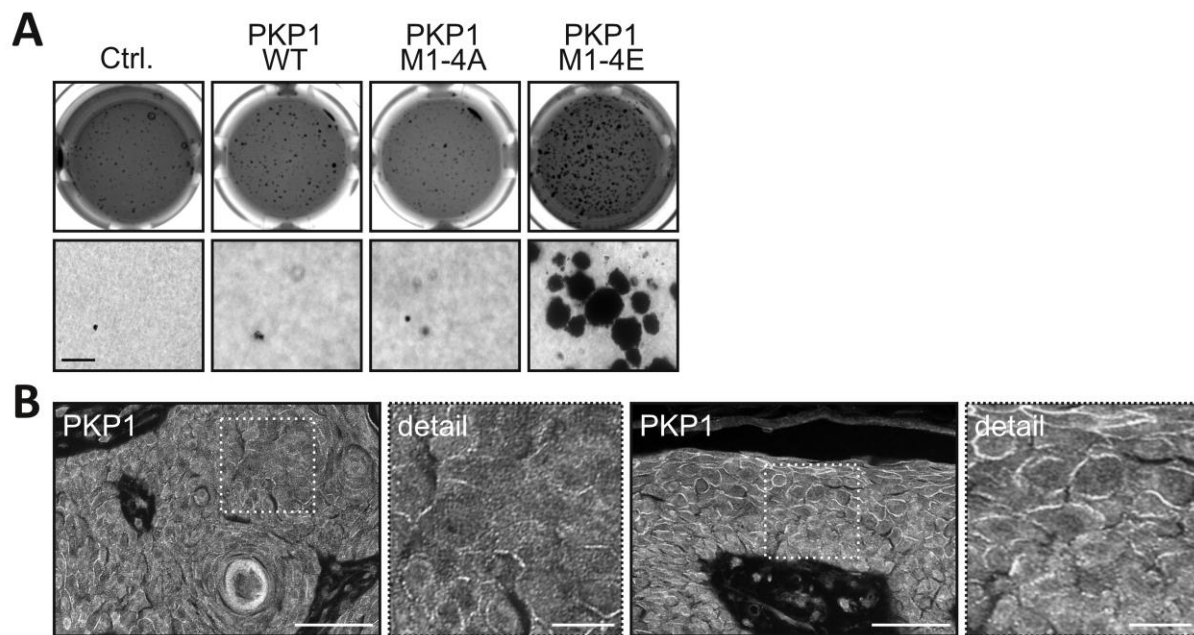


Fig. 34| PKP1 phospho-mimetic mutant promotes anchorage-independent growth and carcinogenesis in an Akt2-dependent manner.

(A) Colony forming in soft agar was performed with MCF-7 cells stably expressing PKP1 mutants as indicated. At three weeks after plating, colonies were stained with iodinitrotetrazolium chloride. A detail image is depicting below. Scale bar: 200 μ m. (B) Characterization of SSC paraffin sections from mice transgenic for HPV8 revealed a considerably elevated cytoplasmic localization of PKP1 and reduced desmosomes. Scale bar: 50 μ m, detail: 10 μ m. A, alanine; Ctrl., control; E, glutamate; HPV8, cutaneous human papillomavirus type 8; M1-4; phosphorylation motif 1-4; PKP, plakophilin; SCC, squamous cell carcinoma; WT; wildtype.

Studies analyzing the expression of desmosomal proteins in human tumors are contradictory with upregulation, downregulation, or maintenance of desmosomal protein expression reported (Chidgey and Dawson, 2007, Dusek and Attardi, 2011). Human papilloma virus (HPV) has been associated with squamous cell carcinoma (SCC). HPV down-regulates Akt1, whereas Akt2 upregulation and activation was reported in tumors (O'Shaughnessy et al.,

2007). In order to test whether the regulation of PKP1 by Akt2 may play a role in SCC, the localization of PKP1 was analyzed in tissue samples of mice transgenic for HPV8 (kindly provided by Prof. Dr. Werner; ETH, Institute of Molecular Health Science, Zurich). These HPV8 transgenic mice develop skin cancer. In comparison to the preferential desmosomal localization of PKP1 in the epidermis of healthy WT mice (Fig. 10E), SCC tissue samples showed a considerably elevated cytoplasmic localization of PKP1 along with reduced desmosomes (Fig. 34B). These results support the hypothesis, that unregulated activation of the Akt2 pathway may induce cytoplasmic accumulation of PKP1 accompanied by a destabilization of desmosomal adhesion on the one hand and an increase in translation and proliferation on the other hand. In this scenario, PKP1 could actively contribute to carcinogenesis.

In this chapter it was shown that the equilibrium between the desmosomal and cytosolic pools of PKP1 is accurately regulated by insulin/IGF1 signaling. Upon activation of the PI3K/Akt2 pathway, PKP1 was phosphorylated by Akt2, resulting in its cytoplasmic accumulation and delayed degradation. This correlated with weakened intercellular cohesion, but enhanced translation, proliferation, wound healing, and anchorage-independent growth. This study predicts an important role of PKP1 in contributing to tumorigenesis in a context-dependent way.

3.3. 14-3-3 proteins regulate desmosomal adhesion via PKPs

The last chapter revealed site specific phosphorylation of PKP1 by the kinase Akt2 leading to its shift from the desmosomes to the cytoplasm, which correlated with distinct functions. Based on these findings, it raised the question whether this pathway is involved in the regulation of desmosomal adhesion by generating 14-3-3 binding sites and interactions. The family of 14-3-3 proteins is known to recognize and specifically bind phosphoserine/threonine motifs, which can result in an altered localization and function of the targets (chapter 2.4.). Therefore, these proteins participate in and modulate several signal transduction pathways. This last chapter will give insights, how growth factor signaling regulates the association of the desmosomal plaque proteins PKP1 and PKP3 with 14-3-3 proteins and uncover unique and partially antagonistic functions of members of the 14-3-3 family in the regulation of desmosomes.

14-3-3 γ and 14-3-3 σ affect intercellular adhesion of keratinocytes

14-3-3 proteins are a family of highly conserved regulatory molecules found in all eukaryotic cells. In mammals, seven isoforms named γ , σ , η , ϵ , β , ζ , and τ have been identified (Ichimura et al., 1988). To assess, which 14-3-3 isoform may contribute to the regulation of desmosomal adhesion in keratinocytes, the expression of all seven proteins was tested. Because of considerable sequence conservation between the 14-3-3 proteins, the specificity of all used isoform-specific 14-3-3 antibodies was probed on recombinant GST-14-3-3 fusion proteins (Fig. 35A). While most antibodies were specific, 14-3-3 η antibody cross-reacted with 14-3-3 γ ; 14-3-3 β antibody with 14-3-3 τ ; and 14-3-3 ζ antibody with 14-3-3 β and 14-3-3 σ . 14-3-3 γ , - σ , - ϵ , and - η were highly expressed compared to the other isoforms (Fig. 35B, C). Given the abundance of desmosomal proteins in the skin, it was assumed that regulatory proteins, which bind in a stoichiometric fashion, occur at similar abundance. Thus, the four highly expressed 14-3-3 isoforms were selected to analyze their contribution to keratinocyte cohesion. Therefore, mouse keratinocytes were transfected with GFP-fused 14-3-3 proteins or 14-3-3-directed siRNAs and cultured in HCM to induce cell contact formation. Dispase was used to detach confluent keratinocyte monolayers and subjected them to mechanical stress to examine intercellular cohesion.

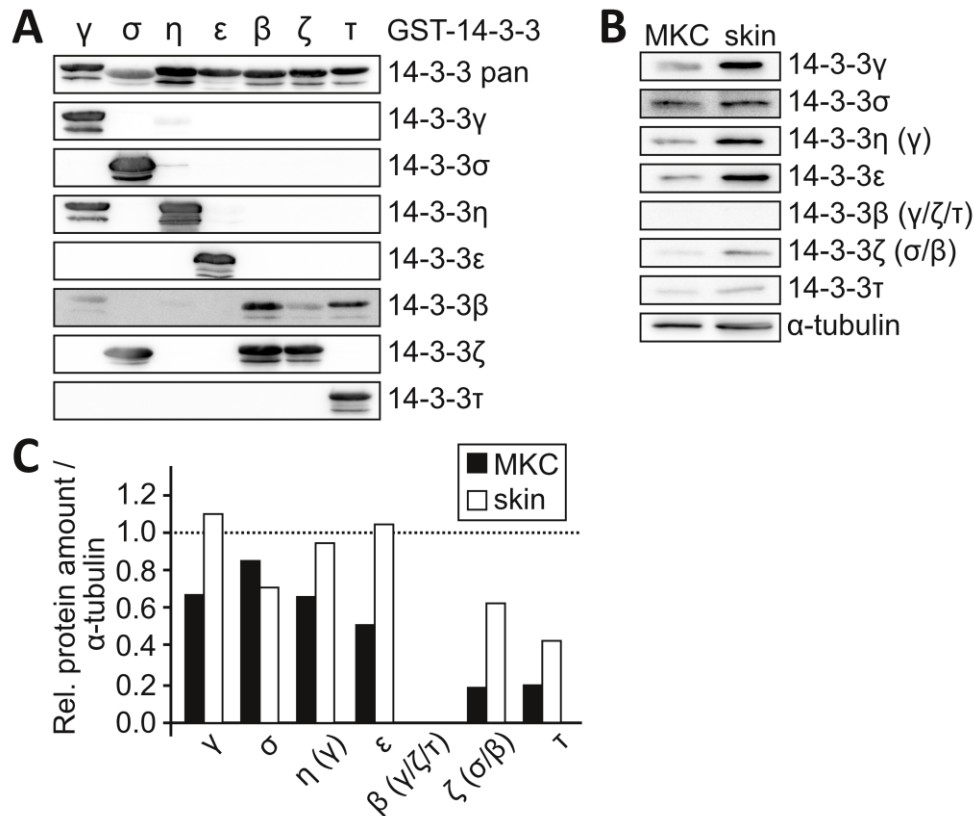


Fig. 35| 14-3-3 isoform expression in murine skin and keratinocytes.

(A) GST-tagged 14-3-3 proteins were expressed in *E. coli* BL21DE3. Total cell extracts were analyzed by Western blot with the indicated 14-3-3 antibodies to determine antibody specificity. Note that 14-3-3η, β and ζ show cross-reactions with other isoforms. (B) Western blot analysis of total protein extracts from mouse keratinocytes (MKC) grown for 6 days in HCM in comparison to murine skin. α-tubulin was used as loading control. Antibody cross-reactivities are indicated in brackets. (C) Quantification of 14-3-3 isoform amounts relative to α-tubulin in mouse keratinocytes (MKC) and murine skin. GST, glutathione S-transferase; HCM, high calcium medium; MKC, mouse keratinocytes; Rel., relative.

Epithelial sheet assays revealed that 14-3-3γ overexpression destabilized intercellular adhesion of mouse keratinocytes, whereas its knockdown did not interfere with strong intercellular cohesion. In contrast, 14-3-3σ overexpression was compatible with strong adhesion, whereas its knockdown significantly reduced intercellular cohesion of mouse keratinocytes (Fig. 36A-C). 14-3-3γ as well as 14-3-3σ knockdown did not affect expression levels of other 14-3-3 proteins indicative of the specificity of the targeting siRNAs (Fig. 36D, E). Since 14-3-3η and -ε did not reveal consistent effects on intercellular cohesion (not shown), 14-3-3γ and 14-3-3σ were selected for further studies. Taken together, these data suggest a destabilizing role of 14-3-3γ and a stabilizing role of 14-3-3σ in keratinocyte cohesion.

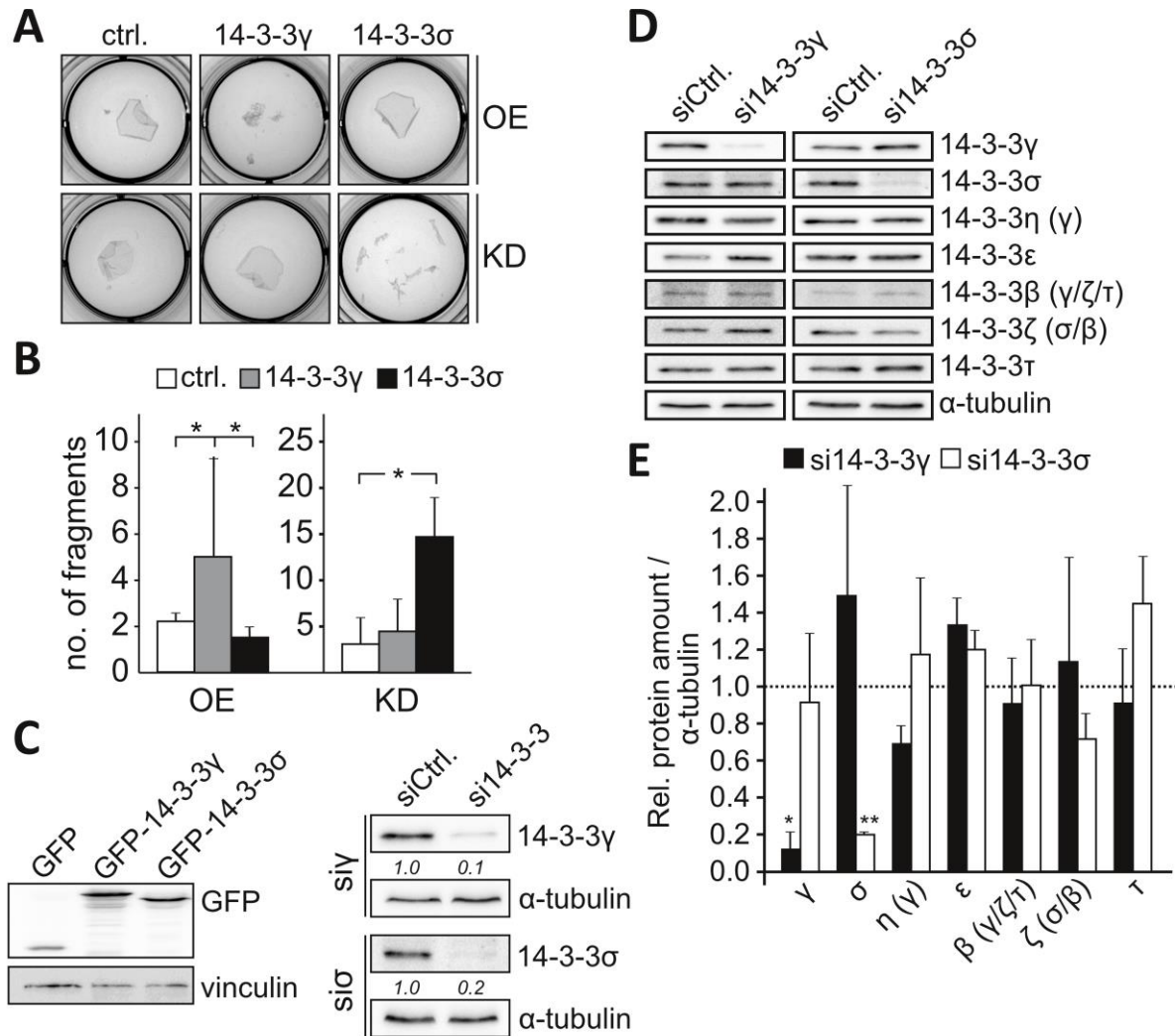


Fig. 36| 14-3-3 γ/σ have opposing effects on intercellular cohesion of murine keratinocytes.

(A) Disperse assays of keratinocytes after overexpression (OE) of GFP (ctrl.), GFP-14-3-3 γ , or GFP-14-3-3 σ (upper row) and after transfection of non-targeting (ctrl.), 14-3-3 γ -, or 14-3-3 σ -directed siRNAs (KD, lower row). Representative images of detached epithelial sheets after application of mechanical stress (rotation) are shown. (B) Quantification of the number of fragments (mean \pm SD, n=8). Statistical significance was determined by 1-way ANOVA testing (Tukey's multiple comparison test). * $P \leq 0.05$. (C) Western blot analysis using an anti-GFP antibody confirms overexpression of the indicated constructs (left). Vinculin served as loading control. Knockdown efficiencies were determined by Western blot using 14-3-3 γ and 14-3-3 σ specific antibodies, respectively. α -tubulin served as loading control. Knockdown efficiencies are given below the lanes. (D) Mouse keratinocytes were transfected with 14-3-3 γ and 14-3-3 σ -directed siRNAs, grown for 24 hours in HCM and lysed in SDS-lysis buffer. Total cell extracts were analyzed by Western blot using the indicated antibodies. Cross-reactivities of the 14-3-3 antibodies are written in brackets. α -tubulin was used as loading control. Depicted are representative images of Western blots. (E) Quantification of 14-3-3 isoform amounts upon knockdown of 14-3-3 γ and 14-3-3 σ . The diagram depicts the relative protein amounts normalized to α -tubulin (mean \pm SD, n=3). Statistical significance was determined by 1-way ANOVA testing (Tukey's multiple comparison test). * $P \leq 0.05$, ** $P \leq 0.005$. ctrl., control; GFP, green fluorescent protein; HCM, high calcium medium; KD, knockdown; no., number; OE, overexpression; Rel., relative.

14-3-3 proteins affect desmosomal protein localization

When tissues are exposed to mechanical stress, the stability, which is required to maintain tissue integrity, is preferentially provided by desmosomes (Hatzfeld et al., 2017). Since the abundance of 14-3-3 γ and 14-3-3 σ affected intercellular cohesion of keratinocytes (Fig. 36A, B), it raised the question whether desmosomal proteins are regulated by 14-3-3 proteins. To analyze the contribution of 14-3-3 γ and 14-3-3 σ on the localization of PKP1 and PKP3, 14-3-3 proteins were overexpressed and immunofluorescence microscopy was examined. In agreement with its role in destabilizing cell cohesion, 14-3-3 γ induced a redistribution of junctional PKP1 to the cytoplasm (Fig. 37A, B and 56A, C in appendix). In differentiated mouse keratinocytes, PKP3 accumulates at tricellular contact sites, whereas bicellular contacts reveal much weaker PKP3 association (Keil et al., 2016). This distribution was changed upon 14-3-3 γ overexpression, where an increased association of PKP3 with lateral contacts was observed (Fig. 37C, D and 56B, C in appendix), similar to the redistribution of tricellular PKP3 towards bicellular contacts in PKP1-KO keratinocytes (Fig. 24C). 14-3-3 σ overexpression had no major effect on the localization of either PKP (Fig. 37 and 56 in appendix).

To test whether depletion of 14-3-3 γ or 14-3-3 σ might also affect the localization of PKP1 and PKP3, knockdown experiments were performed. To initially ascertain the knockdown efficiencies of 14-3-3 γ - and 14-3-3 σ -directed siRNAs on a microscopic level, mouse keratinocytes were transfected with the specific siRNA pool and grown for 24 h in HCM. Due to their solubility and predominant cytoplasmic localization, the cells were fixed in formaldehyde to preserve 14-3-3 localization. Almost all cells showed strongly reduced levels of both 14-3-3 isoforms compared to keratinocytes transfected with non-targeting siRNA pool suggesting a high knockdown efficiency (Fig. 38A), which was also quantified by Western blot analysis (Fig. 38B).

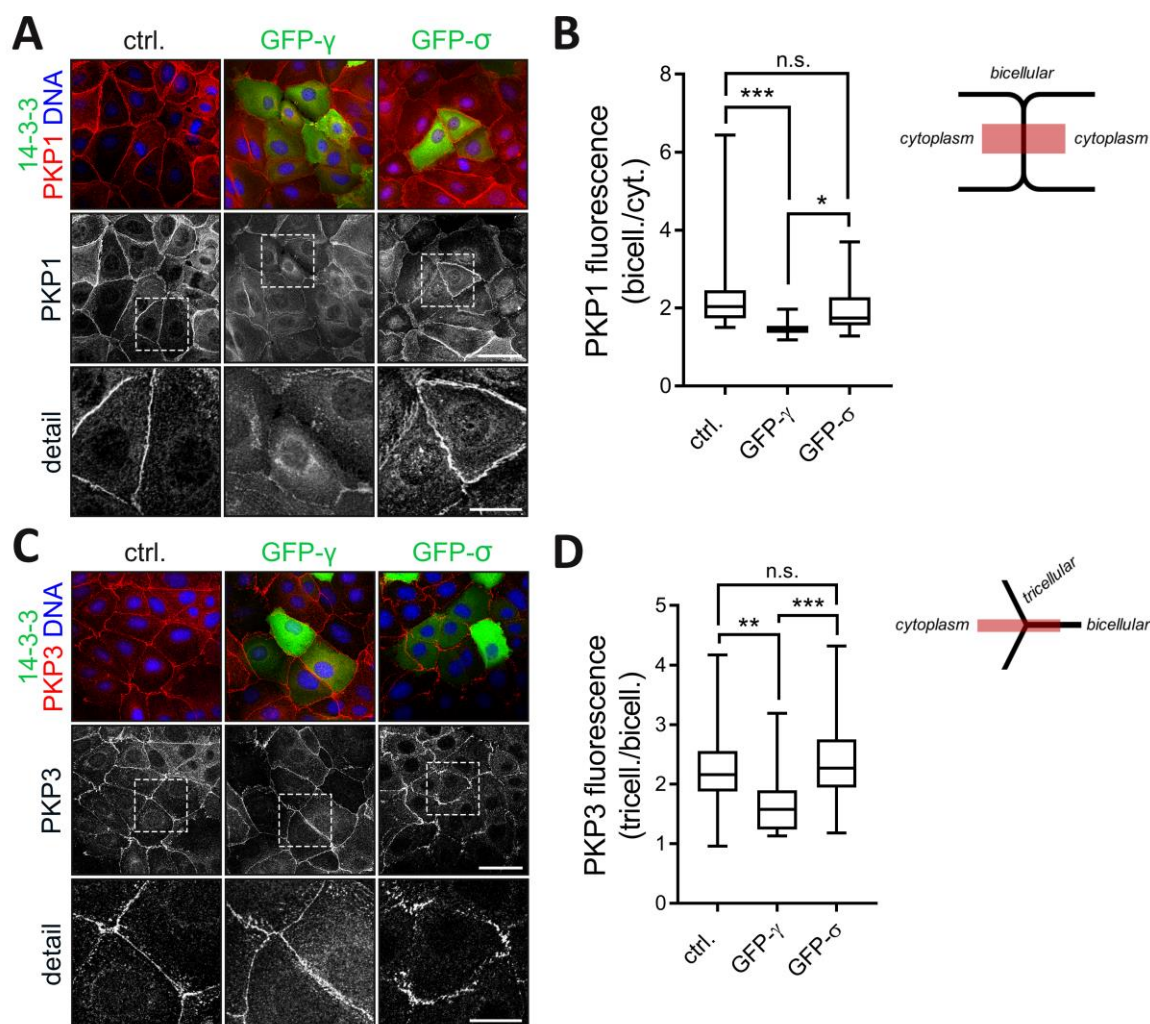


Fig. 37 | 14-3-3 proteins affect the localization of PKP1 and PKP3.

Mouse keratinocytes were transfected with GFP-14-3-3 γ or GFP-14-3-3 σ , grown for 24 hours in HCM, methanol-fixed and immunostained with antibodies against PKP1 (A) or PKP3 (C) shown in red. Hoechst 3342 staining served as nuclear marker (in blue). Depicted are confocal images of single optical sections. Scale bar: 50 μ m, detail: 10 μ m. To compare fluorescence intensities, all images were collected with equal hardware settings. Fluorescence intensities of PKP1 (B) and PKP3 (D) were determined using ImageJ by measuring a segment of equal length and width across 30 individual bicellular or tricellular contacts as illustrated by red bars in the schematics (see also Fig. 56 in appendix). For each line scan the mean junctional (bicellular, tricellular) value was normalized to the mean cytoplasmic value. The boxplots depict the enrichment of PKP1 at bicellular contacts (B) or the ratio of PKP3 (D) at tricellular vs. bicellular contacts and display the 1st to 3rd quartile with full range of variation (whiskers from minimum to maximum). Statistical significance was determined by 1-way ANOVA testing (Tukey's multiple comparison test). * $P \leq 0.05$, ** $P \leq 0.005$, *** $P \leq 0.0005$, n.s. = not significant. bicell., bicellular; ctrl., control; cyt., cytoplasm; GFP, green fluorescent protein; HCM, high calcium medium; PKP, plakophilin; tricell., tricellular.

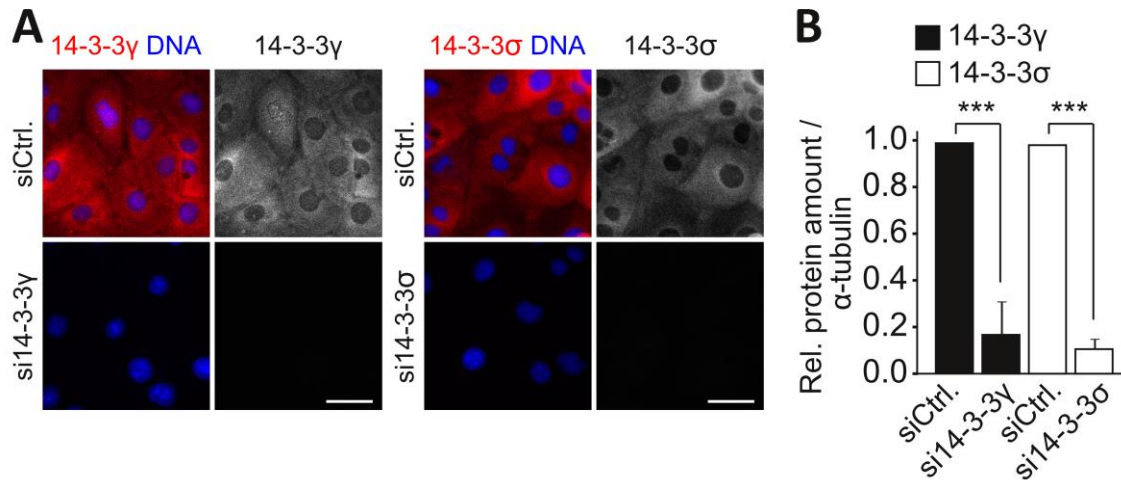


Fig. 38I Quantification of knockdown efficiencies of 14-3-3 γ - and 14-3-3 σ -siPools.

(A) Mouse keratinocytes were transfected with non-targeting (siCtrl.), 14-3-3 γ - or 14-3-3 σ -directed siRNAs, grown for 24 hours in HCM and processed for immunofluorescence after formaldehyde fixation to preserve 14-3-3 localization and stained for 14-3-3 γ or 14-3-3 σ as indicated (in red). DNA was stained with Hoechst 33342 (in blue). To compare knockdown efficiencies, all images were collected with equal hardware settings. Scale bar: 50 μ m. (B) Western blot based quantification of 14-3-3 expression in 14-3-3 γ - and 14-3-3 σ -depleted keratinocytes. α -tubulin was used as loading control. The bars show relative protein amounts normalized to α -tubulin (mean \pm SD, n=4). Statistical significance was determined by a two-tailed Student's *t*-test. *** $P \leq 0.0005$. Ctrl., control; HCM, high calcium medium; Rel., relative.

To further label PKP1 and PKP3 in 14-3-3 γ - and 14-3-3 σ -depleted cells, mouse keratinocytes were transfected with non-targeting, 14-3-3 γ - or 14-3-3 σ -directed siRNAs, cultured for 24 h in HCM to induce cell contact formation and fixed with methanol as formaldehyde fixation reduces the accessibility of PKPs epitopes, which lie in the center of the tightly packed desmosomal plaque. Depletion of 14-3-3 γ had minor effects and correlated with a strong cell border localization of PKP1 (Fig. 39A, B and 57A, C in appendix) and PKP3 accumulation at tricellular contact sites (Fig. 39A, C and 57B, C in appendix). In 14-3-3 σ knockdown cells, changes in PKP1 and PKP3 distribution were not significant, although 14-3-3 γ and 14-3-3 σ had opposing effects and induced significant changes in PKP1 and 3 distribution, when compared with each other (Fig. 39 and 57 in appendix). Taken together, these data suggest that 14-3-3 γ and 14-3-3 σ target desmosomal proteins to regulate their localization as well as intercellular cohesion of keratinocytes.

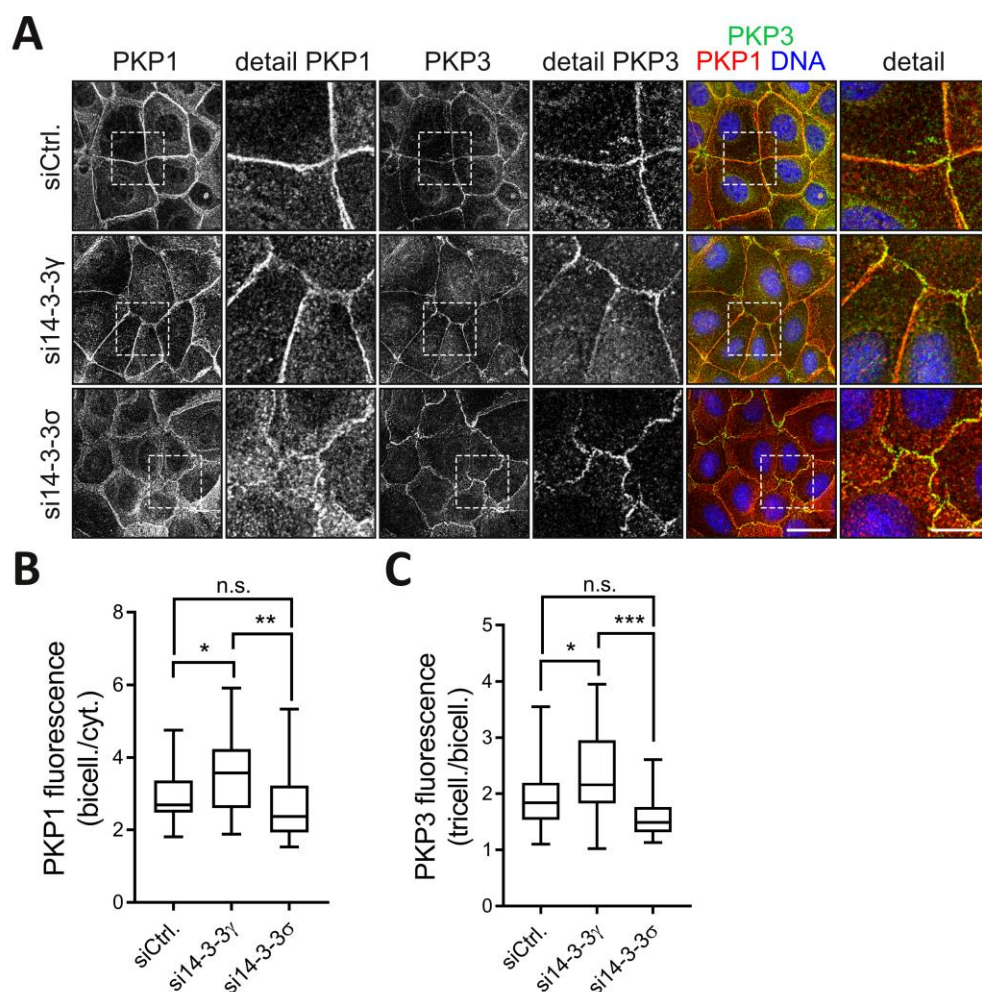


Fig. 39| Depletion of 14-3-3 σ primarily affects the localization of PKP3 at tricellular contacts.

(A) Mouse keratinocytes were transfected with non-targeting (siCtrl.), 14-3-3 γ , or 14-3-3 σ -directed siRNAs, grown for 24 hours in HCM, methanol-fixed and co-immunostained with antibodies against PKP1 and PKP3 (in red). Hoechst 3342 staining served as nuclear marker (in blue). Depicted are confocal images of single optical sections. To compare fluorescence intensities, all images were collected with equal hardware settings. Scale bar: 50 μ m, detail: 10 μ m. Fluorescence intensities of PKP1 (B) and PKP3 (C) were determined using ImageJ by measuring a segment of equal length and width across 30 individual bicellular or tricellular contacts (see also Fig. 57 in appendix). For each line scan the mean junctional (bicellular, tricellular) value was normalized to the mean cytoplasmic value. The boxplots depict the enrichment of PKP1 at bicellular contacts (B) or the ratio of PKP3 (C) at tricellular vs. bicellular contacts and display the 1st to 3rd quartile with full range of variation (whiskers from minimum to maximum). Statistical significance was determined by 1-way ANOVA testing (Tukey's multiple comparison test). n.s. = not significant, * $P \leq 0.05$, ** $P \leq 0.005$, *** $P \leq 0.0005$. bicell., bicellular; ctrl., control; cyt., cytoplasm; HCM, high calcium medium; PKP, plakophilin; tricell., tricellular.

14-3-3 proteins interact with PKPs in a phosphorylation-dependent manner

In order to identify desmosomal interaction partners of 14-3-3-proteins, GFP-14-3-3 γ and GFP-14-3-3 σ were immunoprecipitated from mouse keratinocytes (Fig. 40A). 14-3-3 γ co-precipitated with PKP1. A weak interaction with DSP was also detected, although this could represent an indirect association via PKP1. 14-3-3 σ co-precipitated preferentially with PKP3 in agreement with a previous report (Roberts et al., 2013), but in addition revealed a weaker association with PKP1.

Since 14-3-3 proteins typically interact with their targets by binding to specific phospho-serine/threonine motifs, it was asked whether the interaction of 14-3-3 with PKPs was phosphorylation-dependent. Since Roberts et al. identified S285 as essential for the 14-3-3 σ -PKP3 complex formation (Fig. 8), PKP1 was analyzed in this study. Based on the findings that PKP1 is a substrate of the Akt2 kinase (Fig. 53 in appendix), constitutive active myr-Akt2 was overexpressed in serum-starved HEK293 cells to induce PKP1 phosphorylation. The precipitate was analyzed using an anti-phospho-PKA substrate antibody that was expected to recognize S118 located in the 3th phosphorylation motif of PKP1 (Fig. 27A and 40B).

In cells transfected with active Akt2, PKP1 immunoprecipitates were detected by the phospho-PKA-motif antibody (Fig. 40C) indicating that Akt2 modified PKP1 at S118. Additionally, a band shift was observed for PKP1 upon co-transfection with Akt2 suggesting that the kinase or downstream kinases phosphorylated PKP1. The activity of Akt2 was confirmed by increased phospho-eIF4B, a well-known target of the Akt-dependent signaling pathway. The complete absence of 14-3-3 proteins in immunoprecipitates from serum-starved cells suggests that PKP1 phosphorylation by Akt-signaling is necessary for 14-3-3 binding (Fig. 40C).

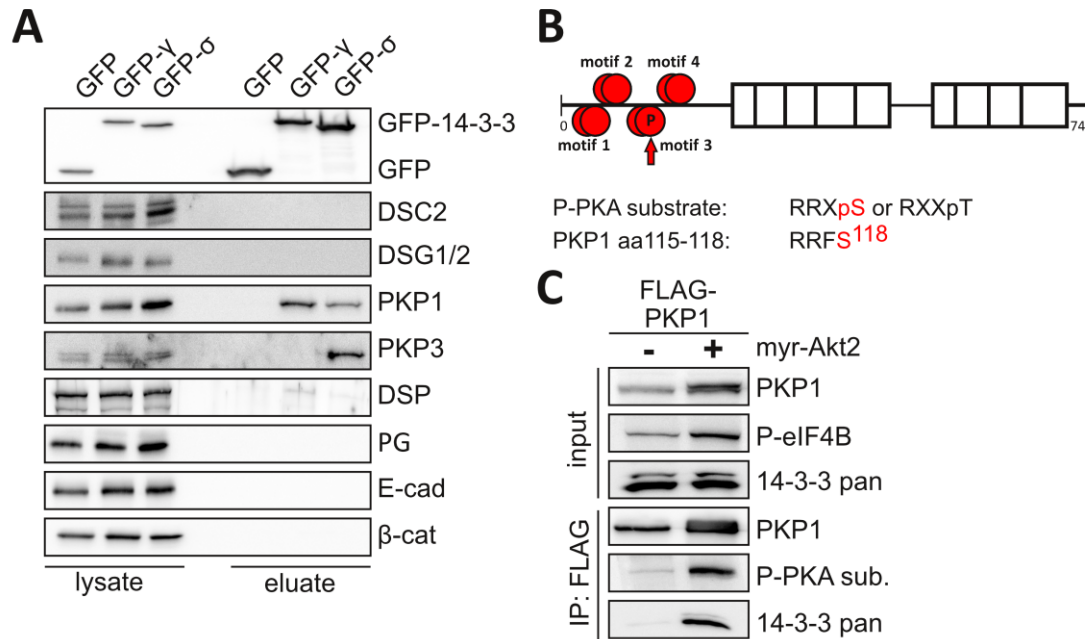


Fig. 40| Growth factor signaling affects the PKP1-14-3-3 association.

(A) GFP-14-3-3 γ , GFP-14-3-3 σ , or GFP were precipitated using GFP-trap agarose and probed for interactions with the indicated proteins. (B) Schematic protein structure of PKP1 illustrating the four phosphorylation motifs identified by peptide microarrays (see also Fig. 53A in appendix). Only motif three corresponds to a phosphorylation site recognized by a PKA phospho-substrate antibody, which detects RRXpS or RXXpT. (C) Lysates of serum-starved HEK293 cells expressing FLAG-PKP1 with or without active myr-Akt2 as indicated were used for FLAG-Co-IPs. Phospho-eIF4B confirms phosphorylation of Akt targets. PKP1 phosphorylation at S118 was determined using a phospho-PKA-substrate antibody. aa, amino acid; cad, cadherin; cat, catenin; DSC, desmocollin; DSG, desmoglein; DSP, desmoplakin; IF, eukaryotic initiation factor; GFP, green fluorescent protein; IP, immunoprecipitation; myr, myristoyl; P, phospho; PG, plakoglobin; PKP, plakophilin.

To validate these findings, the effects of 14-3-3 expression in keratinocytes kept in serum-free versus serum-containing medium were compared. 14-3-3 proteins were overexpressed in PKP1-KO keratinocytes expressing PKP1-GFP to facilitate PKP1 detection at desmosomes and in the cytoplasm at the same time, but avoiding artefacts due to PKP1 overexpression. Whereas PKP1-GFP distribution was essentially unaltered by 14-3-3 γ or 14-3-3 σ in serum-starved cells, 14-3-3 γ overexpression induced a redistribution of PKP1-GFP into the cytoplasm in keratinocytes cultured in the presence of growth factors confirming the observations for endogenous PKP1 (Fig. 41 and 58 in appendix). These data support the conclusion that the PKP1-14-3-3 γ interaction depends on PKP1 phosphorylation.

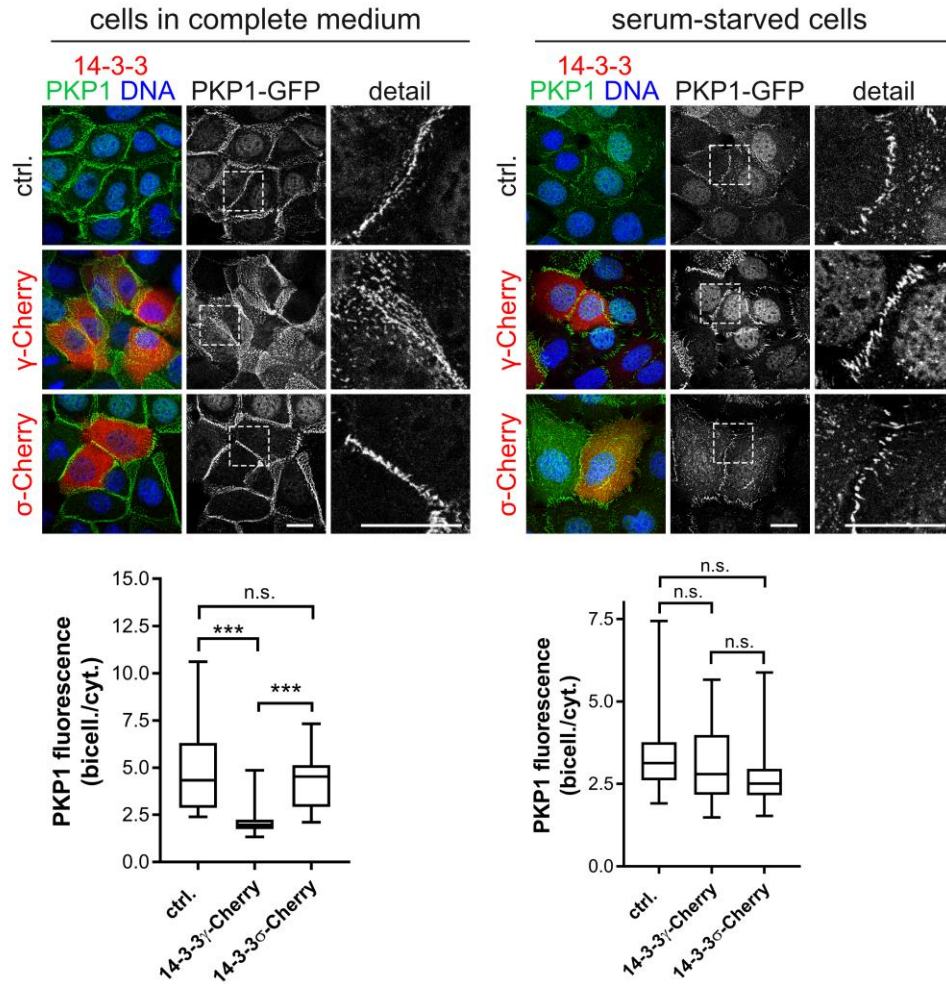


Fig. 41| Growth factor signaling affects the localization of PKP1 via 14-3-3 γ .

PKP1-KO keratinocytes expressing PKP1-GFP were transfected with the indicated 14-3-3-Cherry constructs, followed by serum-stimulation (left) or -starvation (right). Depicted are confocal images of single optical sections. To compare fluorescence intensities, all images were collected with equal hardware settings. Scale bars: 20 μ m. PKP1-GFP distribution was quantified using ImageJ by measuring fluorescence intensities of segments of equal length and width across 30 individual bicellular contacts (see also Fig. 58). For each line scan the mean bicellular value was normalized to the mean cytoplasmic value. The boxplots depict the enrichment of PKP1-GFP at bicellular contacts (left: serum-stimulated cells, right: serum-starved cells) and display the 1st to 3rd quartile with full range of variation (whiskers from minimum to maximum). Statistical significance was determined by 1-way ANOVA testing (Tukey's multiple comparison test). *** $P \leq 0.0005$, n.s. = not significant. bicell., bicellular; ctrl., control; cyt., cytoplasm; GFP, green fluorescent protein; PKP, plakophilin.

14-3-3 γ and 14-3-3 σ differentially regulate adhesion via PKP1 and PKP3

The protein interaction studies suggest that 14-3-3 γ acts preferentially through PKP1 to regulate desmosomal adhesion, whereas 14-3-3 σ probably controls adhesive strength via PKP3. In order to test this more rigorously, the effects of 14-3-3 overexpression were compared in WT and PKP1-KO keratinocytes. DSP was used to identify desmosomes in both cell

lines. Compared to WT keratinocytes, PKP1-KO cells revealed a reduced DSP membrane association along with an increased cytoplasmic pool (Fig. 24C and 42A). This distribution was not altered by 14-3-3 γ expression, but improved after 14-3-3 σ overexpression. In contrast, DSP showed strong plasma membrane association in WT cells with or without 14-3-3 σ overexpression, but was redistributed to the cytoplasm by 14-3-3 γ overexpression (Fig. 42 and 59 in appendix).

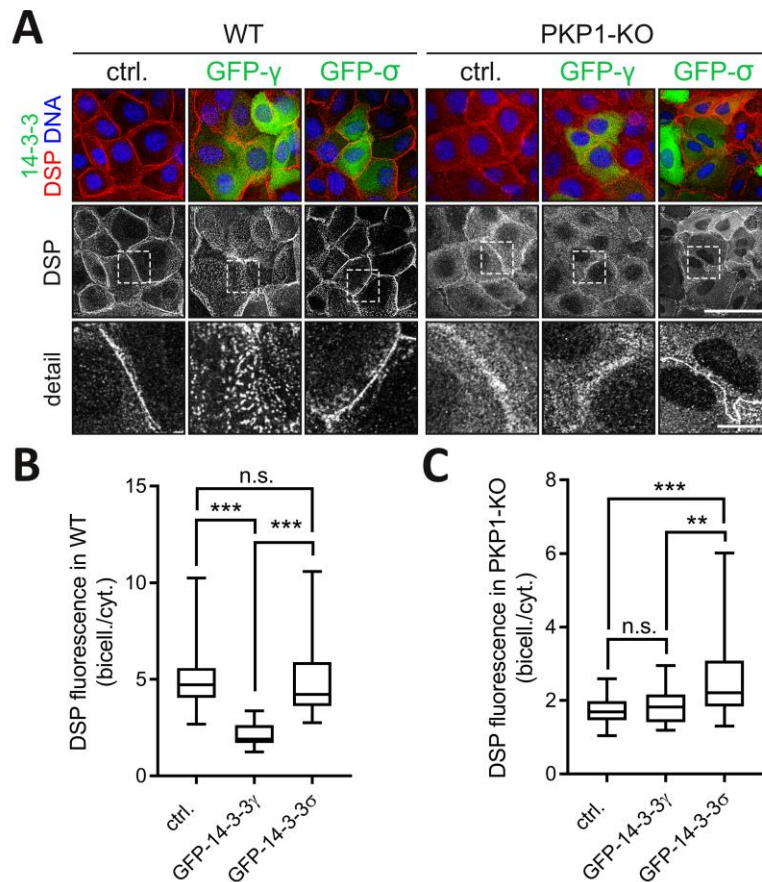


Fig. 42| 14-3-3 γ acts preferentially through PKP1 to regulate desmosomal adhesion.

(A) WT and PKP1-KO keratinocytes were transfected with the indicated GFP-14-3-3 constructs, grown for 24 hours in HCM and immunostained for DSP. Depicted are confocal images of single optical sections. To compare fluorescence intensities, all images were collected with equal hardware settings. Scale bar: 50 μ m, detail: 10 μ m. Fluorescence intensities of DSP in transfected WT or PKP1-KO were determined by measuring a segment of equal length and width across 30 individual bicellular contacts for each condition (see also Fig. 59 in appendix). The boxplots depict the enrichment of DSP at bicellular contacts in WT (B) or PKP1-KO (C) cells and display the 1st to 3th quartile with full range of variation (whiskers from minimum to maximum). Statistical significance was determined by 1-way ANOVA testing (Tukey's multiple comparison test, n=30). ** $P \leq 0.005$, *** $P \leq 0.0005$, n.s. = not significant. bicell., bicellular; ctrl., control; cyt., cytoplasm; DSP, desmoplakin; GFP, green fluorescent protein; HCM, high calcium medium; KO, knockout; WT, wildtype.

In order to further validate the conclusion that 14-3-3 γ acts primarily through PKP1, the intercellular cohesion of WT and PKP1-KO cells was compared by dispase assay. As shown in Fig. 24D, intercellular cohesion is considerably reduced in PKP1-KO keratinocytes. Overexpression of 14-3-3 γ destabilized the WT keratinocyte sheet (Fig. 36A, B), but did not further weaken intercellular cohesion in PKP1-KO cells (Fig. 43). However, 14-3-3 σ slightly stabilized intercellular cohesion even in the absence of PKP1 indicating that this function does not critically depend on PKP1 (Fig. 43). To confirm the assumption that 14-3-3 σ acts primarily via PKP3, PKP3-KO keratinocytes were also used in the dispase assay. Knockdown of 14-3-3 σ decreased mechanical resistance of WT keratinocytes (Fig. 36A, B), but had no effect in PKP3-KO keratinocytes (Fig. 43). Taken together, these data indicate that the role of 14-3-3 γ in destabilizing keratinocyte cohesion depends on PKP1, whereas the impact of 14-3-3 σ on desmosome adhesive function appears primarily mediated by PKP3.

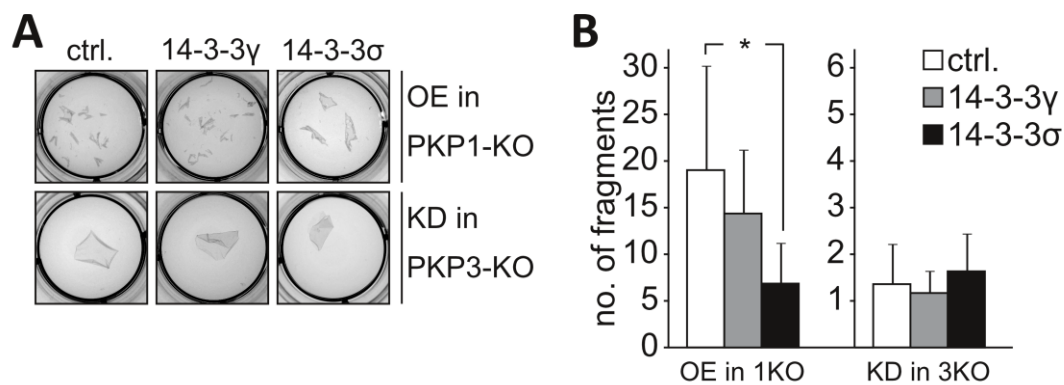


Fig. 43| Distinct PKP-14-3-3 complexes regulate intercellular cohesion of keratinocytes.

Dispase assays of PKP1-KO keratinocytes after overexpression (OE) of GFP (ctrl.), GFP-14-3-3 γ , or GFP-14-3-3 σ (upper row) and PKP3-KO keratinocytes after transfection of non-targeting (ctrl.), 14-3-3 γ -, or 14-3-3 σ -directed siRNAs (lower row). Representative images of epithelial sheets after application of mechanical stress (PKP1-KO 10 min, PKP3-KO 60 min) are shown. (B) Quantification of the number of fragments (mean \pm SD, n=8). Statistical significance was determined by 1-way ANOVA testing (Tukey's multiple comparison test). * $P \leq 0.05$. ctrl., control; GFP, green fluorescent protein; KD, knockdown; KO, knockout; no., number; OE, overexpression; PKP, plakophilin.

Insulin/Akt2-dependent phosphorylation is required for the PKP1-14-3-3 γ association

Studies by Roberts et al. revealed that S285-phosphorylation was required for the 14-3-3 σ -PKP3 interaction (Roberts et al., 2013). As PKP1 is regulated by insulin/Akt2 signaling (chapter 3.2.), it was examined whether this signaling pathway also promotes the PKP1-14-3-3 γ interaction. Prediction tools (<http://scansite.mit.edu>) identified pS54, pS118, pS119, pS155, and pT171 as putative 14-3-3 binding motifs (Fig. 44A). Whereas S54, S118, S119, and

T171 were directly phosphorylated by Akt2 *in vitro* (Fig. 53A in appendix), S155 phosphorylation was only observed in cells after myr-Akt2 expression suggesting that S155 is an indirect target of Akt2 signaling (experiment by Dr. Annika Wolf, not shown). Serine to alanine mutants of all predicted 14-3-3 binding sites of PKP1 were expressed in HEK293 cells that were either co-transfected with a control plasmid or a plasmid expressing constitutive active myr-Akt2. Cell extracts were then incubated with GST-14-3-3 γ to analyze whether phosphorylation of these sites is essential for PKP1-14-3-3 γ interaction. The PKP1 S155A mutant almost completely abolished the interaction with 14-3-3 γ , S118/119A reduced the association, whereas S54A and T171A still bound to 14-3-3 γ and complex formation was increased by Akt2-expression (Fig. 44B). This identifies PKP1-S155 as an essential binding site for 14-3-3 γ . S118/119 might contribute to binding by providing a second binding site for a 14-3-3 dimer, which could enhance complex stability.

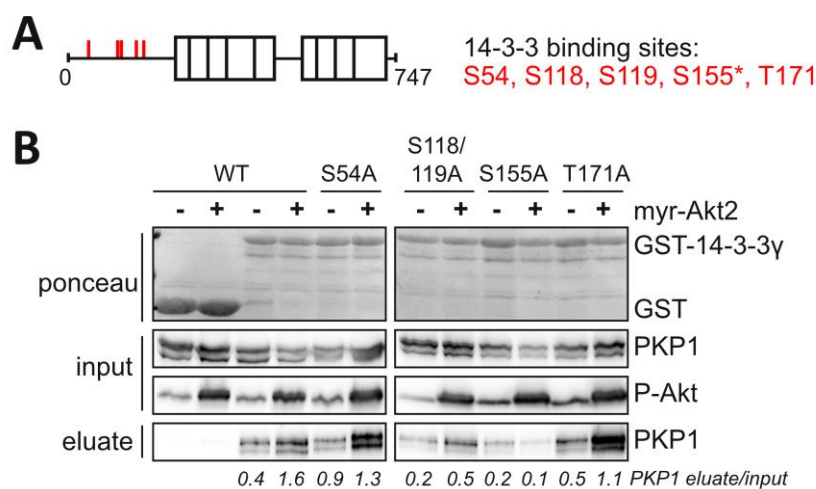


Fig. 44| S155 phosphorylation is essential for 14-3-3 γ binding to PKP1.

(A) Putative 14-3-3 binding sites in the PKP1 N-terminal domain as revealed by Scansite Motif Scan. S155* indicates an indirect phosphorylation site of Akt2. (B) PKP1-WT and mutants of the corresponding serine/threonine residues were co-expressed in HEK293 cells with and without constitutive active myr-Akt2 as indicated and probed for their interaction with GST-14-3-3 γ . GST was used as control. Phospho-Akt confirms the presence of active Akt2. PKP1 amounts in the eluate relative to the input are given below the Western blot. A, alanine; GST, glutathione s-transferase; myr, myristoyl; PKP, plakophilin; S, serine; T, threonine; WT, wildtype.

14-3-3 γ interferes with desmosomal adhesion by sequestering PKP1 in the cytoplasm

Having identified PKP1 as a binding partner of 14-3-3 γ that is regulated by insulin/Akt signaling, it raised the question, how this interaction affects desmosomal adhesion at the mechanistic level. 14-3-3 proteins can regulate target proteins by controlling their intracellu-

lar localization (Aghazadeh and Papadopoulos, 2016, Obsilova et al., 2014). In fact, a redistribution of PKP1 from lateral membranes to the cytoplasm was observed upon 14-3-3 γ overexpression (Fig. 37A, B).

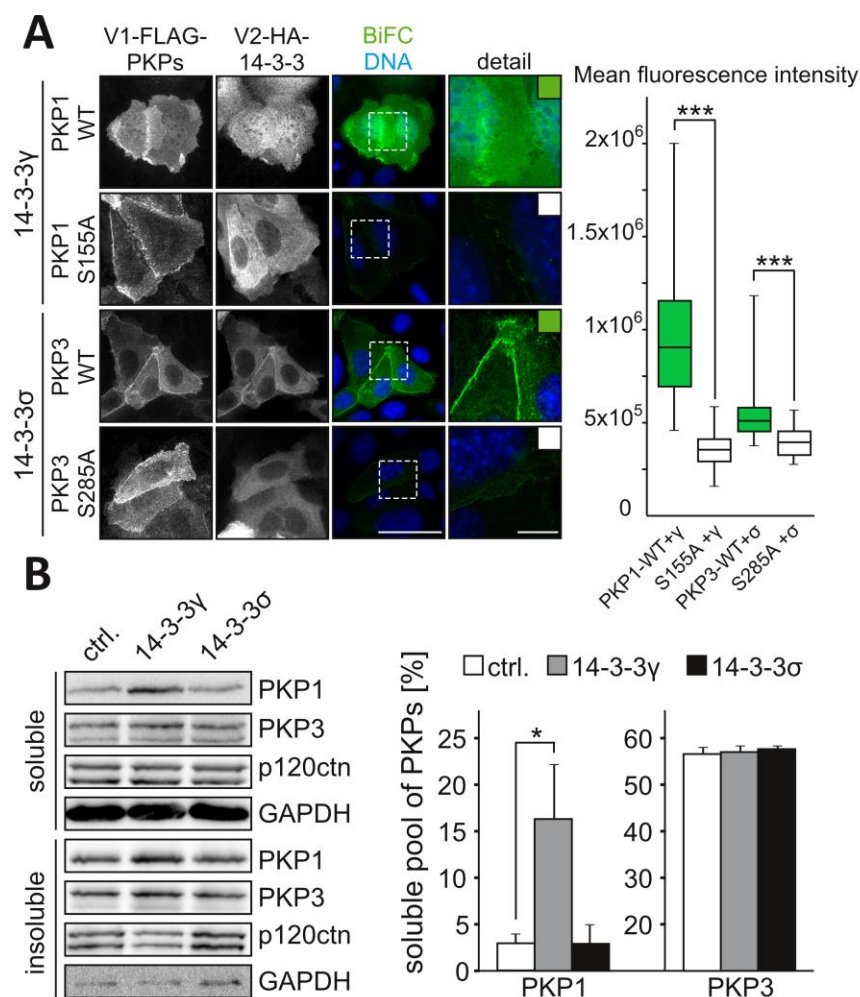


Fig. 45I 14-3-3 γ modulates the solubility of PKP1.

(A) Keratinocytes were co-transfected with BiFC-constructs as indicated. Co-transfected cells were identified by staining for the FLAG and HA epitope. Nuclei were stained with Hoechst 33342 (in blue). To compare BiFC fluorescence intensities, all images were collected with equal hardware settings. Scale bar: 50 μ m, detail: 10 μ m. Boxplots (right) depict the mean BiFC intensities of co-transfected keratinocytes ($n=30$) and display the 1st to 3rd quartile with full range of variation (whiskers from minimum to maximum). Statistical significance was determined by a two-tailed Student's *t*-test. *** $P \leq 0.0005$. (B) Triton X-100 soluble and insoluble fractions of keratinocytes stably expressing GFP-14-3-3 γ , GFP-14-3-3 σ or GFP (ctrl.) were analyzed by Western blot. GAPDH was used as loading control for the soluble fraction. Diagrams on the right show the relative proportion of PKP1 and PKP3 in the soluble fractions (mean \pm SD, $n=3$). Statistical significance was determined by 1-way ANOVA testing (Tukey's multiple comparison test). ** $P \leq 0.005$. A, alanine; BiFC, bimolecular fluorescence complementation; ctrl., control; GAPDH, glyceraldehyde 3-phosphate dehydrogenase; p120ctn, p120-catenin; PKP, plakophilin; S, serine; V1/2, venus-1/2; WT, wildtype.

To validate this, the subcellular localization of the 14-3-3 γ -PKP1 complex was examined using bimolecular fluorescence complementation (BiFC). Venus2-14-3-3 γ overexpression confirmed the shift of PKP1-WT from desmosomes to the cytoplasm (Fig. 45A). Moreover, the complex primarily localized in the cytoplasm as identified by the BiFC signal. The BiFC signal was almost completely abolished, when 14-3-3 γ was co-expressed with the PKP1-S155A mutant, again confirming that phosphorylation of this residue is essential for the association with 14-3-3 γ and cytoplasmic accumulation of PKP1. In contrast, the 14-3-3 σ -PKP3 complex primarily localized at the plasma membrane suggesting that complex formation does not interfere with PKP3 incorporation into desmosomes. The PKP3-S285A mutant failed to produce a BiFC signal (Fig. 45A), confirming previous findings that this mutant precludes a 14-3-3 σ interaction (Roberts et al., 2013).

To further validate the effect of the 14-3-3 γ -PKP1 interaction on its subcellular localization, the soluble versus insoluble pools of PKPs were quantified (Fig. 45B). 14-3-3 γ overexpression significantly increased the cytosolic fraction of PKP1, but did not affect PKP3 solubility. In contrast, 14-3-3 σ overexpression did not alter the solubility of either PKP. Taken together, these data indicate that PKP1's subcellular localization is regulated by 14-3-3 γ in a signaling-dependent manner, whereas PKP3's distribution between the cytoplasm and the plasma membrane was unaltered.

14-3-3 proteins differentially modulate PKP dynamics at the desmosome

If 14-3-3 γ retains PKP1 in the cytoplasm, its replacement rate at the desmosome should be decreased. To test this hypothesis, FRAP was measured in PKP1-GFP expressing keratinocytes. In order to avoid artefacts caused by imbalanced PKP1 overexpression, PKP1-KO keratinocytes expressing PKP1-GFP were used and PKP1 dynamics were examined in control-transfected as well as 14-3-3 γ - or 14-3-3 σ -depleted cells by FRAP (Fig. 46A). Knockdown of both, 14-3-3 γ and 14-3-3 σ increased PKP1 dynamics at the desmosome despite their opposing effects on intercellular cohesion (Fig. 36).

In a similar approach PKP3-KO keratinocytes expressing PKP3-GFP were used and the effect of 14-3-3 γ and 14-3-3 σ depletion on PKP3 dynamics was analyzed. As reported before, desmosomal PKP3 is more dynamic than PKP1 (Keil et al., 2016). Whereas 14-3-3 γ had no significant effect on PKP3-GFP exchange rates at the desmosome, 14-3-3 σ depletion slightly reduced PKP3-GFP dynamics (Fig. 46B).

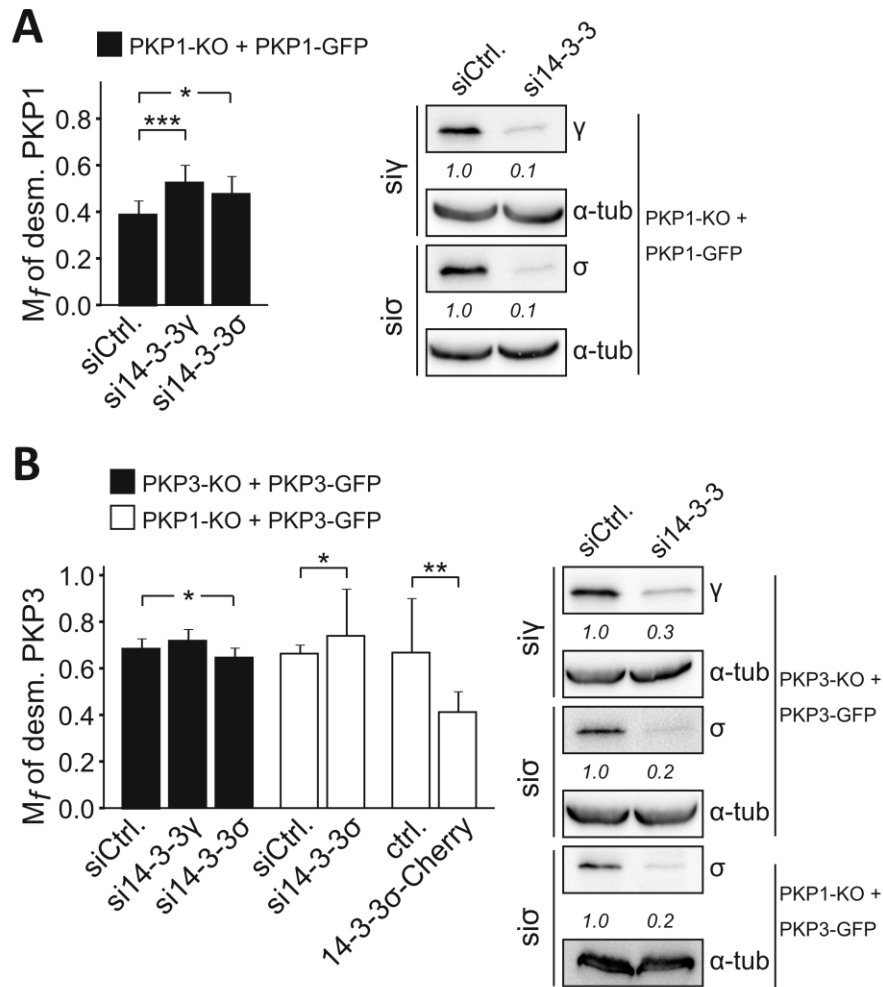


Fig. 46| 14-3-3 proteins differentially modulate PKP dynamics.

(A) PKP1-KO keratinocytes expressing PKP1-GFP (PKP1-KO + PKP1-GFP) or (B) PKP3-GFP (PKP1-KO + PKP3-GFP) and PKP3-KO keratinocytes expressing PKP3-GFP (PKP3-KO + PKP3-GFP) were transfected with the indicated siRNAs or 14-3-3 σ expression vector, grown for 24 hours in HCM and used for FRAP experiments. The diagrams show the mobile fractions (mean \pm SD, $n \geq 10$ cells) of desmosomal PKP1-GFP (A) or PKP3-GFP (B) for the indicated conditions. Statistical significance was determined using a two-tailed Student's *t*-test. * $P \leq 0.05$, ** $P \leq 0.005$, *** $P \leq 0.0005$. To control knockdown efficiencies of 14-3-3 γ and 14-3-3 σ siRNAs in keratinocyte cell lines, total cell extracts were analyzed by Western blot using the indicated antibodies (on the right). α -tubulin served as loading control. Depicted are images of representative Western blots. The mean relative 14-3-3 protein amount is given below the respective image. α -tub, α -tubulin; Ctrl., control; desm., desmosomal; FRAP, fluorescence recovery after photobleaching; GFP, green fluorescent protein; HCM, high calcium medium; KO, knockout; M_f , mobile fraction; PKP, plakophilin.

This is in apparent contradiction to the previous report, where reduced 14-3-3 σ expression lead to an increase in PKP3 dynamics (Roberts et al., 2013). Since PKP3 localization at tricellular contacts depends on PKP1, it was further examined whether the contradictory results depended on PKP1 expression. In order to mimic a PKP1-free situation, PKP3-GFP dynamic was analyzed in PKP1-KO keratinocytes. In fact, 14-3-3 σ depletion slightly increased PKP3 dynam-

ics, whereas 14-3-3 σ overexpression significantly reduced PKP3 exchange rates at lateral desmosomes in the absence of PKP1 (Fig. 46B), in full agreement with the results reported previously (Roberts et al., 2013). In summary, these data indicate that 14-3-3 proteins differentially modulate PKP dynamics at the desmosome.

Taken together, in this chapter it was shown that 14-3-3 γ and 14-3-3 σ have opposing effects on desmosomal adhesion in mouse keratinocytes by exerting distinct preferences for PKP1 and PKP3: a destabilizing effect of 14-3-3 γ was mediated via PKP1, whereas 14-3-3 σ preferentially targeted PKP3 to stabilize intercellular cohesion. These findings identify isoform-specific interactions of PKPs and 14-3-3 proteins in the control of desmosome stability.

4 DISCUSSION

PKP1 is considered as a multifunctional protein that localizes in several cellular compartments. A function of PKP1 in regulating desmosomal adhesion is well established and supported by *in vitro* studies (Hatzfeld et al., 2000, Kowalczyk et al., 1999, South, 2004, South et al., 2003) as well as by the phenotype of a genetic skin disease (EDSFS, see page 11) caused by PKP1 mutations (McGrath and Mellerio, 2010). A cytoplasmic function of PKP1 in the regulation of translation and proliferation has also been reported (Wolf and Hatzfeld, 2010). In the context of this study it was examined whether phosphorylation of PKP1 modifies the equilibrium between its desmosomal and cytoplasmic functions. Indeed, phosphorylation of PKP1 affects the subcellular localization of PKP1. And it was quite surprising that these modifications affect not only the intracellular distribution of PKP1, but exert a major effect on intercellular adhesion, cell migration, proliferation rates, and significantly affect anchorage-independent cell growth. Moreover, the finding that PKP1 phosphorylation promotes binding to 14-3-3 proteins regulating its intracellular localization and exchange rates at the desmosome obtained new insights regarding fine-tuning of desmosomal adhesive strength. In addition, the contribution of PKP1 in differentially regulating desmosome function was studied in PKP1-null mice and identified PKP1 as a protein essential for growth control and integrity of the epidermis. The outcome of this study will be discussed in the following chapters. The compiled summarizing models will illustrate the results and serve as working hypotheses for open questions.

4.1. The role of PKP1 in skin homeostasis

The epidermis is unique with respect to the complexity of desmosome composition (Yin and Green, 2004). However, isotype-specific functions and differentiation-specific expression of desmosomal proteins remain incompletely understood. Gene ablation in mice has been used to establish the role of several desmosomal proteins *in vivo*. In this study it was shown that homozygous PKP1-null mice die postnatally, reveal a reduced birth weight (Fig. 11B) as well as fragile skin (Fig. 12A, B). Desmosome number and size were significantly decreased (Fig. 15), despite the upregulation of most desmosomal proteins (Fig. 18A-C). Additionally, PKP1-KO mice have an impaired inside-out skin barrier (Fig. 17B) caused by disturbed TJs function (Fig. 25). This finding is of particular interest, because it uncovered a role of PKP1 in TJ function that was hitherto unknown.

As PKP2 is the only PKP in the heart, the ablation of the *Pkp2* gene in mice resulted in lethal alterations in heart morphogenesis and stability at mid-gestation caused by dissociation of DSP from the plaques of desmosomes that connect the cardiomyocytes and forms granular aggregates in the cytoplasm (Grossmann et al., 2004) indicating that PKP2 is an essential architectural component of the developing heart. In contrast, loss of PKP3 caused a mild phenotype with defective hair morphogenesis and an increased susceptibility for dermatitis (Sklyarova et al., 2008). Despite the slight upregulation of PKP3 in PKP1-null epidermis (Fig. 18A-C), PKP3 is insufficient to compensate for the lack of PKP1, strongly suggesting that PKP1 and PKP3 fulfill non-overlapping functions in the regulation of intercellular adhesion and growth control. In conclusion, the differences in phenotypes between PKP1, 2, and 3 knockout mice may be explained by their tissue-specific expression and elucidates that at least one PKP is required for stable intercellular adhesion.

The skin fragility (Fig. 11A) along with severely disturbed desmosomes underscores the importance of PKP1 for desmosomal adhesion in the skin, in agreement with previous findings (McGrath et al., 1997, McGrath and Mellerio, 2010) based on a human skin disease. Several features of the PKP1-null mice closely resemble the phenotype of patients with PKP1 mutations causing EDSFS (chapter 2.2.). Prevalence of EDSFS is unknown, because only a few patients carrying a variety of different mutations have been reported (Table 21). As mentioned in the introduction, most PKP1 mutations lie in splice donor or acceptor sites, which may result in exon skipping or cryptic splicing rather than complete ablation of the protein (McGrath and Mellerio, 2010, Sprecher et al., 2004). In general, mutations that do not completely abolish PKP1 expression are associated with a milder phenotype (Hamada et al., 2002). In one patient, a heterozygous Y71X mutation at the start of exon 2 combined with a splice-site mutation of exon 2 was identified (McGrath, 1999), thus retaining only exon 1, as described in this study for the PKP1-null mice.

At the ultrastructural level, the PKP1-KO mice closely mimic the phenotype of PKP1 mutant carriers with acantholysis and detachment of the upper epidermal layers (Fig. 12A), but no involvement of the heart (not shown). Electron microscopy of patient biopsy samples and immortalized patient keratinocytes showed smaller and sparse desmosomes with an increase in cytoplasmic DSP (McMillan et al., 2003, South et al., 2003) similar to my observations (Fig. 15 and 18A-C). Moreover, upregulation of DSG1 and PKP3 with increased membrane association was observed in human mutant biopsy samples and in PKP1-KO tissue samples (Fig.

18A-C) indicating a conserved mechanism of compensatory regulation. However, the upregulation of PKP2 as observed in human biopsy samples (McMillan et al., 2003) was not detected in PKP1-null mice (Fig. 18D). This lack of compensation by PKP2 might contribute to the early death of the PKP1-KO mice, whereas several humans and dogs carrying PKP1 mutations survived despite significant morbidity (Bergman and Sprecher, 2005, McGrath and Mellerio, 2010, Olivry et al., 2012).

Mice lacking PKP1 exhibited all stages of terminal differentiation, although mild changes in the expression and localization of epidermal differentiation marker were examined. Keratins are thought to contribute to the morphological transformation of keratinocytes as they move upwards in the epithelium, such as through their intrinsic bundling properties, their association with filaggrin and their crosslinking to desmosomes and cornified envelopes (Candi et al., 2005, Lee and Coulombe, 2009, Simpson et al., 2011). Keratins 5 and 14 revealed an increased expression (Fig. 20A) and extended localization towards suprabasal layers in PKP1-null epidermis compared to WT (Fig. 19) indicating that the coordinated expression and interaction of desmosomal proteins and keratins are interdependent and that the differentiation-specific isotype composition of the cytoskeleton and desmosomes is a major determinant of adhesive strength. In addition, keratin 17 expression was increased in PKP1-null skin (Fig. 19 and 20). This finding is consistent with the observation that induction of keratin 17 occurs rapidly during barrier disruption and tissue regeneration (Mazzalupo et al., 2003). Besides keratins, loricrin and involucrin are important proteins facilitating terminal differentiation of the epidermis and formation of the skin barrier (Segre, 2006, Steinert and Marekov, 1995). However, loricrin expression was only slightly, non-significantly upregulated in PKP1-null skin and involucrin remained unaffected in PKP1-null skin (Fig. 21B, C). Corneocytes consists mainly of keratins aggregated by filaggrin, which is cross-linked into a mechanically robust cornified cell envelope (Kezic and Jakasa, 2016). Filaggrin degradation products account in part for the maintenance of acidic pH of the *stratum corneum* and water-holding capacity, both essential for the epidermal barrier (Kezic and Jakasa, 2016). However, also profilaggrin to filaggrin processing pattern appeared similar in PKP1-KO mice compared to WT (Fig. 21D). Taken together, the overall epidermal differentiation is not PKP1-dependent, although the coordinated interplay between desmosomal proteins and keratin filaments is essential for the homeostasis and proper function of the skin.

Moreover, this study revealed the important finding that PKP1 affects TJ assembly and function (Fig. 16C, D and 25) and thus the liquid barrier of the epidermis (Fig. 16B and 17B) and transepithelial electrical resistance in keratinocytes (Fig. 25D). The high water loss (Fig. 16B) and postnatal lethality resulting from compromised TJs supports the involvement of TJs in the barrier defect in PKP1-KO mice (Furuse et al., 2002). Loss of PKP1 resulted in an altered localization of TJ proteins (Fig. 16C), decreased OCLN expression (Fig. 25A, B) as well as delayed TJ assembly (Fig. 25C). Considerably less is known regarding crosstalk between TJs and desmosomes. A study in the intestinal epithelium documented a localization of the TJs protein JAM-C at the desmosome and proposed JAM-C's involvement in neutrophil transepithelial migration at this site (Zen et al., 2004). An interconnection between desmosomes and TJs is further supported by ultrastructural analyses that showed an extended subapical system integrating desmosomes and TJ structures in the *stratum corneum* (Schluter et al., 2004). A report by Lie et al. (2010) showed that DSG2 associated with tyrosine kinase c-Src. Interestingly, simultaneous knockdown of DSG2 and DSC2 by RNAi led to the relocation of c-Src from the Sertoli cell surface to the cytoplasm suggesting that DSG2 is a docking site for c-Src (Lie et al., 2010). Concurrent with the altered localization of c-Src, a decrease in the integrity of the TJ barrier was noted, presumably resulting from the disruptive effects of c-Src on ZO-1 (Kale et al., 2003) as well as connexin-43-ZO-1 (Gilleron et al., 2008) interactions, which are critical for barrier dynamics (Li et al., 2009). As PKP1-null keratinocytes revealed a significantly decreased DSG1/2 expression (Fig. 24A, B), an impact on c-Src and thereby TJ functionality in keratinocytes could be one possibility. This assumption might be in good accordance with an emerging concept that desmosomes can serve as a platform for signal transduction pathways (Green and Simpson, 2007, Hatzfeld et al., 2014). In addition, Miyazaki et al. (2016) determined the role of PKP1 in tooth development and reported that PKP1 interacts with ZO-1. In agreement with the discontinuous distribution of ZO-1 in PKP1-KO epidermis (Fig. 16C), they showed that PKP1 knockdown disrupted the localization of ZO-1 in TJs and inhibited ameloblast differentiation (Miyazaki et al., 2016) suggesting that participation of PKP1 in early tooth morphogenesis controls ameloblast differentiation. Moreover, dental abnormalities have been reported in a few cases of EDSFS patients [(Abdalla and Has, 2014, Boyce et al., 2012, Hamada et al., 2002, Kashyap et al., 2015), Table 21]. However, the precise mechanism how PKP1 participates in TJ assembly remains to be studied.

In conclusion, this mouse model shows several functions of PKP1 *in vivo*: (1) it underscores its importance in intercellular adhesion in the suprabasal layers of the skin as described in patients, (2) it shows that PKP1 is essential for skin barrier function, and (3) it is compatible with the role of PKP1 in cell signaling and growth control, defects that have also been noted in patients and in postnatal survival. Therefore, this mouse model provides an excellent basis for unravelling the molecular mechanism underlying EDSFS. In addition, a conditional PKP1-KO will improve the understanding of the role of PKP1 in growth control, a function that is crucial in wound healing and epidermal carcinogenesis.

4.2. Post-translational regulation of PKP1 by insulin signaling

Preliminary results revealed that PKP1 is phosphorylated by Akt2 at four phosphorylation motifs in its N-terminal head domain. As post-translational modifications can modulate protein interactions and as a consequence control protein stability, transport, and localization and finally determine the function of the protein, PKP1's behavior was suggested to be affected by phosphorylation events. To ascertain the biological significance of the identified phosphorylation sites, PKP1 phosphosite-mutants were generated (Fig. 27B) and characterized by examining their intracellular localization, dynamic at the desmosome and their capacity to affect intercellular cohesion, proliferation, wound healing, and anchorage-independent growth.

The potential phosphorylation site (serine/threonine) was mutated to a phosphomimetic residue (glutamic acid) in the attempt to study the constitutively phosphorylated state. However, this approach has significant limitations. Some reports have shown prevented interaction between phospho-mimetic mutants and adapter proteins such as SH2-domain proteins (Zisch et al., 2000), and demonstrated that a glutamic acid residue cannot replace a phosphorylated amino acid (Dephoure et al., 2013). It also has to be mentioned that the phosphate group, with its large hydrated shell and its negative charge greater than 1, is chemically quite distinct from the negatively charge of glutamate, whose carboxyl side chains only contains a single negative charge and a smaller hydrated shell than phosphate (Hunter, 2012). In view of these limitations, the behavior of phospho-mimetic mutants has to be interpreted cautiously. However, acidic amino acids have been successfully used to mimic functions of a phosphorylated residue, e.g. to study Mek1 or eIF-2 α (Huang and Erikson, 1994, Kaufman et al., 1989, McKay and Morrison, 2007). Moreover, GST pulldown experiments were performed using PKP1-WT, PKP1M1-4A, and PKP1M1-4E mutants and DSP N-terminal peptide, DSG1 cyto-

plasmic domain as well as eIF4A (performed by Dr. Annika Wolf) and revealed that both PKP1 mutants were able to associate with all three proteins *in vitro* indicating that these PKP1 mutants were functional and not misfolded.

In this study it was shown that non-phosphorylatable PKP1 was enriched in desmosomes, whereas the phospho-mimetic mutants of PKP1 accumulated in the cytoplasm. Moreover, the impact of phosphorylation on the intracellular localization of PKP1 was conserved in several cell types (Fig. 28 and 54 in appendix). More importantly, PKP1M1-4E-expressing MCF-7 cells revealed a reduced intercellular adhesion compared to PKP1-WT- or M1-4A-expressing cells (Fig. 31A). On this basis, these findings provide strong evidence that unphosphorylated PKP1 preferentially localizes in desmosomes, thereby promoting desmosomal adhesion, whereas the phosphorylated form functions predominantly in the cytoplasm leading to decreased desmosomal adhesion. This indicates that PKP1's functions are regulated predominantly via its phosphorylation-dependent subcellular localization. The observation that desmosomal PKP1 stabilizes cell-cell adhesion is in good agreement with several previous reports showing that PKP1 contributes to keratinocyte cohesion by promoting desmosome formation via recruiting and clustering desmosomal proteins at the plasma membrane and within desmosomes (Bornslaeger et al., 2001, Hatzfeld, 2007, Hatzfeld et al., 2000, Kowalczyk et al., 1999, Smith and Fuchs, 1998, Wahl, 2005). Additionally, PKP1 has been associated with the formation of calcium-independent desmosomes, which exhibit increased intercellular adhesion strength (Garrod and Kimura, 2008, Keil et al., 2016, South et al., 2003). In normal tissues, desmosomes adopt this calcium-independent state, also referred to as hyperadhesion (Garrod et al., 2005, Kimura et al., 2007, Wallis et al., 2000). However, during regeneration and wound healing, desmosomal adhesion becomes calcium-dependent resulting in weaker intercellular cohesion allowing for tissue remodeling (Kimura et al., 2012, Wallis et al., 2000).

To elucidate the mechanism by which phosphorylation of PKP1 influences desmosome stability, the dynamic of PKP1 phosphosite mutants was analyzed by FRAP imaging resulting in considerably altered exchange rates of the non-phosphorylated versus the phospho-mimetic forms in the desmosome (Fig. 32A). Only the non-phosphorylatable mutant displayed a large immobile fraction in desmosomes in agreement with the enhancement of intercellular adhesion observed for this mutant (Fig. 31A). Modification of PKP1 could alter its turnover at the desmosome by modulating internalization and endocytic trafficking. Endocytosis is an important mechanism to counteract junction assembly to maintain junctional homeostasis and it

appears that dynamics of junctional complexes allows the rapid remodeling of these adhesive structures to adapt to various stimuli (Hong et al., 2010, Yap et al., 2007). Accordingly, endocytosis of the AJ protein E-cadherin (Fig. 1C) controls processes such as junction maintenance, cell movement, and polarity. The armadillo protein p120ctn regulates the rate of E-cadherin endocytosis as p120ctn binding prevents E-cadherin's internalization by blocking an E3 ligase that ubiquitinylates the E-cadherin cytoplasmic domain, targeting the complex to the endocytic machinery (Hartsock and Nelson, 2012, Xiao et al., 2005). In line with this, PKP1 stably associates with desmosomal cadherins, thereby promoting the high stability of epithelial sheets. In contrast, phosphorylation of PKP1 may disrupt the cadherin-PKP complex, which could regulate the rate of cadherin endocytosis, leading to increased PKP1 dynamic and thereby weakening intercellular cohesion. The finding that PKP1M1-4E does not associate with the DSG1 cytoplasmic tail using the BiFC approach (by Dr. Annika Wolf, not shown) supports this assumption. Although desmosome turnover is less well characterized, caveolin- or raft-dependent endocytic routes for desmosomal proteins have been reported (Brennan et al., 2012, Delva et al., 2008, Resnik et al., 2011, Stahley et al., 2014). Alternatively, the differential turnover of the PKP1 mutant proteins in the desmosome could reflect a modulation of the desmosome-cytoskeleton association.

Whereas un-phosphorylated PKP1 stabilizes cell adhesion in the desmosome, its phosphorylated form accumulated in the cytoplasm (Fig. 28, 29 and 54 in appendix), thereby reducing intercellular adhesion (Fig. 31A). The increased cytoplasmic pool presumably mediates an increase in mRNA translation by stimulating eIF4A (Wolf et al., 2010), resulting finally in enhanced cell proliferation (Fig. 33) and wound healing (Fig. 32B). Thus, phosphorylation of PKP1 switches its function from stabilizing intercellular adhesion to promoting cell proliferation, an important mechanism to ensure tissue integrity on the one hand and to allow for tissue remodeling during processes such as regeneration and wound healing on the other hand. In support, co-expression of PKP1 and a constitutively active Akt2 (myr-Akt2) induced relocalization of PKP1 to the cytoplasm (Fig. 30A). Akt kinase is an essential component of the PI3K pathway (Fig. 6). Its activity is stimulated by receptor tyrosine kinases and G-protein coupled receptors and tightly regulated, because it controls a broad spectrum of pro-growth and pro-survival activities (Bozulic and Hemmings, 2009, Meier and Hemmings, 1999). Consistently, stimulation of keratinocytes with insulin or IGF1 and thereby activation of Akt increased the cytoplasmic pool of endogenous PKP1 (Fig. 30B).

Insulin and IGF1 have been shown to be important mediators for skin function (Benoliel et al., 1997, Smola et al., 1998). Both hormones promote proliferation and migration of human and mouse keratinocytes. *In vitro* insulin is an essential component in the growth medium of human keratinocytes (Tsao et al., 1982) and when applied topically to skin excision wounds, it accelerated re-epithelialization and stimulated “maturation” of the healing tissue and these effects were dependent on the insulin receptor, but independent of EGFR (Liu et al., 2009). Consistently, EGF treatment showed no obvious change in the subcellular localization of endogenous PKP1 in keratinocytes (Fig. 30B). The fact that cells, which express the phospho-mimetic mutant, exhibit a significantly elevated wound healing (Fig. 32B) is supporting this conjecture. Concomitantly with this, PKP1M1-4E-expressing MCF-7 cells revealed a reduced intercellular adhesion compared to PKP1-WT- or M1-4A-expressing cells (Fig. 31A). Additionally, insulin stimulation reduced cell-cell adhesion similarly (Fig. 31B).

The data of this study suggest that PKP1 may be one critical effector of insulin/IGF1 signaling in the skin. Consistent with this, on the one hand PKP1 phospho-mimetic mutants stimulated proliferation (Fig. 33), whereas on the other hand proliferation was reduced in isolated PKP1-null keratinocytes (Fig. 26) and paw skin thickness was reduced in neonatal PKP1-null mice (Fig. 12C). Although a corresponding reduction in cell proliferation in the dorsal epidermis was not observed (Fig. 14), growth defects may be partially masked *in vivo* by growth factors that are secreted by the dermis (Povoa and Diniz, 2011). In support of a role of PKP1 in insulin/IGF1 signaling, the global deletion of either IGF1 or IGF1R lead to growth retardation and fragile skin (Liu et al., 1993, Powell-Braxton et al., 1993) and a keratinocyte-specific KO of IGF1R, insulin receptor, or both correlated with reduced proliferation of keratinocytes *in vitro* but not *in vivo* (Stachelscheid et al., 2008), as observed for the PKP1-KO mice.

Moreover, the finding that expression of the phospho-mimetic mutant of PKP1 in MCF-7 cells not only stimulated proliferation (Fig. 33), but also conferred the capacity of anchorage-independent growth (Fig. 34A) is of particular interest, because it suggests that the Akt2-mediated modification of PKP1 might play a role in tumorigenesis. Unregulated activation of the growth factor/Akt pathway as described in several tumors (Cheng et al., 2008, Memmott and Dennis, 2009, Qiao et al., 2008, Steelman et al., 2008, Tokunaga et al., 2008) could induce the cytoplasmic accumulation of PKP1 accompanied by a destabilization of desmosomal adhesion and an increase in translation and proliferation. In such a context, PKP1 could actively contribute to carcinogenesis. Indeed, SCC samples of mice transgenic for HPV8

revealed an upregulation of activated Akt2 (O'Shaughnessy et al., 2007) and a considerably elevated cytoplasmic localization of PKP1 (Fig. 34C). In agreement, an overexpression of PKP1 and PKP3 have been described in several tumors, including SCC of the head and neck, lung carcinoma as well as Ewing sarcoma (Cheung et al., 2007, Furukawa et al., 2005, Kundu et al., 2008, Valladares-Ayerbes et al., 2010, Villaret et al., 2000). Notably, in actinic keratosis, a pre-cancerous lesion of the skin, as well as in SCC an elevated cytoplasmic pool of PKP1 has been reported (Kurzen et al., 2003, Narayana et al., 2010) supporting the notion that cytoplasmic PKP1 promotes tumorigenesis. Although melanocytes typically do not express PKP1, some melanoma cell lines acquire PKP1 expression (Rickelt et al., 2008, Schmitt et al., 2007). A phospho-proteome screen of skin melanoma revealed S63, S65, S118, S121, S185, and S191 – sites also being phosphorylated by Akt2 (Fig. 53A in appendix) – as phosphorylation sites emphasizing the relevance of this study in the context of tumor development (Zanivan et al., 2008). Interestingly, activated Akt2 or Akt3 are also upregulated in many melanoma biopsies (Robertson, 2005, Shin et al., 2010, Stahl et al., 2004). In contrast, when the PI3K/Akt pathway is not activated, the loss of PKP1 expression could contribute to reduced intercellular adhesion and thereby also promote carcinogenesis. This correlates with reports showing reduced expression of PKPs in some tumor samples, such as in colorectal, pancreatic, or prostate cancer (Breuninger et al., 2010, Moll et al., 1986, Schwarz et al., 2006, Yang et al., 2013). Thus, a conclusion might be that the localization of PKP1, regulated by phosphorylation, is one of the key factors, which determines whether PKP1 fulfills a tumor protective or a tumor promoting function.

The findings can be summarized in the following simplified model of PKP1's functions (Fig. 47): in the absence of growth factor signaling PKP1 associates with desmosomes leading to an increase in number and size of desmosomes, thereby stabilizing desmosomal adhesion. Excess PKP1 in the cytoplasm is degraded in this situation. This scenario would correlate with a tumor suppressive function of PKP1. After growth factor stimulation however, PKP1 becomes phosphorylated and accumulates in the cytoplasm, where it stimulates translation and proliferation. It still associates with desmosomes, but is less stably integrated facilitating the remodeling of desmosomes. In such a context, PKP1 would acquire a growth-promoting function.

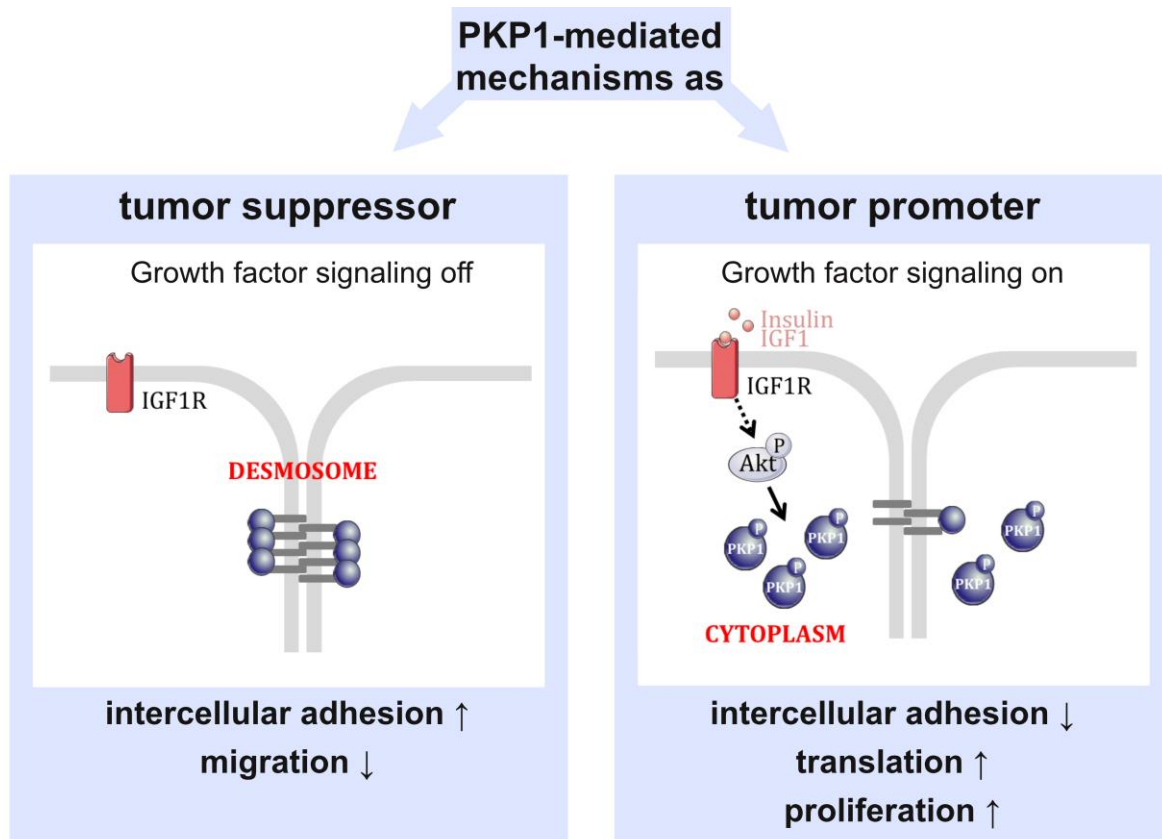


Fig. 47| Model for PKP1 regulation by growth factor signaling.

Schematic model predicting that regulation of PKP1 localization by phosphorylation is one of the key factors, which determines whether it fulfills a tumor protective or a tumor promoting function. In the absence of growth factors (left), PKP1 localizes in the desmosome resulting in enhanced intercellular adhesion and decreased cell migration. Upon activation of the insulin/IGF1 growth factor signaling cascade (right), PKP1 is phosphorylated by Akt2 and accumulates in the cytoplasm. The cytoplasmic pool of PKP1 presumably stimulates translation via interaction with eIF4A (Wolf et al., 2010), enhances proliferation and reduces intercellular cohesion. IGF1(R), insulin-like growth factor 1 (receptor); P, phospho; PKP, plakophilin.

The spatio-temporal control of multifunctional proteins during cell and tissue differentiation remains a challenging task. The decision on where PKP1 localizes within in the cell and with which proteins it interacts seems to have a major impact on keratinocyte cohesion. An imbalance in the regulation of PKP1 may lead to diseases such as cancer. In this study post-translational phosphorylation of PKP1 was examined. Once desmosomes are assembled, phosphorylation of desmosomal proteins may be one possibility to affect their dynamic in order to facilitate remodeling in response to changes in the surrounding environment. Preliminary results suggest that PKP1 could also play a regulatory role in the PI3K/Akt pathway. As the activity of the PI3K/Akt pathway is tightly and coordinately regulated by diverse molecular mechanisms (Altomare and Khaled, 2012), it is conceivable that PKP1 is not only an effec-

tor of Akt2-mediated signaling, but may be also a mediator causing a positive or negative feedback loop. For this purpose, phosphoproteomics by mass spectrometry performed in PKP1-null versus WT keratinocytes will reveal, which changes in the phosphorylation of desmosomal proteins and members of PI3K/Akt pathway are PKP1-dependent. The role of PKP1 as a putative mediator of PI3K/Akt signaling will be deciphered by Western blot analysis using PKP1-null skin and keratinocytes, respectively, compared to WT. However, also other PTMs like methylation or palmitoylation (<http://www.phosphosite.org/>) need further characterization with respect to PKP1's associations, localizations, and functions.

4.3. Isoform-specific PKP-14-3-3-interactions regulate desmosomal adhesion in keratinocytes

Posttranslational modifications such as phosphorylation offer a dynamic way to regulate subcellular localization as shown here for PKP1, protein activity, or stability (Olsen et al., 2006, Ptacek and Snyder, 2006, Schlessinger, 2000). The nature and the strength of protein-protein interactions can be modulated by phosphorylation and de-phosphorylation, thereby controlling protein binding and coordinating distinct pathways (Nishi et al., 2011). Together with kinases and phosphatases, the regulatory 14-3-3 proteins are essential components of phosphorylation-mediated signaling (Beltrao et al., 2013).

14-3-3s are highly homologous proteins encoded by separate genes. There are seven known mammalian 14-3-3 isoforms, named γ , σ , ϵ , η , β , ζ and τ (Ichimura et al., 1988), of which 14-3-3 γ , σ , η and ϵ were found to be highly expressed in mouse keratinocytes and skin (Fig. 35B, C). However, the semi-quantitative Western blot analyses only provide a relative comparison of protein levels, but not an absolute measure of quantity due to the use of monoclonal vs. polyclonal antibodies from different species, which presumably display different affinities. Because only 14-3-3 γ and 14-3-3 σ significantly affected intercellular adhesion in keratinocytes as shown by epithelial sheet assays (Fig. 36A-C and 43), I focused on 14-3-3 γ and 14-3-3 σ in this study, although it cannot be excluded, that additional 14-3-3 isoforms might play a role in the regulation of keratinocytes.

In this study it was shown that distinct PKP-14-3-3 complexes modulate desmosomal adhesion by altering PKP-dynamics and thereby the localization. The association of 14-3-3 proteins with endogenous PKP1 was investigated by a GFP-trap using lysates from mouse keratinocytes (Fig. 40A). The fact that both interaction partners are able to associate within

the cell as well as the lack of unspecific binding or antibody fragments, are major advantages of the GFP-trap. Additionally, this approach confirmed the interaction of 14-3-3 σ with PKP3 as described by Roberts et al. (2013). In transiently transfected HEK293 cells, 14-3-3 proteins co-immunopurified with PKP1 upon Akt2 activation, whereas no association was observed in unstimulated cells indicating that phosphorylation of PKP1 is required for 14-3-3 association (Fig. 40C). Phosphorylation-dependent interaction of 14-3-3 proteins with target proteins is well established and many reviews have been published on this subject (Aitken, 2006, Mackintosh, 2004, Wilker and Yaffe, 2004). Examination of PKP1 amino acids using Scansite search (<http://scansite.mit.edu>) predicted pS54, pS118, pS119, pS155, and pT171 as potential residues capable of mediating the interaction with 14-3-3 proteins. Mutation of S155 to alanine and to a lesser extent also S118/119 to alanine abrogated or weakened the association of PKP1 with 14-3-3 γ , while the other PKP1 mutants were still able to associate with 14-3-3 γ after Akt2 activation (Fig. 44B). These findings may be interpreted to indicate that (1) phosphorylation of PKP1 (by Akt2 or a downstream kinase) is necessary for 14-3-3 binding and (2) S155 as well as S118/119 are important sites for this association. As 14-3-3 proteins are known to act as homo- or heterodimers and each dimer contains two binding pockets, 14-3-3 proteins can interact with two motifs simultaneously (Yaffe et al., 1997). In particular, several proteins were identified to have one high-affinity binding motif as well as an additional low-affinity site that contribute to 14-3-3 binding (Giles et al., 2003). The high-affinity motif has been proposed to act as a “gatekeeper”, recruiting the 14-3-3 dimer (Yaffe, 2002). Binding of a 14-3-3 monomer to this site could then allow other, low-affinity sites to engage the second monomer, stabilizing the overall target-14-3-3 dimer complex (Dougherty and Morrison, 2004). In this assumption pS155 could function as high-affinity site, whereas pS118/119 as low-affinity site(s) could be important for stabilization of the 14-3-3 binding. However, to analyze the binding affinities in detail further approaches are needed such as isothermal titration calorimetry to measure the equilibrium dissociation constant (K_D). Interestingly, phosphorylation of PKP1 at S155 was identified in several studies (Mertins et al., 2016, Mertins et al., 2014, Yi et al., 2014). In good accordance, S155 was not phosphorylated by Akt2 *in vitro*, but *in vivo* (Wolf et al., 2013) suggesting that a kinase downstream of Akt2 such as p70S6K may phosphorylate PKP1 leading to 14-3-3 binding.

What is the functional relevance of isoform-specific 14-3-3 binding to PKPs? It has to be remembered that PKP1 and PKP3 reveal overlapping but distinct expression patterns within

the human epidermis (Fig. 2), with PKP3 detected in all layers without changes during epidermal differentiation (Schmidt et al., 1999) and an increased PKP1 expression from basal to suprabasal layers (Schmidt and Jager, 2005) indicating differential functions in the regulation of desmosomal adhesion. Interestingly, it was shown that Ca^{2+} -independence of desmosomes strictly depends on PKP1, whereas elevated levels of PKP3 prevent the formation of hyperadhesive desmosomes in a PKC α -dependent manner (Keil et al., 2016). Moreover, the segregation of PKP-isoforms, with PKP1 preferentially found along bicellular contacts and PKP3 accumulating at tricellular contacts (Keil et al., 2016), might represent one possibility to build up distinct types of desmosomes. However, the mechanisms regulating desmosome dynamics as well as isoform segregation are not well understood. To analyze the contribution of 14-3-3 γ and 14-3-3 σ to regulate PKP dynamics, FRAP experiments were performed. Depletion of both isoforms increased PKP1 dynamics at the desmosome (Fig. 46A) despite their opposing effects on intercellular cohesion (Fig. 36A-C). These results may be interpreted as follows: 14-3-3 γ sequesters PKP1 in the cytoplasm (Fig. 37A, B and 45A), thereby reducing its exchange rate at the desmosome (Fig. 46A). This leads to a loss of desmosomal PKP1 concomitant with reduced intercellular adhesion (Fig. 36A-C). In contrast, 14-3-3 σ associates preferentially with PKP3 (Fig. 40A) to facilitate its displacement from bicellular to tricellular contact sites (Fig. 37C, D, 39A, C and 56, 57 in appendix). This increases the stability of PKP1 at the desmosome, which correlates with slightly reduced PKP1 dynamics and increased intercellular cohesion (Fig. 43). Taken together, a destabilizing effect of 14-3-3 γ is mediated by PKP1, whereas 14-3-3 σ targets primarily PKP3 to stabilize intercellular cohesion.

Sehgal et al. (2014) proposed a model, where 14-3-3 γ binds to PG in a PKC γ -dependent fashion, which leads to a MT-dependent transport of PG to the cell border to initiate desmosome formation. These findings in HCT116 (human colon carcinoma) cells differ somewhat from the results in this study. For instance, using GST pulldown experiments an interaction of 14-3-3 γ with PG was found in HCT116 cells (Sehgal et al., 2014), whereas 14-3-3 γ revealed no association with PG in mouse keratinocytes shown by GFP-trap (Fig. 40A). Furthermore, Sehgal et al. (2014) reported that loss of 14-3-3 γ decreased desmosome formation and cell-cell adhesion *in vitro*, whereas in my experiments depletion of 14-3-3 γ resulted in no significantly weakened intercellular adhesion shown by epithelial sheet assays (Fig. 36A-C and 43). Nonetheless, how a role of 14-3-3 γ in strengthening desmosomal adhesion as predicted by Sehgal et al. (2014) might correlate with its overexpression in cancer remains to be elucidated.

A function of 14-3-3 γ as an oncogene is well established and supported by the finding that mRNA expression and copy numbers analyses demonstrated an upregulation of 14-3-3 γ in various cancers (<http://nextbio.com/>). Based on the observation that 14-3-3 γ -expressing NIH3T3 fibroblasts grow in soft agar and form tumors in SCID mice, the oncogenic potential of 14-3-3 γ was reported. Furthermore, Radhakrishnan et al. (2010) reported that overexpression of 14-3-3 γ induced activation of MAPK and PI3K signaling (Radhakrishnan and Martinez, 2010) indicating that these pathways generate 14-3-3 target sites. In agreement, 14-3-3 γ positively regulated protein translation and cell proliferation in bovine mammary epithelial cells (Yu et al., 2014). Interestingly, p53 can suppress 14-3-3 γ by stimulating proteasome-mediated 14-3-3 γ degradation (Chen et al., 2015).

In contrast, 14-3-3 σ is highly expressed in the epidermis and its overexpression inhibits proliferation and induces premature differentiation by suppressing IGF1 signaling (Cianfarani et al., 2011). Inactivation of 14-3-3 σ immortalized keratinocytes by an unknown mechanism (Dellambra et al., 2000) and epigenetic silencing of 14-3-3 σ was reported in basal cell carcinoma supporting a tumor-suppressing role (Lodygin and Hermeking, 2005). In addition, 14-3-3 σ is down-regulated in several types of cancer, such as breast (Ferguson et al., 2000), skin (Lodygin et al., 2003), or prostate cancer (Lodygin et al., 2004). A heterozygous inactivating mutation of 14-3-3 σ in mice caused the repeated epilation (*Er*) phenotype with hair loss and regrowth, and hyperproliferation of interfollicular epidermis, while homozygous *14-3-3 σ -Er/Er* mice died at birth (Herron et al., 2005, Li et al., 2005, Sambandam et al., 2015). Overexpression of 14-3-3 σ suppresses anchorage-independent growth of several breast cancer cell lines (Laronga et al., 2000). Interestingly, previous research has reported that 14-3-3 σ negatively regulates Akt and inhibits Akt-mediated cell survival, cell proliferation, transformation, and tumorigenesis. These studies in human breast cancers revealed that low expression of 14-3-3 σ is associated with Akt activation, providing a mechanistic role for 14-3-3 σ down-regulation in cancer formation (Yang et al., 2006).

In accord with the opposing functions of 14-3-3 γ and 14-3-3 σ , the following hypothetical model might illustrate their roles in controlling desmosomal adhesion via PKP1 and PKP3: in the presence of PKP1, PKP3 interacts with 14-3-3 σ at the lateral (bicellular) plasma membrane, which increases PKP3's exchange rates. Since PKP1 is more stable at lateral desmosomes, it outcompetes PKP3 along lateral membranes over time, which results in an accumulation of PKP3 at tricellular contact sites as observed during differentiation and junction matu-

ration. This promotes the high stability of epithelial sheets mediated by PKP1 (Keil et al., 2016). Thus, 14-3-3 σ promotes strong adhesion mediated by PKP1 by an indirect mechanism that targets PKP3. Basal PKP3-S285 phosphorylation may facilitate the PKP3-14-3-3 σ interaction in a growth factor-independent fashion.

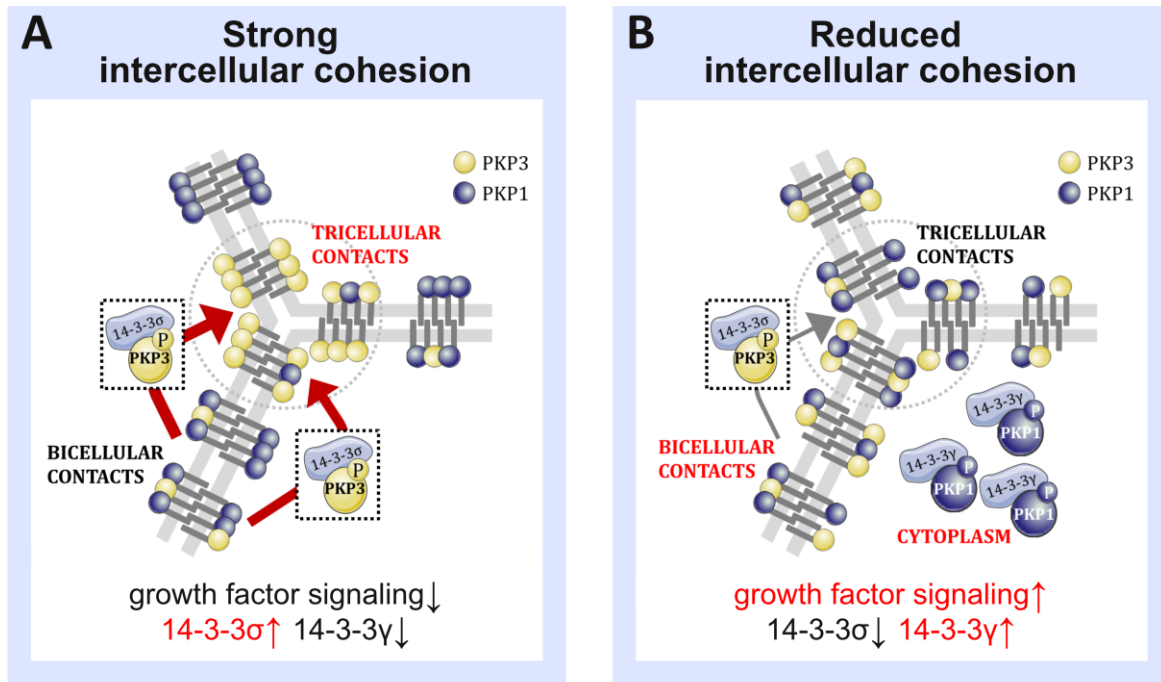


Fig. 48I Model depicting the regulation of intercellular cohesion via 14-3-3 γ and - σ .

Schematic model predicting the regulation of PKPs 1 and 3 by distinct 14-3-3 proteins. While 14-3-3 σ stabilized intercellular cohesion of keratinocytes, 14-3-3 γ had an opposite effect. This correlates with specific protein interactions: (A) 14-3-3 σ associates preferentially with PKP3 at the plasma membrane to promote its accumulation at tricellular contact sites (shown in red), whereas PKP1 becomes enriched at bicellular desmosomes providing strong cell-cell adhesion. (B) In contrast, growth factor signaling stimulates the association of 14-3-3 γ with PKP1 resulting in its accumulation in the cytoplasm and reduced incorporation into desmosomes. This leads to its loss from lateral contacts and reduced intercellular adhesion. PKP3 becomes more uniformly distributed along the membrane and renders desmosomes more dynamic facilitating tissue remodeling as required during regeneration and wound healing. P, phospho; PKP, plakophilin.

In the absence of PKP1, 14-3-3 σ reduces PKP3's exchange at the desmosomes by retaining the complex at the desmosome leading to increased intercellular cohesion. Activation of growth factor signaling stimulates proliferation and migration, which requires dynamic remodeling of cell contacts. This is achieved by PKP1 phosphorylation via Akt2 signalling resulting in its accumulation in the cytoplasm (chapter 3.2.). Phospho-PKP1 interacts with 14-3-3 γ , which promotes its retention in the cytoplasm. As 14-3-3 γ is known to stimulate PI3K signalling and regulates protein translation, one can hypothesize that 14-3-3 γ joins PKP1 with cytoplasmic proteins such as eIF4A facilitating translation. Overexpression of 14-3-3 γ as observed

in several tumors would retain phosphorylated PKP1 in the cytoplasm resulting in its depletion from desmosomes and as a consequence in reduced intercellular cohesion. Since loss of intercellular adhesion is a hallmark of cancer, 14-3-3 γ -mediated attenuation of desmosome function could contribute to its oncogenic potential in stratified epithelia. Due to the loss of PKP1 from lateral desmosomes, PKP3 is no longer displaced from the lateral membranes and becomes more uniformly distributed along the membrane leading to weaker and more dynamic adhesion.

Taken together, this study has identified a hitherto unappreciated, isoform-dependent role of 14-3-3 γ and 14-3-3 σ in the regulation of desmosome stability that depends on their interaction with distinct PKPs. At a mechanistic level, 14-3-3 γ and 14-3-3 σ control the segregation of PKP1 and PKP3 into bi- and tricellular contacts by regulating PKP dynamic. However, the kinase(s), which phosphorylate PKP1 and PKP3 leading to their association with 14-3-3 γ/σ are still unknown. Moreover, by the use and analysis of tumor samples the working hypothesis would be further strengthened and might validate that a destabilizing role of 14-3-3 γ affecting PKP1 and a stabilizing role of 14-3-3 σ indirectly regulating PKP1 by binding to PKP3 in keratinocyte cohesion is in line with their reported roles in cancer.

4.4. PKP1 and β -catenin: comparison of two multifunctional proteins

The armadillo proteins PKP1 and β -catenin are multifunctional and evolutionary conserved molecules that in metazoans exert essential roles in a multitude of developmental and homeostatic processes (Valenta et al., 2012). Both proteins have many things in common, but reveal also significant differences, which will be briefly discussed in this chapter (a schematic comparison is shown in Fig. 49). β -catenin contains 12 arm repeats flanked by rather short N- and C-terminal domains. These arm repeats form a superhelix with a long, positively charged groove, which serves as an interaction platform for several binding partners and is therefore considered as a scaffold for protein complex formation (Huber et al., 1997). In contrast, PKP1 consists of a central domain of nine arm repeats and interacts with binding partners preferentially by its N-terminal head domain, which is much larger than in β -catenin. PKP1 and β -catenin are both plaque proteins functioning as structural components in the particular cell-cell contact: β -catenin is located in AJs (Fig. 1C), where it binds cadherins through the arm repeats and establishes a link to the actin cytoskeleton via N-terminally bound α -catenin (Aberle et al., 1996, Hulsken et al., 1994, Nieset et al., 1997), whereas PKP1 is a desmosomal plaque

protein (Fig. 1D) interacting through its N-terminal domain with the cadherins DSGs and DSCs and via DSP to keratins. However, desmosomes and AJs link adjacent cells together and connect their cytoskeletal elements.

Loss of β -catenin in mice resulted in embryonic lethality; more specifically, the analyses pointed to a primary defect in the embryonic ectodermal cell layer of day 6.5-7.5 p.c. embryos (Haegel et al., 1995) indicating that β -catenin plays a major role during the development of multicellular organisms. However, in a study conducted by Huelsken et al. (2001) loss of β -catenin in the epidermis of mice blocked the formation of placodes that generate hair follicles. When β -catenin was deleted after hair follicles have formed, the hair was completely lost after the first hair cycle (Huelsken et al., 2001). Moreover, in the absence of β -catenin, stem cells failed to differentiate into follicular keratinocytes, but instead adopted an epidermal fate suggesting that β -catenin is essential for fate decisions of skin stem cells (Huelsken et al., 2001). However, hair follicle development was not examined in PKP1-null mice, but notably newborn PKP1-KO pups lacked whiskers (not shown) suggesting a defect in hair development. Additionally, subcutaneous adipocyte layer thickness was considerably reduced in PKP1-KO mice (Fig. 12D). Interestingly and in good accordance with my findings, hair follicle growth and subcutaneous adipocyte layer thickness are synchronized in mice and epidermal Wnt/ β -catenin signaling is essential for activation of proadipogenic pathways including insulin/IGF signaling (Donati et al., 2014) suggesting similar roles for β -catenin and PKP1 in hair follicle development. Wnt signaling is crucial for maintaining the balance between proliferation and differentiation throughout embryogenesis and tissue regeneration. In addition, Miyazaki et al. (2016) hypothesized that PKP1 regulates Wnt signaling via its arm repeat domain in manner similar to β -catenin using CLDE (cervical-loop derived dental epithelium) cells (Miyazaki et al., 2016). Upon Wnt stimulation during early tooth development, PKP1 translocates to the nucleus and acts as a Wnt signal transducer (Miyazaki et al., 2016). However, the nuclear function of PKP1 is less defined than its desmosomal and cytoplasmic role. Future work will be required to determine whether nuclear PKP1 interacts with transcription factors or whether it controls gene transcription of distinct targets.

Like PKP1, β -catenin is also found in the cytoplasm and the nucleus. Normally cytosolic levels of β -catenin are low due to coordinated phosphorylation by CK1 and the APC/Axin/GSK3 β -complex leading to its ubiquitination and proteasomal degradation (Aberle et al., 1997, Orford et al., 1997). However, in the presence of Wnt ligand, the co-receptor

LRP5/6 is brought in complex with Wnt-bound Frizzled leading to activation of Dishevelled by sequential phosphorylation, poly-ubiquitination, and polymerization, which displaced GSK3 β from APC/Axin. Stabilized β -catenin is translocated to the nucleus via Rac1 and other factors, where it binds to LEF/TCF transcription factors, displacing co-repressors and recruiting additional co-activators to Wnt target genes (Behrens, 2000, Brembeck et al., 2006, Cadigan and Waterman, 2012, Clevers, 2006, Polakis, 2000). Thus, β -catenin exhibits distinct changes in its subcellular localization reflecting its new functions similar to PKP1. PKP1's regulation strongly resembles that of β -catenin. On the one hand β -catenin functions in E-cadherin-mediated cell-cell adhesion, where it supports the tumor suppressive function of E-cadherin and on the other hand stimulation of Wnt signaling leads to β -catenin accumulation in the cytoplasm and translocation into the nucleus, where it stimulates together with LEF/TCF the transcription of several target genes involved in growth control, thereby acquiring an oncogenic function. Mutations in either β -catenin or its regulatory proteins are common events in the development of colon (Morin et al., 1997) and other cancers [reviewed in (Morin, 1999)].

Similar to PKP1, the function of β -catenin can be regulated through phosphorylation by various kinases. Fang et al. (2007) reported, that Akt-mediated phosphorylation of β -catenin at S552 caused its dissociation from cell-cell contacts and accumulation in both the cytoplasm and the nucleus and enhanced its interaction with 14-3-3 ζ . Moreover, phosphorylation of β -catenin by Akt increased its transcriptional activity and promoted tumor cell invasion suggesting that Akt-dependent regulation of β -catenin plays a critical role in tumor development (Dovrat et al., 2014, Fang et al., 2007, Tian et al., 2004). 14-3-3 proteins regulate the shuttling of β -catenin between cytoplasm and nucleus, whereas 14-3-3 γ affects PKP1's cytoplasmic-desmosomal localization. In a study conducted by Li et al. (2008), the molecular mechanism underlying β -catenin's translocation in and out of the nucleus by 14-3-3 proteins was examined in detail. 14-3-3 and β -catenin formed a stable tripartite complex with chibby (Cby) causing β -catenin to partition into the cytoplasm suggesting that Cby acts together with 14-3-3 proteins to promote nuclear export of β -catenin, thereby antagonizing β -catenin signaling (Li et al., 2008).

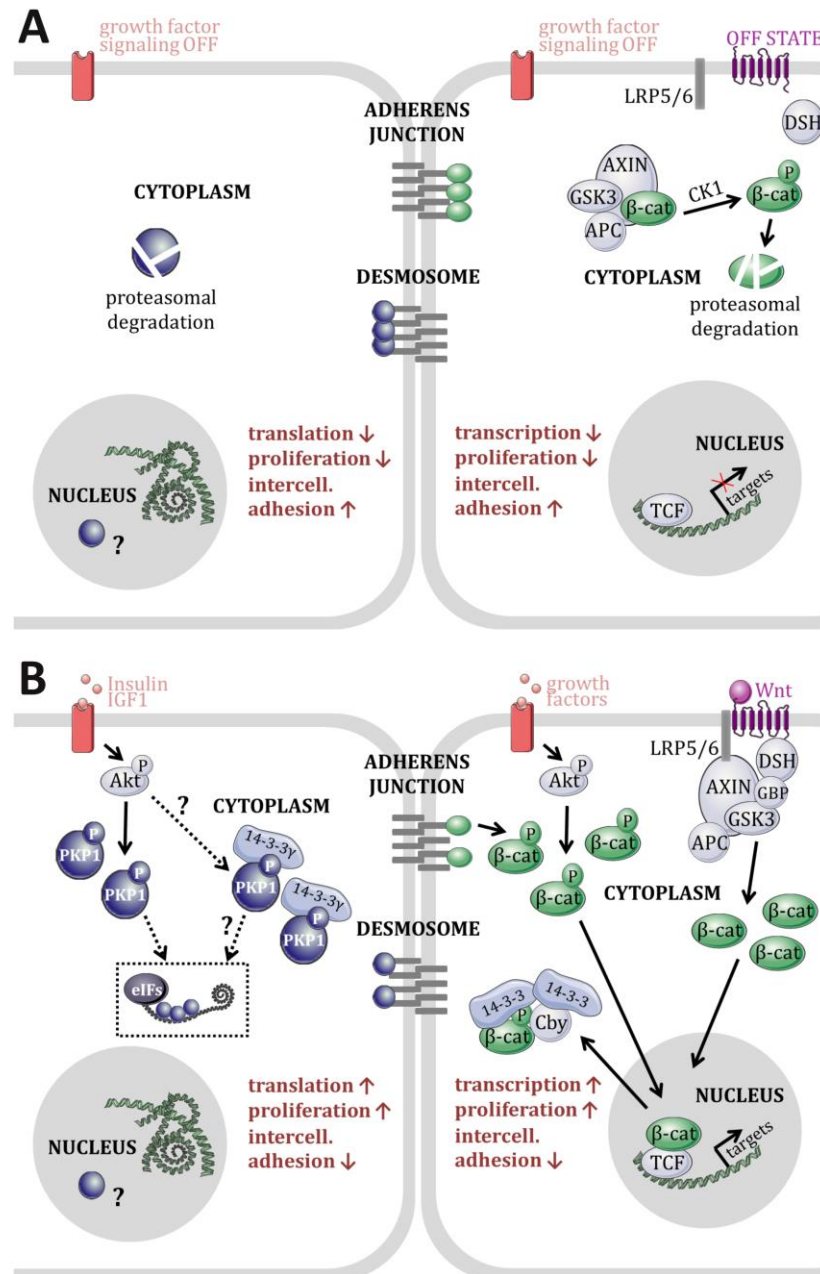


Fig. 49| Schematic comparison of multifunctional PKP1 and β -catenin.

Regulation of PKP1 (in dark blue, left) and β -catenin (in green, right) in the absence (A) or presence (B) of growth factors or Wnt, respectively, based on (Fang et al., 2007, Hatzfeld et al., 2014, Li et al., 2008, Moon et al., 2004, Wolf et al., 2010). (A) In the absence of growth factors (left), PKP1 localizes at desmosomes thereby promoting intercellular adhesion. Excess PKP1 in the cytoplasm gets degraded. In the absence of active Wnt (right), β -catenin is bound by a multiprotein complex consisting of APC, axin, GSK3 β and CK1, phosphorylated by CK1 and proteasomal degraded leading to a low cytosolic pool of β -catenin and repressed prospective target genes. A second pool of β -catenin is located at AJs. In this scenario, E-cadherin mediated cell-cell-adhesion is increased, whereas transcription and proliferation are decreased.

Continued on next page

Fig. 49 continued

(B) In the presence of insulin/IGF1 (left), PKP1 is phosphorylated by Akt2 leading to its cytosolic accumulation and increased protein synthesis, presumably by interaction with the helicase eIF4A. 14-3-3 γ associates and sequesters PKP1 in the cytoplasm leading to weakened intercellular adhesion. In a similar way, Akt-mediated phosphorylation of β -catenin causes its disassociation from AJs and accumulation in the cytoplasm as well as nucleus and enhances its interaction with 14-3-3. Moreover, when Wnt signaling is active, β -catenin degradation is reduced. β -catenin accumulates in the cytoplasm and enters the nucleus, where it binds to TCF- and LEF-family transcription factors and activates transcription and proliferation. Furthermore, Cby and 14-3-3 form a stable tripartite complex with β -catenin causing its partition into the cytoplasm. AJ, adherence junction; APC, adenomatous polyposis coli; AXIN, axis inhibition protein; cat, catenin; Cby, chibby; CK, casein kinase; DSH, Dishevelled; eIF, eukaryotic initiation factor; GSK, glycogen synthase kinase; IGF1, insulin-like growth factor 1; LRP, LDL-receptor-related protein; P, phospho; TCF, T-cell factor.

In conclusion, PKP1 and β -catenin exhibit distinct activities in addition to their originally identified functions. Apart from their structural role in desmosomes and AJs, respectively, they participate in several pathways such as insulin/PI3K or Wnt signaling. Regulatory mechanisms such as phosphorylation and 14-3-3 binding exist to control their subcellular translocation and highlight the importance of precise regulation and crosstalk between different subcellular sites. This study provides an integrated and dynamic picture of the multiple roles of PKP1 and defines it as an abundant component to ensure epidermal homeostasis by controlling intercellular adhesion as well as proliferation and consequently the integrity of the tissue in steady-state conditions.

5 MATERIAL & METHODS

5.1. Chemicals and general lab material

Unless otherwise stated, all used chemicals were purchased from Applichem (Darmstadt, Germany), Carl Roth (Karlsruhe, Germany), Sigma Aldrich (St. Louis, Missouri, USA), Roche (Basel, Switzerland), Thermo Fisher Scientific (Waltham, Massachusetts, USA) and Merck (Darmstadt, Germany). Cell culture media and supplements were purchased from PAA (Pasching, Austria) and Sigma Aldrich (St. Louis, Missouri, USA). All plastic ware, sterile cell culture ware, pipet tips, tubes, sterile filters and cryo tubes were purchased from VWR (West Chester, Pennsylvania, USA), BD Bioscience (San José, California, USA), TPP (Trasadingen, Switzerland), and Corning (Tewksbury, Massachusetts, USA). Glass coverslips were purchased from glassware factory Karl Hecht (Sondheim, Germany), Menzel-Gläser (Braunschweig, Germany) or Superfrost Ultra Plus® glass slides from Thermo Fisher Scientific (Waltham, Massachusetts, USA). Rotilabo blotting paper was purchased from Carl Roth (Karlsruhe, Germany), Protran nitrocellulose transfer membrane from Whatman (Kent, UK) and nylon membrane from Altmann Analytik (Munich, Germany).

5.2. Phenotypic analysis of PKP1 knockout mice

5.2.1. Animals

All mouse strains used in this study were kept and bred at the ZAMED (Zentrum für Angewandte Medizinische und Humanbiologische Forschung) animal facility of the Medical Faculty (Martin-Luther-University Halle-Wittenberg). The mice had standard rodent diet and water. The light cycle was set to 12 h. From an age of 8 weeks mice were used for breeding. 3 weeks after birth, mice were separated according to the sex, marked with ear tags and kept in separated cages. For genotyping, mice tails were clipped and used for DNA isolation immediately. All experiments were approved by the local authorities (Landesverwaltungsamt Sachsen-Anhalt, reference number 425022-1166 MLU) and carried out according to the German Animal Protection Law.

5.2.2. Documentation of weight development

Material: Incucell-incubator (MMM Medcenter Einrichtungen GmbH; Planegg, Germany), SBC 51 precision balance (Scaltec; Göttingen, Germany).

The weight of newborn WT and PKP1-KO mice was monitored every hour for 8 h. Therefore, mice were kept at 37°C without feeding. Results are displayed as relatives of initial body weight.

5.2.3. Transepidermal water loss (TEWL) assay

Material: Tewameter® TM 300 (Courage & Khazaka; Cologne, Germany).

To measure the water evaporation rates of the skin a Tewameter® TM 300 was used. By two pairs of sensors (temperature and relative humidity) inside a hollow cylinder of the Tewameter® probe, the density gradient of the water evaporation from the skin was measured. The conditions were stabilized for 30 min, in a climate- and humidity-controlled room. The ambient temperature was between 21°C and 23°C with a mean relative humidity of 36-44%. For measurement, the Tewameter® was applied on the ventral skin of newborn mice. A microprocessor analyzed the values and expressed the evaporation rate in g/h/m².

5.2.4. Detection of TJ barrier function *in vitro* by biotin diffusion assay

Material: 2 M CaCl₂ (see 7.1.4), 3.7% (w/v) FA [(formaldehyde), see 7.1.4], EZ-Link sulfo-NHS-LC-biotin (Pierce Chemical Co.; Rockford, IL), PBS (see 7.1.4), polyfreeze tissue freezing medium (Polyscience; Eppenheim, Germany), precooled isopentane.

To analyze inside-out barrier of the murine skin, 10 mg/ml EZ-Link sulfo-NHS-LC-biotin/PBS containing 1 mM CaCl₂ was injected intradermally into the back skin of newborn mice (Furuse et al., 2002). After 30 min, mice were sacrificed and skin was embedded in polyfreeze tissue freezing medium and snap-frozen in isopentane precooled to -80°C for cryosections (see 5.2.9). The cryosections were fixed in 3.7% FA and stained with Cy3-conjugated streptavidin. To mark the TJs, sections were counterstained using anti-ZO-1 followed by A488-labelled secondary antibody (see 5.2.13 and 7.1.6).

5.2.5. Toluidine blue dye penetration assay

Material: 0.2% (w/v) Toluidine blue (Sigma Aldrich; St. Louis, Missouri, USA) freshly diluted in water and filtered; ice-cold methanol series [25% (v/v), 50% (v/v), 75% (v/v), 100% (v/v)], PBS (see 7.1.4), Sony Cyber Shot DSC-H300 camera (Sony; Tokyo, Japan).

Outside-in skin barrier function of the skin was analyzed in neonatal mice via the Toluidine blue dye penetration assay according to Hardman et al. (Hardman et al., 1998). Briefly, pups were washed in PBS, dehydrated by methanol series [25% (v/v), 50% (v/v), 75% (v/v),

100% (v/v), 75% (v/v), 50% (v/v), 25% (v/v) ice-cold methanol for 2 min each], equilibrated in PBS for 2 min and subsequently incubated for 5 min with 0.2% (w/v) Toluidine blue. After a brief washing step in PBS images were acquired.

5.2.6. Preparation and analysis of corneocytes

Material: extraction buffer (see below), glass slides (Menzel-Gläser; Braunschweig, Germany), Hettich Universal 16 centrifuge (Hettich GmbH & Co.KG; Tuttlingen, Germany), microscope EVOS FL Cell Imaging System (Thermo Fischer Scientific; Waltham, Massachusetts, USA), washing buffer (see below), and water bath (Mettler; Shanghai, China).

To isolate corneocytes, dorsal skin of newborn mice was cut into small pieces and incubated for 10 min in extraction buffer (see below) in a boiling water bath. The suspensions were centrifuged for 10 min at 3,500x g and RT, the supernatants were discarded and the pellets were re-extracted under the same conditions. Subsequently, the pellets were washed three times with washing buffer (see below), centrifuged for 10 min at 3,500x g and RT, resuspended in washing buffer and stored at 4°C. The isolated corneocytes were applied on glass slides and images were acquired using an EVOS FL Cell Imaging System. The relative area of corneocytes was quantified using the MiToBo plugin for ImageJ.

Extraction buffer: 0.1 M Tris, pH 8.0, 2% (w/v) SDS, 5 mM EDTA, 2 mM DTT

Washing buffer: 0.1 M Tris, pH 8.0, 0.2% (w/v) SDS, 5 mM EDTA, 2 mM DTT

5.2.7. Ultrastructural analysis of skin samples

Material: 1% (w/v) osmiumtetroxide (Carl Roth; Karlsruhe, Germany), 3% (v/v) glutaraldehyde (Sigma Aldrich; St. Louis, Missouri, USA) in 0.1 M sodium cacodylate buffer, epoxy resin (EMBed-812 Embedding Kit, Science Services; Munich, Germany), stain apparatus (EM-STAIN, Leica; Wetzlar, Germany), Ultramicrotome S (Leica; Wetzlar, Germany), Zeiss Libra 120 transmission electron microscope (Carl Zeiss Microscopy; Oberkochen, Germany).

For electron microscopy the tissue was fixed with 3% glutaraldehyde in 0.1 M sodium cacodylate buffer pH 7.2 (SCB), washed, post-fixed with 1% osmiumtetroxide in SCB, dehydrated in a graded series of acetone and embedded in epoxy resin. After polymerization the material was sectioned with an Ultramicrotome S. The ultrathin sections (80 nm) were transferred to formvar-coated grids and post-stained with uranyl acetate and lead citrate using a stain apparatus. The sections were observed with a Zeiss Libra 120 transmission electron microscope operating at 120 kV. Images were taken applying a Dual-Speed on axis SSCCD camera (BM-2k-120; TRS, Moorenweis) using the iTEM software from Olympus SIS (Münster, Germany). The same software was used for morphometric measurements. Tissue processing and electron microscopy was kindly performed by Dr. Dr. Gerd Hause and

Annekathrin Rother (Biozentrum, Martin-Luther-University).

5.2.8. Preparation of paraffin sections

Material: 3.7% (w/v) FA (see 7.1.4), ethanol series [50% (v/v), 70% (v/v), 80% (v/v), 90% (v/v) and 100%], Leica ASP200 S processor for paraffin infiltration of tissue (Leica; Wetzlar, Germany), Leica EG1160 paraffin embedding center (Leica; Wetzlar, Germany), microtome (Leica; Wetzlar, Germany), Superfrost Ultra Plus® glass slides (Thermo Fisher Scientific; Waltham, Massachusetts, USA), xylol (Merck; Darmstadt, Germany).

For histology, dorsal skin and paws were cut and fixed overnight in 3.7% (w/v) FA. The following day, samples were dehydrated in consecutive baths with a gradually increasing concentration of ethanol: 50%, 70% and 80% for 60 min each, 90% for overnight and 100% - 3 x 60 min. Then, samples were treated with xylol for 2 x 15 min and subsequently transferred to a container with liquid paraffin. Skin samples embedded in paraffin blocks using an embedding device and stored at RT. Before cutting, paraffin blocks were cooled down on ice. The paraffin embedded tissue was cut into 6 µm thick sections using a microtome, collected on glass slides and stored at RT.

5.2.9. Preparation of cryosections

Material: cryostat (Leica CM3050 S; Wetzlar, Germany), PolyFreeze tissue freezing medium (Polyscience; Eppelheim, Germany), precooled isopentane, Superfrost Ultra Plus® glass slides (Thermo Fisher Scientific; Waltham, Massachusetts, USA).

For histology, dorsal skin was embedded in tissue freezing medium, snap-frozen in isopentane precooled to -80°C and kept at -80°C. Before cutting, samples were equilibrated at -20°C. 8-10 µm frozen tissue sections were cut at -20°C in a cryostat and placed on glass slides. Before using for further applications (see 5.2.13), cryosections were air-dried for 1 h at RT.

5.2.10. Hematoxylin & Eosin (H&E) staining

Material: DPX Mountant (Sigma Aldrich; St. Louis, Missouri, USA), Eosin Y (Sigma Aldrich; St. Louis, Missouri, USA), ethanol series [100%, 96% (v/v), 95% (v/v), 90% (v/v), 80% (v/v), 70% (v/v), 50% (v/v)], Hematoxylin (Mayers hemalaun, Merck; Darmstadt, Germany), xylol (Merck; Darmstadt, Germany), Zeiss Axioplan 2 imaging microscope (Carl Zeiss Microscopy; Oberkochen, Germany).

For histological analysis of paraffin sections, H&E staining was done. Paraffin sections were deparaffinized by xylol treatment for 2 x 5 min. Then, sections were rehydrated in 100%, 95%, 90%, 80%, 70%, 50% (v/v) ethanol series for 2 min each and washed in aqua bidest. The slides were treated with hematoxylin for 30 sec and rinsed with warm tap water. Subsequently, samples were treated with eosin for 1 min, rinsed with tap water and dehydrat-

ed in 70% (v/v), 2 x 96% (v/v) and 2 x 100% ethanol series for 30 sec, each. Finally, the slides were washed in xylol for 2 x 2 min and mounted in DPX Mountant. H&E staining was kindly performed by Anja Doering (Magin Lab, University Leipzig). H&E images were taken at a Zeiss Axioplan 2 imaging microscope equipped with a CCD camera (AxioCam HR3c) and the AxioVision Software using a LCI “Plan-Neofluar” 25x/0.8 Imm Korr DIC objective.

5.2.11. Connective tissue stain

Material: Trichrome Stain Kit (Abcam; Cambridge, UK), Zeiss Axioplan 2 imaging microscope (Carl Zeiss Microscopy; Oberkochen, Germany).

To analyze the thickness of subcutaneous adipocytes, Trichrome Stain Kit was used to stain paraffin embedded skin sections for collagen, muscle fibers and nuclei according to the manufacturer’s protocol. Images were taken at a Zeiss Axioplan 2 imaging microscope equipped with a CCD camera (AxioCam HR3c) and the AxioVision Software using a LCI “Plan-Neofluar” 25x/0.8 Imm Korr DIC objective.

5.2.12. Immunohistochemistry (IHC) of paraffin sections

Material: 0.1 M citrate buffer (see below), blocking solution (see below), DPX Mountant (Sigma Aldrich; St. Louis, Missouri, USA), ethanol series [100%, 96% (v/v), 95% (v/v), 90% (v/v), 80% (v/v), 70% (v/v), 50% (v/v)], Hoechst 33342 (stock 10 µg/µl, Thermo Fisher Scientific; Waltham, USA), PBS (see 7.1.4), primary antibody anti-Ki67 (see 7.1.6), proteinase K (Sigma Aldrich; St. Louis, Missouri, USA), secondary antibody (see 7.1.6), TBS (see 7.1.4), Triton X-100 (Sigma Aldrich; St. Louis, Missouri, USA), xylol (Merck; Darmstadt, Germany).

In order to mark proliferating cells in murine skin samples, Ki-67 staining was used (Gerdes et al., 1983). Paraffin embedded specimen (see 5.2.8) were sectioned at 4 µm, deparaffinized by xylol treatment for 2 x 5 min. Then, sections were rehydrated in 100%, 95%, 90%, 80%, 70% and 50% (v/v) ethanol series for 2 min each and treated in 0.1 M citrate buffer (see below) for Ki-67 detection. Ki-67 primary antibody (see 7.1.6) was diluted in blocking solution (see below) and incubated for 1 h at RT in a humid chamber. Slides were washed 3 x 10 min in PBS and incubated with the indicated secondary antibody (diluted in blocking solution, see 7.1.6) for 1 h at RT in a dark, humid chamber. To visualize the nuclei, each immunostaining was finalized by 10 min staining with Hoechst 33342 (1:1,000 in blocking solution). Then, slides were washed 3 x 10 min in PBS. Sections were mounted in DPX Mountant and stored in the dark at 4°C.

SCC paraffin samples (kindly provided by Prof. Dr. Werner; ETH, Institute of Molecular Health Science, Zurich) were used to analyze the localization of PKP1. Paraffin embedded

and sectioned specimen were deparaffinized by xylol treatment for 2 x 5 min. Sections were rehydrated in 100%, 95%, 90%, 80%, 70%, 50% (v/v) ethanol series for 2 min each, treated in 0.05 M Tris/HCl buffer (pH 10.2) for 12 min at 120°C, washed in TBS for 5 min and incubated in 0.5% (v/v) Triton X-100/TBS for 5 min at RT. Then, sections were incubated with 2 µg/ml proteinase K (diluted in TBS) for 8 min at 37°C and washed in TBS for 5 min at RT. PKP1 staining was performed as described above for Ki-67 staining.

0.1 M citrate buffer: 0.1 M citric acid, 0.1 M trisodium citrate, pH 6.0

Blocking solution: 0.5% (v/v) Triton X-100, 1% (w/v) BSA, 5% (v/v) normal donkey serum/TBS

5.2.13. Immunofluorescence (IF) of cryosections

Material: 3.7% (w/v) FA (see 7.1.4), acetone (Sigma Aldrich; St. Louis, Missouri, USA), blocking solution (see below), BSA (Carl Roth; Karlsruhe Germany), DPX Mountant (Sigma Aldrich; St. Louis, Missouri, USA), Hoechst 33342 (stock 10 µg/µl, Thermo Fisher Scientific; Waltham, Massachusetts, USA), Leica - TCS SP5 AOBs confocal microscope, PBS (see 7.1.4), primary/secondary antibody (see 7.1.6), TBS (see 7.1.4), Triton X-100 (Sigma Aldrich; St. Louis, Missouri, USA).

To mark desmosomal and AJs proteins, keratins and differentiation marker proteins, cryosections were fixed in acetone at -20°C for 10 min and dried for 1 h before further processing. To mark the TJs, cryosections were fixed in 3.7% (w/v) FA for 10 min at RT followed by incubation in 0.2% (v/v) Triton X-100/PBS for 5 min and blocking in 5% (v/v) normal donkey serum/1% (w/v) BSA/PBS.

All antibodies (see 7.1.6) were diluted in blocking solution (see below) and incubated overnight at 4°C in a dark, humid chamber. Next day, slides were washed 3 x 10 min in PBS and incubated with the indicated secondary antibody (see 7.1.6) for 1 h at RT in a dark, humid chamber. To visualize the nuclei each immunostaining was finalized by 10 min staining with Hoechst 33342 (1:1,000 in blocking solution) and washed 3 x 10 min in PBS. Sections were mounted in DPX Mountant and stored in the dark at 4°C. For IF microscopy, image stacks were collected at the confocal microscope (Leica - TCS SP5 AOBs) using a HCX PL APO lambda blue 63x1.40 OIL objective and Leica LAS AF software (Leica Microsystems). Maximum intensity projections of at least 45 optical sections are depicted.

Blocking solution: 0.5% (v/v) Triton X-100, 1% (w/v) BSA in TBS

Blocking solution (TJ): 5% (v/v) normal donkey serum, 1% (w/v) BSA in PBS

5.3. Cell culture methods

5.3.1. Cultivation of eukaryote cell lines

Material: 2.5% (w/v) trypsin (Life Technologies; Carlsbad, California, USA), DMEM [(Dulbecco's Modified Eagle Medium), Sigma Aldrich; St. Louis, Missouri, USA], DMSO (Sigma Aldrich; St. Louis, Missouri, USA), FCS (fetal calf serum), glutamate (Sigma Aldrich; St. Louis, Missouri, USA), Hera Safe – Biological Safety Cabinet (Kendro; Langensfeld, Germany), Heraeus cytoperm 2 – CO₂-incubator (Thermo Fisher Scientific; Waltham, USA), Hettich Universal 16 – centrifuge (Hettich GmbH & Co.KG; Tuttlingen, Germany), isopropanol (Sigma Aldrich; St. Louis, Missouri, USA), PBSE (see 7.1.4), sodium pyruvate (Sigma Aldrich; St. Louis, Missouri, USA), water bath (Mettler; Shanghai, China), Wilovert A – microscope (Hund; Wetzlar, Germany).

All cells used in this study are listed in chapter 7.1.7. HaCaT, HEK293 and MCF-7 were cultured on 10 cm dishes in cell culture medium (see below) at 37°C, 5% CO₂ and 90% humidity. Every 2-3 days, the medium was disposed, cells were washed twice with PBSE and incubated with 0.05% trypsin/PBSE at 37°C until they detached from the cell dish. Fresh medium was added and cells were pelleted by low speed centrifugation (3 min at 1,000x g). The supernatant was aspirated. Cells were resuspended in fresh medium and replated at the required density. To freeze cells, cell pellets were resuspended in freezing medium [90% (v/v) FCS, 10% (v/v) DMSO], aliquoted in cell culture cryogenic tubes and stored at -80°C. To thaw cells, vials were placed in a 37°C water bath and thawed cells were immediately transferred to a centrifuge tube containing 9 ml cell culture medium and centrifuged at 1,000x g and RT for 3 min. The cells were resuspended in fresh medium and plated on 10 cm plates.

Cell culture medium: high glucose (4.5g/l) DMEM flask, 1 mM sodium pyruvate, 1mM glutamate, 10% (v/v) FCS

5.3.2. Isolation, culture and differentiation of mouse keratinocytes

Material: beta-iodine, 2 M CaCl₂ (see 7.1.4), Collagen I rat tail (Thermo Fisher Scientific; Waltham, Massachusetts, USA), dispase II (Roche; Basel, Switzerland), sterile dissecting set, Hettich Universal 16 – centrifuge (Hettich GmbH & Co.KG; Tuttlingen, Germany), PBS (see 7.1.4), solutions used for keratinocyte culture (see below), water bath (Mettler; Shanghai, China), Wilovert A – microscope (Hund; Wetzlar, Germany).

Primary keratinocytes of WT, PKP1-KO and PKP3-KO mice [gift from F. Van Roy (Sklyarova et al., 2008)] were isolated from newborn pups. The embryos were sacrificed by decapitation and the bodies were cooled in a 50 ml falcon on ice for 1 h. Embryos were washed and disinfected (50% (v/v) beta-iodine/PBS, PBS, 70% (v/v) ethanol/PBS, PBS for 1 min each) and transferred to a sterile 100 mm dish. Tail tips were cut off and used for genotyping (see

5.5.11). The skin was dissected and incubated with 5 mg/ml dispase II in PBS overnight at 4°C. On the next day, the dermis was peeled off and discarded. The epidermal sheet (with the basal layer facing the bottom of the plate) was incubated with trypsin solution (see below) for 5-10 min at 37°C / 5% CO₂. Trypsin reaction was stopped by adding mouse keratinocyte medium (see below). All viable cells from the basal layer were released in the medium leaving behind the transparent *stratum corneum*. The cell suspension was carefully recovered, transferred into a falcon tube and centrifuged at 1,000x g for 3 min (Kashiwagi and Huh, 2005). The isolated keratinocytes were cultured on collagen I-coated cell culture dishes in 0.1 mM CaCl₂ and 24 h later in 50 µM CaCl₂ containing mouse keratinocyte medium (see below) at 5% CO₂ and 32°C to permit immortalization. The duration of immortalization took around 15-20 passages until cells showed up an epithelial phenotype. Cell culture experiments were started at passage ~20. To induce differentiation of keratinocytes, LCM (low calcium medium) was changed to 1.2 mM CaCl₂ (HCM, high calcium medium).

To freeze keratinocytes, cell pellets were resuspended in freezing medium (see below), aliquoted in cell culture cryogenic tubes and stored at -80°C. To thaw cells, vials were placed in a 37°C water bath, immediately transferred to a centrifuge tube containing 9 ml medium and centrifuged at 1,000x g for 3 min. The cells were resuspended in fresh medium and plated in 10 cm plates.

For growth factor stimulation, keratinocytes were cultured on collagen I-coated glass coverslips. 24 h after plating cells were serum-starved (HCM without FCS, insulin, cholera toxin, EGF) for 24 h and stimulated with 5 µg/ml insulin, 100 ng/ml IGF1 or 10 ng/ml EGF for additional 24 h and further processed for IF staining (see 5.3.5).

Table 1| Solutions used for keratinocyte culture.

Name	Final concentration	Constituents and their amounts
Collagen I	50 µg/µl	3.75 mg/ml Collagen I rat tail (Thermo Fisher Scientific; Waltham, Massachusetts, USA) in 0.02 N acidic acid
DMEM/Ham's F12 medium		350 ml: DMEM 4,5 g/l D-glucose, without L-glutamine, without sodium pyruvate, without CaCl ₂ 110 ml: Ham's F-12, without L-glutamine, without CaCl ₂ , 50 µM CaCl ₂
FCS Superior (Biochrom GmbH)		To remove calcium ions, serum was pretreated with 8 g/50 ml Chelex® 100 (Bio-Rad, Hercules, USA) overnight on a rotating wheel at 4°C. Procedure was 1x repeated followed by sterile filtration (0.1 µm filter).
Keratinocytes medium (LCM)	10% (v/v) 1x 0.18 mM 0.5 µg/ml 5 µg/ml 10 ng/ml 100 pM	460 ml DMEM/Ham's F12 medium 50 ml FCS (Chelex treated) 5 ml sodium pyruvat 5 ml GlutaMax (100x) (Invitrogen) 2 ml 45 mM adenine (Sigma) in 0.05 N HCl 250 µl 1 mg/ml hydrocortison in EtOH (Sigma) 500 µl 5 mg/ml insulin (Sigma) in 5 mM HCl 500 µl 10 µg/ml EGF (Sigma) in FAD 5 µl 1 µM cholera toxin (Sigma) in sterile water
Keratinocyte freezing medium	10% (v/v) 90% (v/v)	5 ml DMSO 45 ml FCS (Chelex treated) Aliquoted and stored at -20°C.
Trypsin solution	0.025% (v/v) 0.025% (v/v)	468 ml cell culture grade PBS 27 ml ES-EDTA-Solution (1.85 g/l in cell culture grade water) 5 ml trypsin, 2.5% Solution was stored at -20°C.

5.3.3. Generation of stable cell lines

Generation of stable cell lines by single cell cloning

Material: 2.5% (w/v) trypsin (Life Technologies; Carlsbad, California, USA), G418 selection agent (PAA; Pasching, Austria), Hera Safe – Biological Safety Cabinet (Kendro; Langensfeld, Germany), Heraeus cytoperm 2 – CO₂ incubator (Thermo Fisher Scientific; Waltham, Massachusetts, USA), Hettich Universal 16 – centrifuge (Hettich GmbH & Co.KG; Tuttingen, Germany), Neubauer cell counter (Laboroptik; Friedrichsdorf, Germany), PBSE (see 7.1.4), water bath (Mettler; Shanghai, China), Wilovert A – microscope (Hund; Wetzlar, Germany).

All generated cell lines used in this study are listed in chapter 7.1.7. To generate MCF-7 cells stably expressing DsRed, PKP1-WT-, PKP1M1-4A and PKP1M1-4E-DsRed, MCF-7 cells were transfected (see 5.3.4) with the indicated plasmids encoding a neomycin resistance gene. 48 h after transfection, MCF-7 cells were diluted (2.5 cells/200 µl) and plated onto 96-well plates in fresh medium containing 600 µg/ml G418. Every 2-3 days the medium was changed and cells were checked for colony forming. When confluent, cells were transferred

into larger culture vessels until culturing in 10 cm culture dishes.

Cell culture medium: high glucose (4.5g/l) DMEM flask, 1 mM sodium pyruvate, 1mM glutamate, 10% (v/v) FCS, 600 µg/ml G418 optional for selection

Generation of stable cell lines by lentiviral transduction

Material: 2 M CaCl₂ (see 7.1.4), 2.5% (w/v) trypsin (Life Technologies; Carlsbad, California, USA), cell culture medium for HEK293T (5.3.1) and keratinocytes (5.3.2), Hera Safe – Biological Safety Cabinet (Kendro; Langensfeld, Germany), Heraeus cytoperm 2 – CO₂ incubator (Thermo Fisher Scientific; Waltham, USA), Hettich Mikro 220R – centrifuge (Hettich GmbH & Co.KG; Tuttlingen, Germany), Lenti-X concentrator (Takara Bio Inc.; Japan), Poly-L-Lysine (Sigma Aldrich; St. Louis, Missouri, USA), 2x DNA precipitation buffer (see below), puromycin (Thermo Fisher Scientific; Waltham, USA), RNase/DNase-free water (Sigma Aldrich; St. Louis, Missouri, USA), water bath (Mettler; Shanghai, China), Wilovert A – microscope (Leica; Wetzlar, Germany).

All generated cell lines used in this study are listed in chapter 7.1.7. The cDNA of human PKP1, PKP3, 14-3-3 γ and 14-3-3 σ was subcloned into pLVX-IRES-puro (Takara Bio Inc.) containing an EGFP ORF. Vectors for production of lentiviral particles; pMD2.G and psPAX2 were a gift from D. Trono (Addgene plasmids #12259, #12260). To generate stable keratinocytes, HEK293T cells were plated onto Poly-L-Lysine-coated dishes and 24 h after plating co-transfected by CaPO₄ precipitation (see 5.3.4). The transfection reaction included 24.8 µg plasmid DNA [50% plasmid DNA of interest (hPKP1-GFP, hPKP3-GFP, GFP-h14-3-3 γ , GFP-14-3-3 σ , or GFP), 36% psPAX2 and 14% pMD2.G] in 280 µl RNase/DNase-free water and 40 µl 2 mM CaCl₂. The solution was gently mixed, subsequently pipetted dropwise to 310 µl 2x DNA precipitation buffer (see below). The solution was incubated for 20 min at RT and added to the HEK293T cells. Next day, the media containing lentiviral particles was removed from the wells and fresh media was added. 48 h after transfection, the media was collected and the lentiviral particles were purified using Lenti-X concentrator according to the manufacturer's protocol. Keratinocytes were incubated with the lentiviral particles for 24 h and subsequently puromycin (1 µg/ml) selected. The resulting cell lines were analyzed by flow cytometry and Western blot (see 5.4.6) to monitor expression of the transgenes (Keil et al., 2016). Lentiviral transduction of PKP1 and PKP3 rescue cell lines was kindly performed by Dr. René Keil (Hatzfeld Lab, Martin-Luther-University).

2x DNA precipitation buffer: 280 mM NaCl, 10 mM KCl, 1.5 mM Na₂HPO₄ (x2 H₂O), 12 mM glucose, 50 mM HEPES, pH 7.05 (filtered through 0.2 µm filter)

5.3.4. Transfection of eukaryote cell lines

DNA transfection with calcium phosphate (CaPO₄)

Material: 2 M CaCl₂ (see 7.1.4), 2x DNA precipitation buffer (see below), 2.5% (w/v) trypsin (Life Technologies; Carlsbad, California, USA), 12 mm coverslips (glassware factory Karl Hecht; Sondheim, Germany), cell culture medium (see below), glycerol shock buffer (see below), Hera Safe – Biological Safety Cabinet (Kendro; Langensfeld, Germany), Heraeus cytoperm 2 – CO₂ incubator (Thermo Fisher Scientific; Waltham, Massachusetts, USA), Hettich Universal 16 – centrifuge (Hettich GmbH & Co.KG; Tuttlingen, Germany), Neubauer cell counter (Laboroptik; Friedrichsdorf, Germany), water bath (Mettler; Shanghai, China), PBSE (see 7.1.4), Wilovert A – microscope (Leica; Wetzlar, Germany).

Cells were plated on dishes or wells corresponding to the experiment one day before transfection. To perform IF analysis (see 5.3.5), sterile coverslips were placed into the wells before adding cells. 2 h before starting, the cell culture medium (see below) was changed. According to dish/well size the CaPO₄/DNA precipitation solution was mixed (Table 2). Therefore the calculated amount of water and DNA was added to a 2 ml microcentrifuge tube and carefully mixed. After adding of CaCl₂, 2x DNA precipitation buffer (see below) was slowly added dropwise to the microcentrifuge tube. The mixture was mildly swirled and incubated for 20 min at RT. The precipitate was gently mixed and dropwise added to the cells. During this procedure the dish was carefully moved to mix the medium with the precipitate. The cells were incubated for 6 h in the CO₂-incubator (37°C, 5% CO₂). After 6 h the cells were washed 3-4 times with cell culture medium without FCS and a glycerol shock was performed. For this approach the medium was discarded and the cells were covered with glycerol shock buffer (see below) and incubated at RT. The length of incubation depended upon the degree of tolerance of the cell line and was checked under the microscope (~1 min HEK293, ~2 min MCF-7/HaCaT). Immediately the cells were washed 3x with medium without FCS. Fresh cell culture medium was added to the cells and cells were incubated at 37°C and 5% CO₂.

Table 2| DNA transfection by CaPO₄ precipitation.

Culture vessel	H ₂ O	DNA	2 M CaCl ₂	2x DNA precipitation buffer
6-well plate	200 µl	10 µg	13 µl	100 µl
6 cm dish	600 µl	30 µg	38 µl	300 µl
10 cm dish	1680 µl	70 µg	105 µl	840 µl

2x DNA precipitation buffer: 280 mM NaCl, 10 mM KCl, 1.5 mM Na₂HPO₄ (x2 H₂O), 12 mM glucose, 50 mM HEPES, pH 7.05 (filtered through 0.2 µm filter)

- Cell culture medium: high glucose (4.5g/l) DMEM flask, 1 mM sodium pyruvate, 1mM glutamate, 10% (v/v) FCS
- Glycerol shock buffer (1 ml): 300 μ l 50% (v/v) glycerol, 200 μ l cell culture grade H₂O, 500 μ l 2x DNA precipitation buffer

DNA transfection with Xfect™

Material: 12 mm coverslips (glassware factory Karl Hecht; Sondheim, Germany), cell culture medium (see 5.3.1 or 5.3.2), Hera Safe – Biological Safety Cabinet (Kendro; Langensfeld, Germany), Heraeus cytoperm 2 – CO₂ incubator (Thermo Fisher Scientific; Waltham, USA), Hettich Universal 16 – centrifuge (Hettich GmbH & Co.KG; Tuttlingen, Germany), Neubauer cell counter (Laboroptik; Friedrichsdorf, Germany), PBSE (see 7.1.4), Rotilabo® mini-centrifuge (Carl Roth; Karlsruhe, Germany), Vortex-Genie 2 (Scientific Industries; NY, USA), water bath (Mettler; Shanghai, China), Wilovert A – microscope (Leica; Wetzlar, Germany), Xfect™ (Clontech; Mountain View, California, USA).

The transfection of plasmid DNA was done using Xfect™ transfection reagent (Table 3). Plasmid DNA used in this study is listed in chapter 7.1.8. One day prior to the transfection, cells were plated to allow 50-70% confluency at the time of transfection. To perform IF analysis (see 5.3.5), sterile coverslips were placed into the wells before adding cells. Xfect polymer was thoroughly vortexed. In a microcentrifuge tube, the appropriate μ g of plasmid DNA was diluted with Xfect reaction buffer and mixed by vortexing for 5 sec at high speed. Xfect polymer was added to the diluted plasmid DNA and mixed by vortexing for 10 sec at high speed. To allow formation of nanoparticle complexes, the solution was incubated for 10 min at RT. After spinning down for 1 sec to collect the contents at the bottom of the tube, the entire nanoparticle complex solution was added dropwise to the cell culture medium. Thereby the plate was gently rocked back and forth to mix the medium with the solution. The plate was incubated at 37°C and 5% CO₂ for at least 4 h up to 48 h before further processing of the transfected cells.

Table 3| DNA transfection by Xfect reagent.

Culture vessel	Growth medium	DNA	Final dilution volume (in Xfect reaction buffer)	Xfect polymer volume
24-well plate	250 μ l	1 μ g	25 μ l	always 0.3 μ l of Xfect polymer for every 1 μ g of plasmid used
12-well plate	500 μ l	2.5 μ g	50 μ l	
6-well plate	1 ml	7.5 μ g	100 μ l	
10 cm dish	10 ml	30 μ g	600 μ l	

siRNA transfection with Lipofectamine® RNAiMax

Material: 12 mm coverslips (glassware factory Karl Hecht; Sondheim, Germany), cell culture medium for mouse keratinocytes (see 5.3.2), Hera Safe – Biological Safety Cabinet (Kendro; Langensfeld, Germany), Heraeus cytoperm 2 – CO₂ incubator (Thermo Fisher Scientific; Waltham, USA), Hettich Universal 16 – centrifuge (Hettich GmbH & Co.KG; Tuttingen, Germany), Lipofectamine® RNAiMax reagent (Thermo Fisher Scientific; Waltham, Massachusetts, USA), Rotilabo® mini-centrifuge (Carl Roth; Karlsruhe, Germany), water bath (Mettler; Shanghai, China), Wilovert A – microscope (Leica; Wetzlar, Germany), Vortex-Genie 2 (Scientific Industries; NY, USA).

For knockdown analyses in mouse keratinocytes, siRNA pools were transfected using Lipofectamine® RNAiMax reagent. siRNAs used in this study were listed in chapter 7.1.9. To transfect keratinocytes in suspension, the cells were plated in the appropriate density just prior to preparing transfection complexes. To perform IF analyses (see 5.3.5), sterile coverslips were placed into the wells before adding cells. Lipofectamine® RNAiMax reagent was thoroughly vortexed. For each sample two microcentrifuge tubes were prepared (Table 4), vortexed and incubated for 5 min at RT. The polymer solution was added to the siRNA pool solution and well vortexed at a medium speed for 10 sec. The entire siRNA-lipid complex was added dropwise to the freshly plated cells suspension by gently rocking the plate back and forth to mix. The keratinocytes were incubated at 32°C and 5% CO₂ until the time of analysis (24-48 h post transfection).

Table 4| siRNA transfection by Lipofectamine® RNAiMax reagent.

Culture vessel	Lipofectamine® RNAiMax reagent	siRNA
24-well plate	3 µl in 50 µl serum-free medium (SFM*)	1 µl (10 pmol) in 50 µl SFM
12-well plate	6 µl in 100 µl SFM	2 µl (20 pmol) in 100 µl SFM
6-well plate	9 µl in 150 µl SFM	3 µl (30 pmol) in 150 µl SFM

*SFM = serum-free medium

5.3.5. Indirect immunofluorescence

Material: -20°C acetone (Merck; Darmstadt, Germany), -20°C methanol (Merck; Darmstadt, Germany), 12 mm coverslips (glassware factory Karl Hecht; Sondheim, Germany), 3.7% (w/v) FA (see 7.1.4), BSA (bovine serum albumin from Carl Roth; Karlsruhe, Germany), Collagen I rat tail (Thermo Fisher Scientific; Waltham, Massachusetts, USA), Hoechst 33342 (stock 10 µg/µl, Thermo Fisher Scientific; Waltham, Massachusetts, USA), MT-stabilizing buffer (see below), Mowiol (see below), PBS (see 7.1.4), Poly-L-Lysine (Sigma Aldrich; St. Louis, Missouri, USA), primary and secondary antibody (see 7.1.6), skimmed milk (Milupa; Friedrichsdorf, Germany), tweezer.

To visualize proteins in fixed cells, two types of antibodies were used. The primary antibodies are unconjugated and recognize a specific target protein (or molecule) of interest within the cell. A fluorophore-conjugated secondary antibody directed against the primary anti-

body is then used for detection. For this approach, cells were grown on poly-L-lysine- (MCF-7) or collagen I-coated (mouse keratinocytes) coverslips and processed according to the experiment [transfection with plasmid or siRNA (5.3.4), switching LCM to HCM (5.3.2)]. The cells were then fixed according to the protein of interest.

Formaldehyde fixation

The cells growing on coverslips were washed with PBS and fixed in 3.7% (w/v) FA for 15 min at RT. After 3 x 10 min washing in PBS, cells were permeabilized in MT-stabilizing buffer (see below) at RT for 15 min at RT.

Methanol fixation

The cells growing on coverslips were washed with PBS and fixed in methanol for 10 min at -20°C. Subsequently, cells were permeabilized in MT-buffer (see below) at RT for 15 min.

Methanol/acetone fixation

The cells growing on coverslips were washed with PBS and fixed in methanol for 10 min at -20°C and subsequently in acetone for 30 sec at -20°C. Before further processing, cells were air-dried for 30 min.

After fixation and permeabilization of the cells on the glass coverslips, cells were incubated in blocking solution [1% (w/v) skimmed milk/PBS or 1% (w/v) BSA/PBS depending on primary antibody, see 7.1.6] for 30 min at RT. The primary antibody was diluted in blocking solution and incubated overnight at 4°C in a dark, humid chamber. Next day, coverslips were washed 3 x 10 min with PBS at RT. Cells were briefly blocked in blocking solution for 10 min at RT and a fluorophore-conjugated secondary antibody (see 7.1.6) was incubated for 1 h at RT. Finally, all samples were stained with Hoechst 33342 (1:1,000 in blocking solution) for 10 min at RT to visualize nuclei and the glass coverslips were mounted in Mowiol (see below).

Mowiol: 5% (w/v) Mowiol, 30% (v/v) glycerol, 0.25% (w/v) 1,4-diazabicyclo[2.2.2]octane (DABCO)

MT-buffer: 100 mM pipes (pH 6.9), 4 M glycerol, 2 mM EDTA, 1 mM EGTA, 0.5% (v/v) Triton X-100

5.3.6. Bimolecular fluorescence complementation (BiFC)

Material: 12 mm coverslips (glassware factory Karl Hecht; Sondheim, Germany), 3.7% (w/v) FA (see 7.1.4), Collagen I rat tail (Thermo Fisher Scientific; Waltham, Massachusetts, USA), Hoechst 33342 (stock 10 µg/µl, Thermo Fisher Scientific; Waltham, Massachusetts, USA), Mowiol (see above), PBS (see 7.1.4), primary and secondary antibody (see 7.1.6), skimmed milk (Milupa; Friedrichsdorf, Germany), tweezer.

For BiFC analysis, mouse keratinocytes were seeded onto Collagen-coated coverslips and co-transfected with pVen1 and pVen2 (see 1.5.6.7.1.8) constructs. 4 h post transfection, LCM was switched to HCM and cells incubated for 12 h before fixation in 3.7% (w/v) FA/PBS and immunostained with FLAG- and HA-tag-directed antibodies (see 1.5.6.7.1.6). DNA was stained with Hoechst 33342. Coverslips were mounted in Mowiol (see above). Images of cells expressing both FLAG- and HA-tagged fusion proteins were taken with identical exposure times (1,500 ms) to enable a comparison of BiFC efficiencies. Image processing and mean BiFC fluorescence intensities of two adjacent cells (n=30 images) were determined using ImageJ.

5.3.7. Dispase/epithelial sheet assay

Material: Dispase II (Roche; Basel, Switzerland), HEPES (Sigma Aldrich; St. Louis, Missouri, USA), Hera Safe – Biological Safety Cabinet (Kendro; Langensfeld, Germany), Heraeus cytoperm 2 – CO₂ incubator (Thermo Fisher Scientific; Waltham, USA), MS1 small orbital shaker (IKA; Staufen, Germany), PBS (see 7.1.4), Sony Cyber Shot DSC-H300 camera (Sony; Tokyo, Japan), Vortex-Genie 2 (Scientific Industries; NY, USA).

For analysis of intercellular cohesion, MCF-7 cells or keratinocytes were seeded in triplicates onto 12-well plates and grown to confluence (and switched to HCM for 24 h for keratinocyte differentiation, see 5.3.2). The confluent cell monolayer was washed twice with PBS (+1.2 mM CaCl₂ for keratinocytes) and incubated for 30 min with dispase solution (see below) at 37°C/5% CO₂. Free-floating monolayers were shaken on an orbital shaker for 30 min at RT and images were taken.

Dispase solution (MCF-7): Cell culture medium (see 5.3.1), 2.4 U/ml Dispase II, 25 mM HEPES

Dispase solution (keratinocytes): Cell culture medium (see 5.3.2), 2.4 U/ml Dispase II, 25 mM HEPES, 1.2 mM CaCl₂

5.3.8. Measurement of transepithelial electrical resistance (TER)

Material: LCM and HCM for mouse keratinocytes (see 5.3.2), Hera Safe – Biological Safety Cabinet (Kendro; Langensfeld, Germany), Heraeus cytoperm 2 – CO₂ incubator (Thermo Fisher Scientific; Waltham, USA), PBS (see 7.1.4), PET 24-well plate inserts with 0.4 µm pore size (Sigma Aldrich; Karlsruhe, Germany), voltmeter (World Precision Instruments; Sarasota, FL, USA).

To evaluate TJ-associated barrier function of keratinocytes, cells were seeded onto PET 24-well plate inserts, grown to confluence and switched to HCM. TER was monitored at indicated time points using a voltmeter with a chopstick electrode. Precautions were taken to maintain sterility during TER measurements.

5.3.9. Fluorescence recovery after photobleaching (FRAP)

Material: cell culture medium for MCF-7 (see 5.3.1) or mouse keratinocytes (see 5.3.2), Collagen I rat tail (Thermo Fisher Scientific; Waltham, Massachusetts, USA), glass-bottomed dishes (IBIDI; Martinsried, Germany), HEPES (Sigma Aldrich; St. Louis, Missouri, USA), Leica – TCS SP5 AOBs confocal microscope.

The dynamics of GFP-tagged PKP1-WT, PKP1M1-4A and PKP1M1-4E in MCF-7 cells was analyzed by FRAP kindly performed by Dr. Markus Glass (AG Hüttelmaier, Martin-Luther-University). Cells were plated on glass-bottomed dishes, transfected with the indicated plasmids (see 5.3.4) and analyzed 48 h after transfection. Before FRAP experiment, cell culture medium was changed and supplemented with 25 mM HEPES as a buffering agent. Bleaching and imaging was performed on a confocal microscope (Leica – TCS SP5 AOBs) using a HCX PL APO lambda blue 63x1.40 OIL objective and an argon laser at 488 nm. Ten images were taken before the bleach pulse and 300 images after bleaching with an image acquisition frequency of 5 frames/sec. For each time point, the background intensity was subtracted and the data were normalized by dividing each data point by the average unbleached value. The average fluorescence recovery curve was fitted to a single exponential function, given by $F(t)=A(1-e^{-t/\tau})+B$, where $F(t)$ is the intensity at time t , A the plateau level after recovery (mobile fraction), B the level after bleaching and τ the slope of the exponential term (time constant). The recovery half-times were obtained by calculating the time when the cells reached half of the final intensity. The mobile (M_f) and immobile fractions (I_f) were determined by calculating $M_f=A/(1-B)$ and $I_f=1-M_f$.

The dynamic of GFP-tagged PKP1 and PKP3 in PKP1- and PKP3 knockout keratinocytes plated on collagen I-coated glass-bottomed dishes was analyzed by FRAP 24 h after addition of 1.2 mM CaCl_2 . Before FRAP experiment, cell culture medium was changed and supplemented with 25 mM HEPES as a buffering agent. The setting for FRAP analysis was similar as above. Five images were taken before the bleach pulse and 200 images after bleaching with an image acquisition frequency of 4 frames/second. For data analysis the fluorescence intensities from three regions of interest per cell (ROI1 = bleached intercellular contact,

ROI2 = total cell and ROI3 = background) were determined. For each time point, the background intensity was subtracted and the data were full scale normalized using the following formula based on easyFRAP tool (Rapsomaniki et al., 2012):

$$I(t)^{dn} = \left[\left(\frac{1}{n_{pre}} \times \sum_{t=1}^{n_{pre}} I(t)ROI2' \right) \div I(t)ROI2' \right] \times \left[I(t)ROI1' \div \left(\frac{1}{n_{pre}} \times \sum_{t=1}^{n_{pre}} I(t)RPI1' \right) \right]$$

$$I(t)^{fullscale} = \left[I(t)^{dn} - I(t_{postbleach})^{dn} \right] \div \left[1 - I(t_{postbleach})^{dn} \right]$$

I = fluorescence intensity; t = time; dn = double normalized; ROI1'/ROI2' = background subtracted ROIs

The fluorescence recovery curve was fitted to a single exponential function (as above):

$$I(t) = A(1 - e^{-t\tau})$$

5.3.10. Cell migration assay

Material: cell culture medium for MCF-7 (see 5.3.1), culture-insert 2 well (IBIDI; Martinsried, Germany), Hera Safe – Biological Safety Cabinet (Kendro; Langensfeld, Germany), Heraeus cytoperm 2 – CO₂ incubator (Thermo Fisher Scientific; Waltham, USA), HEPES (Sigma Aldrich; St. Louis, Missouri, USA), PBSE (see 7.1.4), Zeiss Axio Imager microscope (Carl Zeiss; Jena, Germany).

To analyze cell migration into a cell free gap, culture-inserts consisting of two reservoirs separated by a 500 µm thick wall were placed onto a culture plate. MCF-7 cells stably expressing DsRed, PKP1-WT-, PKP1M1-4A- or PKP1M1-4E-DsRed (see 5.3.3) were seeded in duplicate into the two reservoirs (4x10⁵ cells/ml; 70 µl/reservoir) and grown to confluency for 48 h. Before the insert was removed creating a gap of ~500 µm, the medium was refreshed supplemented with 25 mM HEPES as a buffering agent. Migration was observed by live cell imaging using a Zeiss Axio Imager microscope (Carl Zeiss) in an incubation chamber allowing temperature (37°C), humid and CO₂ (10%) control. Brightfield images were acquired every 1 h for a period of 24 h using a 10x Ex Plan Neofluar objective (NA 0.3) and standardized microscope settings. The area of migrated cells into the gap was quantified using the MiToBo plugin for ImageJ.

5.3.11. Soft agar assay for colony formation

Material: agar (Carl Roth; Karlsruhe, Germany), agarose (Carl Roth; Karlsruhe, Germany), culture medium for MCF-7 (see 5.3.1), EOS 40D camera (Canon; Tokyo, Japan), G418 selection agent (PAA; Pasching, Austria), Hera Safe – Biological Safety Cabinet (Kendro; Langensfeld, Germany), Heraeus cytoperm 2 – CO₂ incubator (Thermo Fisher Scientific; Waltham, USA), Hettich Universal 16 – centrifuge (Hettich GmbH & Co.KG; Tuttlingen, Germany), iodonitrotetrazolium chlorid (Applichem; Darmstadt, Germany), microwave, Neubauer cell counter (Laboroptik; Friedrichsdorf, Germany), PBSE (see 7.1.4), water bath (Memmert; Shanghai, China), Wilovert A – microscope (hund; Wetzlar, Germany).

The soft agar colony formation assay is a method used to analyze cellular anchorage-independent growth *in vitro*. The setup is shown in Fig. 50. To prepare base agar, all steps were done sterilely. 1% (w/v) agar was melted in a microwave and cooled to 40°C in a water bath. Using falcon tubes, 2x cell culture medium supplemented with 20% (v/v) FCS and 1.2 mg/μl G418 was warmed to 40°C in water bath. The temperature was equilibrated at least 30 min. Equal volumes of the two solutions were mixed to give 0.5% (w/v) agar in 1x cell culture medium supplemented with 10% (v/v) FCS and 600 μg/μl G418. 200 μl/well of the mixed solution was added in a 48well-plate and set aside for 5 min to allow agar to solidify. To prepare top agarose, 0.7% (w/v) agarose was melted in a microwave and cooled to 40°C in a water bath. Using falcon tubes, 2x cell culture medium supplemented with 20% (v/v) FCS and 1.2 mg/μl G418 was warmed to 40°C in water bath. The temperature was equilibrated at least 30 min. During that time, MCF-7 cells stably expressing DsRed, PKP1-WT-, PKP1M1-4A- or PKP1M1-4E-DsRed (see 5.3.3) were trypsinized and cell count was determined. To seed 1,000 cells/well, the appropriate cell suspension was added to a falcon tube. Equal volumes of the two solutions were mixed to give 0.35% (w/v) agarose in 1x cell culture medium supplemented with 10% (v/v) FCS and 600 μg/μl G418 together with the appropriate cell density. 200 μl/well of the mixed solution was added in sextuple in a 48well-plate and incubated at 37°C and 5% CO₂ for approximately 3 weeks. 1-2 times a week, fresh medium (100 μl/well) was added. Cell colonies were stained overnight using 5 mg/ml iodinitrotetrazolium chlorid (diluted in H₂O and sterile filtered) and images were acquired using an EOS 40D with an EFS 60 mm macro lens.

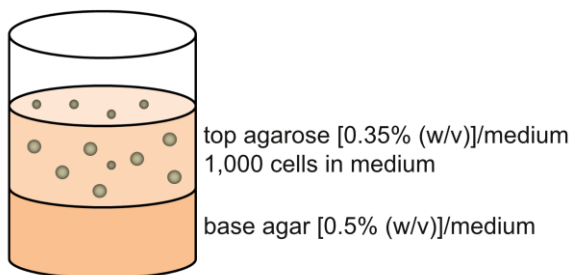


Fig. 50| Soft agar assay setup.

The image illustrates the setup of the soft agar assay. On the base, 0.5% (w/v) agar + medium was added. On the top, a semisolid culture consisting of 0.35% (w/v) agarose + 1,000 cells/medium was added. 100 μl medium was added 1-2 times a week. Colony formation was checked for 3 weeks and finally stained with iodinitrotetrazolium chlorid.

5.3.12. Cell count analysis

Material: 2.5% (w/v) trypsin (Life Technologies; Carlsbad, California, USA), Hera Safe – Biological Safety Cabinet (Kendro; Langenselbold, Germany), Heraeus cytoperm 2 – CO₂ incubator (Thermo Fisher Scientific; Waltham, Massachusetts, USA), Hettich Universal 16 – centrifuge (Hettich GmbH & Co.KG; Tuttlingen, Germany), mouse keratinocyte medium (5.3.2), Neubauer cell counter (Laboroptik; Friedrichsdorf, Germany), PBS (7.1.4), water bath (Memmert; Shanghai, China), Wilovert A – microscope (hund; Wetzlar, Germany).

For analysis of cell count, spontaneously immortalized WT and PKP1-KO keratinocytes, and PKP1-KO cells expressing either GFP or hPKP1-GFP (see 5.3.3) were seeded in quadruple onto 96-well plates (0.2×10^5 cells/cm²) and cell number was counted 48 h after plating. Therefore, cells were detached from the well using 50 µl trypsin. Trypsin reaction was stopped by adding fresh cell culture medium and cell count was determined using Neubauer cell counter. Results are displayed as relatives of cell counts. PKP1-KO cell counts were normalized to WT cell counts. Cell count analysis was kindly performed by Dr. René Keil (Hatzfeld Lab, Martin-Luther-University).

5.3.13. Cell proliferation assay (BrdU)

Material: 12 mm coverslips (glassware factory Karl Hecht; Sondheim, Germany), 3.7% (w/v) FA (see 7.1.4), 4 M HCl, anti-BrdU antibody and secondary antibody (see 7.1.6), blocking solution (see below), BrdU (Roche; Basel, Switzerland), BSA (Carl Roth; Karlsruhe, Germany), Hera Safe – Biological Safety Cabinet (Kendro; Langenselbold, Germany), Heraeus cytoperm 2 – CO₂ incubator (Thermo Fisher Scientific; Waltham, Massachusetts, USA), Hettich Universal 16 – centrifuge (Hettich GmbH & Co.KG; Tuttlingen, Germany), Hoechst 33342 (stock 10 µg/µl, Thermo Fisher Scientific; Waltham, Massachusetts, USA), Mowiol (see below), PBS & PBSE (see 7.1.4), Triton X-100 (Sigma Aldrich; St. Louis, Missouri, USA).

5-bromo-2'-deoxyuridine (BrdU) is a thymidine analog, which is incorporated into DNA during DNA synthesis when added exogenously. An anti-BrdU antibody is then used to label proliferating cells that have incorporated BrdU. For this approach, MCF-7 cells were transfected (see 5.3.4) and 24 h later serum-starved for additional 24 h (0.1% FCS), refreshed with 10% FCS for 16 h and subsequently incubated with 10 µM BrdU for 1 h. After fixation in 3.7% (w/v) FA for 20 min at RT, the DNA was denatured with 4 M HCl for 10 min at RT. Specimen were washed 3 times in blocking solution (see below) for 10 min at RT followed by BrdU antibody staining (1:250 in blocking solution) overnight at 4°C in a humid, dark chamber. Next day, coverslips were washed 3 x 10 min with PBS. Cells were briefly blocked in blocking solution (see below) for 10 min at RT and a fluorophore-conjugated secondary antibody was incubated for 1 h at RT in a humid, dark chamber. Finally, Hoechst 33342

staining (1:1,000 in blocking solution) was done for 10 min at RT to visualize nuclei and the glass coverslips were mounted in Mowiol (see below). More than 200 transfected cells were checked for BrdU incorporation in each independent assay.

Blocking solution: 1% (w/v) BSA, 0.1% (v/v) Triton X-100, in PBS

Mowiol: 5% (w/v) Mowiol, 30% (v/v) glycerol, 0.25% (w/v) 1,4-diazabicyclo[2.2.2]octane (DABCO)

5.3.14. Cell viability assay (crystal violet)

Material: 3.7% (w/v) FA (see 7.1.4), crystal violet (Sigma Aldrich; St. Louis, Missouri, USA), Hera Safe – Biological Safety Cabinet (Kendro; Langenselbold, Germany), Heraeus cytoperm 2 – CO₂ incubator (Thermo Fisher Scientific; Waltham, Massachusetts, USA), Hettich Universal 16 – centrifuge (Hettich GmbH & Co.KG; Tuttlingen, Germany), LabSystems Multiscan RC microplate reader (Thermo Fisher Scientific; Waltham, Massachusetts, USA), MS1 small orbital shaker (IKA; Staufen, Germany), PBS (see 7.1.4), SDS (Carl Roth; Karlsruhe, Germany).

MCF-7 cells stably expressing DsRed, PKP1-WT-, PKP1M1-4A- or PKP1M1-4E-DsRed (see 5.3.3) were seeded in triplicate onto 98-well plates (5,000 cells/well) and cultured for 24, 48, 72 and 96 h at 37°C and 5% CO₂. Cells were gently washed in PBS, fixed in 3.7% (w/v) FA for 20 min at RT and 3 times washed in PBS. Cells were stained with 0.05% (w/v) crystal violet/PBS for 1 h at RT and 3 times washed with water followed by a washing step in PBS for 15 min at RT on an orbital shaker. PBS was removed and the plates were left to dry at 37°C. The dye was dissolved by shaking the cells in 1% (v/v) SDS/PBS for 30 min at RT. Absorption was measured at 550 nm. To avoid bias by variability in cell seeding, all data were normalized to values determined at 24 h.

5.4. Biochemical methods

5.4.1. Preparation of protein lysates

Preparation of protein lysates from mouse skin

Material: dissecting set, Dry bath FB15103 (Thermo Fisher Scientific; Waltham, Massachusetts, USA), Heraeus Pico 17 – centrifuge (Thermo Fisher Scientific; Waltham, Massachusetts, USA), protease (10 µg/ml aprotinin, 10 µg/ml leupeptin, 1 mM pepabloc) and phosphatase (1 mM NaVO₃, 10 mM NaF) inhibitors (Sigma Aldrich; St. Louis, Missouri, USA), SDS lysis buffer (see below), Ultra-Turrax T25 - homogenizer (IKA; Staufen, Germany).

For analysis of protein expression, pieces of dorsal skin from newborn mice were homogenized using a homogenizer and subsequently boiled for 5 min in SDS lysis buffer (see below). Prior the lysis buffer was freshly supplemented with protease and phosphatase inhibitors. Skin extracts were centrifuged for 15 min at 14,000x g and RT. The supernatant was

transferred into a new microcentrifuge tube and the protein concentration was determined (see 5.4.2). The lysates were either stored at -80°C or directly used for SDS-PAGE (see 5.4.4).

SDS lysis buffer: 20 mM Tris-HCl, pH 7.5, 1% (w/v) SDS, 10 $\mu\text{g}/\text{ml}$ aprotinin, 10 $\mu\text{g}/\text{ml}$ leupeptin, 1 mM pefabloc, 5 mM NaF, 1 mM NaVO_3

Preparation of protein lysates from adherent cells

Material: 4x SDS loading buffer (see 7.1.4), Benzonase[®] nuclease (Santa Cruz; Dallas, Texas, USA), Heraeus Pico 17 – centrifuge (Thermo Fisher Scientific; Waltham, USA), PBS (see 7.1.4), protease (10 $\mu\text{g}/\text{ml}$ aprotinin, 10 $\mu\text{g}/\text{ml}$ leupeptin, 1 mM pefabloc) and phosphatase (1 mM NaVO_3 , 10 mM NaF) inhibitors (Sigma Aldrich; St. Louis, Missouri, USA), rubber cell scraper, SDS lysis buffer (see below).

The adherent cells were washed twice with ice cold PBS and incubated with the appropriate lysis buffer [e.g. SDS lysis buffer (see below)] for 10 min. Prior the lysis buffer was supplemented with protease and phosphatase inhibitors. The cells were scraped off using a rubber cell scraper. The cell suspension was transferred to a microcentrifuge tube, frozen in liquid nitrogen and stored at -80°C . The deep-frozen samples were thawed in a water bath at RT and centrifuged for 10 min at 14,000x g at RT. The supernatant was transferred into a new microcentrifuge tube and the protein concentration was determined (see 5.4.2). Cell lysates were used for SDS-PAGE (see 5.4.4) and Western blot analysis (see 5.4.6). For the direct use of cell lysates for SDS-PAGE without determination of protein concentration, cells were washed twice with ice cold PBS and incubated with SDS loading buffer (see below) for 5 min. The cells were scraped off, transferred to a microcentrifuge tube, boiled at 95°C for 5 min, centrifuged for 10 min at 14,000x g and RT and loaded onto a gel (see 5.4.4).

SDS lysis buffer: 20 mM Tris-HCl, pH 7.5, 1% (w/v) SDS, [fresh: 10 $\mu\text{g}/\text{ml}$ aprotinin, 10 $\mu\text{g}/\text{ml}$ leupeptin, 1 mM pefabloc, 5 mM NaF, 1 mM NaVO_3 , 250 U/ml Benzonase[®] nuclease]

5.4.2. Solubility assay

Material: 4x SDS loading buffer (see 7.1.4), Heraeus Pico 17 – centrifuge (Thermo Fisher Scientific; Waltham, USA), PBS (see 7.1.4), non-denaturing lysis buffer (see below), protease (10 $\mu\text{g}/\text{ml}$ aprotinin, 10 $\mu\text{g}/\text{ml}$ leupeptin, 1 mM pefabloc) and phosphatase (1 mM NaVO_3 , 10 mM NaF) inhibitors (Sigma Aldrich; St. Louis, Missouri, USA), rubber cell scraper, SDS lysis buffer (see above).

The adherent cells were washed twice with ice cold PBS and suspended for 15 min in non-denaturing lysis buffer (see below). After centrifugation for 30 min at 13,000x g, the supernatant (soluble fraction) was collected and the pellet (insoluble fraction) was resuspended in the same volume of SDS lysis buffer (see above). The fractions were resolved by SDS-

PAGE (5.4.4), transferred to nitrocellulose and probed with the appropriate antibodies (5.4.6).

Non-denaturing lysis buffer: 20 mM Tris-HCl, pH 7.5, 140 mM NaCl, 10% (v/v) glycerol, 1.5% (v/v) Triton X-100, 2 mM EDTA, [fresh: 10 µg/ml aprotinin, 10 µg/ml leupeptin, 1 mM pepabloc, 5 mM NaF, 1 mM NaVO₃, 250 U/ml Benzonase® nuclease]

5.4.3. Determination of protein concentration by BCA assay

Material: BSA stock (2 mg/ml), GeneQuant 1300 V1.6.1 – Spectrophotometer (GE Healthcare; Munich, Germany), Incucell – incubator (MMM Medcenter Einrichtungen GmbH; Planegg, Germany), Pierce® BCA Protein Assay Kit (Life Technologies; Carlsbad, California, USA), Vortex-Genie 2 (Scientific Industries; NY, USA).

The BCA protein assay is used for quantitation of total protein in a sample. The principle of this method is the ability of proteins to reduce Cu⁺² to Cu⁺¹ in an alkaline solution (the biuret reaction), which results in a purple color formation by bicinchoninic acid (BCA) and was detected with a spectrophotometer at 562 nm. The reduction of copper is mainly caused by four amino acid residues including cysteine or cystine, tyrosine and tryptophan that are present in protein molecules. The assay was performed according to the manufacturer's instructions. Therefore a diluted BSA standard was prepared (Table 5) to construct a calibration curve.

Table 5| Preparation of diluted BSA standard.

Sample	BSA concentration	to pipette
1	100 µg/ml	25 µl BSA stock (2 mg/ml) + 475 µl H ₂ O
2	50 µg/ml	250 µl from sample 1 + 250 µl H ₂ O
3	25 µg/ml	250 µl from sample 2 + 250 µl H ₂ O
4	10 µg/ml	200 µl from sample 3 + 300 µl H ₂ O
5	5 µg/ml	250 µl from sample 4 + 250 µl H ₂ O
6	2.5 µg/ml	250 µl from sample 5 + 250 µl H ₂ O
7	0 µg/ml	250 µl H ₂ O (blank)

The unknown samples were diluted (1:100 – 1:200 in H₂O). To perform BCA assay, 100 µl of the diluted BSA standard samples or diluted unknown samples were mixed with 100 µl of a freshly prepared 25:25:1 ABC solution (from the Pierce® BCA Protein Assay Kit). The mixture was vortexed and incubated for 1 h at 37°C. Next, the absorbances of the standard BSA solutions as well as the unknown samples were measured at 562 nm with a spectrophotometer. The responses of the standards were used to plot a standard curve using the software Microsoft Excel. Absorbance values of the unknown samples were interpolated onto

the plot for the standard curve to determine their concentrations.

5.4.4. Sodium dodecyl sulfate polyacrylamide gel electrophoresis (SDS-PAGE)

Material: 4x SDS loading buffer (see 7.1.4), Dry bath FB15103 (Thermo Fisher Scientific; Waltham, Massachusetts, USA), Electrophoresis Power Supply Consort EV231 (Sigma Aldrich; St. Louis, Missouri, USA), Heraeus Pico 17 – centrifuge (Thermo Fisher Scientific; Waltham, Massachusetts, USA), Mini-PROTEAN-System – Electrophoresis chamber (Bio-Rad; Munich, Germany), PageRuler™ Plus Prestained protein ladder (life technologies; Carlsbad, California, USA), SDS running buffer (see below).

To separate proteins under denaturing conditions, sodium dodecyl sulfate polyacrylamide gel electrophoresis (SDS-PAGE) was used (Laemmli, 1970). Proteins become negatively charged in SDS and can be separated by their electrical charge according to the molecular size. Protein lysates were separated on SDS-polyacrylamide gels prepared according to the compositions (8-15% PAA). After the polymerization of the gel and assembly of electrophoresis system, samples were mixed with 4x SDS loading buffer, boiled for 5 min at 95°C and briefly centrifuged. 20 µl was loaded in the stacking gel. 8 µl of the PageRuler™ Plus Prestained protein ladder was loaded in one pocket of the gel as protein standard. The electrophoresis module was filled with SDS running buffer (see below) and electrophoresis was carried out at 75 V for 20 min and 95 V for approximately 2 h.

SDS running buffer: 25 mM Tris/HCl, 19.2 mM glycine, 0.1% (v/v) SDS

5.4.5. Coomassie staining of polyacrylamide gels

Material: Coomassie staining and unstaining solution (see below), Coomassie Brilliant Blue R250 (Carl Roth; Karlsruhe, Germany), Heidolph Duomax 1030 – Rocking Shaker (Schütt Labortechnik GmbH; Göttingen, Germany), microwave.

To stain protein samples after electrophoretic separation in a polyacrylamide gel (see 5.4.4), Coomassie Brilliant Blue R250 was used. The dye binds to proteins through ionic interactions between dye sulfonic acid groups and positive protein amine groups. Therefore, the gels were boiled in Coomassie staining solution (see below) and incubated for 5 min. To remove unbound staining solution, the gels were boiled in unstaining solution (see below) for 5 min. Gels were incubated with refreshed unstaining solution overnight at RT on a rocking shaker.

Coomassie staining solution: 0.25% (w/v) Coomassie Brilliant Blue R250, 9.2% (v/v) acetic acid, 45% (v/v) methanol

Coomassie unstaining solution: 7.5% (v/v) acetic acid, 5% (v/v) methanol

5.4.6. Western blot

Material: blotting buffer I, II, III (see below), BSA (Carl Roth; Karlsruhe, Germany), chemiluminescence solution (CLS) 1 and 2 (see below), Fusion-SL – Chemiluminescence- and Fluorescence system Imager (Pierce; Erlangen, Germany), Heidolph Duomax 1030 – Rocking Shaker (Schütt Labortechnik GmbH; Göttingen, Germany), Impuls Sealer (Burghardt GmbH; Stuttgart, Germany), PerfectBlue Semi-Dry blotter (Pierce; Erlangen, Germany), Ponceau S (Carl Roth; Karlsruhe; Germany), primary and secondary antibodies (see 7.1.6), Rotilabo filter paper (Carl Roth; Karlsruhe, Germany), SB3 Stuart – overhead rotator (Dunn Labortechnik GmbH; Asbach, Germany), skimmed milk (Milupa; Friedrichsdorf, Germany), TBS & TBST (see 7.1.4), VWR® Power Source (VWR; Radnor, Pennsylvania, USA), Wet blot buffer (see below), Wet blot equipment (Pierce; Erlangen, Germany), Whatman Protran Nitrocellulose Transfer Membrane (Whatman; Kent, UK).

Proteins were transferred from the SDS-PAA gel to nitrocellulose membranes using a PerfectBlue Semi-Dry blotter (Renart et al., 1979). The composition of the blotting device was:

Setup semi-dry blot	<i>anode (+)</i> 3x whatman cellulose filter paper in blotting buffer I 3x whatman cellulose filter paper in blotting buffer II nitrocellulose membrane in blotting buffer II SDS-PAA gel 3x whatman cellulose filter paper in blotting buffer III <i>cathode (-)</i>
----------------------------	---

The transfer was performed at 1 mA/cm² for 45 min, followed by 1.5 mA/cm² for 30 min. Proteins larger than 200 kDa were transferred to nitrocellulose membrane using a Wet blot approach:

Setup wet blot	<i>anode (+)</i> sponge in wet blot buffer 2x whatman cellulose filter paper in wet blot buffer nitrocellulose membrane in blotting buffer II SDS-PAA gel 2x whatman cellulose filter paper in wet blot buffer sponge in wet blot buffer <i>cathode (-)</i>
-----------------------	--

The protein transfer using the Wet blot approach was performed at 400 mA for 3 h. The efficiency of the transfer was monitored by staining the membrane with 1x Ponceau S (see below) for 10 min. Afterwards the membrane was briefly washed in TBST and incubated with blocking solution 5% (w/v) skimmed milk/TBST or 3% (w/v) BSA/TBST depending on primary antibody (see 7.1.6) and incubated on a rocking shaker for 30 min at RT. The primary antibodies were incubated at 4°C overnight on an overhead rotator in the appropriate blocking solution. Next day, membranes were washed 3 x 10 min in TBST. Horseradish peroxidase (HRP) conjugated secondary antibodies were diluted in 5% (w/v) milk/TBST (see 7.1.6), added to the membrane and incubated for 1 h at RT on a rocking

shaker. Membranes were washed 3 x 10 min in TBST and once in TBS for 5 min. Finally, membranes were immersed with ECL [equal parts chemiluminescence solution (CLS) 1 and 2 (see below)] and chemiluminescence was detected using Imager Fusion-SL.

10x Ponceau S:	2% (w/v) Ponceau S, 30% (w/v) TCA, 30% (w/v) sulfosalicylic acid
Blotting buffer I:	0.3 M Tris/HCl (pH 10.4), 20% (v/v) methanol
Blotting buffer II:	25 mM Tris/HCl (pH 10.4), 20% (v/v) methanol
Blotting buffer III:	25 mM Tris/HCl (pH 9.4), 40 mM ϵ -aminocaproic acid, 20% (v/v) methanol
CLS 1:	100 mM Tris/HCl (pH 8.5), 25 mM luminol, 0.4 mM coumaric acid
CLS 2:	100 mM Tris/HCl (pH 8.5), 0.02% (v/v) H ₂ O ₂
Wet blot buffer:	48 mM Tris/HCl, 39 mM glycerol, 0.0375% (v/v) SDS, pH 9.2

5.4.7. Expression of GST-fusion proteins

Material: 2xYT medium (see below), 4x SDS loading buffer (see 7.1.4), ampicillin (Carl Roth; Karlsruhe, Germany), Dry bath FB15103 (Thermo Fisher Scientific; Waltham, USA), GeneQuant 1300 Spectrophotometer (GE Healthcare; Munich, Germany), GST buffer (see below), Hettich Mikro 220R – centrifuge (Hettich GmbH & Co.KG; Tuttlingen, Germany), Incubator Shaker Series I26 (Eppendorf; Hamburg, Germany), isopropyl- β -D-1-thiogalactopyranoside [(IPTG), Carl Roth; Karlsruhe, Germany], PBS (see 7.1.4), SB3 Stuart – overhead rotator (Dunn Labortechnik GmbH; Asbach Germany), Triton X-100 (Sigma Aldrich; St. Louis, Missouri, USA), UP 200S – Ultrasonic processor (Hielscher Ultrasonics GmbH; Teltow, Germany).

E. coli cells [strain BL21(DE3)] were transformed with plasmids encoding for the GST-fusion proteins of interest (see 0) and plated on agar plates containing 100 μ g/ml ampicillin. To inoculate the preculture, bacterial colonies containing the transformed *E. coli* were transferred to a flask containing 25 ml 2xYT medium (see below) with 100 μ g/ml ampicillin. The culture was incubated on an environmental shaker at 37°C until the OD₆₀₀ reaches a maximum of 1.2. Next, the complete preculture was used to inoculate the 250 ml 2xYT medium main culture (100 μ g/ml ampicillin), which was incubated at 37°C until an OD₆₀₀ of 0.4. The expression of the proteins was induced by adding 0.2 mM IPTG and the culture was incubated for 3 h at 30°C. The bacteria were harvested by centrifugation for 10 min at 4,000x g and 4°C. Pellets were resuspended in ice-cold PBS, aliquoted, centrifuged (10 min, 4,000x g, 4°C) and stored at -80°C. To analyze the expression of the protein as well as its solubility, the bacteria was resuspended in ice-cold GST buffer (see below) and sonicated on ice (amplitude 90%, pulse cycle 0.9 for 30sec; 3 times each probe). Triton X-100 was added to a final concentration of 1% (v/v), incubated for 30 min at 4°C on an overhead rotator and centrifuged (30 min, 14,000x g, 4°C) to remove insoluble proteins and cell debris. The pellet

was resuspended in 4 x SDS loading buffer (see below), boiled for 5 min at 95°C, briefly centrifuged and analyzed by SDS-PAGE (see 5.4.4) and following Coomassie brilliant blue staining (see 5.4.5).

2x YT medium: 10 g/l NaCl, 10 g/l yeast extract, 16 g/l tryptone

GST buffer: 50 mM Tris/HCl (pH 7.5), 150 mM NaCl, 1 mM EDTA, 10% (v/v) glycerol, protease/phosphatase inhibitors (fresh): 10 µg/ml aprotinin, 10 µg/ml leupeptin, 1 mM pepabloc, 1 mM DTT, 5 mM NaF, 1 mM NaVO₃

5.4.8. Glutathione S-transferase (GST) pulldown

Material: 4x SDS loading buffer (see 7.1.4), cell lysis buffer (see below), Dry bath FB15103 (Thermo Fisher Scientific; Waltham, USA), glutathione sepharose (Thermo Fisher Scientific; Waltham, Massachusetts, USA), GST buffer (see below), Hettich Mikro 220R – centrifuge (Hettich GmbH & Co.KG; Tuttlingen, Germany), SB3 Stuart – overhead rotator (Dunn Labortechnik GmbH; Asbach, Germany), Triton X-100 (Sigma Aldrich; St. Louis, Missouri, USA), UP 200S – Ultrasonic processor (Hielscher Ultrasonics GmbH; Teltow, Germany).

Pulldown analyses are *in vitro* methods used to determine a physical interaction between two or more proteins. The pulldown assay is a form of affinity purification and is similar to immunoprecipitation (see 5.4.9) except that a “bait” protein is used instead of an antibody. In this approach the protein of interest is tagged with glutathione S-transferase (GST) and captured on an immobilized affinity ligand specific for the tag (glutathione sepharose). The immobilized bait is then incubated with cell lysate that contains putative “prey” proteins. The binding of proteins can be analyzed by SDS-PAGE (see 5.4.4) and Western blotting (see 5.4.6). To perform GST pulldown analyses, 14-3-3 γ in pGEX-5X-1 (Amersham) was expressed in *E. coli* BL21(DE3) (see 5.4.7). Bacteria were harvested by centrifugation at 4,000x g and 4°C for 10 min, resuspended in GST buffer (see below) and sonicated on ice (amplitude 90%, pulse cycle 0.9 for 30 sec; 3 times each probe). Triton X-100 was added to a final concentration of 1% (v/v) and the lysates were incubated for 30 min at 4°C on an overhead rotator. Lysates were centrifuged for 30 min at 14,000x g and 4°C. The supernatant was added into a new tube and the amount of GST-14-3-3 was checked by SDS-PAGE (see 5.4.4) and Western blot (see 5.4.6). The appropriate amount of glutathione sepharose (20 µl/pulldown) was equilibrated by washing 3 times in 800 µl GST buffer (see below) and collecting by centrifugation for 1 min at 4,000x g at 4°C. The bacterial lysates were incubated with the equilibrated glutathione sepharose (10-20 volumes of bacterial lysates to sepharose) for 2 h at 4°C on an overhead rotator. After 3 times washing in GST buffer (see below), equal amounts of cell lysate (~500 µl) were added to 30 µl GST or GST-14-3-3 γ se-

pharose, respectively, and incubated for additional 2 h at 4°C on an overhead rotator. Prior the cell lysates were prepared (see 5.4.1) using cell lysis buffer (see below) for GST pull-down and one part (~150 µl) was saved for input. After 3 times washing of the glutathione sepharose in GST lysis buffer the bound proteins were eluted in 4x SDS loading buffer (50 µl/pulldown), boiled for 5 min at 95°C, briefly centrifuged, separated by SDS-PAGE (see 5.4.4), and analyzed by Western blot (see 5.4.6).

GST buffer: 50 mM Tris/HCl (pH 7.5), 150 mM NaCl, 1 mM EDTA, 10% (v/v) glycerol
 Cell lysis buffer: 20 mM Tris/HCl (pH 7.5), 137 mM NaCl, 2 mM EDTA, 10% (v/v) glycerol, 1% (v/v) NP-40 (IPEGAL), protease inhibitors (fresh): 10 µg/ml aprotinin; 10 µg/ml leupeptin, 1 mM pefabloc; phosphatase inhibitors (fresh): 1 mM DTT, 5 mM NaF, 1 mM NaVO₃

5.4.9. Immunoprecipitation (IP)

Material: 4x SDS loading buffer (see 7.1.4), ChromoTek GFP-trap® (ChromoTek GmbH; Martinsried, Germany) or anti-FLAG M2 affinity gel (Sigma Aldrich; St. Louis, Missouri, USA), Dry bath FB15103 (Thermo Fisher Scientific; Waltham, Massachusetts, USA), GFP-trap lysis buffer & GFP-trap dilution buffer (see below), Hettich Mikro 220R – centrifuge (Hettich GmbH & Co.KG; Tuttlingen, Germany), IP buffer (see below), PBS (see 7.1.4), SB3 Stuart – overhead rotator (Dunn Labortechnik GmbH; Asbach, Germany).

GFP-immunoprecipitation

ChromoTek GFP-trap®, which utilizes small recombinant alpaca antibody fragments covalently coupled to the surface of agarose beads to recognize GFP, was used to search for 14-3-3 γ and 14-3-3 σ association partners in mouse keratinocytes. For this approach, mouse keratinocytes were cultured in 10 cm culture dishes. 24 h after plating, cells were transfected with plasmids encoding GFP-14-3-3 γ , GFP-14-3-3 σ , or GFP, respectively (see 5.3.4). 48 h after transfection, cells were washed twice with ice cold PBS and lysed in 500 µl of cold GFP-trap lysis buffer (see below). Lysates were transferred to 1.5 ml tubes, incubated 30 min on ice and clarified by centrifugation at 14,000x g for 15 min at 4°C. One part (~150 µl) was saved for input. Vortexed GFP-Trap® beads were pipetted into 500 µl ice cold GFP-trap washing buffer (see below) and centrifuged at 4,000x g for 1 min at 4°C. The supernatant was discarded and the pellet was washed twice in GFP-trap washing buffer (see below). Equal amounts of cell lysates (~500 µl) were added to the equilibrated GFP-trap® beads (30 µl) and incubated for 1 h at 4°C on an overhead rotator. After centrifugation at 4,000x g for 1 min at 4°C, beads were washed with 800 µl GFP-trap® washing buffer. The supernatant (unbound proteins) was discarded and the washing step was repeated twice. Finally, GFP-trap® beads were resuspended in 50 µl 4x SDS loading buffer and boiled for

10 min at 95°C to dissociate immunocomplexes from the beads. GFP-trap® beads were collected by centrifugation at 4,000x g for 2 min at RT. The supernatants were analyzed by SDS-PAGE (see 5.4.4) and Western blot (see 5.4.6).

GFP-trap lysis buffer: 10 mM Tris/HCl (pH 7.5), 150 mM NaCl, 0.5 mM EDTA, 0.5% (v/v) NP-40 (IPEGAL), protease inhibitors (fresh): 10 µg/ml aprotinin; 10 µg/ml leupeptin, 1 mM pefabloc; phosphatase inhibitors (fresh): 1 mM DTT, 5 mM NaF, 1 mM NaVO₃

GFP-trap washing buffer: 10 mM Tris/HCl (pH 7.5), 150 mM NaCl, 0.5 mM EDTA

FLAG-immunoprecipitation

To analyze the association of 14-3-3 proteins to phosphorylated PKP1, HEK293 cells were seeded on poly-L-lysine-coated 10 cm dishes and transfected 24h later with plasmids encoding for FLAG-tagged PKP1 in presence or absence of myr-HA-Akt2 (see 5.3.4). The next day, HEK293 cells were serum-starved for additional 24 h. For co-IP, cells were washed twice with ice cold PBS and lysed with 500 µl of IP buffer (see below). Lysates were transferred to 1.5 ml tubes, incubated 30 min on ice and clarified by centrifugation at 14,000x g for 15 min at 4°C. One part (~150 µl) was saved for input. 500 µl of cell lysates were incubated with 30 µl equilibrated anti-FLAG M2 affinity gel for at least 1 h at 4°C on an overhead rotator. The affinity gel was separated from the supernatant by centrifugation at 4,000x g for 1 min at 4°C and was washed 3 times in IP buffer. Bound proteins were solubilized in 4x SDS loading buffer, separated on SDS-PAA gels (see 5.4.4) and analyzed by Western blot (see 5.4.6).

IP buffer: 20 mM Tris/HCl (pH 7.5), 137 mM NaCl, 2 mM EDTA, 10% (v/v) glycerol, 1% (v/v) NP-40 (IPEGAL), protease inhibitors (fresh): 10 µg/ml aprotinin; 10 µg/ml leupeptin, 1 mM pefabloc; phosphatase inhibitors (fresh): 1 mM DTT, 5 mM NaF, 1 mM NaVO₃

5.5. Molecular biological methods

5.5.1. Reverse transcription (cDNA synthesis)

Material: dNTPs (Thermo Fisher Scientific; Waltham, Massachusetts, USA), DTT, Heraeus Pico 17 – centrifuge (Thermo Fisher Scientific; Waltham, Massachusetts, USA), random primer (Roche; Mannheim, Germany), RNase/DNase-free water (Thermo Fisher Scientific; Waltham, Massachusetts, USA), Superscript™-II Reverse Transcriptase (Thermo Fisher Scientific; Waltham, Massachusetts, USA), Thermocycler T3 (Biometra; Göttingen, Germany), Vortex-Genie 2 (Scientific Industries; NY, USA).

To synthesize complementary DNA (cDNA) from RNA template, reverse transcription was done using random primers. These oligonucleotides are six nucleotides long (random hexamers) and bind randomly with no template specificity. The random primers hybridize to

the RNA. In a next step they are elongated by reverse transcriptase through dNTPs (deoxynucleotide triphosphate) to produce cDNA. This can be used directly as a template for the polymerase chain reaction (see 5.5.2).

reaction	2 μ l RNA (1 μ g/ μ l)
	1 μ l random primer (100 μ M)
	9 μ l RNase/DNase-free H ₂ O

The reaction was incubated for 10 min at 70°C to denature secondary structures of the RNA and snap-cooled on ice for 5 min. Reverse transcription reaction mixture (4 μ l 5x reaction buffer), 2 μ l DTT (100 mM), 2 μ l dNTPs (2.5 mM each) and 1 μ l Superscript™-II (200 U/ μ l) were added. The reaction mixture was briefly centrifuged and incubated for 10 min at 20°C, 60 min at 42°C and 5 min at 90°C using a thermocycler. The synthesized cDNA was mixed with 80 μ l RNase/DNase-free water, aliquoted and stored at -20°C.

5.5.2. Polymerase chain reaction (PCR)

Materials: dNTPs (Thermo Fisher Scientific; Waltham, Massachusetts, USA), Heraeus Pico 17 – centrifuge (Thermo Fisher Scientific; Waltham, Massachusetts, USA), oligonucleotides (see 7.1.5), Phusion High-Fidelity DNA Polymerase (Thermo Fisher Scientific; Waltham, Massachusetts, USA), RNase/DNase-free H₂O (Thermo Fisher Scientific; Waltham, Massachusetts, USA), template DNA (e.g. cDNA, see 5.5.1), Thermocycler T3 (Biometra; Göttingen, Germany), Vortex-Genie 2 (Scientific Industries; NY, USA).

PCR is a commonly used method, which allows for the amplification of a specific DNA fragment from a complex pool of DNA. Each PCR assay requires the presence of template DNA, two oligonucleotides, dNTPs and a thermostable DNA polymerase. The oligonucleotides (see 1.5.6.7.1.5) in the reaction specify the exact DNA product to be amplified. They are short DNA fragments with a defined sequence complementary to the target DNA and serve as an extension point for the DNA polymerase to build on. During the PCR process the reaction solution is first heated above the melting point of the two complementary DNA strands of the target DNA to separate the strands (denaturation at 96°C for 30 sec). To allow the specific oligonucleotides to bind to the target DNA segments, the temperature is lowered (annealing at 50-65°C for 30 sec). Only if oligonucleotides and target DNA are complementary in sequence, annealing will occur. During DNA synthesis (68°C or 72°C, 60 sec/1 kb fragment) the DNA polymerase extends the oligonucleotides by adding nucleotides to the developing DNA strand. With each repetition of these three steps, the number of copied DNA molecules doubles. In this study PCR was used for cloning of different gene products. For this approach the High Fidelity PCR enzyme mix was used according to the manufactur-

er's protocol.

5.5.3. Site-directed mutagenesis

Material: dNTPs (Thermo Fisher Scientific; Waltham, Massachusetts, USA), DpnI (Thermo Fisher Scientific; Waltham, Massachusetts, USA), Heraeus Pico 17 – centrifuge (Thermo Fisher Scientific; Waltham, Massachusetts, USA), oligonucleotides (see 7.1.5), PfuUltra High-Fidelity DNA Polymerase (Stratagene; San Diego, California, USA), RNase/DNase-free H₂O (Thermo Fisher Scientific; Waltham, Massachusetts, USA), template DNA, Thermocycler T3 (Biometra; Göttingen, Germany), Vortex-Genie 2 (Scientific Industries; NY, USA).

reaction A	25-50 ng template 1x reaction buffer 20 µM primer (for) 10 mM dNTPs 1.25 U PfuUltra polymerase ad 25 µl RNase/DNase-free H ₂ O	reaction B	25-50 ng template 1x reaction buffer 20 µM primer (rev) 10 mM dNTPs 1.25 U PfuUltra polymerase ad 25 µl RNase/DNase-free H ₂ O
1. PCR program	2 min 95°C 30 sec 95°C 1 min 45°C/48°C 14 min 68°C		initial denaturation denaturation annealing elongation
			} 4x
reaction C	pooled reaction A and B 10 mM dNTPs 2.5 U PfuUltra polymerase		
2. PCR program	30 sec 95°C 1 min 45°C/48°C 14 min 68°C 14 min 68°C 4°C		denaturation annealing elongation finale elongation stop of reaction
			} 20x

Fig. 51| PCR reaction and program for site-directed mutagenesis.

The overview shows the reactions and programs used for site-directed mutagenesis. Two separate PCR reactions 1 and 2 containing the forward (for) or reversed (rev) primer were generated. After the 1st PCR program, which serves to anneal the primers to the template, both reactions were pooled and a 2nd PCR program was performed. For annealing step, the temperature was selected according to the length and GC-content of the corresponding primers. dNTPs, desoxyribonukleosidtriphosphate; for, forward; rev, reversed.

To create specific non-phosphorylatable (Ser/Thr to Ala) as well as phospho-mimetic (Ser/Thr to Glu) mutations in the known PKP1 sequence, PCR-based site-directed mutagenesis was performed by using oligonucleotides with specifically altered sequences compared to the template DNA [(Hutchison et al., 1978), Fig. 51]. In this study, cDNA sequences already cloned in appropriate vectors were used (see 5.5.6). The used oligonucleotides are

listed in chapter 1.5.6.7.1.5. During PCR, the mutation is incorporated into the amplicon, replacing the original PKP1 sequence. As a result, circular and double-stranded DNA with two single-strand breaks and the desired mutation were emerged. PCR was followed by DpnI digestion cleaving at methylated sites to degrade template plasmid. The mutated DNA molecule was transformed in the *E. coli* strain JM109 (see 0) and further analyzed by sequencing (see 5.5.12).

5.5.4. Agarose gel electrophoresis

Material: 6x DNA loading buffer (see below), agarose (Carl Roth; Karlsruhe, Germany), Biometra® Standard Power Pack P25 (Analytik Jena AG; Jena, Germany), ethidium bromide (Merck; Darmstadt, Germany), Fusion-SL – Chemiluminescence- and Fluorescence system (Peqlab; Erlangen, Germany), GeneRuler 1 kb Plus DNA ladder (Thermo Fisher Scientific; Waltham, Massachusetts, USA), RNase/DNase-free H₂O (Thermo Fisher Scientific; Waltham, Massachusetts, USA), TBE buffer (see below), UV table (bts Biotech Trade & Service GmbH; Kraichtal, Germany).

To separate nucleic acids by length, agarose gel electrophoresis was performed. Electrophoresis uses an electrical field to move the negatively charged nucleic acid through an agarose gel matrix toward a positive anode. Shorter DNA fragments migrate through the gel more quickly than larger ones. The migration speed and separation of DNA or RNA fragments is also dependent on the conformation of the fragments, the concentration of the agarose [0.6% (w/v) – 2% (w/v) agarose] and the electric tension. By running the nucleic acids on an agarose gel alongside a ladder (see 1.5.6.7.1.3), one can determine the approximate length of the nucleic acid fragment. The appropriate amount of agarose was dissolved in TBE buffer (see below) and 0.3 µg/ml ethidium bromide was added. Ethidium bromide is a fluorescence dye inserting in the nucleic acids. The DNA samples were diluted in RNase/DNase-free H₂O and 6x DNA loading buffer (see below) and loaded on the agarose gel. The gel electrophoresis was performed in horizontal electrophoresis chambers filled with TBE buffer (see below) at 100 V for 30-90 min.

6x DNA loading buffer: 0.25% (w/v) bromophenol blue, 40% (v/v) glycerol, 100 mM EDTA, 0.1% (v/v) SDS

TBE buffer: 445 mM Tris, 445 mM boric acid, 10 mM EDTA

5.5.5. Purification of nucleic acids

Material: Fusion-SL – Chemiluminescence- and Fluorescence system (Peqlab; Erlangen, Germany), Heraeus Pico 17 – centrifuge (Thermo Fisher Scientific; Waltham, Massachusetts, USA), Jetquick Gel Extraction Spin Kit (Genomed; Löhne, Germany), Jetquick PCR Purification Kit (Genomed; Löhne, Germany), scalpel, Thermomixer comfort (Eppendorf; Hamburg, Germany), UV table (bts Biotech Trade & Service GmbH; Kraichtal, Germany).

The purification of DNA fragments was done using the PCR Purification and Gel Extraction Kit. Therefore, the samples were diluted in 6x DNA loading buffer (see 7.1.4) and loaded on an agarose gel (see 0). After separation of the DNA fragments by gel electrophoresis the DNA bands were excised and extracted from the agarose gel. The excised DNA was used to extract the DNA from the agarose gel using the Gel Extraction Kit according to the manufacturer's instructions. 300 µl buffer H1 was added to 100 mg gel and incubated for 10 min at 50°C. Afterwards DNA purification was performed using the Purification Kit according to the manufacturer's instructions.

5.5.6. Cloning of PCR products by use of TA system

Material: dNTPs (Thermo Fisher Scientific; Waltham, Massachusetts, USA), Heraeus Pico 17 – centrifuge (Thermo Fisher Scientific; Waltham, Massachusetts, USA), Taq polymerase (Thermo Fisher Scientific; Waltham, Massachusetts, USA), Thermocycler T3 (Biometra; Göttingen, Germany), TOPO TA Cloning kit (Thermo Fisher Scientific; Waltham, USA), Vortex-Genie 2 (Scientific Industries; NY, USA).

TA cloning was used as method for the cloning of PCR products. The procedure exploits the terminal transferase activity of the thermophilic DNA polymerase (Taq polymerase). Taq polymerase has non-template dependent activity which preferentially adds a single adenosine to the 3'-ends of a double stranded DNA molecule and thus the molecule PCR amplified by Taq polymerase possess single 3'-A overhangs. The use of a linearized "T-vector" with single 3'-T (thymidine) overhangs on both ends allows the direct ligation of the PCR products, facilitated by complementarity between the PCR product 3'-A overhangs and vector 3'-T overhangs. The ligation was done for 30 min at RT according to the manufacturer's instructions. Following the product was transformed in the *E. coli* strain JM109 (see 0).

5.5.7. Restriction endonuclease digestion of nucleic acids

Material: Heraeus Pico 17 – centrifuge (Thermo Fisher Scientific; Waltham, Massachusetts, USA), restriction endonucleases and buffers (Thermo Fisher Scientific; Waltham, Massachusetts, USA), RNase/DNase-free H₂O (Thermo Fisher Scientific; Waltham, Massachusetts, USA), Thermocycler T3 (Biometra; Göttingen, Germany), Vortex-Genie 2 (Scientific Industries; NY, USA).

Restriction endonucleases are bacterial enzymes that hydrolyze DNA at specific restriction

sites. They are classified into four types on the basis of subunit composition, cleavage position, sequence specificity, and cofactor requirements. Type II endonucleases are the only class used in the laboratory for routine DNA analysis and gene cloning. They cut DNA at defined positions close to or within their recognition sequences to produce discrete restriction fragment and distinct gel banding patterns.

preparative approach	10 µl DNA (1 µg/µl)
	5 µl 10x buffer
	33 µl RNase/DNase-free water
	2 µl restriction endonuclease (10 U/µl)
analytical approach	1 µl plasmid DNA
	1.5 µl 10x buffer
	13 µl RNase/DNase-free water
	0.25 µl restriction endonuclease (10 U/µl)

The reactions were incubated for 3 h at 37°C in the thermocycler. The DNA was separated by agarose gel electrophoresis (see 0) and in the case of a preparative approach the DNA was purified by Gel Extraction Kit (see 0).

5.5.8. Ligation

Material: Heraeus Pico 17 – centrifuge (Thermo Fisher Scientific; Waltham, Massachusetts, USA), RNase/DNase-free H₂O (Thermo Fisher Scientific; Waltham, Massachusetts, USA), T4 DNA ligase and buffers (Thermo Fisher Scientific; Waltham, Massachusetts, USA), Vortex-Genie 2 (Scientific Industries; NY, USA).

Ligation is the final step in the generation of a recombinant plasmid and describes the connection of the insert DNA into a compatibly digested (see 5.5.7) vector backbone. This reaction was performed by the T4 DNA ligase, which catalyzed the formation of covalent phosphodiester linkages to permanently join the nucleotides together. The quantity ratio between vector and insert should be between 1:1 and 1:5. To estimate these, an agarose gel electrophoresis (see 0) was done prior the ligation. Ligation was performed for 2 h at RT. After ligation, the complete plasmid was transformed into *E. coli* JM109 (see 0) for propagation.

ligation	x µl PCR fragment (insert)
	x µl vector
	1 µl 10x ligase buffer
	0.5 µl T4 DNA ligase (1 U/µl)
	add 10 µl RNase/DNase-free H ₂ O

5.5.9. Preparation and transformation of competent *E. coli*

Material: ampicillin (Carl Roth; Karlsruhe, Germany), GeneQuant 1300 Spectrophotometer (GE Healthcare; Munich, Germany), Hettich Mikro 220R – centrifuge (Hettich GmbH & Co.KG; Tuttlingen, Germany), Incubator Shaker Series I26 (Eppendorf; Hamburg, Germany), Incucell – incubator (MMM Medcenter Einrichtungen GmbH, Planegg, Germany), kanamycin (Carl Roth; Karlsruhe, Germany), LB agar plates, LB medium (see below), Purification NucleoSpin® Plasmid Kit or Purification NucleoBond® XtraMidi Kit (Macherey-Nagel GmbH; Berlin, Germany), RNase/DNase-free H₂O (Thermo Fisher Scientific; Waltham, Massachusetts, USA), TFB-I and -II buffer (see below), Thermomixer comfort (Eppendorf; Hamburg, Germany).

To prepare competent *E. coli* strains JM109 and BL21(DE3), one colony was incubated at 37°C in 10 ml LB medium (see below) on an environmental shaker (preculture). On the next day, the preculture was used to inoculate the main culture (100 ml LB medium). This culture was incubated at 37°C on an environmental shaker until an OD₆₀₀ of 0.3. The suspension was centrifuged for 10 min at 3.000x g and 4°C and the pellet was resuspended in 30 ml TFB-I buffer (see below). The solution was incubated for 8 min on ice. After centrifugation for 10 min at 3,000x g at 4°C the bacterial pellet was gently resuspended in 4 ml TFB-II buffer (see below) in an ice bath. The bacteria were aliquoted in -80°C pre-cold 1.5 ml microcentrifuge tubes (100 µl each) and stored at -80°C. Preparation of competent *E. coli* strains was kindly done by Andrej Mun (AG Hatzfeld, Martin-Luther-University).

LB medium: 10 g/l NaCl, 10 g/l tryptone, 5 g/l yeast extract, pH 7.0

TFB-I buffer: 30 mM potassium acetate (pH 5.8), 50 mM MgCl₂, 100 mM KCl, 15% (v/v) glycerol

TFB-II buffer: 10 mM 3-(N-morpholino)-propanesulfonic acid (MOPS; pH 7.0), 10 mM KCl, 75 mM CaCl₂, 15% (v/v) glycerol

To transform plasmid DNA, one aliquot of competent *E. coli* (100 µl) was defrosted on ice. 10 µl of the ligation reaction or 50 ng plasmid DNA in 10 µl RNase/DNase-free H₂O was added to the bacteria and incubated for 30 min on ice, heat-shocked at 42°C for 90 sec and incubated for 2 min on ice. The transformed bacteria were mixed with 900 µl LB medium (see above), incubated for 1 h at 37°C on a shaker and plated on LB agar plates with the appropriate selection antibiotics (100 µg/ml ampicillin or 50 µg/ml kanamycin). The LB agar plates were incubated overnight at 37°C.

5.5.10. Preparation of plasmid DNA

Material: ampicillin (Carl Roth; Karlsruhe, Germany), GeneQuant 1300 Spectrophotometer (GE Healthcare; Munich, Germany), GET buffer (see below), Heraeus Pico 17 – centrifuge (Thermo Fisher Scientific; Waltham, USA), Incubator Shaker Series I26 (Eppendorf; Hamburg, Germany), isopropanol (Sigma Aldrich; St. Louis, Missouri, USA), kanamycin (Carl Roth; Karlsruhe, Germany), LB medium (see below), SDS (Carl Roth; Karlsruhe, Germany), Vortex-Genie 2 (Scientific Industries; NY, USA).

Bacterial colonies were inoculated into 5 ml LB medium with the appropriate antibiotic (100 µg/ml ampicillin or 50 µg/ml kanamycin) and incubated overnight at 37°C on an environmental shaker. 1.5 ml of the overnight culture was centrifuged at 13.000x g for 1 min at RT and pellets were resuspended in 100 µl GET buffer (see below). To lyse bacteria, 200 µl 0.2 M NaOH + 1% (w/v) SDS was added, the suspension inverted several times and incubated for 5 min at RT. By adding of 150 µl 3 M sodium acetate (pH 4.8) the DNA and soluble proteins were precipitated. After centrifugation for 10 min at 13,000x g and RT the supernatant was transferred to a new microcentrifuge tube and the solved plasmid DNA was precipitated by adding 2 volumes of isopropanol and incubating for 30 min at RT. After centrifugation for 15 min at 13,000x g and RT the pellet was washed in 70% (v/v) EtOH and centrifuged for 5 min. The pellet was dried and solved in 50 µl 10 mM Tris/HCl (pH 8.0) supplemented with 50 ng RNase A und incubated at 37°C for 30 min. To prepare plasmids for transfection of cell lines the Purification NucleoSpin® Plasmid Kit or Purification NucleoBond® XtraMidi Kit was used. The prepared plasmids were further analyzed using restriction endonucleases (see 5.5.7) and sequencing (see 5.5.12). The plasmid concentration was measured at 260 nm using a spectrophotometer. The concentration of pure dddDNA (double-stranded DNA) with an A_{260} of 1.0 is 50 µg/ml.

LB medium: 10 g/l NaCl, 10 g/l tryptone, 5 g/l yeast extract, pH 7.0

GET buffer: 25 mM Tris/HCl (pH 8.0), 50 mM glucose, 10 mM EDTA

5.5.11. Preparation of genomic DNA from mouse tails for PCR genotyping

Material: Dry bath FB15103 (Thermo Fisher Scientific; Waltham, Massachusetts, USA), Heraeus Pico 17 – centrifuge (Thermo Fisher Scientific; Waltham, USA), KAPA Mouse Genotyping Hot Start Kit (peqlab; Erlangen, Germany), Reax top test tube shaker (Heidolph Instruments; Schwabach, Germany), Thermocycler T3 (Biometra; Göttingen, Germany), Thermomixer comfort (Eppendorf; Hamburg, Germany).

Genomic DNA was isolated from tail biopsies and used as a template for PCR genotyping with the KAPA Mouse Genotyping Hot Start Kit. PCR was carried out according to the manufacturer's protocol using primers p1 – p5 (see 1.5.6.7.1.5). To isolate genomic DNA from

mouse tail, a tail tip was cut and transferred into a microcentrifuge tube and components from the Kit were added as shown in Table 6.

Table 6| Extraction of genomic DNA from mouse tail by KAPA Mouse Genotyping Kit.

Component	Per 100 µl reaction	Final concentration
PCR-grade water	88 µl	N/A
10x KAPA Express extract buffer	10 µl	1x
1 U/µl KAPA Express extract enzyme	2 µl	2 U/rxn
mouse tail tip	as required	2 mm section

The lysis was performed by heating the samples at 75°C for 10 min and 95°C for 5 min. After a brief centrifugation step to pellet cellular debris, the supernatant was transferred to a new microcentrifuge tube. To prepare the master mix, the appropriate volumes of master mix, template and oligonucleotides were transferred to individual PCR tubes (Table 7).

Table 7| KAPA2G Fast Genotyping PCR Protocol.

Component	Per 25 µl reaction	Final concentration
PCR-grade water	up to 25 µl	N/A
2x KAPA2G Fast Genotyping Mix with dye	12.5 µl	1x
10 µM forward primer	1.25 µl	0.5 µM
10 µM reverse primer	1.25 µl	0.5 µM
template DNA	as required	1 µl of 1:10 dilution

The individual reactions were mixed and centrifuged briefly. PCR was performed according to manufacturer's protocol. PCR products were loaded onto a 0.8% (w/v) agarose gel and electrophoresis was performed (see 0).

5.5.12. Sequencing

2 µg plasmid DNA was dried and send for sequencing to company Eurofins MWG Operon (Ebersberg, Germany).

5.5.13. Southern blot

Material: 5x SSPE buffer (see below), 6x DNA loading buffer (see 7.1.4), 20x SSC (see below), BglII restriction endonuclease and buffer (Thermo Fisher Scientific; Waltham, Massachusetts, USA), clean tweezers, DecaLabel DNA Labeling Kit (Thermo Fisher Scientific; Waltham, USA), Denhardt's solution (see below), ethidium bromide (Merck; Darmstadt, Germany), Fusion-SL – Chemiluminescence- and Fluorescence system (Peqlab; Erlangen, Germany), Glycogen, RNA grade (Thermo Fisher Scientific; Waltham, USA), Heraeus Pico 17 – centrifuge (Thermo Fisher Scientific; Waltham, USA), hybridization buffer (see below), nylon membrane (Altmann Analytik; Munich, Germany), scintillation counter, SDS (Carl Roth, Karlsruhe, Germany), TBE (see 7.1.4), Thermomixer comfort (Eppendorf; Hamburg, Germany), UV table (bts Biotech Trade & Service GmbH; Kraichtal, Germany), washing solution (see below), Yeastmaker™ Carrier DNA (Clontech Laboratories; Mountain View, California, USA).

The knockout of PKP1 was verified by Southern blot using BglIII digested genomic DNA (see 5.5.7) and two internal probes. The probes (P1 – 555 bp and P2 – 529 bp) were amplified by PCR with primers listed in chapter 1.5.6.7.1.5. To perform Southern blot, 10 µg of genomic DNA (see 5.5.11) was digested in 50 µl reaction volume with 50 U BglIII overnight at 37°C. Restriction was stopped by adding 6x DNA loading buffer and 1 µl of 20% (w/v) SDS. The sample was heated for 5 min at 70°C, centrifuged briefly, loaded onto a 0.8% (w/v) agarose gel (see 0) in TBE buffer (see 7.1.4) with 0.3 µg/ml ethidium bromide and run for ~6 h at 80 V. To document the gel, it was exposed only shortly to UV-light and photographed with a ruler to the left. After documentation, the gel was incubated for 30 min in 0.4 M NaOH. For Southern blot approach, 3 sheets of filter paper and nylon membrane were moisten in water, then in 20x SSC (see below). To arrange Southern blot, a sheet of nylon membrane was placed on top of the gel. Pressure was applied evenly to the gel by placing a stack of paper towels and a weight on the top of the membrane and gel to ensure even contact between gel and membrane. To perform a transferring by suction, 20x SSC buffer (see below) was used to ensure a seal and prevent drying of the gel. Therefore the buffer reservoir was filled with ~300-400 ml 20x SSC (see below). The transfer was performed for at least 12 h at RT. After transfer, the filter paper was removed and the position of the gel pockets was marked on the membrane. For orientation, the lower corner of the membrane was cut off. Membrane was washed for 15 sec in 2x SSC and dried on filter paper. To fix DNA, membrane was baked at 80°C for 2 h. To prehybridize, the membrane was cut according to the probes. The membrane strips were moisten in 5x SSPE buffer (see below), transferred to 50 ml Falcon tubes and incubated for 30 min at 42°C in 10 ml hybridization buffer (see below). To label the probes, 35 ng DNA was mixed with 10 µl decanucleotide 5x reaction buffer, filled to 40 µl with nuclease-free water, vortexed and briefly centrifuged. To denature DNA, samples were boiled for 10 min in water bath and snap-cooled on ice. Next steps were performed at isotope laboratory. 3 µl dNTPs (0.33 mM dGTP, 0.33 mM dATP, 0.33 mM dTTP aqueous solution, without dCTP), 10 µCi of [α -³²P]dCTP and 1 µl Klenow (5 U/µl) enzyme was added, gently mixed, centrifuged and incubated for 5 min at 37°C. 4 µl dNTP was added and incubated another 10 min at 37°C. The reaction was stopped by adding 1 µl EDTA (0.5 M). The volume was filled up to 200 µl with nuclease-free water and mixed carefully. For precipitation 400 µl EtOH, 40 µl 3 M sodium acetate (pH 5.0) and 1 µl

glycogen (20 mg/ml aqueous solution) was added and centrifuged at 13.000x g and RT for 15 min. The supernatant was transferred into a new tube and collected for scintillation counter. The pellet was washed twice with 400 μ l 70% (v/v) EtOH, centrifuged at 13.000x g and RT for 2 min and air dried. The pellet was solved in 50 μ l RNase/DNase-free water. To calculate the incorporation rate of [α -³²P]dCTP the radioactivity of the collected supernatant and the samples was measured. For hybridization, the labelled probe was mixed with 100 μ l salmon sperm DNA, incubated 5 min at 95°C, briefly centrifuged and added to the hybridization tubes (with membrane). Hybridization was performed overnight at 42°C on an overhead rotator. After hybridization, 1 l washing solution (see below) was prepared and pre-warmed at 68°C in a water bath. The probe was discarded. ~25 ml pre-warmed washing solution was added to the Falcon tube and incubated at 68°C for 30 min. The washing step was repeated twice to remove excess probe. DNA fragments were visualized by autoradiography. The size of the expected fragments is:

Probe 1: PKP1^{+/+}: 6.7 kb, PKP1^{+/-}: 6.7 and 14.85 kb, PKP1^{-/-}: 14.85 kb;

Probe 2: PKP1^{+/+}: 8.37 kb, PKP1^{+/-}: 8.37 and 14.85 kb, PKP1^{-/-}: 14.85 kb.

100x Denhardt's solution: 2% (w/v) Ficoll 400, 2% (w/v) polyvinylpyrrolidone, 2% (w/v) BSA

Hybridization buffer: 6x SSPE, 1% (v/v) SDS, 5x Denhardt's solution, 10% (w/v) dextran sulfate, 50% formamide, 0.1 mg/ml denatured herring sperm

20x SSC buffer: 3 M NaCl, 0.3 M sodium citrate, pH 7.0

20x SSPE buffer: 3 M NaCl, 0.2 M NaH₂PO₄, 0.02 M EDTA, pH 7.4

Washing solution: 0.1x SSC, 0.1% (w/v) SDS

5.6. Image processing, quantification and statistical analysis

All data sets were processed using standard software Excel, Word and PowerPoint (Microsoft Office 2010). Images were taken using the iTEM software from Olympus SIS (Münster, Germany), AxioVision software (Carl Zeiss) or Leica LAS AF software (Leica Microsystems). Figures were arranged using Adobe Photoshop CS5 (Adobe), Scribus 1.4.5., or ImageJ. Adjustments of brightness, contrast, or color balance were applied to the whole image. Schematic overviews were arranged using images from Medical Art (Servier; Neuilly-sur-Seine, France). Statistical analysis and diagram illustrations were done using SigmaPlot 10.0 (Systat Software; Erkrath, Germany) and GraphPad Prism 7 (GraphPad Software; La Jolla, San Diego, USA).

To determine average fluorescence intensities for PKP1, PKP3, and DSP (chapter 3.3.), ImageJ was used for measuring a segment of equal length and width across 30 individual bi- and tricellular cell contacts for each condition. The corresponding graphs (shown in chapter 7.2. in appendix) depict the mean fluorescence intensities for PKP1, PKP3, and DSP relative to the value at the appropriate cellular contact sites. To quantify the enrichment of PKP1 and DSP at bicellular contacts, the mean bicellular value was normalized to the mean cytoplasmic value for each line scan. To determine the ratio of PKP3 at tricellular vs. bicellular contacts, the mean junctional (bicellular and tricellular) values were normalized to the mean cytoplasmic value for each line scan. The resulting mean tricellular values were divided by the mean bicellular values. All ratios (bicellular/cytoplasm for PKP1 and DSP, tricellular/bicellular for PKP3) are shown as boxplots displaying the first to third quartile with full range of variation (whiskers from minimum to maximum).

For all measurements, the error bars represent the standard deviation (SD) of $n \geq 3$. The means of two independent samples were compared for statistically significant differences by two-tailed Student's *t*-test. One-way analysis of variance (ANOVA) was used to compare the means of more than two independent data sets that were normally distributed. To compare the means of more than two independent data sets based on multiple characteristics that were normally distributed, two-way analysis of variance (ANOVA) was used. In addition to analyze data that were known not to be normally distributed, the Mann-Whitney U-test as the nonparametric counterpart of the unpaired Student's *t*-test was run. Probability (*P*) values are given as follows: * $P \leq 0.05$, ** $P \leq 0.005$ and *** $P \leq 0.0005$.

6 REFERENCES

- Abdalla EM, Has C. A plakophilin-1 gene mutation in an Egyptian family with ectodermal dysplasia-skin fragility syndrome. *Molecular syndromology* 2014;5(6):304-6.
- Aberle H, Bauer A, Stappert J, Kispert A, Kemler R. beta-catenin is a target for the ubiquitin-proteasome pathway. *The EMBO journal* 1997;16(13):3797-804.
- Aberle H, Schwartz H, Hoschuetzky H, Kemler R. Single amino acid substitutions in proteins of the armadillo gene family abolish their binding to alpha-catenin. *The Journal of biological chemistry* 1996;271(3):1520-6.
- Adhe VS, Dongre AM, Khopkar US. Ectodermal dysplasia-skin fragility syndrome. *Indian journal of dermatology, venereology and leprology* 2011;77(4):503-6.
- Aghazadeh Y, Papadopoulos V. The role of the 14-3-3 protein family in health, disease, and drug development. *Drug discovery today* 2016;21(2):278-87.
- Aitken A. 14-3-3 and its possible role in co-ordinating multiple signalling pathways. *Trends in cell biology* 1996;6(9):341-7.
- Aitken A. Functional specificity in 14-3-3 isoform interactions through dimer formation and phosphorylation. Chromosome location of mammalian isoforms and variants. *Plant molecular biology* 2002;50(6):993-1010.
- Aitken A. 14-3-3 proteins: a historic overview. *Seminars in cancer biology* 2006;16(3):162-72.
- Aitken A, Baxter H, Dubois T, Clokie S, Mackie S, Mitchell K, et al. Specificity of 14-3-3 isoform dimer interactions and phosphorylation. *Biochemical Society transactions* 2002;30(4):351-60.
- Aitken A, Howell S, Jones D, Madrazo J, Patel Y. 14-3-3 alpha and delta are the phosphorylated forms of raf-activating 14-3-3 beta and zeta. In vivo stoichiometric phosphorylation in brain at a Ser-Pro-Glu-Lys MOTIF. *The Journal of biological chemistry* 1995;270(11):5706-9.
- Aktories K, Barbieri JT. Bacterial cytotoxins: targeting eukaryotic switches. *Nature reviews Microbiology* 2005;3(5):397-410.
- Al-Amoudi A, Castano-Diez D, Devos DP, Russell RB, Johnson GT, Frangakis AS. The three-dimensional molecular structure of the desmosomal plaque. *Proceedings of the National Academy of Sciences of the United States of America* 2011;108(16):6480-5.
- Altomare DA, Khaled AR. Homeostasis and the importance for a balance between AKT/mTOR activity and intracellular signaling. *Current medicinal chemistry* 2012;19(22):3748-62.
- Altomare DA, Lyons GE, Mitsuuchi Y, Cheng JQ, Testa JR. Akt2 mRNA is highly expressed in embryonic brown fat and the AKT2 kinase is activated by insulin. *Oncogene* 1998;16(18):2407-11.
- Amagai M, Klaus-Kovtun V, Stanley JR. Autoantibodies against a novel epithelial cadherin in pemphigus vulgaris, a disease of cell adhesion. *Cell* 1991;67(5):869-77.
- Anastasiadis PZ. p120-ctn: A nexus for contextual signaling via Rho GTPases. *Biochimica et biophysica acta* 2007;1773(1):34-46.
- Anderson P, Kedersha N. Stress granules: the Tao of RNA triage. *Trends in biochemical sciences* 2008;33(3):141-50.
- Andrade MA, Petosa C, O'Donoghue SI, Muller CW, Bork P. Comparison of ARM and HEAT protein repeats. *Journal of molecular biology* 2001;309(1):1-18.
- Bass-Zubek AE, Godsel LM, Delmar M, Green KJ. Plakophilins: multifunctional scaffolds for adhesion and signaling. *Current opinion in cell biology* 2009;21(5):708-16.
- Behrens J. Control of beta-catenin signaling in tumor development. *Annals of the New York Academy of Sciences* 2000;910:21-33; discussion -5.
- Beltrao P, Bork P, Krogan NJ, van Noort V. Evolution and functional cross-talk of protein post-translational modifications. *Molecular systems biology* 2013;9:714.

- Benoliel AM, Kahn-Perles B, Imbert J, Verrando P. Insulin stimulates haptotactic migration of human epidermal keratinocytes through activation of NF-kappa B transcription factor. *Journal of cell science* 1997;110 (Pt 17):2089-97.
- Bergman R, Sprecher E. Histopathological and ultrastructural study of ectodermal dysplasia/skin fragility syndrome. *Am J Dermatopathol* 2005;27(4):333-8.
- Bertani G. Studies on lysogenesis. I. The mode of phage liberation by lysogenic *Escherichia coli*. *Journal of bacteriology* 1951;62(3):293-300.
- Bikle DD. Vitamin D: a calciotropic hormone regulating calcium-induced keratinocyte differentiation. *Journal of the American Academy of Dermatology* 1997;37(3 Pt 2):S42-52.
- Bikle DD, Xie Z, Tu CL. Calcium regulation of keratinocyte differentiation. *Expert review of endocrinology & metabolism* 2012;7(4):461-72.
- Blume-Jensen P, Hunter T. Oncogenic kinase signalling. *Nature* 2001;411(6835):355-65.
- Bonne S, van Hengel J, Nollet F, Kools P, van Roy F. Plakophilin-3, a novel armadillo-like protein present in nuclei and desmosomes of epithelial cells. *Journal of cell science* 1999;112 (Pt 14):2265-76.
- Bonne S, van Hengel J, van Roy F. Chromosomal mapping of human armadillo genes belonging to the p120(ctn)/plakophilin subfamily. *Genomics* 1998;51(3):452-4.
- Bornslaeger EA, Corcoran CM, Stappenbeck TS, Green KJ. Breaking the connection: displacement of the desmosomal plaque protein desmoplakin from cell-cell interfaces disrupts anchorage of intermediate filament bundles and alters intercellular junction assembly. *J Cell Biol* 1996;134(4):985-1001.
- Bornslaeger EA, Godsel LM, Corcoran CM, Park JK, Hatzfeld M, Kowalczyk AP, et al. Plakophilin 1 interferes with plakoglobin binding to desmoplakin, yet together with plakoglobin promotes clustering of desmosomal plaque complexes at cell-cell borders. *Journal of cell science* 2001;114(Pt 4):727-38.
- Bose A, Teh MT, Mackenzie IC, Waseem A. Keratin k15 as a biomarker of epidermal stem cells. *International journal of molecular sciences* 2013;14(10):19385-98.
- Boukamp P, Petrussevska RT, Breitkreutz D, Hornung J, Markham A, Fusenig NE. Normal keratinization in a spontaneously immortalized aneuploid human keratinocyte cell line. *The Journal of cell biology* 1988;106(3):761-71.
- Boyce AE, McGrath JA, Techanukul T, Murrell DF, Chow CW, McGregor L, et al. Ectodermal dysplasia-skin fragility syndrome due to a new homozygous internal deletion mutation in the PKP1 gene. *Australas J Dermatol* 2012;53(1):61-5.
- Bozulic L, Hemmings BA. PIKKing on PKB: regulation of PKB activity by phosphorylation. *Current opinion in cell biology* 2009;21(2):256-61.
- Brandner JM, McIntyre M, Kief S, Wladykowski E, Moll I. Expression and localization of tight junction-associated proteins in human hair follicles. *Archives of dermatological research* 2003;295(5):211-21.
- Brembeck FH, Rosario M, Birchmeier W. Balancing cell adhesion and Wnt signaling, the key role of beta-catenin. *Current opinion in genetics & development* 2006;16(1):51-9.
- Brennan D, Peltonen S, Dowling A, Medhat W, Green KJ, Wahl JK, 3rd, et al. A role for caveolin-1 in desmoglein binding and desmosome dynamics. *Oncogene* 2012;31(13):1636-48. doi: 10.038/onc.2011.346. Epub Aug 15.
- Breuninger S, Reidenbach S, Sauer CG, Strobel P, Pfitzenmaier J, Trojan L, et al. Desmosomal plakophilins in the prostate and prostatic adenocarcinomas: implications for diagnosis and tumor progression. *The American journal of pathology* 2010;176(5):2509-19.
- Cadigan KM, Waterman ML. TCF/LEFs and Wnt signaling in the nucleus. *Cold Spring Harbor perspectives in biology* 2012;4(11).
- Candi E, Schmidt R, Melino G. The cornified envelope: a model of cell death in the skin. *Nature reviews Molecular cell biology* 2005;6(4):328-40.

- Cantley LC. The phosphoinositide 3-kinase pathway. *Science* 2002;296(5573):1655-7.
- Chan TO, Rittenhouse SE, Tsichlis PN. AKT/PKB and other D3 phosphoinositide-regulated kinases: kinase activation by phosphoinositide-dependent phosphorylation. *Annual review of biochemistry* 1999;68:965-1014.
- Chen DY, Dai DF, Hua Y, Qi WQ. p53 suppresses 14-3-3gamma by stimulating proteasome-mediated 14-3-3gamma protein degradation. *International journal of oncology* 2015;46(2):818-24.
- Chen S, Synowsky S, Tinti M, MacKintosh C. The capture of phosphoproteins by 14-3-3 proteins mediates actions of insulin. *Trends in endocrinology and metabolism: TEM* 2011;22(11):429-36.
- Cheng GZ, Park S, Shu S, He L, Kong W, Zhang W, et al. Advances of AKT pathway in human oncogenesis and as a target for anti-cancer drug discovery. *Current cancer drug targets* 2008;8(1):2-6.
- Cheung IY, Feng Y, Danis K, Shukla N, Meyers P, Ladanyi M, et al. Novel markers of subclinical disease for Ewing family tumors from gene expression profiling. *Clinical cancer research : an official journal of the American Association for Cancer Research* 2007;13(23):6978-83.
- Chiba H, Osanai M, Murata M, Kojima T, Sawada N. Transmembrane proteins of tight junctions. *Biochimica et biophysica acta* 2008;1778(3):588-600.
- Chidgey M, Brakebusch C, Gustafsson E, Cruchley A, Hail C, Kirk S, et al. Mice lacking desmocollin 1 show epidermal fragility accompanied by barrier defects and abnormal differentiation. *J Cell Biol* 2001;155(5):821-32.
- Chidgey M, Dawson C. Desmosomes: a role in cancer? *British journal of cancer* 2007;96(12):1783-7.
- Choi HJ, Weis WI. Structure of the armadillo repeat domain of plakophilin 1. *Journal of molecular biology* 2005;346(1):367-76.
- Cianfarani F, Bernardini S, De Luca N, Dellambra E, Tatangelo L, Tiveron C, et al. Impaired keratinocyte proliferative and clonogenic potential in transgenic mice overexpressing 14-3-3sigma in the epidermis. *J Invest Dermatol* 2011;131(9):1821-9. doi: 10.038/jid.2011.137. Epub Jun 9.
- Clerk A, Aggeli IK, Stathopoulou K, Sugden PH. Peptide growth factors signal differentially through protein kinase C to extracellular signal-regulated kinases in neonatal cardiomyocytes. *Cellular signalling* 2006;18(2):225-35.
- Clevers H. Wnt/beta-catenin signaling in development and disease. *Cell* 2006;127(3):469-80.
- Coffer PJ, Jin J, Woodgett JR. Protein kinase B (c-Akt): a multifunctional mediator of phosphatidylinositol 3-kinase activation. *The Biochemical journal* 1998;335 (Pt 1):1-13.
- Collins JE, Legan PK, Kenny TP, MacGarvie J, Holton JL, Garrod DR. Cloning and sequence analysis of desmosomal glycoproteins 2 and 3 (desmocollins): cadherin-like desmosomal adhesion molecules with heterogeneous cytoplasmic domains. *The Journal of cell biology* 1991;113(2):381-91.
- Collins LJ, Kurland CG, Biggs P, Penny D. The modern RNP world of eukaryotes. *The Journal of heredity* 2009;100(5):597-604.
- Cotsarelis G, Kaur P, Dhouailly D, Hengge U, Bickenbach J. Epithelial stem cells in the skin: definition, markers, localization and functions. *Experimental dermatology* 1999;8(1):80-8.
- Cowin P, Kapprell HP, Franke WW, Tamkun J, Hynes RO. Plakoglobin: a protein common to different kinds of intercellular adhering junctions. *Cell* 1986;46(7):1063-73.
- Dale BA, Resing KA, Lonsdale-Eccles JD. Filaggrin: a keratin filament associated protein. *Annals of the New York Academy of Sciences* 1985;455:330-42.
- de Azambuja E, Cardoso F, de Castro G, Jr., Colozza M, Mano MS, Durbecq V, et al. Ki-67 as prognostic marker in early breast cancer: a meta-analysis of published studies involving 12,155 patients. *British journal of cancer* 2007;96(10):1504-13.

- Dellambra E, Golisano O, Bondanza S, Siviero E, Lacal P, Molinari M, et al. Downregulation of 14-3-3sigma prevents clonal evolution and leads to immortalization of primary human keratinocytes. *The Journal of cell biology* 2000;149(5):1117-30.
- Delva E, Jennings JM, Calkins CC, Kottke MD, Faundez V, Kowalczyk AP. Pemphigus vulgaris IgG-induced desmoglein-3 endocytosis and desmosomal disassembly are mediated by a clathrin- and dynamin-independent mechanism. *The Journal of biological chemistry* 2008;283(26):18303-13.
- Delva E, Tucker DK, Kowalczyk AP. The desmosome. *Cold Spring Harbor perspectives in biology* 2009;1(2):a002543.
- Demlehner MP, Schafer S, Grund C, Franke WW. Continual assembly of half-desmosomal structures in the absence of cell contacts and their frustrated endocytosis: a coordinated Sisyphus cycle. *The Journal of cell biology* 1995;131(3):745-60.
- Den Z, Cheng X, Merched-Sauvage M, Koch PJ. Desmocollin 3 is required for pre-implantation development of the mouse embryo. *J Cell Sci* 2006;119(Pt 3):482-9.
- Dephoure N, Gould KL, Gygi SP, Kellogg DR. Mapping and analysis of phosphorylation sites: a quick guide for cell biologists. *Molecular biology of the cell* 2013;24(5):535-42.
- Depianto D, Kerns ML, Dlugosz AA, Coulombe PA. Keratin 17 promotes epithelial proliferation and tumor growth by polarizing the immune response in skin. *Nat Genet* 2010;42(10):910-4.
- Dohn MR, Brown MV, Reynolds AB. An essential role for p120-catenin in Src- and Rac1-mediated anchorage-independent cell growth. *The Journal of cell biology* 2009;184(3):437-50.
- Donati G, Proserpio V, Lichtenberger BM, Natsuga K, Sinclair R, Fujiwara H, et al. Epidermal Wnt/beta-catenin signaling regulates adipocyte differentiation via secretion of adipogenic factors. *Proc Natl Acad Sci U S A* 2014;111(15):E1501-9.
- Dougherty MK, Morrison DK. Unlocking the code of 14-3-3. *Journal of cell science* 2004;117(Pt 10):1875-84.
- Dovrat S, Caspi M, Zilberberg A, Lahav L, Firsow A, Gur H, et al. 14-3-3 and beta-catenin are secreted on extracellular vesicles to activate the oncogenic Wnt pathway. *Molecular oncology* 2014;8(5):894-911.
- Dubash AD, Green KJ. Desmosomes. *Current biology : CB* 2011;21(14):R529-31.
- Dusek RL, Attardi LD. Desmosomes: new perpetrators in tumour suppression. *Nature reviews Cancer* 2011;11(5):317-23.
- Dusek RL, Godsel LM, Green KJ. Discriminating roles of desmosomal cadherins: beyond desmosomal adhesion. *Journal of dermatological science* 2007;45(1):7-21.
- Ersoy-Evans S, Erkin G, Fassihi H, Chan I, Paller AS, Surucu S, et al. Ectodermal dysplasia-skin fragility syndrome resulting from a new homozygous mutation, 888delC, in the desmosomal protein plakophilin 1. *Journal of the American Academy of Dermatology* 2006;55(1):157-61.
- Fang D, Hawke D, Zheng Y, Xia Y, Meisenhelder J, Nika H, et al. Phosphorylation of beta-catenin by AKT promotes beta-catenin transcriptional activity. *The Journal of biological chemistry* 2007;282(15):11221-9.
- Fanning AS, Jameson BJ, Jesaitis LA, Anderson JM. The tight junction protein ZO-1 establishes a link between the transmembrane protein occludin and the actin cytoskeleton. *The Journal of biological chemistry* 1998;273(45):29745-53.
- Ferguson AT, Evron E, Umbricht CB, Pandita TK, Chan TA, Hermeking H, et al. High frequency of hypermethylation at the 14-3-3 sigma locus leads to gene silencing in breast cancer. *Proceedings of the National Academy of Sciences of the United States of America* 2000;97(11):6049-54.
- Fischer-Keso R, Breuninger S, Hofmann S, Henn M, Rohrig T, Strobel P, et al. Plakophilins 1 and 3 bind to FXR1 and thereby influence the mRNA stability of desmosomal proteins. *Molecular and cellular biology* 2014;34(23):4244-56.

- Freedman VH, Shin SI. Cellular tumorigenicity in nude mice: correlation with cell growth in semi-solid medium. *Cell* 1974;3(4):355-9.
- Fresno Vara JA, Casado E, de Castro J, Cejas P, Belda-Iniesta C, Gonzalez-Baron M. PI3K/Akt signalling pathway and cancer. *Cancer treatment reviews* 2004;30(2):193-204.
- Fuchs E. Epidermal differentiation and keratin gene expression. *Journal of cell science Supplement* 1993;17:197-208.
- Fuchs E, Raghavan S. Getting under the skin of epidermal morphogenesis. *Nature reviews Genetics* 2002;3(3):199-209.
- Furukawa C, Daigo Y, Ishikawa N, Kato T, Ito T, Tsuchiya E, et al. Plakophilin 3 oncogene as prognostic marker and therapeutic target for lung cancer. *Cancer research* 2005;65(16):7102-10.
- Furuse M, Hata M, Furuse K, Yoshida Y, Haratake A, Sugitani Y, et al. Claudin-based tight junctions are crucial for the mammalian epidermal barrier: a lesson from claudin-1-deficient mice. *The Journal of cell biology* 2002;156(6):1099-111.
- Gardien KL, Baas DC, de Vet HC, Middelkoop E. Transepidermal water loss measured with the Tewameter TM300 in burn scars. *Burns : journal of the International Society for Burn Injuries* 2016;42(7):1455-62.
- Garrod D. Desmosomes in vivo. *Dermatol Res Pract* 2010;2010:212439.
- Garrod D, Chidgey M. Desmosome structure, composition and function. *Biochimica et biophysica acta* 2008;1778(3):572-87.
- Garrod D, Kimura TE. Hyper-adhesion: a new concept in cell-cell adhesion. *Biochemical Society transactions* 2008;36(Pt 2):195-201.
- Garrod DR, Berika MY, Bardsley WF, Holmes D, Tabernero L. Hyper-adhesion in desmosomes: its regulation in wound healing and possible relationship to cadherin crystal structure. *Journal of cell science* 2005;118(Pt 24):5743-54.
- Garrod DR, Merritt AJ, Nie Z. Desmosomal cadherins. *Current opinion in cell biology* 2002;14(5):537-45.
- Gerdes J, Schwab U, Lemke H, Stein H. Production of a mouse monoclonal antibody reactive with a human nuclear antigen associated with cell proliferation. *International journal of cancer* 1983;31(1):13-20.
- Ghose S, Min Y, Lin PC. delta-Catenin activates Rho GTPase, promotes lymphangiogenesis and growth of tumor metastases. *PloS one* 2015;10(1):e0116338.
- Giles N, Forrest A, Gabrielli B. 14-3-3 acts as an intramolecular bridge to regulate cdc25B localization and activity. *The Journal of biological chemistry* 2003;278(31):28580-7.
- Gilleron J, Fiorini C, Carette D, Avondet C, Falk MM, Segretain D, et al. Molecular reorganization of Cx43, Zo-1 and Src complexes during the endocytosis of gap junction plaques in response to a non-genomic carcinogen. *Journal of cell science* 2008;121(Pt 24):4069-78.
- Gillies RJ, Didier N, Denton M. Determination of cell number in monolayer cultures. *Analytical biochemistry* 1986;159(1):109-13.
- Glisovic T, Bachorik JL, Yong J, Dreyfuss G. RNA-binding proteins and post-transcriptional gene regulation. *FEBS letters* 2008;582(14):1977-86.
- Gonzalez-Mariscal L, Tapia R, Chamorro D. Crosstalk of tight junction components with signaling pathways. *Biochimica et biophysica acta* 2008;1778(3):729-56.
- Goodfellow IG, Roberts LO. Eukaryotic initiation factor 4E. *The international journal of biochemistry & cell biology* 2008;40(12):2675-80.
- Graff JR, Konicek BW, Carter JH, Marcusson EG. Targeting the eukaryotic translation initiation factor 4E for cancer therapy. *Cancer research* 2008;68(3):631-4.
- Graham FL, Smiley J, Russell WC, Nairn R. Characteristics of a human cell line transformed by DNA from human adenovirus type 5. *The Journal of general virology* 1977;36(1):59-74.

- Green KJ, Gaudry CA. Are desmosomes more than tethers for intermediate filaments? *Nat Rev Mol Cell Biol* 2000;1(3):208-16.
- Green KJ, Parry DA, Steinert PM, Virata ML, Wagner RM, Angst BD, et al. Structure of the human desmoplakins. Implications for function in the desmosomal plaque. *The Journal of biological chemistry* 1990;265(19):11406-7.
- Green KJ, Simpson CL. Desmosomes: new perspectives on a classic. *The Journal of investigative dermatology* 2007;127(11):2499-515.
- Grossmann KS, Grund C, Huelsken J, Behrend M, Erdmann B, Franke WW, et al. Requirement of plakophilin 2 for heart morphogenesis and cardiac junction formation. *The Journal of cell biology* 2004;167(1):149-60.
- Guillemot L, Paschoud S, Pulimeno P, Foglia A, Citi S. The cytoplasmic plaque of tight junctions: a scaffolding and signalling center. *Biochimica et biophysica acta* 2008;1778(3):601-13.
- Gunschmann C, Stachelscheid H, Akyuz MD, Schmitz A, Missero C, Bruning JC, et al. Insulin/IGF-1 controls epidermal morphogenesis via regulation of FoxO-mediated p63 inhibition. *Dev Cell* 2013;26(2):176-87. doi: 10.1016/j.devcel.2013.05.017.
- Haegel H, Larue L, Ohsugi M, Fedorov L, Herrenknecht K, Kemler R. Lack of beta-catenin affects mouse development at gastrulation. *Development* 1995;121(11):3529-37.
- Haghighat A, Mader S, Pause A, Sonenberg N. Repression of cap-dependent translation by 4E-binding protein 1: competition with p220 for binding to eukaryotic initiation factor-4E. *The EMBO journal* 1995;14(22):5701-9.
- Hamada T, South AP, Mitsuhashi Y, Kinebuchi T, Bleck O, Ashton GH, et al. Genotype-phenotype correlation in skin fragility-ectodermal dysplasia syndrome resulting from mutations in plakophilin 1. *Experimental dermatology* 2002;11(2):107-14.
- Hara K, Yonezawa K, Kozlowski MT, Sugimoto T, Andrabi K, Weng QP, et al. Regulation of eIF-4E BP1 phosphorylation by mTOR. *The Journal of biological chemistry* 1997;272(42):26457-63.
- Hardman MJ, Sisi P, Banbury DN, Byrne C. Patterned acquisition of skin barrier function during development. *Development* 1998;125(8):1541-52.
- Hartsock A, Nelson WJ. Adherens and tight junctions: structure, function and connections to the actin cytoskeleton. *Biochimica et biophysica acta* 2008;1778(3):660-9.
- Hartsock A, Nelson WJ. Competitive regulation of E-cadherin juxtamembrane domain degradation by p120-catenin binding and Hakai-mediated ubiquitination. *PloS one* 2012;7(5):e37476.
- Hatzfeld M. The p120 family of cell adhesion molecules. *European journal of cell biology* 2005;84(2-3):205-14.
- Hatzfeld M. Plakophilins: Multifunctional proteins or just regulators of desmosomal adhesion? *Biochimica et biophysica acta* 2007;1773(1):69-77.
- Hatzfeld M, Haffner C, Schulze K, Vinzens U. The function of plakophilin 1 in desmosome assembly and actin filament organization. *The Journal of cell biology* 2000;149(1):209-22.
- Hatzfeld M, Keil R, Magin TM. Desmosomes and Intermediate Filaments: Their Consequences for Tissue Mechanics. *Cold Spring Harbor perspectives in biology* 2017;9(6).
- Hatzfeld M, Kristjansson GI, Plessmann U, Weber K. Band 6 protein, a major constituent of desmosomes from stratified epithelia, is a novel member of the armadillo multigene family. *Journal of cell science* 1994;107 (Pt 8):2259-70.
- Hatzfeld M, Wolf A, Keil R. Plakophilins in desmosomal adhesion and signaling. *Cell communication & adhesion* 2014;21(1):25-42.
- Hay N, Sonenberg N. Upstream and downstream of mTOR. *Genes & development* 2004;18(16):1926-45.
- Heid HW, Schmidt A, Zimbelmann R, Schafer S, Winter-Simanowski S, Stumpp S, et al. Cell type-specific desmosomal plaque proteins of the plakoglobin family: plakophilin 1 (band 6 protein). *Differentiation; research in biological diversity* 1994;58(2):113-31.

- Hennings H, Holbrook KA. Calcium regulation of cell-cell contact and differentiation of epidermal cells in culture. An ultrastructural study. *Experimental cell research* 1983;143(1):127-42.
- Henriksson ML, Francis MS, Peden A, Aili M, Stefansson K, Palmer R, et al. A nonphosphorylated 14-3-3 binding motif on exoenzyme S that is functional in vivo. *European journal of biochemistry* 2002;269(20):4921-9.
- Hernandez-Martin A, Torreló A, Ciria S, Colmenero I, Aguilar A, Grimalt R, et al. Ectodermal dysplasia-skin fragility syndrome: a novel mutation in the PKP1 gene. *Clin Exp Dermatol* 2013;38(7):787-90.
- Hernandez S, Chavez Munguia B, Gonzalez-Mariscal L. ZO-2 silencing in epithelial cells perturbs the gate and fence function of tight junctions and leads to an atypical monolayer architecture. *Experimental cell research* 2007;313(8):1533-47.
- Herron BJ, Liddell RA, Parker A, Grant S, Kinne J, Fisher JK, et al. A mutation in stratifin is responsible for the repeated epilation (Er) phenotype in mice. *Nature genetics* 2005;37(11):1210-2.
- Hinton TM, Coldwell MJ, Carpenter GA, Morley SJ, Pain VM. Functional analysis of individual binding activities of the scaffold protein eIF4G. *The Journal of biological chemistry* 2007;282(3):1695-708.
- Hofmann I, Casella M, Schnolzer M, Schlechter T, Spring H, Franke WW. Identification of the junctional plaque protein plakophilin 3 in cytoplasmic particles containing RNA-binding proteins and the recruitment of plakophilins 1 and 3 to stress granules. *Molecular biology of the cell* 2006;17(3):1388-98.
- Holz MK, Ballif BA, Gygi SP, Blenis J. mTOR and S6K1 mediate assembly of the translation preinitiation complex through dynamic protein interchange and ordered phosphorylation events. *Cell* 2005;123(4):569-80.
- Homberg M, Magin TM. Beyond expectations: novel insights into epidermal keratin function and regulation. *International review of cell and molecular biology* 2014;311:265-306.
- Hong S, Troyanovsky RB, Troyanovsky SM. Spontaneous assembly and active disassembly balance adherens junction homeostasis. *Proceedings of the National Academy of Sciences of the United States of America* 2010;107(8):3528-33.
- Hsu CK, Liu L, Can PK, Kocaturk E, McMillan JR, Gungor S, et al. Ectodermal dysplasia-skin fragility syndrome resulting from a new atypical homozygous cryptic acceptor splice site mutation in PKP1. *Journal of dermatological science* 2016;84(2):210-2.
- Huang W, Erikson RL. Constitutive activation of Mek1 by mutation of serine phosphorylation sites. *Proceedings of the National Academy of Sciences of the United States of America* 1994;91(19):8960-3.
- Huber AH, Nelson WJ, Weis WI. Three-dimensional structure of the armadillo repeat region of beta-catenin. *Cell* 1997;90(5):871-82.
- Huelsken J, Vogel R, Erdmann B, Cotsarelis G, Birchmeier W. beta-Catenin controls hair follicle morphogenesis and stem cell differentiation in the skin. *Cell* 2001;105(4):533-45.
- Hulsken J, Birchmeier W, Behrens J. E-cadherin and APC compete for the interaction with beta-catenin and the cytoskeleton. *The Journal of cell biology* 1994;127(6 Pt 2):2061-9.
- Hunter T. Why nature chose phosphate to modify proteins. *Philosophical transactions of the Royal Society of London Series B, Biological sciences* 2012;367(1602):2513-6.
- Hutchison CA, Phillips S, Edgell MH, Gillam S, Jahnke P, Smith M. Mutagenesis at a specific position in a DNA sequence. *The Journal of biological chemistry* 1978;253:6551-60.
- Ichimura T, Isobe T, Okuyama T, Takahashi N, Araki K, Kuwano R, et al. Molecular cloning of cDNA coding for brain-specific 14-3-3 protein, a protein kinase-dependent activator of tyrosine and tryptophan hydroxylases. *Proceedings of the National Academy of Sciences of the United States of America* 1988;85(19):7084-8.

- Jensen ON. Interpreting the protein language using proteomics. *Nature reviews Molecular cell biology* 2006;7(6):391-403.
- Johnson C, Crowther S, Stafford MJ, Campbell DG, Toth R, MacKintosh C. Bioinformatic and experimental survey of 14-3-3-binding sites. *The Biochemical journal* 2010;427(1):69-78.
- Jones DH, Ley S, Aitken A. Isoforms of 14-3-3 protein can form homo- and heterodimers in vivo and in vitro: implications for function as adapter proteins. *FEBS letters* 1995;368(1):55-8.
- Kale G, Naren AP, Sheth P, Rao RK. Tyrosine phosphorylation of occludin attenuates its interactions with ZO-1, ZO-2, and ZO-3. *Biochemical and biophysical research communications* 2003;302(2):324-9.
- Kapprell HP, Owaribe K, Franke WW. Identification of a basic protein of Mr 75,000 as an accessory desmosomal plaque protein in stratified and complex epithelia. *The Journal of cell biology* 1988;106(5):1679-91.
- Kashiwagi M, Huh NH. Organ culture of developing mouse skin and its application for molecular mechanistic studies of morphogenesis. *Methods in molecular biology* 2005;289:39-46.
- Kashyap S, Shanker V, Sharma N. Ectodermal Dysplasia-Skin Fragility Syndrome: A Rare Case Report. *Indian J Dermatol* 2015;60(4):421. doi: 10.4103/0019-5154.160525.
- Kasturi L, Sizemore N, Eckert RL, Martin K, Rorke EA. Calcium modulates cornified envelope formation, involucrin content, and transglutaminase activity in cultured human ectocervical epithelial cells. *Experimental cell research* 1993;205(1):84-90.
- Kaufman RJ, Davies MV, Pathak VK, Hershey JW. The phosphorylation state of eucaryotic initiation factor 2 alters translational efficiency of specific mRNAs. *Molecular and cellular biology* 1989;9(3):946-58.
- Kedersha N, Stoecklin G, Ayodele M, Yacono P, Lykke-Andersen J, Fritzler MJ, et al. Stress granules and processing bodies are dynamically linked sites of mRNP remodeling. *The Journal of cell biology* 2005;169(6):871-84.
- Keil R, Rietscher K, Hatzfeld M. Antagonistic Regulation of Intercellular Cohesion by Plakophilins 1 and 3. *The Journal of investigative dermatology* 2016;136(10):2022-9.
- Keil R, Wolf A, Huttelmaier S, Hatzfeld M. Beyond regulation of cell adhesion: local control of RhoA at the cleavage furrow by the p0071 catenin. *Cell cycle* 2007;6(2):122-7.
- Kezic S, Jakasa I. Filaggrin and Skin Barrier Function. *Current problems in dermatology* 2016;49:1-7.
- Kilani RT, Medina A, Aitken A, Jalili RB, Carr M, Ghahary A. Identification of different isoforms of 14-3-3 protein family in human dermal and epidermal layers. *Molecular and cellular biochemistry* 2008;314(1-2):161-9.
- Kim W, Bennett EJ, Huttlin EL, Guo A, Li J, Possemato A, et al. Systematic and quantitative assessment of the ubiquitin-modified proteome. *Molecular cell* 2011;44(2):325-40.
- Kimura TE, Merritt AJ, Garrod DR. Calcium-independent desmosomes of keratinocytes are hyper-adhesive. *The Journal of investigative dermatology* 2007;127(4):775-81.
- Kimura TE, Merritt AJ, Lock FR, Eckert JJ, Fleming TP, Garrod DR. Desmosomal adhesiveness is developmentally regulated in the mouse embryo and modulated during trophectoderm migration. *Developmental biology* 2012;369(2):286-97.
- Koch PJ, de Viragh PA, Scharer E, Bundman D, Longley MA, Bickenbach J, et al. Lessons from loricrin-deficient mice: compensatory mechanisms maintaining skin barrier function in the absence of a major cornified envelope protein. *The Journal of cell biology* 2000;151(2):389-400.
- Koch PJ, Walsh MJ, Schmelz M, Goldschmidt MD, Zimbelmann R, Franke WW. Identification of desmoglein, a constitutive desmosomal glycoprotein, as a member of the cadherin family of cell adhesion molecules. *European journal of cell biology* 1990;53(1):1-12.
- Kolly C, Suter MM, Muller EJ. Proliferation, cell cycle exit, and onset of terminal differentiation in cultured keratinocytes: pre-programmed pathways in control of C-Myc and Notch1 prevail over extracellular calcium signals. *The Journal of investigative dermatology* 2005;124(5):1014-25.

- Kong J, Lasko P. Translational control in cellular and developmental processes. *Nature reviews Genetics* 2012;13(6):383-94.
- Kowalczyk AP, Hatzfeld M, Bornslaeger EA, Kopp DS, Borgwardt JE, Corcoran CM, et al. The head domain of plakophilin-1 binds to desmoplakin and enhances its recruitment to desmosomes. Implications for cutaneous disease. *The Journal of biological chemistry* 1999;274(26):18145-8.
- Kowalczyk AP, Stappenbeck TS, Parry DA, Palka HL, Virata ML, Bornslaeger EA, et al. Structure and function of desmosomal transmembrane core and plaque molecules. *Biophysical chemistry* 1994;50(1-2):97-112.
- Kröger C, Loschke F, Schwarz N, Windoffer R, Leube RE, Magin TM. Keratins control intercellular adhesion involving PKC- α -mediated desmoplakin phosphorylation. *J Cell Biol* 2013;201(5):681-92. doi: 10.1083/jcb.201208162. Epub 2013 May 20.
- Kundu ST, Gosavi P, Khapare N, Patel R, Hosing AS, Maru GB, et al. Plakophilin3 downregulation leads to a decrease in cell adhesion and promotes metastasis. *International journal of cancer* 2008;123(10):2303-14.
- Kurzen H, Munzing I, Hartschuh W. Expression of desmosomal proteins in squamous cell carcinomas of the skin. *J Cutan Pathol* 2003;30(10):621-30.
- Laemmli UK. Cleavage of structural proteins during the assembly of the head of bacteriophage T4. *Nature* 1970;227(5259):680-5.
- Lai-Cheong JE, Arita K, McGrath JA. Genetic diseases of junctions. *The Journal of investigative dermatology* 2007;127(12):2713-25.
- Laronga C, Yang HY, Neal C, Lee MH. Association of the cyclin-dependent kinases and 14-3-3 sigma negatively regulates cell cycle progression. *The Journal of biological chemistry* 2000;275(30):23106-12.
- Lee CH, Coulombe PA. Self-organization of keratin intermediate filaments into cross-linked networks. *Journal of Cell Biology* 2009;186(3):409-21.
- Letterio JJ, Bottinger EP. TGF- β knockout and dominant-negative receptor transgenic mice. *Mineral and electrolyte metabolism* 1998;24(2-3):161-7.
- Levy L, Broad S, Diekmann D, Evans RD, Watt FM. β 1 integrins regulate keratinocyte adhesion and differentiation by distinct mechanisms. *Molecular biology of the cell* 2000;11(2):453-66.
- Li FQ, Mofunanya A, Harris K, Takemaru K. Chibby cooperates with 14-3-3 to regulate beta-catenin subcellular distribution and signaling activity. *The Journal of cell biology* 2008;181(7):1141-54.
- Li MW, Mruk DD, Lee WM, Cheng CY. Connexin 43 and plakophilin-2 as a protein complex that regulates blood-testis barrier dynamics. *Proceedings of the National Academy of Sciences of the United States of America* 2009;106(25):10213-8.
- Li Q, Lu Q, Estepa G, Verma IM. Identification of 14-3-3sigma mutation causing cutaneous abnormality in repeated-epilation mutant mouse. *Proceedings of the National Academy of Sciences of the United States of America* 2005;102(44):15977-82.
- Liao Y, Hung MC. Physiological regulation of Akt activity and stability. *American journal of translational research* 2010;2(1):19-42.
- Lie PP, Cheng CY, Mruk DD. Crosstalk between desmoglein-2/desmocollin-2/Src kinase and coxsackie and adenovirus receptor/ZO-1 protein complexes, regulates blood-testis barrier dynamics. *The international journal of biochemistry & cell biology* 2010;42(6):975-86.
- Lim W, Mayer B, Pawson T. *Cell signaling: principles and mechanisms* [eBook, Garland Science, Taylor & Francis Group, LLC, New York, NY]. NY: Garland Science, Taylor & Francis Group, LLC, 2015.
- Liu D, Bienkowska J, Petosa C, Collier RJ, Fu H, Liddington R. Crystal structure of the zeta isoform of the 14-3-3 protein. *Nature* 1995;376(6536):191-4.

- Liu JP, Baker J, Perkins AS, Robertson EJ, Efstratiadis A. Mice carrying null mutations of the genes encoding insulin-like growth factor I (Igf-1) and type 1 IGF receptor (Igf1r). *Cell* 1993;75(1):59-72.
- Liu Y, Petreaca M, Yao M, Martins-Green M. Cell and molecular mechanisms of keratinocyte function stimulated by insulin during wound healing. *BMC cell biology* 2009;10:1.
- Lodygin D, Diebold J, Hermeking H. Prostate cancer is characterized by epigenetic silencing of 14-3-3sigma expression. *Oncogene* 2004;23(56):9034-41.
- Lodygin D, Hermeking H. The role of epigenetic inactivation of 14-3-3sigma in human cancer. *Cell research* 2005;15(4):237-46.
- Lodygin D, Yazdi AS, Sander CA, Herzinger T, Hermeking H. Analysis of 14-3-3sigma expression in hyperproliferative skin diseases reveals selective loss associated with CpG-methylation in basal cell carcinoma. *Oncogene* 2003;22(35):5519-24.
- Lorch JH, Klessner J, Park JK, Getsios S, Wu YL, Stack MS, et al. Epidermal growth factor receptor inhibition promotes desmosome assembly and strengthens intercellular adhesion in squamous cell carcinoma cells. *The Journal of biological chemistry* 2004;279(35):37191-200.
- Loschke F, Homberg M, Magin TM. Keratin Isotypes Control Desmosome Stability and Dynamics through PKCalpha. *The Journal of investigative dermatology* 2016;136(1):202-13.
- Loschke F, Seltmann K, Bouameur JE, Magin TM. Regulation of keratin network organization. *Current opinion in cell biology* 2015;32:56-64.
- Mackintosh C. Dynamic interactions between 14-3-3 proteins and phosphoproteins regulate diverse cellular processes. *The Biochemical journal* 2004;381(Pt 2):329-42.
- Mahoney MG, Hu Y, Brennan D, Bazzi H, Christiano AM, Wahl JK, 3rd. Delineation of diversified desmoglein distribution in stratified squamous epithelia: implications in diseases. *Experimental dermatology* 2006;15(2):101-9.
- Masters SC, Pederson KJ, Zhang L, Barbieri JT, Fu H. Interaction of 14-3-3 with a nonphosphorylated protein ligand, exoenzyme S of *Pseudomonas aeruginosa*. *Biochemistry* 1999;38(16):5216-21.
- Matsui T, Amagai M. Dissecting the formation, structure and barrier function of the stratum corneum. *Int Immunol* 2015;27(6):269-80.
- Mazzalupo S, Wong P, Martin P, Coulombe PA. Role for keratins 6 and 17 during wound closure in embryonic mouse skin. *Developmental dynamics : an official publication of the American Association of Anatomists* 2003;226(2):356-65.
- McGowan KM, Coulombe PA. Onset of keratin 17 expression coincides with the definition of major epithelial lineages during skin development. *The Journal of cell biology* 1998;143(2):469-86.
- McGrath JA. A novel genodermatosis caused by mutations in plakophilin 1, a structural component of desmosomes. *J Dermatol* 1999;26(11):764-9.
- McGrath JA, Hoeger PH, Christiano AM, McMillan JR, Mellerio JE, Ashton GH, et al. Skin fragility and hypohidrotic ectodermal dysplasia resulting from ablation of plakophilin 1. *Br J Dermatol* 1999;140(2):297-307.
- McGrath JA, McMillan JR, Shemanko CS, Runswick SK, Leigh IM, Lane EB, et al. Mutations in the plakophilin 1 gene result in ectodermal dysplasia/skin fragility syndrome. *Nat Genet* 1997;17(2):240-4.
- McGrath JA, Mellerio JE. Ectodermal dysplasia-skin fragility syndrome. *Dermatologic clinics* 2010;28(1):125-9.
- McKay MM, Morrison DK. Integrating signals from RTKs to ERK/MAPK. *Oncogene* 2007;26(22):3113-21.
- McMillan JR, Haftek M, Akiyama M, South AP, Perrot H, McGrath JA, et al. Alterations in desmosome size and number coincide with the loss of keratinocyte cohesion in skin with homozygous

- and heterozygous defects in the desmosomal protein plakophilin 1. *The Journal of investigative dermatology* 2003;121(1):96-103.
- Mechanic S, Raynor K, Hill JE, Cowin P. Desmocollins form a distinct subset of the cadherin family of cell adhesion molecules. *Proceedings of the National Academy of Sciences of the United States of America* 1991;88(10):4476-80.
- Meier R, Hemmings BA. Regulation of protein kinase B. *Journal of receptor and signal transduction research* 1999;19(1-4):121-8.
- Memmott RM, Dennis PA. Akt-dependent and -independent mechanisms of mTOR regulation in cancer. *Cellular signalling* 2009;21(5):656-64.
- Mendoza MC, Er EE, Blenis J. The Ras-ERK and PI3K-mTOR pathways: cross-talk and compensation. *Trends in biochemical sciences* 2011;36(6):320-8.
- Menon GK, Grayson S, Elias PM. Ionic calcium reservoirs in mammalian epidermis: ultrastructural localization by ion-capture cytochemistry. *The Journal of investigative dermatology* 1985;84(6):508-12.
- Mertens C, Kuhn C, Franke WW. Plakophilins 2a and 2b: constitutive proteins of dual location in the karyoplasm and the desmosomal plaque. *The Journal of cell biology* 1996;135(4):1009-25.
- Mertins P, Mani DR, Ruggles KV, Gillette MA, Clauser KR, Wang P, et al. Proteogenomics connects somatic mutations to signalling in breast cancer. *Nature* 2016;534(7605):55-62.
- Mertins P, Yang F, Liu T, Mani DR, Petyuk VA, Gillette MA, et al. Ischemia in tumors induces early and sustained phosphorylation changes in stress kinase pathways but does not affect global protein levels. *Molecular & cellular proteomics : MCP* 2014;13(7):1690-704.
- Miyazaki K, Yoshizaki K, Arai C, Yamada A, Saito K, Ishikawa M, et al. Plakophilin-1, a Novel Wnt Signaling Regulator, Is Critical for Tooth Development and Ameloblast Differentiation. *PLoS one* 2016;11(3):e0152206.
- Moll R, Cowin P, Kapprell HP, Franke WW. Desmosomal proteins: new markers for identification and classification of tumors. *Laboratory investigation; a journal of technical methods and pathology* 1986;54(1):4-25.
- Moon RT, Kohn AD, De Ferrari GV, Kaykas A. WNT and beta-catenin signalling: diseases and therapies. *Nature reviews Genetics* 2004;5(9):691-701.
- Moore BW, Perez VJ. *Specific Acid Proteins in the Nervous System*. Englewood Cliffs, New Jersey: Prentice-Hall 1967.
- Moreira JM, Shen T, Ohlsson G, Gromov P, Gromova I, Celis JE. A combined proteome and ultrastructural localization analysis of 14-3-3 proteins in transformed human amnion (AMA) cells: definition of a framework to study isoform-specific differences. *Molecular & cellular proteomics : MCP* 2008;7(7):1225-40.
- Morin PJ. beta-catenin signaling and cancer. *BioEssays : news and reviews in molecular, cellular and developmental biology* 1999;21(12):1021-30.
- Morin PJ, Sparks AB, Korinek V, Barker N, Clevers H, Vogelstein B, et al. Activation of beta-catenin-Tcf signaling in colon cancer by mutations in beta-catenin or APC. *Science* 1997;275(5307):1787-90.
- Morris MA, Young LS, Dawson CW. DNA tumour viruses promote tumour cell invasion and metastasis by deregulating the normal processes of cell adhesion and motility. *European journal of cell biology* 2008;87(8-9):677-97.
- Morrison DK. The 14-3-3 proteins: integrators of diverse signaling cues that impact cell fate and cancer development. *Trends in cell biology* 2009;19(1):16-23.
- Müller J, Ritt DA, Copeland TD, Morrison DK. Functional analysis of C-TAK1 substrate binding and identification of PKP2 as a new C-TAK1 substrate. *The EMBO journal* 2003;22(17):4431-42.
- Muslin AJ, Tanner JW, Allen PM, Shaw AS. Interaction of 14-3-3 with signaling proteins is mediated by the recognition of phosphoserine. *Cell* 1996;84(6):889-97.

- Nakatani K, Sakaue H, Thompson DA, Weigel RJ, Roth RA. Identification of a human Akt3 (protein kinase B gamma) which contains the regulatory serine phosphorylation site. *Biochemical and biophysical research communications* 1999;257(3):906-10.
- Narayana N, Gist J, Smith T, Tylka D, Trogdon G, Wahl JK. Desmosomal component expression in normal, dysplastic, and oral squamous cell carcinoma. *Dermatol Res Pract* 2010;2010:649731.(doi):10.1155/2010/649731. Epub 2010 Mar 18.
- Neuber S, Muhmer M, Wratten D, Koch PJ, Moll R, Schmidt A. The desmosomal plaque proteins of the plakophilin family. *Dermatol Res Pract* 2010;2010:101452.
- Nieset JE, Redfield AR, Jin F, Knudsen KA, Johnson KR, Wheelock MJ. Characterization of the interactions of alpha-catenin with alpha-actinin and beta-catenin/plakoglobin. *Journal of cell science* 1997;110 (Pt 8):1013-22.
- Nishi H, Hashimoto K, Panchenko AR. Phosphorylation in protein-protein binding: effect on stability and function. *Structure* 2011;19(12):1807-15.
- North AJ, Bardsley WG, Hyam J, Bornslaeger EA, Cordingley HC, Trinnaman B, et al. Molecular map of the desmosomal plaque. *Journal of cell science* 1999;112 (Pt 23):4325-36.
- North AJ, Chidgey MA, Clarke JP, Bardsley WG, Garrod DR. Distinct desmocollin isoforms occur in the same desmosomes and show reciprocally graded distributions in bovine nasal epidermis. *Proc Natl Acad Sci U S A* 1996;93(15):7701-5.
- O'Shaughnessy RF, Akgul B, Storey A, Pfister H, Harwood CA, Byrne C. Cutaneous human papillomaviruses down-regulate AKT1, whereas AKT2 up-regulation and activation associates with tumors. *Cancer research* 2007;67(17):8207-15.
- Obsil T, Ghirlando R, Klein DC, Ganguly S, Dyda F. Crystal structure of the 14-3-3zeta:serotonin N-acetyltransferase complex. a role for scaffolding in enzyme regulation. *Cell* 2001;105(2):257-67.
- Obsil T, Obsilova V. Structural basis of 14-3-3 protein functions. *Seminars in cell & developmental biology* 2011;22(7):663-72.
- Obsilova V, Kopecka M, Kosek D, Kacirova M, Kylarova S, Rezabkova L, et al. Mechanisms of the 14-3-3 protein function: regulation of protein function through conformational modulation. *Physiological research* 2014;63 Suppl 1:S155-64.
- Olivry T, Linder KE, Wang P, Bizikova P, Bernstein JA, Dunston SM, et al. Deficient plakophilin-1 expression due to a mutation in PKP1 causes ectodermal dysplasia-skin fragility syndrome in Chesapeake Bay retriever dogs. *PLoS One* 2012;7(2):e32072.
- Olsen JV, Blagoev B, Gnad F, Macek B, Kumar C, Mortensen P, et al. Global, in vivo, and site-specific phosphorylation dynamics in signaling networks. *Cell* 2006;127(3):635-48.
- Orford K, Crockett C, Jensen JP, Weissman AM, Byers SW. Serine phosphorylation-regulated ubiquitination and degradation of beta-catenin. *The Journal of biological chemistry* 1997;272(40):24735-8.
- Paris L, Tonutti L, Vannini C, Bazzoni G. Structural organization of the tight junctions. *Biochimica et biophysica acta* 2008;1778(3):646-59.
- Parker AE, Wheeler GN, Arnemann J, Pidsley SC, Ataliotis P, Thomas CL, et al. Desmosomal glycoproteins II and III. Cadherin-like junctional molecules generated by alternative splicing. *The Journal of biological chemistry* 1991;266(16):10438-45.
- Pearce LR, Komander D, Alessi DR. The nuts and bolts of AGC protein kinases. *Nature reviews Molecular cell biology* 2010;11(1):9-22.
- Perez-Moreno M, Fuchs E. Catenins: keeping cells from getting their signals crossed. *Developmental cell* 2006;11(5):601-12.
- Piepkorn M, Pittelkow MR, Cook PW. Autocrine regulation of keratinocytes: the emerging role of heparin-binding, epidermal growth factor-related growth factors. *The Journal of investigative dermatology* 1998;111(5):715-21.

- Pokutta S, Weis WI. Structure and mechanism of cadherins and catenins in cell-cell contacts. *Annual review of cell and developmental biology* 2007;23:237-61.
- Polakis P. Wnt signaling and cancer. *Genes & development* 2000;14(15):1837-51.
- Povoa G, Diniz LM. Growth hormone system: skin interactions. *Anais brasileiros de dermatologia* 2011;86(6):1159-65.
- Powell-Braxton L, Hollingshead P, Warburton C, Dowd M, Pitts-Meek S, Dalton D, et al. IGF-I is required for normal embryonic growth in mice. *Genes Dev* 1993;7(12B):2609-17.
- Prabakaran S, Lippens G, Steen H, Gunawardena J. Post-translational modification: nature's escape from genetic imprisonment and the basis for dynamic information encoding. *Wiley interdisciplinary reviews Systems biology and medicine* 2012;4(6):565-83.
- Prevot D, Darlix JL, Ohlmann T. Conducting the initiation of protein synthesis: the role of eIF4G. *Biology of the cell* 2003;95(3-4):141-56.
- Proud CG, Denton RM. Molecular mechanisms for the control of translation by insulin. *The Biochemical journal* 1997;328 (Pt 2):329-41.
- Ptacek J, Snyder M. Charging it up: global analysis of protein phosphorylation. *Trends in genetics : TIG* 2006;22(10):545-54.
- Qiao M, Sheng S, Pardee AB. Metastasis and AKT activation. *Cell cycle* 2008;7(19):2991-6.
- Radhakrishnan VM, Martinez JD. 14-3-3gamma induces oncogenic transformation by stimulating MAP kinase and PI3K signaling. *PloS one* 2010;5(7):e11433.
- Rapley J, Oshiro N, Ortiz-Vega S, Avruch J. The mechanism of insulin-stimulated 4E-BP protein binding to mammalian target of rapamycin (mTOR) complex 1 and its contribution to mTOR complex 1 signaling. *The Journal of biological chemistry* 2011;286(44):38043-53.
- Rapsomaniki MA, Kotsantis P, Symeonidou IE, Giakoumakis NN, Taraviras S, Lygerou Z. easyFRAP: an interactive, easy-to-use tool for qualitative and quantitative analysis of FRAP data. *Bioinformatics* 2012;28(13):1800-1.
- Renart J, Reiser J, Stark GR. Transfer of proteins from gels to diazobenzoyloxymethyl-paper and detection with antisera: a method for studying antibody specificity and antigen structure. *Proceedings of the National Academy of Sciences of the United States of America* 1979;76(7):3116-20.
- Resnik N, Sepcic K, Plemenitas A, Windoffer R, Leube R, Veranic P. Desmosome assembly and cell-cell adhesion are membrane raft-dependent processes. *J Biol Chem* 2011;286(2):1499-507. doi: 10.074/jbc.M110.189464. Epub 2010 Nov 11.
- Rickelt S, Franke WW, Doerflinger Y, Goerdts S, Brandner JM, Peitsch WK. Subtypes of melanocytes and melanoma cells distinguished by their intercellular contacts: heterotypic adherens junctions, adhesive associations, and dispersed desmoglein 2 glycoproteins. *Cell and tissue research* 2008;334(3):401-22.
- Rimpler U. Funktionelle Charakterisierung von Desmocollin 2 während der Embryonalentwicklung und im adulten Herzen in der Maus [dissertation] Humboldt-Universität zu Berlin. 2014.
- Rinnerthaler M, Streubel MK, Bischof J, Richter K. Skin aging, gene expression and calcium. *Experimental gerontology* 2015;68:59-65.
- Rittinger K, Budman J, Xu J, Volinia S, Cantley LC, Smerdon SJ, et al. Structural analysis of 14-3-3 phosphopeptide complexes identifies a dual role for the nuclear export signal of 14-3-3 in ligand binding. *Molecular cell* 1999;4(2):153-66.
- Roberts BJ, Johnson KE, McGuinn KP, Saowapa J, Svoboda RA, Mahoney MG, et al. Palmitoylation of plakophilin is required for desmosome assembly. *J Cell Sci* 2014;127(Pt 17):3782-93. doi: 10.1242/jcs.149849. Epub 2014 Jul 7.
- Roberts BJ, Reddy R, Wahl JK, 3rd. Stratifin (14-3-3 sigma) limits plakophilin-3 exchange with the desmosomal plaque. *PloS one* 2013;8(10):e77012.

- Roberts BJ, Svoboda RA, Overmiller AM, Lewis JD, Kowalczyk AP, Mahoney MG, et al. Palmitoylation of Desmoglein 2 Is a Regulator of Assembly Dynamics and Protein Turnover. *The Journal of biological chemistry* 2016;291(48):24857-65.
- Robertson GP. Functional and therapeutic significance of Akt deregulation in malignant melanoma. *Cancer metastasis reviews* 2005;24(2):273-85.
- Sambandam SAT, Kasetti RB, Xue L, Dean DC, Lu Q, Li Q. 14-3-3sigma regulates keratinocyte proliferation and differentiation by modulating Yap1 cellular localization. *The Journal of investigative dermatology* 2015;135(6):1621-8.
- Sandilands A, Sutherland C, Irvine AD, McLean WH. Filaggrin in the frontline: role in skin barrier function and disease. *Journal of cell science* 2009;122(Pt 9):1285-94.
- Sawada N, Murata M, Kikuchi K, Osanai M, Tobioka H, Kojima T, et al. Tight junctions and human diseases. *Medical electron microscopy : official journal of the Clinical Electron Microscopy Society of Japan* 2003;36(3):147-56.
- Schackmann RC, Tenhagen M, van de Ven RA, Derksen PW. p120-catenin in cancer - mechanisms, models and opportunities for intervention. *Journal of cell science* 2013;126(Pt 16):3515-25.
- Schafer S, Koch PJ, Franke WW. Identification of the ubiquitous human desmoglein, Dsg2, and the expression catalogue of the desmoglein subfamily of desmosomal cadherins. *Experimental cell research* 1994;211(2):391-9.
- Schlessinger J. Cell signaling by receptor tyrosine kinases. *Cell* 2000;103(2):211-25.
- Schluter H, Wepf R, Moll I, Franke WW. Sealing the live part of the skin: the integrated meshwork of desmosomes, tight junctions and curvilinear ridge structures in the cells of the uppermost granular layer of the human epidermis. *Eur J Cell Biol* 2004;83(11-12):655-65.
- Schmidt A, Jager S. Plakophilins--hard work in the desmosome, recreation in the nucleus? *European journal of cell biology* 2005;84(2-3):189-204.
- Schmidt A, Langbein L, Pratzel S, Rode M, Rackwitz HR, Franke WW. Plakophilin 3--a novel cell-type-specific desmosomal plaque protein. *Differentiation; research in biological diversity* 1999;64(5):291-306.
- Schmidt A, Langbein L, Rode M, Pratzel S, Zimbelmann R, Franke WW. Plakophilins 1a and 1b: widespread nuclear proteins recruited in specific epithelial cells as desmosomal plaque components. *Cell Tissue Res* 1997a;290(3):481-99.
- Schmidt A, Langbein L, Rode M, Pratzel S, Zimbelmann R, Franke WW. Plakophilins 1a and 1b: widespread nuclear proteins recruited in specific epithelial cells as desmosomal plaque components. *Cell and tissue research* 1997b;290(3):481-99.
- Schmitt CJ, Franke WW, Goerdts S, Falkowska-Hansen B, Rickelt S, Peitsch WK. Homo- and heterotypic cell contacts in malignant melanoma cells and desmoglein 2 as a novel solitary surface glycoprotein. *The Journal of investigative dermatology* 2007;127(9):2191-206.
- Schmitz A, Garg K, Koumaki D, Kuonen F, Lazic E, Verykiou S, et al. Assessing the in vivo epidermal barrier in mice: dye penetration assays. *The Journal of investigative dermatology* 2015;135(2):e29.
- Schwarz J, Ayim A, Schmidt A, Jager S, Koch S, Baumann R, et al. Differential expression of desmosomal plakophilins in various types of carcinomas: correlation with cell type and differentiation. *Hum Pathol* 2006;37(5):613-22.
- Segre JA. Epidermal barrier formation and recovery in skin disorders. *The Journal of clinical investigation* 2006;116(5):1150-8.
- Sehgal L, Mukhopadhyay A, Rajan A, Khapare N, Sawant M, Vishal SS, et al. 14-3-3gamma-Mediated transport of plakoglobin to the cell border is required for the initiation of desmosome assembly in vitro and in vivo. *Journal of cell science* 2014;127(Pt 10):2174-88.
- Serre G, Mils V, Haftek M, Vincent C, Croute F, Reano A, et al. Identification of late differentiation antigens of human cornified epithelia, expressed in re-organized desmosomes and bound to cross-linked envelope. *The Journal of investigative dermatology* 1991;97(6):1061-72.

- Shin SI, Freedman VH, Risser R, Pollack R. Tumorigenicity of virus-transformed cells in nude mice is correlated specifically with anchorage independent growth in vitro. *Proceedings of the National Academy of Sciences of the United States of America* 1975;72(11):4435-9.
- Shin SS, Wall BA, Goydos JS, Chen S. AKT2 is a downstream target of metabotropic glutamate receptor 1 (Grm1). *Pigment cell & melanoma research* 2010;23(1):103-11.
- Simpson CL, Patel DM, Green KJ. Deconstructing the skin: cytoarchitectural determinants of epidermal morphogenesis. *Nature reviews Molecular cell biology* 2011;12(9):565-80.
- Sklyarova T, Bonne S, D'Hooge P, Denecker G, Goossens S, De Rycke R, et al. Plakophilin-3-deficient mice develop hair coat abnormalities and are prone to cutaneous inflammation. *The Journal of investigative dermatology* 2008;128(6):1375-85.
- Smith EA, Fuchs E. Defining the interactions between intermediate filaments and desmosomes. *The Journal of cell biology* 1998;141(5):1229-41.
- Smola H, Stark HJ, Thiekotter G, Mirancea N, Krieg T, Fusenig NE. Dynamics of basement membrane formation by keratinocyte-fibroblast interactions in organotypic skin culture. *Experimental cell research* 1998;239(2):399-410.
- Sobolik-Delmaire T, Katafiasz D, Wahl JK, 3rd. Carboxyl terminus of Plakophilin-1 recruits it to plasma membrane, whereas amino terminus recruits desmoplakin and promotes desmosome assembly. *The Journal of biological chemistry* 2006;281(25):16962-70.
- Sobolik-Delmaire T, Reddy R, Pashaj A, Roberts BJ, Wahl JK, 3rd. Plakophilin-1 localizes to the nucleus and interacts with single-stranded DNA. *The Journal of investigative dermatology* 2010;130(11):2638-46.
- Sotiropoulou PA, Blanpain C. Development and homeostasis of the skin epidermis. *Cold Spring Harbor perspectives in biology* 2012;4(7):a008383.
- Soule HD, Vazquez J, Long A, Albert S, Brennan M. A human cell line from a pleural effusion derived from a breast carcinoma. *Journal of the National Cancer Institute* 1973;51(5):1409-16.
- South AP. Plakophilin 1: an important stabilizer of desmosomes. *Clin Exp Dermatol* 2004;29(2):161-7.
- South AP, Wan H, Stone MG, Dopping-Hepenstal PJ, Purkis PE, Marshall JF, et al. Lack of plakophilin 1 increases keratinocyte migration and reduces desmosome stability. *J Cell Sci* 2003;116(Pt 16):3303-14.
- Sprecher E, Molho-Pessach V, Ingber A, Sagi E, Indelman M, Bergman R. Homozygous splice site mutations in PKP1 result in loss of epidermal plakophilin 1 expression and underlie ectodermal dysplasia/skin fragility syndrome in two consanguineous families. *J Invest Dermatol* 2004;122(3):647-51.
- Stachelscheid H, Ibrahim H, Koch L, Schmitz A, Tschardt M, Wunderlich FT, et al. Epidermal insulin/IGF-1 signalling control interfollicular morphogenesis and proliferative potential through Rac activation. *Embo J* 2008;27(15):2091-101. doi: 10.1038/emboj.2008.141. Epub Jul 24.
- Stahl JM, Sharma A, Cheung M, Zimmerman M, Cheng JQ, Bosenberg MW, et al. Deregulated Akt3 activity promotes development of malignant melanoma. *Cancer research* 2004;64(19):7002-10.
- Stahley SN, Saito M, Faundez V, Koval M, Mattheyses AL, Kowalczyk AP. Desmosome assembly and disassembly are membrane raft-dependent. *PLoS One* 2014;9(1):e87809. doi: 10.1371/journal.pone.0087809. eCollection 2014.
- Stappenbeck TS, Bornslaeger EA, Corcoran CM, Luu HH, Virata ML, Green KJ. Functional analysis of desmoplakin domains: specification of the interaction with keratin versus vimentin intermediate filament networks. *The Journal of cell biology* 1993;123(3):691-705.
- Steed E, Balda MS, Matter K. Dynamics and functions of tight junctions. *Trends in cell biology* 2010;20(3):142-9.

- Steelman LS, Stadelman KM, Chappell WH, Horn S, Basecke J, Cervello M, et al. Akt as a therapeutic target in cancer. *Expert opinion on therapeutic targets* 2008;12(9):1139-65.
- Steijlen PM, van Steensel MA, Jansen BJ, Blokx W, van de Kerkhof PC, Happle R, et al. Cryptic splicing at a non-consensus splice-donor in a patient with a novel mutation in the plakophilin-1 gene. *The Journal of investigative dermatology* 2004;122(5):1321-4.
- Steinert PM, Marekov LN. The proteins elafin, filaggrin, keratin intermediate filaments, loricrin, and small proline-rich proteins 1 and 2 are isodipeptide cross-linked components of the human epidermal cornified cell envelope. *The Journal of biological chemistry* 1995;270(30):17702-11.
- Stulke J. More than just activity control: phosphorylation may control all aspects of a protein's properties. *Molecular microbiology* 2010;77(2):273-5.
- Svitkin YV, Pause A, Haghighat A, Pyronnet S, Witherell G, Belsham GJ, et al. The requirement for eukaryotic initiation factor 4A (eIF4A) in translation is in direct proportion to the degree of mRNA 5' secondary structure. *Rna* 2001;7(3):382-94.
- Tanaka A, Lai-Cheong JE, Cafe ME, Gontijo B, Salomao PR, Pereira L, et al. Novel truncating mutations in PKP1 and DSP cause similar skin phenotypes in two Brazilian families. *The British journal of dermatology* 2009;160(3):692-7.
- Tian Q, Feetham MC, Tao WA, He XC, Li L, Aebersold R, et al. Proteomic analysis identifies that 14-3-3zeta interacts with beta-catenin and facilitates its activation by Akt. *Proceedings of the National Academy of Sciences of the United States of America* 2004;101(43):15370-5.
- Tokunaga E, Oki E, Egashira A, Sadanaga N, Morita M, Kakeji Y, et al. Deregulation of the Akt pathway in human cancer. *Current cancer drug targets* 2008;8(1):27-36.
- Tsao MC, Walthall BJ, Ham RG. Clonal growth of normal human epidermal keratinocytes in a defined medium. *Journal of cellular physiology* 1982;110(2):219-29.
- Valenta T, Hausmann G, Basler K. The many faces and functions of beta-catenin. *The EMBO journal* 2012;31(12):2714-36.
- Valladares-Ayerbes M, Diaz-Prado S, Reboredo M, Medina V, Lorenzo-Patino MJ, Iglesias-Diaz P, et al. Evaluation of plakophilin-3 mRNA as a biomarker for detection of circulating tumor cells in gastrointestinal cancer patients. *Cancer Epidemiol Biomarkers Prev* 2010;19(6):1432-40.
- van Hemert MJ, Steensma HY, van Heusden GP. 14-3-3 proteins: key regulators of cell division, signalling and apoptosis. *BioEssays : news and reviews in molecular, cellular and developmental biology* 2001;23(10):936-46.
- Vazquez-Osorio I, Chmel N, Rodriguez-Diaz E, Gonzalvo-Rodriguez P, Happle R, Bueno E, et al. A case of mosaicism in ectodermal dysplasia - skin fragility syndrome. *The British journal of dermatology* 2017.
- Villaret DB, Wang T, Dillon D, Xu J, Sivam D, Cheever MA, et al. Identification of genes overexpressed in head and neck squamous cell carcinoma using a combination of complementary DNA subtraction and microarray analysis. *The Laryngoscope* 2000;110(3 Pt 1):374-81.
- Vivanco I, Sawyers CL. The phosphatidylinositol 3-Kinase AKT pathway in human cancer. *Nature reviews Cancer* 2002;2(7):489-501.
- Wagner SA, Beli P, Weinert BT, Scholz C, Kelstrup CD, Young C, et al. Proteomic analyses reveal divergent ubiquitylation site patterns in murine tissues. *Molecular & cellular proteomics : MCP* 2012;11(12):1578-85.
- Wahl JK, 3rd. A role for plakophilin-1 in the initiation of desmosome assembly. *J Cell Biochem* 2005;96(2):390-403.
- Wallis S, Lloyd S, Wise I, Ireland G, Fleming TP, Garrod D. The alpha isoform of protein kinase C is involved in signaling the response of desmosomes to wounding in cultured epithelial cells. *Mol Biol Cell* 2000;11(3):1077-92.
- Waschke J, Spindler V, Bruggeman P, Zillikens D, Schmidt G, Drenckhahn D. Inhibition of Rho A activity causes pemphigus skin blistering. *The Journal of cell biology* 2006;175(5):721-7.

- Watt FM. Epidermal stem cells: markers, patterning and the control of stem cell fate. *Philosophical transactions of the Royal Society of London Series B, Biological sciences* 1998;353(1370):831-7.
- Weng LP, Smith WM, Brown JL, Eng C. PTEN inhibits insulin-stimulated MEK/MAPK activation and cell growth by blocking IRS-1 phosphorylation and IRS-1/Grb-2/Sos complex formation in a breast cancer model. *Human molecular genetics* 2001;10(6):605-16.
- Wheeler GN, Buxton RS, Parker AE, Arnemann J, Rees DA, King IA, et al. Desmosomal glycoproteins I, II and III: novel members of the cadherin superfamily. *Biochemical Society transactions* 1991;19(4):1060-4.
- White FH, Gohari K. Desmosomes in hamster cheek pouch epithelium: their quantitative characterization during epithelial differentiation. *Journal of cell science* 1984;66:411-29.
- Whitman SA, Cover C, Yu L, Nelson DL, Zarnescu DC, Gregorio CC. Desmoplakin and talin2 are novel mRNA targets of fragile X-related protein-1 in cardiac muscle. *Circ Res* 2011;109(3):262-71. doi: 10.1161/CIRCRESAHA.111.244244. Epub 2011 Jun 9.
- Whitlock NV, Bower C. Genetic evidence for a novel human desmosomal cadherin, desmoglein 4. *The Journal of investigative dermatology* 2003;120(4):523-30.
- Whitlock NV, Haftek M, Angoulvant N, Wolf F, Perrot H, Eady RA, et al. Genomic amplification of the human plakophilin 1 gene and detection of a new mutation in ectodermal dysplasia/skin fragility syndrome. *J Invest Dermatol* 2000;115(3):368-74.
- Wilker E, Yaffe MB. 14-3-3 Proteins--a focus on cancer and human disease. *Journal of molecular and cellular cardiology* 2004;37(3):633-42.
- Wolf A, Hatzfeld M. A role of plakophilins in the regulation of translation. *Cell cycle* 2010;9(15):2973-8.
- Wolf A, Keil R, Gotzl O, Mun A, Schwarze K, Lederer M, et al. The armadillo protein p0071 regulates Rho signalling during cytokinesis. *Nature cell biology* 2006;8(12):1432-40.
- Wolf A, Krause-Gruszczynska M, Birkenmeier O, Ostareck-Lederer A, Huttelmaier S, Hatzfeld M. Plakophilin 1 stimulates translation by promoting eIF4A1 activity. *The Journal of cell biology* 2010;188(4):463-71.
- Wolf A, Rietscher K, Glass M, Huttelmaier S, Schutkowski M, Ihling C, et al. Insulin signaling via Akt2 switches plakophilin 1 function from stabilizing cell adhesion to promoting cell proliferation. *Journal of cell science* 2013;126(Pt 8):1832-44.
- Xiao B, Smerdon SJ, Jones DH, Dodson GG, Soneji Y, Aitken A, et al. Structure of a 14-3-3 protein and implications for coordination of multiple signalling pathways. *Nature* 1995;376(6536):188-91.
- Xiao K, Garner J, Buckley KM, Vincent PA, Chiasson CM, Dejana E, et al. p120-Catenin regulates clathrin-dependent endocytosis of VE-cadherin. *Molecular biology of the cell* 2005;16(11):5141-51.
- Yaffe MB. How do 14-3-3 proteins work?-- Gatekeeper phosphorylation and the molecular anvil hypothesis. *FEBS letters* 2002;513(1):53-7.
- Yaffe MB, Rittinger K, Volinia S, Caron PR, Aitken A, Leffers H, et al. The structural basis for 14-3-3:phosphopeptide binding specificity. *Cell* 1997;91(7):961-71.
- Yang C, Strobel P, Marx A, Hofmann I. Plakophilin-associated RNA-binding proteins in prostate cancer and their implications in tumor progression and metastasis. *Virchows Archiv : an international journal of pathology* 2013;463(3):379-90.
- Yang H, Wen YY, Zhao R, Lin YL, Fournier K, Yang HY, et al. DNA damage-induced protein 14-3-3 sigma inhibits protein kinase B/Akt activation and suppresses Akt-activated cancer. *Cancer research* 2006;66(6):3096-105.
- Yap AS, Crampton MS, Hardin J. Making and breaking contacts: the cellular biology of cadherin regulation. *Current opinion in cell biology* 2007;19(5):508-14.

- Yi T, Zhai B, Yu Y, Kiyotsugu Y, Raschle T, Eitzkorn M, et al. Quantitative phosphoproteomic analysis reveals system-wide signaling pathways downstream of SDF-1/CXCR4 in breast cancer stem cells. *Proceedings of the National Academy of Sciences of the United States of America* 2014;111(21):E2182-90.
- Yin T, Getsios S, Caldelari R, Godsel LM, Kowalczyk AP, Muller EJ, et al. Mechanisms of plakoglobin-dependent adhesion: desmosome-specific functions in assembly and regulation by epidermal growth factor receptor. *J Biol Chem* 2005;280(48):40355-63. Epub 2005 Sep 23.
- Yin T, Green KJ. Regulation of desmosome assembly and adhesion. *Semin Cell Dev Biol* 2004;15(6):665-77.
- Yu C, Luo C, Qu B, Khudhair N, Gu X, Zang Y, et al. Molecular network including eIF1AX, RPS7, and 14-3-3gamma regulates protein translation and cell proliferation in bovine mammary epithelial cells. *Archives of biochemistry and biophysics* 2014;564:142-55.
- Zanivan S, Gnad F, Wickstrom SA, Geiger T, Macek B, Cox J, et al. Solid tumor proteome and phosphoproteome analysis by high resolution mass spectrometry. *Journal of proteome research* 2008;7(12):5314-26.
- Zen K, Babbin BA, Liu Y, Whelan JB, Nusrat A, Parkos CA. JAM-C is a component of desmosomes and a ligand for CD11b/CD18-mediated neutrophil transepithelial migration. *Molecular biology of the cell* 2004;15(8):3926-37.
- Zhai J, Lin H, Shamim M, Schlaepfer WW, Canete-Soler R. Identification of a novel interaction of 14-3-3 with p190RhoGEF. *The Journal of biological chemistry* 2001;276(44):41318-24.
- Zheng R, Bu DF, Zhu XJ. Compound heterozygosity for new splice site mutations in the plakophilin 1 gene (PKP1) in a Chinese case of ectodermal dysplasia-skin fragility syndrome. *Acta dermato-venereologica* 2005;85(5):394-9.
- Zisch AH, Pazzagli C, Freeman AL, Schneller M, Hadman M, Smith JW, et al. Replacing two conserved tyrosines of the EphB2 receptor with glutamic acid prevents binding of SH2 domains without abrogating kinase activity and biological responses. *Oncogene* 2000;19(2):177-87.

7 APPENDIX

7.1. Supplementary materials

7.1.1. Lab equipment

Table 8| Lab equipment.

Equipment	Manufacturer
BBD 6620 CO ₂ -incubator	Thermo Fisher Scientific; Waltham, Massachusetts, USA
Biometra® Standard Power Pack P25	Analytik Jena AG; Jena, Germany
Bio-Rad PowerPack 3000	Bio-Rad; Munich, Germany
Comfort NoFrost fridge-freezer	Liebherr; Bulle, Switzerland
Cryostat Leica CM3050 S	Wetzlar; Germany
Dry bath FB15103	Thermo Fisher Scientific; Waltham, Massachusetts, USA
Electrophoresis Power Supply Consort EV231	Sigma Aldrich; St. Louis, Missouri, USA
Electrophoresis Power Supply EC250-90	Savant Instruments , Inc./EC apparatus corporation; NY, USA
EPSON Perfection V600 Photo scanner	EPSON; Suwa, Japan
EVOS FL Cell Imaging System	Thermo Fisher Scientific; Waltham, Massachusetts, USA
Finn pipettes F2	Thermo Fisher Scientific; Waltham, Massachusetts, USA
Fridge profiline	Liebherr; Bulle, Switzerland
Fusion-SL - Chemiluminescence- and Fluorescence system (Imager)	Peqlab; Erlangen, Germany
GeneQuant 1300, Version 4281 V1.6.1 - Spectrophotometer	GE Healthcare; Munich, Germany
Heidolph Duomax 1030 – Rocking Shaker	Schütt Labortechnik GmbH; Göttingen, Germany
Heraeus Biofuge 28RS	Thermo Fisher Scientific; Waltham, Massachusetts, USA
Heraeus cytoperm 2 – CO ₂ -incubator	Thermo Fisher Scientific; Waltham, Massachusetts, USA
Heraeus Pico 17 - centrifuge	Thermo Fisher Scientific; Waltham, Massachusetts, USA
Hera Safe – Biological Safety Cabinet	Kendro; Langenselbold, Germany
Hettich Mikro 220R - centrifuge	Hettich GmbH & Co.KG; Tuttlingen, Germany
Hettich Universal 16 - centrifuge	Hettich GmbH & Co.KG; Tuttlingen, Germany
iCycler IQ5 Systems - qRT-PCR-System	Bio-Rad; Munich, Germany
Impuls Sealer	Burghardt Verpackungsmaschinen GmbH; Stuttgart, Germany
Incubator Shaker Series I26	Eppendorf; Hamburg, Germany
Incucell – incubator	MMM Medcenter Einrichtungen GmbH; Martinsried, Germany
LabSystems Multiscan RC microplate reader	Thermo Fisher Scientific; Waltham, Massachusetts, USA
Leica ASP200 S processor for paraffin infiltration of tissue	(AG Magin; University Leipzig); Leica; Wetzlar, Germany
Leica TCS SP5 microscope	(AG Hüttelmaier; Martin-Luther-University); Leica; Wetzlar, Germany

Equipment	Manufacturer
Leica EG1160 paraffin embedding center	(AG Magin; University Leipzig); Leica; Wetzlar, Germany
Liquid Nitrogen Sample Storage Tank Sanyo	EWALD Innovationstechnik GmbH; Bad Nenndorf, Germany
Liquid Nitrogen Storage Container	Cryotherm; Kirchen (Sieg), Germany
Magnetic stirrer	IKA; Staufen, Germany
Microtome	Leica; Wetzlar, Germany
Mini-PROTEAN-System – Electrophoresis chamber	Bio-Rad; Munich, Germany
MS1 small orbital shaker	IKA; Staufen, Germany
MultiCal pH 526 - pH-meter	WTW GmbH; Weilheim, Germany
Nikon Eclipse E600 - microscope	Nikon; Düsseldorf, Germany
PerfectBlue Semi-Dry blotter	Peqlab; Erlangen, Germany
Reax top test tube shaker	Heidolph Instruments; Schwabach, Germany
Rotilabo® mini-centrifuge	Carl Roth; Karlsruhe, Germany
SBC 51 – precision balance	Scaltec; Göttingen, Germany
SB3 Stuart – overhead rotator	Dunn Labortechnik GmbH; Asbach, Germany
Scotsman AF103 Ice Flaker	Scotsman Ice Systems; Milan, Italy
Shaking incubator 3032	GFL; Burgwedel, Germany
Sigma 2-16PK, Rotor 12151 und 12148 - refrigerated centrifuge	SIGMA Laborzentrifugen GmbH; Osterode am Harz, Germany
Sony Cyber Shot DSC-H300 camera	Sony; Tokyo, Japan
Stirrer Labinco L21	Labinco Beheer B.V.; Breda, Netherlands
Tewameter® TM 300	kindly provided by Prof. Dr. Niessen (CECAD, University of Cologne); Courage & Khazaka; Cologne, Germany
Thermocycler T3	Biometra; Göttingen, Germany
Thermomixer comfort	Eppendorf; Hamburg, Germany
Thermomixer HLC	Science Services GmbH; Munich, Germany
Ultramicrotome S	(Biozentrum; Halle, Wittenberg); Carl Zeiss, Jena, Germany
Ultra-Turrax T25 - Homogenizer	IKA; Staufen, Germany
UP 200S – Ultrasonic processor	Hielscher Ultrasonics GmbH; Teltow, Germany
UV table	bts Biotech Trade & Service GmbH; Kraichtal, Germany
Voltmeter	kindly provided by Dr. med. vet. Schreier (Julius-Bernstein-Institute for Physiology, Halle-Wittenberg); World Precision Instruments; Sarasota, FL, USA
Vortex-Genie 2	Scientific Industries; NY, USA
VWR® Power Source 250V	VWR; Radnor, Pennsylvania, USA
Water bath	Memmert; Shanghai, China
Wet blot equipment	Peqlab; Erlangen, Germany
Wilovert A – microscope	Leica; Wetzlar, Germany
Zeiss Axio Observer - microscope	Carl Zeiss; Jena, Germany
Zeiss Axioplan 2 - microscope	(AG Magin; University Leipzig);

Equipment	Manufacturer
	Carl Zeiss; Jena, Germany
Zeiss Libra 120 TEM	(Biozentrum; Halle, Wittenberg); Carl Zeiss; Jena, Germany
Zeiss TE LAVAL 31 – microscope	Carl Zeiss; Jena, Germany

7.1.2. Kits and ready-to-use reagents

Table 9| Kits and ready-to-use reagents.

Kit/reagent	Manufacturer
Anti-FLAG M2 affinity gel	Sigma Aldrich; St. Louis, Missouri, USA
Cell Proliferation BrdU	Roche; Basel, Switzerland
ChromoTek GFP-trap®	ChromoTek GmbH; Martinsried, Germany
DecaLabel DNA Labeling Kit	Thermo Fisher Scientific; Waltham, Massachusetts, USA
DPX Mountant	Sigma Aldrich; St. Louis, Missouri, USA
Jetquick Gel Extraction Spin Kit	Genomed; Löhne, Germany
Jetquick PCR Purification Kit	Genomed; Löhne, Germany
KAPA Mouse Genotyping Hot Start Kit	Peqlab; Erlangen, Germany
Lipofectamine® RNAiMax reagent	Thermo Fisher Scientific; Waltham, Massachusetts, USA
Mini DNA, RNA and protein purification NucleoSpin® Plasmid Kit	Macherey-Nagel GmbH; Berlin, Germany
DNA, RNA and protein purification Nucleo-Bond® XtraMidi Kit	Macherey-Nagel GmbH; Berlin, Germany
Pierce® BCA Protein Assay Kit	Life Technologies; Carlsbad, California, USA
Pierce® Glutathione Agarose	Thermo Fisher Scientific; Waltham, Massachusetts, USA
Polyfreeze Tissue Freezing Medium	Polyscience; Eppelheim, Germany
TOPO TA Cloning Kit	Thermo Fisher Scientific; Waltham, Massachusetts, USA
Trichrome Stain Kit	Abcam; Cambridge, UK
Xfect™ siRNA Transfection Reagent	Clontech; Mountain View, California, USA
Xfect™ Transfection Reagent	Clontech; Mountain View, California, USA

7.1.3. DNA and protein standards

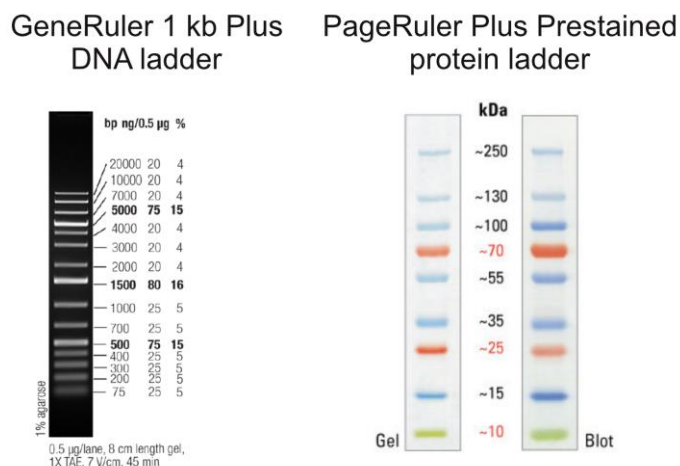


Fig. 52I DNA and protein standards.

For DNA gel electrophoresis the GeneRuler 1 kb Plus DNA ladder (Thermo Fisher Scientific; Waltham, Massachusetts, USA) was used. The PageRuler™ Plus Prestained protein ladder (Life Technologies; Carlsbad, California, USA) was used as protein standard for SDS-PAGE (standards are shown in Fig. 52).

7.1.4. Solutions

Table 10I Solutions and buffers.

Name	Composition
2 M CaCl ₂	29.4 g CaCl ₂ (x2 H ₂ O) in 100 ml autoclaved H ₂ O solved and sterile filtered (0.2 µM)
2x DNA precipitation buffer	280 mM NaCl; 10 mM KCl; 1.5 mM Na ₂ HPO ₄ (x2 H ₂ O); 12 mM glucose; 50 mM HEPES; pH 7.05 (filtered through 0.2 µm filter)
2x YT medium	10 g/l NaCl; 10 g/l yeast extract; 16 g/l tryptone
3.7% FA (formaldehyde)	400 ml aqua bidest was heated to 60°C and 18.5 g paraformaldehyde was added with stirring. 1 N sodium hydroxide was added dropwise until solution was cleared and cooled down to RT. 50 ml 10xPBS was added and pH was equilibrated to 7.3. Volume was filled up to 500 ml and 3.7% FA solution was aliquoted and stored at -20°C.
4x SDS loading buffer	250 mM Tris/HCl (pH 6.8); 8% (v/v) SDS; 10% (v/v) β-mercaptoethanol; 30% (v/v) glycerol; 0.25% (w/v) bromophenol blue
6x DNA loading buffer	0.25% (w/v) bromophenol blue; 40% (v/v) glycerol; 100 mM EDTA; 0.1% (v/v) SDS
10x Ponceau S	2% (w/v) Ponceau S; 30% (w/v) TCA; 30% (w/v) sulfosalicylic acid
20x SSC (Southern blot)	3.0 M NaCl; 0.3 M sodium citrate; pH 7.0
20x SSPE (Southern blot)	3.0 M NaCl; 0.2 M NaH ₂ PO ₄ ; 0.02 M EDTA; pH 7.4
100x Denhardt's solution	2% (w/v) Ficoll 400; 2% (w/v) polyvinylpyrrolidone; 2% (w/v) BSA
Blotting buffer I (WB)	0.3 M Tris/HCl (pH 10.4); 20% (v/v) methanol
Blotting buffer II (WB)	25 mM Tris/HCl (pH 10.4); 20% (v/v) methanol

Name	Composition
Blotting buffer III (WB)	25 mM Tris/HCl (pH 9.4); 40 mM ϵ -aminocaproic acid; 20% (v/v) methanol
Chemiluminescence solution 1	100 mM Tris/HCl (pH 8.5); 25 mM luminol; 0.4 mM coumaric acid
Chemiluminescence solution 2	100 mM Tris/HCl (pH 8.5); 0.02% (v/v) H ₂ O ₂
Citrate buffer for Ki-67 staining	0.1 M citric acid; 0.1 M trisodium citrate; pH 6.0
Coomassie staining solution	0.25% (w/v) Coomassie Brilliant Blue R250; 9.2% (v/v) acetic acid; 45% (v/v) methanol
Coomassie unstaining solution	7.5% (v/v) acetic acid; 5% (v/v) methanol
GET buffer	25 mM Tris/HCl (pH 8.0); 50 mM glucose; 10 mM EDTA
GFP-trap lysis buffer	10 mM Tris/HCl (pH 7.5); 150 mM NaCl; 0.5 mM EDTA; 0.5% (v/v) NP-40 (IPEGAL); protease/phosphatase inhibitors (fresh): 10 μ g/ml aprotinin; 10 μ g/ml leupeptin, 1 mM pefabloc; 1 mM DTT, 5 mM NaF, 1 mM NaVO ₃
GFP-trap washing buffer	10 mM Tris/HCl (pH 7.5); 150 mM NaCl; 0.5 mM EDTA
GST buffer	50 mM Tris/HCl (pH 7.5); 150 mM NaCl; 1 mM EDTA; 10% (v/v) glycerol; protease/phosphatase inhibitors (fresh): 10 μ g/ml aprotinin; 10 μ g/ml leupeptin, 1 mM pefabloc; 1 mM DTT, 5 mM NaF, 1 mM NaVO ₃
LB agar	10 g/l NaCl; 10 g/l tryptone; 5 g/l yeast extract; 20 g/l agar; pH 7.0
Hybridization buffer for Southern blot	6x SSPE; 1% (v/v) SDS; 5x Denhardt's solution; 10% (w/v) dextran sulfate; 50% formamide; 0.1 mg/ml denatured herring sperm
LB medium	10 g/l NaCl; 10 g/l tryptone; 5 g/l yeast extract; pH 7.0
IP buffer	20 mM Tris/HCl (pH 7.5); 137 mM NaCl; 2 mM EDTA; 10% (v/v) glycerol; 1% (v/v) NP-40 (IPEGAL); protease/phosphatase inhibitors (fresh): 10 μ g/ml aprotinin; 10 μ g/ml leupeptin, 1 mM pefabloc; 1 mM DTT, 5 mM NaF, 1 mM NaVO ₃
Mowiol	5% (w/v) Mowiol; 30% (v/v) glycerol; 0.25% (w/v) 1,4-diazabicyclo[2.2.2]octane (DABCO)
MT buffer (IF)	100 mM pipes (pH 6.9); 4 M glycerol; 2 mM EDTA; 1 mM EGTA; 0.5% (v/v) Triton X-100
Non-denaturing lysis buffer	20 mM Tris/HCl (pH 7.5); 140 mM NaCl, 10% (v/v) glycerol; 1.5% (v/v) Triton X-100, 2 mM EDTA; protease/phosphatase inhibitors (fresh): 10 μ g/ml aprotinin; 10 μ g/ml leupeptin, 1 mM pefabloc; 1 mM DTT, 5 mM NaF, 1 mM NaVO ₃
PBS	135 mM NaCl; 2.5 mM KCl; 10 mM Na ₂ HPO ₄ , 1 mM KH ₂ PO ₄ ; pH 7.4
PBSE	135 mM NaCl; 2.5 mM KCl; 10 mM Na ₂ HPO ₄ , 1 mM KH ₂ PO ₄ ; 0.5 mM EDTA; pH 7.4
SDS lysis buffer	20 mM Tris/HCl (pH 7.5); 1% (w/v) SDS; protease/phosphatase inhibitors (fresh): 10 μ g/ml aprotinin; 10 μ g/ml leupeptin, 1 mM pefabloc; 1 mM DTT, 5 mM NaF, 1 mM NaVO ₃
SDS running buffer	25 mM Tris/HCl; 19.2 mM glycine; 0.1% (v/v) SDS
Stripping buffer (WB)	0.2 M glycerol/HCl (pH 2.5); 0.05% (v/v) Tween20
TBE	445 mM Tris, 445 mM boronic acid; 10 mM EDTA
TBS	10 mM Tris/HCl (pH 7.6); 100 mM NaCl
TBST	10 mM Tris/HCl (pH 7.6); 100 mM NaCl; 0.1% (v/v) Tween20
TFB-I buffer	30 mM potassium acetate (pH 5.8), 50 mM MgCl ₂ , 100 mM KCl, 15% (v/v) glycerol

Name	Composition
TFB-II buffer	10 mM 3-(N-morpholino)-propanesulfonic acid (MOPS; pH 7.0); 10 mM KCl; 75 mM CaCl ₂ ; 15% (v/v) glycerol
Wet blot buffer	48 mM Tris/HCl; 39 mM glycerol; 0.0375% (v/v) SDS; pH 9.2

7.1.5. Oligonucleotides

The oligonucleotides were purchased from Eurofins MWG Operon (Ebersberg, Germany). A primer pair is consisting of a forward (for) and a reversed (rev) primer.

Oligonucleotides used for PKP1 KO mouse project

Table 11| Oligonucleotides used for genotyping and probe amplification.

Primer name	Sequence 5' → 3'
p1 (CDS-PKP1-F)	TCAGTGACTTCAGGTACAGCACAGG
p2 (CDS-PKP1-ttR)	CACAAGTCCATGCTCCACAAAGAGG
p3 (CDS-PKP1-R)	AACTCAAGTCCTGGTAGTCGAACCC
p4 (CDS-loxF)	GAGATGGCGCAACGCAATTAATG
p5 (CDS-neoF)	GGGATCTCATGCTGGAGTTCTTCG
probe_1 for	TTGAATTGCTTCTCGTCACCTAATCG
probe_1 rev	TTCTCGAGCCTGGGCATATGCATACAAC
probe_2 for	TTGAATTCCTCCTAGCTGCTTACCTAATTG
probe_2 rev	TTCTCGAGTGAGAAAGAGATTTCCACATTTTC

Oligonucleotides used for site-directed mutagenesis

The site-directed mutagenesis was used to exchange serine (S) or threonine (T) to alanine (A) or glutamate (E).

Table 12| Oligonucleotides used for site-directed mutagenesis.

Primer name	Sequence 5' → 3'
PKP1 mutant S_{54/56/57/59/60}T₆₁S_{63/65/69} → A	
PKP1 S _{54/56/57} for	CCGTC AAGCGGCAGAAGGCCAAGGCTGCCAGTCGTCCACCCTGAGCC
PKP1 S _{54/56/57} rev	GGCTCAGGGTGGACGACTGGGCAGCCTTGGCCTTCTGCCGCTTGACGG
PKP1 S _{54/56/57} S _{59/60} for	AGCGGCAGAAGGCCAAGGCTGCCAGGCGGCCACCCTGAGCCA
PKP1 S _{54/56/57} S _{59/60} rev	TGGCTCAGGGTGGCCGCTGGGCAGCCTTGGCCTCCTGCCGCT
PKP1 S _{56/57/59/60} T ₆₁ S ₆₃ for	GGCTGCCAGGCGCCGCGACTGGCACACTCCAATCGAGGTTCC
PKP1 S _{56/57/59/60} T ₆₁ S ₆₃ rev	GGAACCTCGATTGGAGTGTGCCAGTGCAGGCGCCTGGGCAGCC
PKP1 S ₆₀ T ₆₁ S ₆₃ S ₆₅ for	CGGCCGCACTGGCACACGCAAATCGAGGTTCCATGTATG
PKP1 S ₆₀ T ₆₁ S ₆₃ S ₆₅ rev	CATACATGGAACCTCGATTTGCGTGTGCCAGTGCAGGCGG
PKP1 S _{63/65} S ₆₉ for	CTGGCACACGCAAATCGAGGTGCAATGTATGATGGCTTGGCTGAC
PKP1 S _{63/65} S ₆₉ rev	GTCAGCCAAGCCATCATACATTGCACCTCGATTTGCGTGTGCCAG
PKP1 mutant S_{54/56/57/59/60}T₆₁S_{63/65/69} → E	
PKP1 S _{54/56/57} for	CCGTC AAGCGGCAGAAGGAAAAGGAAGAAGCAGTCGTCCACCCTGAGCC
PKP1 S _{54/56/57} rev	GGCTCAGGGTGGACGACTGTTCTTCTTTCTTCTTCTGCCGCTTGACGG
PKP1 S _{54/56/57} S _{59/60} for	CCGTC AAGCGGCAGAAGGAAAAGGAAGAAGCAGGAAGAAACCTGAGCCAC
PKP1 S _{54/56/57} S _{59/60} rev	GTGGCTCAGGGTTTCTTCTGTTCTTCTTTCTTCTTCTGCCGCTTGACGG
PKP1 S _{56/57/59/60} T ₆₁ S ₆₃ for	GGAAGAAGGAAGAAGCAGGAAGAAGAACTGGAACACTCCAATCGAGGTTCC
PKP1 S _{56/57/59/60} T ₆₁ S ₆₃ rev	GGAACCTCGATTGGAGTGTTCAGTTCTTCTTCTTCTTCTTCTTCC
PKP1 S ₆₀ T ₆₁ S ₆₃ S ₆₅ for	CAGGAAGAAGAACTGGAACACGAAAATCGAGGTTCCATGTATGATG

Primer name	Sequence 5' → 3'
PKP1 S ₆₀ T ₆₁ S ₆₃ S ₆₅ rev	CCATCATACATGGAACCTCGATTTTCGTGTTCCAGTTCTTCTTCCTG
PKP1 S _{63/65} S ₆₉ for	GAACTGGAACACGAAAATCGAGGTGAAATGTATGATGGCTTGGCTGAC
PKP1 S _{63/65} S ₆₉ rev	GTCAGCCAAGCCATCATACATTTACCTCGATTTTCGTGTTCCAGTTC
PKP1 mutant T₈₂S₈₄ → A	
PKP1 T ₈₂ S ₈₄ for	CTGACAATTACAACCTATGGGGCAACCGCAAGGAGCAGCTACTACTCCAAG
PKP1 T ₈₂ S ₈₄ rev	CTTGGAGTAGTAGCTGCTCCTTTCGGTTGCCCATAGTTGTAATTGTCAG
PKP1 mutant T₈₂S₈₄ → E	
PKP1 T ₈₂ S ₈₄ for	CTGACAATTACAACCTATGGGGAAACCGAAAGGAGCAGCTACTACTCCAAG
PKP1 T ₈₂ S ₈₄ rev	CTTGGAGTAGTAGCTGCTCCTTTCGGTTGCCCATAGTTGTAATTGTCAG
PKP1 mutant S_{118/119/121/127} → A	
PKP1 S _{118/119} for	GACAACAGGCGCTTCGCCGCTACAGCCAGATGGAG
PKP1 S _{118/119} rev	CTCCATCTGGCTGTAGGCGGCGAAGCGCCTGTTGTC
PKP1 S _{118/119} S ₁₂₁ for	CGCTTCGCCGCTACGCCAGATGGAGAACTGG
PKP1 S _{118/119} S ₁₂₁ rev	CCAGTTCTCCATCTGGGCGTAGGCGGCGAAGCG
PKP1 S _{118/119/121} S ₁₂₇ for	CAGATGGAGAACTGGGCGGCGACTACCCCCGG
PKP1 S _{118/119/121} S ₁₂₇ rev	CCGGGGGTAGTGCCGGGCCAGTTCTCCATCTG
PKP1 mutant S_{118/119/121/127} → E	
PKP1 S _{118/119} for	GACAACAGGCGCTTCGAGGAGTACAGCCAGATGGAG
PKP1 S _{118/119} rev	CTCCATCTGGCTGTACTCCTCGAAGCGCCTGTTGTC
PKP1 S _{118/119} S ₁₂₁ for	CGCTTCGAGGAGTACGAGCAGATGGAGAACTGG
PKP1 S _{118/119} S ₁₂₁ rev	CCAGTTCTCCATCTGCTCGTACTCCTCGAAGCG
PKP1 S _{118/119/121} S ₁₂₇ for	CAGATGGAGAACTGGGAGCGGCGACTACCCCCGG
PKP1 S _{118/119/121} S ₁₂₇ rev	CCGGGGGTAGTGCCGCTCCAGTTCTCCATCTG
PKP1 mutant S₁₅₅ → A	
PKP1 S ₁₅₅ for	CGAGCCCGACGGTGGTGCAGGGCAGGGG
PKP1 S ₁₅₅ rev	GCGCGGCTCGCAAAGTTCAAAGAAACACTAGCAATTTATTGATTTTCTCT- ATTTCCAAAAAAGC
PKP1 mutant T_{166/171}S₁₇₄T_{179/180}S_{185/188}T₁₈₉S₁₉₁ → A	
PKP1 T ₁₆₆ for	CTACTGTGACCCACGGGGCGCACTGCGCAAGGGCAGCGTG
PKP1 T ₁₆₆ rev	CAGCGTGCCCTTGCAGTTCGCCCCGTGGGTCACAGTAG
PKP1 T ₁₆₆ T ₁₇₁ S ₁₇₄ for	GGCGCACTGCGCAAGGGCGCACTGGGCGCAAAGGGCCAGAAGACCACC
PKP1 T ₁₆₆ T ₁₇₁ S ₁₇₄ rev	GGTGGTCTTCTGGCCCTTTGCGCCAGTGCCTTTCGCGAGTGCGCC
PKP1 S ₁₇₄ T _{179/180} for	GGCGCAAAGGGCCAGAAGGCAGCACAGAACCGCTACAGCTTTTAC
PKP1 S ₁₇₄ T _{179/180} rev	GTAAGAGCTGTAGCGGTTCTGTGCTGCCTTCTGGCCCTTTGCGCC
PKP1 T _{179/180} S ₁₈₅ for	GGCAGCACAGAACCCTACGCATTTTACAGCACCTGCAGTGG
PKP1 T _{179/180} S ₁₈₅ rev	CCACTGCAGGTGCTGTAAGATGCGTAGCGGTTCTGTGCTGCC
PKP1 S ₁₈₅ S ₁₈₈ T ₁₈₉ for	CAGAACCCTACGCATTTTACGCAGCATGCAGTGGTTCAGAAGGCC
PKP1 S ₁₈₅ S ₁₈₈ T ₁₈₉ rev	GGCCTTCTGACCACTGCATGCTGCGTAAAGTGCAGTGGTTCAG
PKP1 S _{185/188} T ₁₈₉ S ₁₉₁ for	GCTACGCATTTTACGCAGCATGCGCAGGTTCAGAAGGCCATAAAGAAG
PKP1 S _{185/188} T ₁₈₉ S ₁₉₁ rev	CCTTCTTTATGGCCTTCTGACCTGCGCATGCTGCGTAAAGTGCAGTGG
PKP1 mutant T_{166/171}S₁₇₄T_{179/180}S_{185/188}T₁₈₉S₁₉₁ → E	
PKP1 T ₁₆₆ for	CTACTGTGACCCACGGGGCGAACTGCGCAAGGGCAGCGTG
PKP1 T ₁₆₆ rev	CAGCGTGCCCTTGCAGTTCGCCCCGTGGGTCACAGTAG
PKP1 T ₁₆₆ T ₁₇₁ S ₁₇₄ for	GGCGAACTGCGCAAGGGCGAACTGGGCGAAAAGGGCCAGAAGACCACC
PKP1 T ₁₆₆ T ₁₇₁ S ₁₇₄ rev	GGTGGTCTTCTGGCCCTTTTCGCCAGTTCGCCCTTTCGCGAGTTCGCC
PKP1 S ₁₇₄ T _{179/180} for	GGCGAAAAGGGCCAGAAGGAAGAACAAGAACCGCTACAGCTTTTAC
PKP1 S ₁₇₄ T _{179/180} rev	GTAAGAGCTGTAGCGGTTCTGTTCTTCTTCTGGCCCTTTTCGCC
PKP1 T _{179/180} S ₁₈₅ for	GAAGGAAGAACAAGAACCGCTACGAATTTTACAGCACCTGCAGTGG

Primer name	Sequence 5' → 3'
PKP1 T _{179/180} S ₁₈₅ rev	CCACTGCAGGTGCTGTAAAATTCGTAGCGGTTCTGTTCTTCCTTC
PKP1 S ₁₈₅ S ₁₈₈ T ₁₈₉ for	GAACAGAACCGCTACGAATTTTACGAAGAATGCAGTGGTCAGAAGGCC
PKP1 S ₁₈₅ S ₁₈₈ T ₁₈₉ rev	GGCCTTCTGACCACTGCATTCTTCGTAAAATTCGTAGCGGTTCTGTTC
PKP1 S _{185/188} T ₁₈₉ S ₁₉₁ for	CTACTGTGACCCACGGGGCGAACTGCGCAAGGGCACGCTG
PKP1 S _{185/188} T ₁₈₉ S ₁₉₁ rev	CAGCGTGCCCTTGCGCAGTTCGCCCCGTGGGTCACAGTAG
PKP3 mutant S₂₈₅ → A	
PKP3 S ₂₈₅ for	CCTCAGCATTCGGCCATGGAGTCCTG
PKP3 S ₂₈₅ rev	GCGAGGCTCTGGGCCAGGAAGTCCT

Oligonucleotides used for cloning

The underlined sequences mark the recognition sequence of the particular restriction endonuclease.

Table 13| Oligonucleotides used for cloning.

Primer name	Sequence 5' → 3'
14-3-3 γ EcoRI for	AAA <u>GAA TTC</u> GCC ATG GTG GAC CGC GAG CAA C
14-3-3 γ +Stop Sall rev	TTT <u>GTC GAC</u> TTA ATT GTT GCC TTC GCC GCC
14-3-3 σ EcoRI for	AAA <u>GAA TTC</u> GCC ATG GAG AGA GCC AGT CTG ATC C
14-3-3 σ +Stop Sall rev	TTT <u>GTC GAC</u> TCA GCT CTG GGG CTC CTG G
14-3-3 η EcoRI for	AAA <u>GAA TTC</u> GCC ATG GGG GAC CGG GAG CAG
14-3-3 η +Stop Sall rev	TTT <u>GTC GAC</u> TCA GTT GCC TTC TCC TGC TTC TTC
14-3-3 ϵ EcoRI for	AAA <u>GAA TTC</u> GCC ATG GAT GAT CGA GAG GAT CTG G
14-3-3 ϵ +Stop Sall rev	TTT <u>GTC GAC</u> TCA CTG ATT TTC GTC TTC CAC GTC
14-3-3 β EcoRI for	AAA <u>GAA TTC</u> GCC ATG ACA ATG GAT AAA AGT GAG CTG G
14-3-3 β +Stop Sall rev	TTT <u>GTC GAC</u> TTA GTT CTC TCC CTC CCC AGC
14-3-3 ζ EcoRI for	AAA <u>GAA TTC</u> GCC ATG GAT AAA AAT GAG CTG GTT CAG AAG
14-3-3 ζ +Stop Sall rev	TTT <u>GTC GAC</u> TTA ATT TTC CCC TCC TTC TCC TGC
14-3-3 τ EcoRI for	TTT <u>GAA TCC</u> GCC ATG GAG AAG ACT GAG CTG ATC
14-3-3 τ +Stop rev	TTT <u>GTC GAC</u> TTA GTT TTC AGC CCC TTC TGC CGC

7.1.6. Antibodies

The listed monoclonal (mAb) and polyclonal (pAb) antibodies were used as shown for immunofluorescence (IF) analysis and Western blot [(WB), Table 14]. For WB analysis the antibodies were diluted in 5% (w/v) skimmed milk/TBST (m) or 3% (w/v) BSA/TBST (b). For IF analysis the antibodies were diluted in 1% (w/v) skimmed milk/PBS (m) or 1% (w/v) BSA/PBS (b).

Table 14| Primary antibodies.

Antibody	Source	Species / type	Clone/antigen	WB	IF
14-3-3 pan	Cell signaling	rabbit pAb	#8312	1:1,000 (b)	-
14-3-3 β	Cell signaling	rabbit pAb	#9636	1:500 (b)	-
14-3-3 γ	Cell signaling	rabbit mAb	D15B7	1:500 (b)	-
14-3-3 γ	Invitrogen	mouse mAb	HS23		1:250 (m)
14-3-3 ϵ	Cell signaling	rabbit pAb	#9635	1:500 (b)	-
14-3-3 ζ	Cell signaling	rabbit mAb	D7H5	1:500 (b)	-
14-3-3 η	Cell signaling	rabbit mAb	D23B7	1:500 (b)	-

APPENDIX

Antibody	Source	Species / type	Clone/antigen	WB	IF
14-3-3 σ	Santa Cruz	goat pAb	C-18	1:500 (m)	1:250 (m)
14-3-3 τ	Cell signaling	rabbit pAb	#9638	1:500 (b)	-
BrdU	Sigma	mouse mAb	BU-33	-	1:250 (b)
CLDN1	Invitrogen	mouse mAb	2H10D10	1:250 (m)	-
CLDN1	Niessen lab	rabbit pAb	-	-	1:1,000 (b)
CLDN4	Invitrogen	rabbit pAb	catalogue number: PA5-34437	1:1,000 (m)	1:500 (b)
DSC2	Progen	rabbit pAb	catalogue number: 610120	1:1,000 (m)	1:500 (m)
DSC2/3	Invitrogen	mouse mAb	7G6	-	1:100 (m)
DSG1/2	Progen	mouse mAb	DG 3.10	1:500 (m)	1:500 (m)
DSP	Hatzfeld lab	rabbit pAb	bovine snout DSP	1:2,000 (m)	1:1,000 (m)
E-cadherin	Transduction	mouse mAb	36	1:1,000 (m)	1:1,000 (m)
FLAG	Sigma	mouse mAb	M2	1:1,000 (m)	1:500 (m)
FLG	Santa Cruz	rabbit pAb	M-290	1:2,000 (m)	1:1,000 (b)
GFP	Rockland	rabbit pAb	600-401-215	1:1,000 (m)	1:1,000 (m)
GST	BD Pharmingen™	mouse mAb	G172-1138	1:2,000 (m)	-
HA	Sigma	Mouse mAb	HA-7		1:500 (m)
involucrin	Biozol	rabbit pAb	Poly19244	1:200,000 (m)	1:1,000 (b)
Ki-67	eBioscience	rat mAb	SolA15	-	1:100 (b)
Krt1	Magin lab (PSL, customized peptide-specific antibodies)	rabbit pAb	VKfVSTSYSRGTK	1:20,000 (m)	1:400 (b)
Krt14	Magin lab (PSL, customized peptide-specific antibodies)	rabbit pAb	KVSTHEQVLRTKN	1:20,000 (m)	1:1,000 (b)
Krt17	Magin lab (PSL, customized peptide-specific antibodies)	rabbit pAb	recombinant C-term. fragment	1:20,000 (m)	1:500 (b)
Krt5	Magin lab (PSL, customized peptide-specific antibodies)	guinea pig pAb	SGSSVKFVSTTSSRRSFKS	1.20,000 (m)	1:200 (b)
loricrin	Biozol	rabbit pAb	Poly19051	1:200,000 (m)	1:1,000 (b)
OCLN	Invitrogen	mouse mAb	OC-3F10	1:200 (m)	1:500 (b)
p120ctn	Transduction	mouse mAb	98	1:1,000 (m)	1:500 (m)
P-Akt	Cell signaling	rabbit pAb	#9271	1:500 (b)	-
P-cadherin	Invitrogen	rat mAb	PCD-1	1:500 (m)	1:500 (m)
P-eIF4B	Cell signaling	rabbit pAb	#3591	1:500 (b)	-
PG	Sigma	mouse mAb	15F11	1:250 (m)	-
PKP1 (N-term.)	Santa Cruz	mouse mAb	10B2	1:500 (m)	1:100 (m)
PKP1 (C-term.)	Hatzfeld lab (PSL, customized peptide-specific antibodies)	guinea pig pAb	PQIARLLQSGNSDVVR, QGVLRRQQGFDRNM	1:5,000 (m)	-
PKP1 (repeats)	Hatzfeld lab	rabbit pAb	recombinant PKP1 repeat domain	1:4,000 (m)	-
PKP2 (a+b)	Progen	mouse mAb	PP2/62	1:500 (m)	-
PKP3	Santa Cruz	mouse mAb	23E3/4	1:500 (m)	-
PKP3 (N-term.)	Hatzfeld lab (PSL, customized peptide-specific antibodies)	guinea pig pAb	GGAQTPPPMPTRPVSFHER	-	1:4,000 (m)
P-PKA substrate	Cell signaling	rabbit pAb	100G7E	1:500 (b)	-
vinculin	Sigma	mouse mAb	hVIN-1	1:1,000 (m)	-
ZO-1	Invitrogen	rabbit pAb	Mid	1:1,000 (m)	1:500 (m)

Antibody	Source	Species / type	Clone/antigen	WB	IF
α -tubulin	Sigma	mouse mAb	DM1A	1:2,000 (m)	1:1,000 (m)
β -catenin	Transduction	mouse mAb	14	1:1,000 (m)	1:500 (m)

The fluorophore-conjugated secondary antibodies were used for IF analysis and the HRP-conjugated antibodies for WB (Table 15).

Table 15| Secondary antibodies.

Antibody	Source	Species / type	Dilution (WB/IF)
anti-mouse Cy3	Dianova	donkey polyclonal	1:250 (IF cells) 1:800 (IF skin)
anti-guinea pig Cy3	Dianova	donkey polyclonal	
anti-guinea pig Alexa 488	Dianova	donkey polyclonal	
anti-rabbit Alexa 488	Dianova	donkey polyclonal	
anti-rabbit DyLight 594	Dianova	donkey polyclonal	
anti-rabbit Cy3	Dianova	donkey polyclonal	
anti-rat Cy3	Dianova	donkey polyclonal	
anti-goat Cy3	Dianova	donkey polyclonal	1:20,000 (WB)
anti-guinea pig HRP	Dianova	donkey polyclonal	
anti-mouse HRP	Dianova	donkey polyclonal	
anti-rabbit HRP	Dianova	donkey polyclonal	
anti-rat HRP	Dianova	donkey polyclonal	
anti-goat HRP	Dianova	donkey polyclonal	

7.1.7. Cell lines

Table 16| Cell lines.

Cell line	Description	Source
HEK293	human embryonic kidney cells	(Graham et al., 1977)
HaCaT	spontaneously transformed human keratinocytes	(Boukamp et al., 1988)
MCF-7	human mamma adenocarcinoma cells	(Soule et al., 1973)
MCF-7 DsRed	generated by transfection of MCF-7 cells, single cell cloning and G418 selection	generated by Dr. A. Wolf & K. Rietscher (Hatzfeld lab)
MCF-7 PKP1 WT-DsRed	generated by transfection of MCF-7 cells, single cell cloning and G418 selection	generated by Dr. A. Wolf & K. Rietscher (Hatzfeld lab)
MCF-7 PKP1M1-4A-DsRed	generated by transfection of MCF-7 cells, single cell cloning and G418 selection	generated by Dr. A. Wolf & K. Rietscher (Hatzfeld lab)
MCF-7 PKP1M1-4E-DsRed	generated by transfection of MCF-7 cells, single cell cloning and G418 selection	generated by Dr. A. Wolf & K. Rietscher (Hatzfeld lab)
WT MKC	spontaneously immortalized murine keratinocytes derived from PKP1 ^{+/+} mice	generated by Dr. A. Wolf & K. Rietscher (Hatzfeld lab)
PKP1-KO MKC	spontaneously immortalized murine keratinocytes derived from PKP1 ^{-/-} mice	generated by Dr. A. Wolf & K. Rietscher (Hatzfeld lab)
PKP1-KO + GFP MKC	generated by lentiviral transduction of PKP1-KO MKC and puromycin selection	generated by Dr. R. Keil (Hatzfeld lab)
PKP1-KO + hPKP1-GFP MKC (1+1)	generated by lentiviral transduction of PKP1-KO MKC and puromycin selection	generated by Dr. R. Keil (Hatzfeld lab)

Cell line	Description	Source
PKP1-KO + hPKP3-GFP MKC (1+3)	generated by lentiviral transduction of PKP1-KO MKC and puromycin selection	generated by Dr. R. Keil (Hatzfeld lab)
PKP3-KO + hPKP3-GFP MKC (3+3)	generated by lentiviral transduction of PKP3-KO MKC and puromycin selection	generated by Dr. R. Keil (Hatzfeld lab)
GFP MKC	generated by lentiviral transduction of WT MKC and puromycin selection	generated by K. Rietscher (Hatzfeld lab)
GFP-14-3-3 γ MKC	generated by lentiviral transduction of WT MKC and puromycin selection	generated by K. Rietscher (Hatzfeld lab)
GFP-14-3-3 σ MKC	generated by lentiviral transduction of WT MKC and puromycin selection	generated by K. Rietscher (Hatzfeld lab)

7.1.8. Plasmids

The listed plasmids were transformed in *E. coli* strain BL21(DE3) (see 0) to express the corresponding protein shown in Table 17. The source of plasmids not generated in this study is shown in brackets.

Table 17| Plasmids for bacterial expression.

Name	Expressed protein	Source or restriction enzymes
pGEX-5x-1	GST	BD Bioscience (Heidelberg, Germany)
pGEX-14-3-3 γ	GST-14-3-3 γ	BD Bioscience (Heidelberg, Germany)
pGEX-14-3-3 σ	GST-14-3-3 σ	EcoRI/Sall
pGEX-14-3-3 η	GST-14-3-3 η	EcoRI/Sall
pGEX-14-3-3 ϵ	GST-14-3-3 ϵ	EcoRI/Sall
pGEX-14-3-3 β	GST-14-3-3 β	EcoRI/Sall
pGEX-14-3-3 ζ	GST-14-3-3 ζ	EcoRI/Sall
pGEX-14-3-3 τ	GST-14-3-3 τ	EcoRI/Sall in XhoI

Table 18| Plasmids for expression in cell lines.

Name	Expressed protein	Vector	Source or restriction enzymes
pMD2.G	VSV-G-expressing envelope plasmid	pMD2.G	Addgene
psPAX2	Gag, Pol, Rev and Tat	psPAX2	Addgene
pCherry-C1	Cherry	pCherry-C1	Takara Bio Inc.
pEGFP-C2	EGFP	pEGFP-C2	BD Bioscience (Heidelberg, Germany)
pDsRed-N1	DsRed	pDsRed-N1	BD Bioscience (Heidelberg, Germany)
pVen1-FLAG-C2	Ven1-FLAG	pVen1-FLAG-C2	Hüttelmaier lab
pVen2-HA-C2	Ven2-HA	pVen2-HA-C2	Hüttelmaier lab
hPKP1-pEGFP	PKP1-GFP	pLVX-IRES-puro containing EGFP ORF	EcoRI/XhoI by Dr. R. Keil (Hatzfeld lab)
hPKP3-pEGFP	PKP3-GFP	pLVX-IRES-puro containing EGFP ORF	EcoRI / Sall in XhoI by Dr. R. Keil (Hatzfeld lab)
PKP1-WT-pEGFP-C2	GFP-PKP1-WT	pEGFR-C2	EcoRI/XhoI in Sall

Name	Expressed protein	Vector	Source or restriction enzymes
PKP1M1-4A-pEGFP-C2	GFP-PKP1M1-4A	pEGFR-C2	EcoRI/XhoI in Sall
PKP1M1-4E-pEGFP-C2	GFP-PKP1M1-4E	pEGFP-C2	EcoRI/XhoI in Sall
14-3-3 γ -pEGFP-C2	GFP-14-3-3 γ	pEGFR-C2	EcoRI/XhoI in Sall
14-3-3 σ -pEGFP-C2	GFP-14-3-3 σ	pEGFR-C2	EcoRI/XhoI in Sall
14-3-3 γ -pLVX-EGFP-C2	GFP-14-3-3 γ	pLVX-EGFP-C2	EcoRI/Sall in XhoI
14-3-3 σ -pLVX-EGFP-C2	GFP-14-3-3 σ	pLVX-EGFP-C2	EcoRI/Sall in XhoI
PKP1-WT-pDsRed-N1	PKP1-WT-DsRed	pDsRed-N1	EcoRI/XhoI in Sall
PKP1M1A-pDsRed-N1	PKP1M1A-DsRed	pDsRed-N1	EcoRI/XhoI in Sall
PKP1M1E-pDsRed-N1	PKP1M1E-DsRed	pDsRed-N1	EcoRI/XhoI in Sall
PKP1M2A-pDsRed-N1	PKP1M2A-DsRed	pDsRed-N1	EcoRI/XhoI in Sall
PKP1M2E-pDsRed-N1	PKP1M2E-DsRed	pDsRed-N1	EcoRI/XhoI in Sall
PKP1M3A-pDsRed-N1	PKP1M3A-DsRed	pDsRed-N1	EcoRI/XhoI in Sall
PKP1M3E-pDsRed-N1	PKP1M3E-DsRed	pDsRed-N1	EcoRI/XhoI in Sall
PKP1M4A-pDsRed-N1	PKP1M4A-DsRed	pDsRed-N1	EcoRI/XhoI in Sall
PKP1M4E-pDsRed-N1	PKP1M4E-DsRed	pDsRed-N1	EcoRI/XhoI in Sall
PKP1M1-4A-pDsRed-N1	PKP1M1-4A-DsRed	pDsRed-N1	EcoRI/XhoI in Sall
PKP1M1-4E-pDsRed-N1	PKP1M1-4E-DsRed	pDsRed-N1	EcoRI/XhoI in Sall
pcDNA3	-	pcDNA3	Addgene
myr-HA-Akt2 (da)	myr-HA-Akt2	pcDNA3	Addgene
pVen2-HA-Akt2dn (K181M/T309A/S474A)	Ven2-HA-Akt2dn	pVen2-HA-C2	EcoRI/XhoI in Sall
pVen1-FLAG-PKP1-WT	Ven1-FLAG-PKP1-WT	pVen1-FLAG-C2	EcoRI/XhoI in Sall
pVen1-FLAG-PKP1 S54/56/57/59/60A	Ven1-FLAG-PKP1 S54/56/57/59/60A	pVen1-FLAG-C2	EcoRI/XhoI in Sall
pVen1-FLAG-PKP1M3A	Ven1-FLAG-PKP1M3A	pVen1-FLAG-C2	EcoRI/XhoI in Sall
pVen1-FLAG-PKP1 S153/155A	Ven1-FLAG-PKP1 S153/155A	pVen1-FLAG-C2	EcoRI / Sall in XhoI
pVen1-FLAG-PKP1M4A	Ven1-FLAG-PKP1M4A	pVen1-FLAG-C2	EcoRI/XhoI in Sall
pVen1-FLAG-PKP3-WT	Ven1-FLAG-PKP3-WT	pVen1-FLAG-C2	EcoRI/XhoI in Sall
pVen1-FLAG-PKP3 S285A	Ven1-FLAG-PKP3 S285A	pVen1-FLAG-C2	EcoRI/XhoI in Sall
pVen2-HA-14-3-3 γ	Ven2-HA-14-3-3 γ	pVen2-HA-C2	EcoRI/XhoI in Sall
pVen2-HA-14-3-3 σ	Ven2-HA-14-3-3 σ	pVen2-HA-C2	EcoRI/XhoI in Sall
14-3-3 γ -pCherry	14-3-3 γ -Cherry	pCherry-C1	EcoRI/Sall
14-3-3 σ -pCherry	14-3-3 σ -Cherry	pCherry-C1	EcoRI/Sall

7.1.9. siRNAs

Table 19| siRNAs.

Name	Repressed gene product	Source
siControl pool	no repressed gene (scrambled control)	siTools Biotech GmbH (Martinsried, Germany)
si14-3-3 γ pool	14-3-3 γ	
si14-3-3 σ pool	14-3-3 σ	

7.1.10. *E. coli* strains

The strain BL21(DE3) was used for the expression of proteins and the strain JM109 was used for cloning (Table 11). The strains were grown standardly in LB medium (Bertani, 1951). To select recombinant clones, the medium was supplemented with 50 μ g/ml kanamycin or 100 μ g/ml ampicillin according to the antibiotic resistance.

Table 20| *E. coli* strains.

Strain	Genotype	Source
BL21(DE3)	<i>F⁻ ompT, hsdSB (r_B, m_B), gal(λclts857 ind1, Sam7, nin5, lacUV5-T7gene1), dcm (DE3)</i>	Stratagene, Ja Jolla, Kalifornien, USA
JM109	<i>e14-(McrA⁻) recA1 endA1 gyrA96 thi-1 hsdR17 (r_K⁻ m_K⁺) supE44 relA1 Δ(lac-proAB) [F' traD36 proAB lacI^qZΔM15]</i>	Stratagene, Ja Jolla, Kalifornien, USA

7.2. Supplementary tables and figures

Table 21| Mutations within PKP1 causing EDSFS and clinical features.

Mutation analyses	Phenotype	Reference
patient compound heterozygote (paternal Q304X within first repeat domain and maternal frameshift mutation 1132ins28 within third repeat domain)	cutaneous fragility, congenital ectodermal dysplasia affecting skin, hair, and nails, growth retardation, astigmatism, small and poorly formed desmosomes with reduced connections to keratins	(McGrath et al., 1997)
patient compound heterozygote (paternal acceptor splice site mutation 203-1G>A and maternal T>G transversion leading to Y71X occurring within N-terminal head domain of PKP1)	trauma-induced skin fragility, congenital ectodermal dysplasia affecting hair, nails and sweat glands, poor weight gain, widening of intercellular spaces between keratinocytes, small and poorly formed desmosomes with reduced connections to keratin	(McGrath et al., 1999)
patient homozygote 1233-2A>T (A>T substitution at the acceptor -2 splice site of intron 6)	skin erosions, dystrophic nails, sparse hair, painful thickening and cracking of palms and soles, mild pruritus, small desmosomes	(Whittock et al., 2000)
patient homozygote 2021+1 G>A (donor splice site mutations in intron 11 occurring within arm repeat domain; but low levels of full-length <i>PKP1</i> transcript elucidated)	mild phenotype with normal skin at birth, loss of scalp hair at 3 months after febrile illness, progressive nail dystrophy during infancy, palmoplantar keratoderma around age 18, trauma-induced skin fragility and blisters from age 20, dental caries, reduced number of hyperplastic desmosomes	(Hamada et al., 2002)
<u>case 1:</u> patient homozygote 847-2A>G (acceptor splice site mutations of intron 4) <u>case 2:</u> patient homozygote 203-1G>A (acceptor splice site mutations of intron 1)	<u>case 1:</u> superficial blisters after birth, prominent nail dystrophy and severe hypotrichosis, intraepidermal separation, widening of intercellular spaces, abnormal desmosome ultrastructure <u>case 2:</u> general erythroderma and skin blisters, nail dystrophy, episodes of pneumonia and sepsis, failure to thrive, palmoplantar keratoderma	(Sprecher et al., 2004)
patient homozygote 1680+1G>A, IVS9+1G>A (G to A transition in the splice donor site of exon 9, expression of a shortened, but partially functional PKP1)	extreme plantar hyperkeratosis, sharply demarcated, oozing erythematous lesions, no blistering, subungual follicular hyperkeratosis, acantholysis, recurrent skin infections	(Steijlen et al., 2004)
patient compound heterozygote, (paternal splice mutation 1835-2A>G near the acceptor end of intron 10 and maternal splice site mutation 1053 T>A + 1054+1 G>T near the 3' end of exon 5 and at the	hyperkeratosis, acantholysis and widening of intercellular spaces in the epidermis, loss of close contact between keratinocytes, decrease in number and size of desmosomes	(Zheng et al., 2005)

Mutation analyses	Phenotype	Reference
donor end of intron 5 on one allele)		
patient homozygote 888delC (frameshift mutation within exon 5)	red skin at birth, skin fragility, progressive plantar keratoderma, nail dystrophy, alopecia, widening of intercellular spaces in the epidermis, reduced number of small, poorly desmosomes	(Ersoy-Evans et al., 2006)
patient homozygote p.R672X (nonsense mutation)	growth retardation, skin blisters, cheilitis, sparse scalp hair, thickening of fingernails, trauma-induced skin erosions, hyperkeratosis of the palms and soles	(Tanaka et al., 2009)
not reported	palmoplantar hyperkeratosis with fissuring, short and sparse scalp hair, nail dystrophy, multiple erosions over the skin, epidermal hyperplasia with widening of intercellular space	(Adhe et al., 2011)
patient homozygote c.897del5 (frame shift mutation due to 5 base pair deletion in exon 5)	neonatal bullae, dystrophic nails, woolly scalp hair, abnormal dental development, desquamating erythematous rash at sites of trauma, suprabasal intraepidermal clefting	(Boyce et al., 2012)
patient homozygote 1223-2A>G (frame shift mutation leading to deletion of exon 7 and premature stop codon)	skin fragility, palmoplantar hyperkeratosis, onychodystrophy, perioral fissuring, noncicatricial alopecia	(Hernandez-Martin et al., 2013)
patient homozygote c.203-1G>T (G>T transversion at nucleotide position c.203-1 within intron 1)	neonatal normal skin, nail dystrophy, scanty abnormal hair, skin blistering, trauma-induced fragile skin, hyperkeratosis of palms and soles, dysplastic dentition, frequent chest infections	(Abdalla and Has, 2014)
not reported	neonatal normal skin, later skin fragility, hair and nail deformities, abnormal dentition, palmoplantar keratoderma, abnormal sweating	(Kashyap et al., 2015)
patient homozygote IVS8-9G>A (single nucleotide transition within intron 8)	trauma-induced skin fragility, cheilitis with perioral fissuring, hypotrichosis and scalp erosions, absence of axillary hair, scattered blisters, erosions and crusts over the face and limbs, subungual hyperkeratosis, plantar keratoderma with fissuring, hyperkeratosis, acanthosis, dissociation between keratinocytes	(Hsu et al., 2016)
patient homozygote c.638delT (heterozygous mutation in exon 3 (c.638delT) in a heterozygous state in the patient's normal skin and blood, and in the father's blood, and homozygous state in patient's affected skin; mosaicism)	unilateral superficial erosions, plantar keratoderma, nail dystrophy, a Blaschko-linear arrangement	(Vazquez-Osorio et al., 2017)

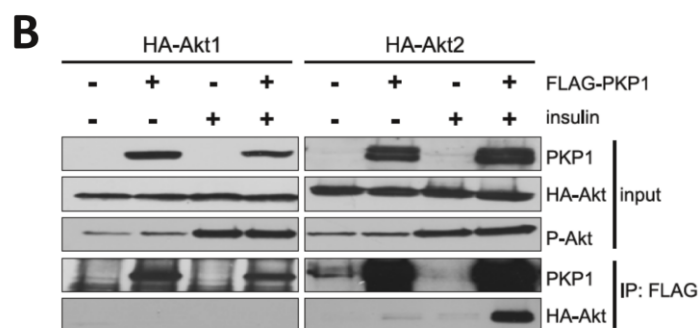
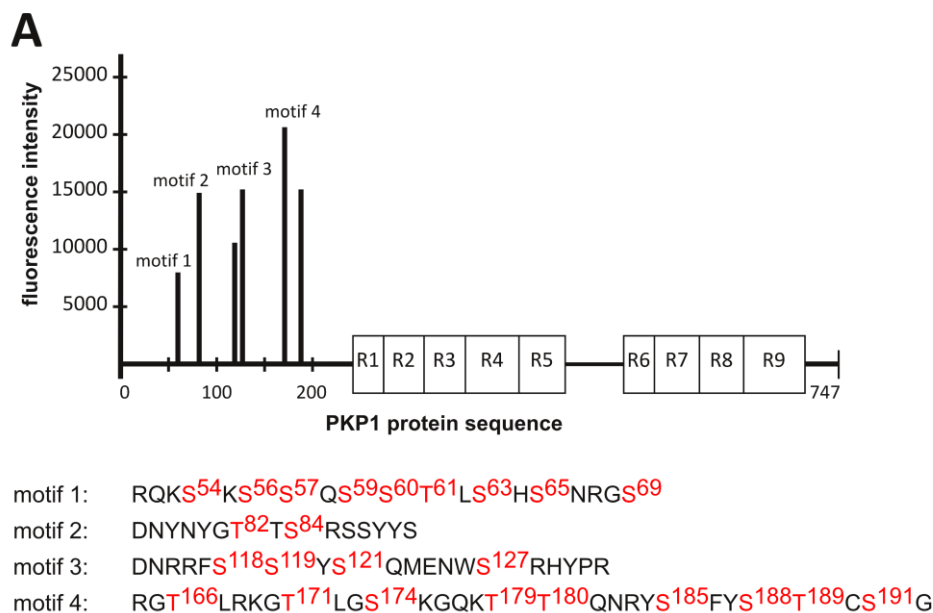


Fig. 53| PKP1 is phosphorylated by Akt2.

(A) Peptide microarrays performed by Dr. Mike Schutkowski and Dr. Annika Wolf identified PKP1 phosphorylation sites within the N-terminal head domain of the protein indicated by a schematic structure of the PKP1 domains. The peptide microarrays were incubated with recombinant active Akt2 and ATP. Phosphorylated peptides were visualized by probing the arrays with Pro-Q Diamond. Phosphorylated amino acids identified by peptide microarray and mass spectrometry are shown in red. (B) Exogenous PKP1 associates with Akt2, but not with Akt1. HEK293 cells were transfected with the indicated constructs, serum-starved (-FCS) for 24 hours, treated with insulin as indicated and harvested for co-immunoprecipitation experiments and Western blot analysis. Phospho-Akt (P-Akt) labeling confirms the activation of Akt by insulin. FCS, fetal calf serum; IP, immunoprecipitation; PKP, plakophilin; R1-R9, arm repeats, S, serine; T, threonine.

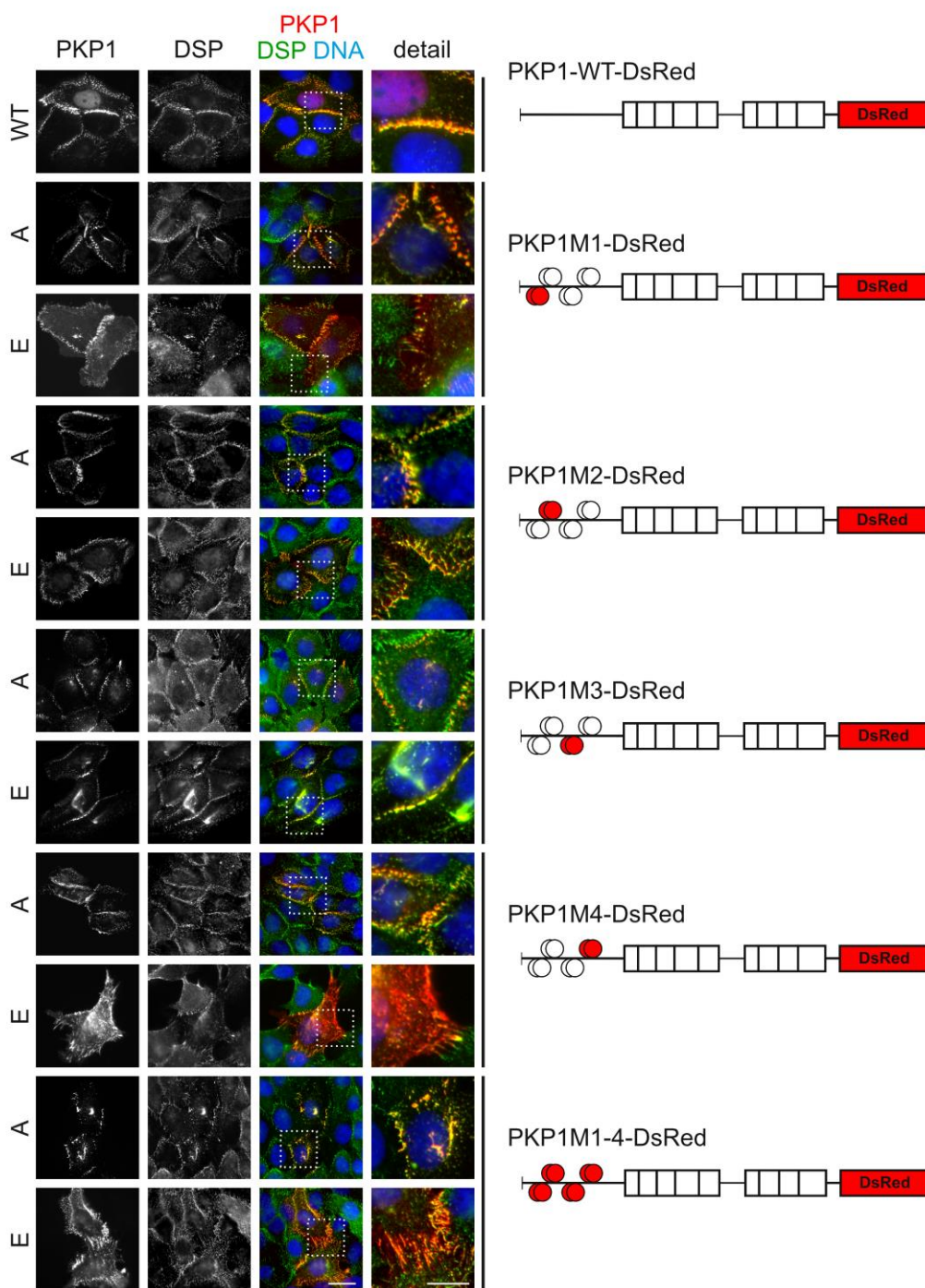


Fig. 54| PKP1 phosphosite mutants reveal distinct localization patterns in HaCaT cells.

HaCaT cells transfected with the indicated PKP1-DsRed constructs were labeled with DSP antibody (in green) and nuclei were stained with Hoechst 33342 (in blue). Dashed boxes indicate the enlarged areas. Scale bar: 20 μm , detail: 10 μm . A, alanine; DSP, desmoplakin; E, glutamate; M1-4, phosphorylation motif 1-4; PKP, plakophilin; WT, wildtype.

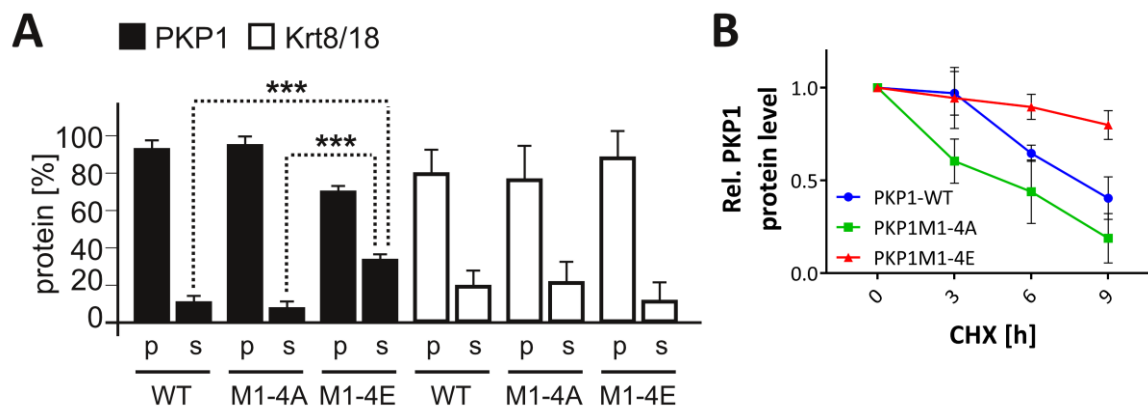


Fig. 55I Phosphorylation of PKP1 by Akt2 affects its solubility and stability.

(A) The PKP1 phospho-mimetic mutant reveals an increased soluble pool. PKP1-WT, PKP1M1-4A, or PKP1M1-4E mutants were transfected into MCF-7 cells and lysates were prepared in non-denaturing lysis buffer. Corresponding amounts of soluble (s) and insoluble (p) fractions were loaded onto a SDS gel. The experiment was performed by Aileen Wingefeld. The diagram depicts the ratio of soluble versus insoluble PKP1 and keratin 8/18 (mean \pm SD, $n=3$). Statistical significance was determined by a two-tailed Student's *t*-test. $***P \leq 0.0005$. (B) Phospho-mimetic mutants of PKP1 lead to increased protein stability. HEK293 cells were transfected with PKP1-WT, PKP1M1-4A, or PKP1M1-4E mutants. 48h post transfection, cells were treated with cycloheximide (CHX). At the indicated time points, whole-cell lysates were prepared and Western blot was performed. The diagram depicts PKP1 band intensity normalized to actin and protein levels are given relative to $t=0$ controls (mean \pm SD, $n=3$). Stability assay was conducted by Dr. Annika Wolf. A, alanine; CHX, cycloheximide; E, glutamate; Krt, keratin; M1-4, phosphorylation motif 1-4; p, insoluble; PKP, plakophilin; Rel., relative; s, soluble; WT, wildtype.

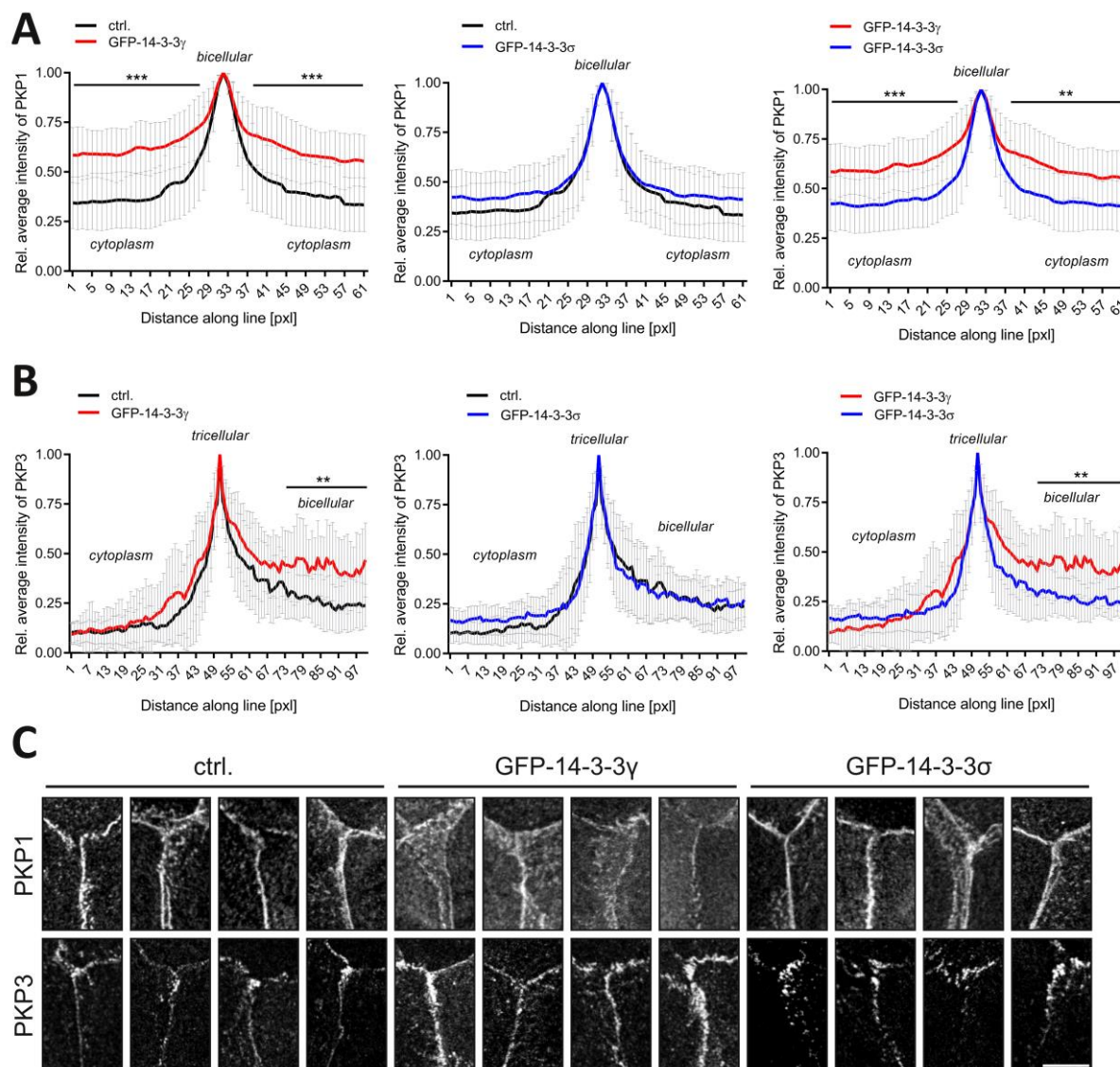


Fig. 56| Overexpression of 14-3-3 γ or 14-3-3 σ affects the localization of PKP1 and PKP3.

Mouse keratinocytes were transfected with GFP (ctrl.), GFP-14-3-3 γ , or GFP-14-3-3 σ , grown for 24 hours in HCM and immunostained for PKP1 (A) or PKP3 (B). Fluorescence intensities of PKPs were determined using ImageJ by measuring a segment of equal length and width across 30 individual bicellular or tricellular contacts for each condition. The graphs depict the fluorescence intensities (mean \pm SD, $n=30$) relative to the value at the respective cell contact. Statistical significance was determined by 2-way ANOVA testing (Tukey's multiple comparison test). ** $P \leq 0.005$, *** $P \leq 0.0005$. (C) Depicted are details from confocal images of single optical sections emphasizing the relocalization of PKP1 (upper row) and PKP3 (lower row) at bicellular and tricellular contacts dependent on the expression of GFP-14-3-3 γ or GFP-14-3-3 σ . To compare fluorescence intensities, images were collected with equal hardware settings. Scale bar: 10 μm . ctrl., control; GFP, green fluorescent protein; HCM, high calcium medium; PKP, plakophilin; pxl, pixel; Rel., relative.

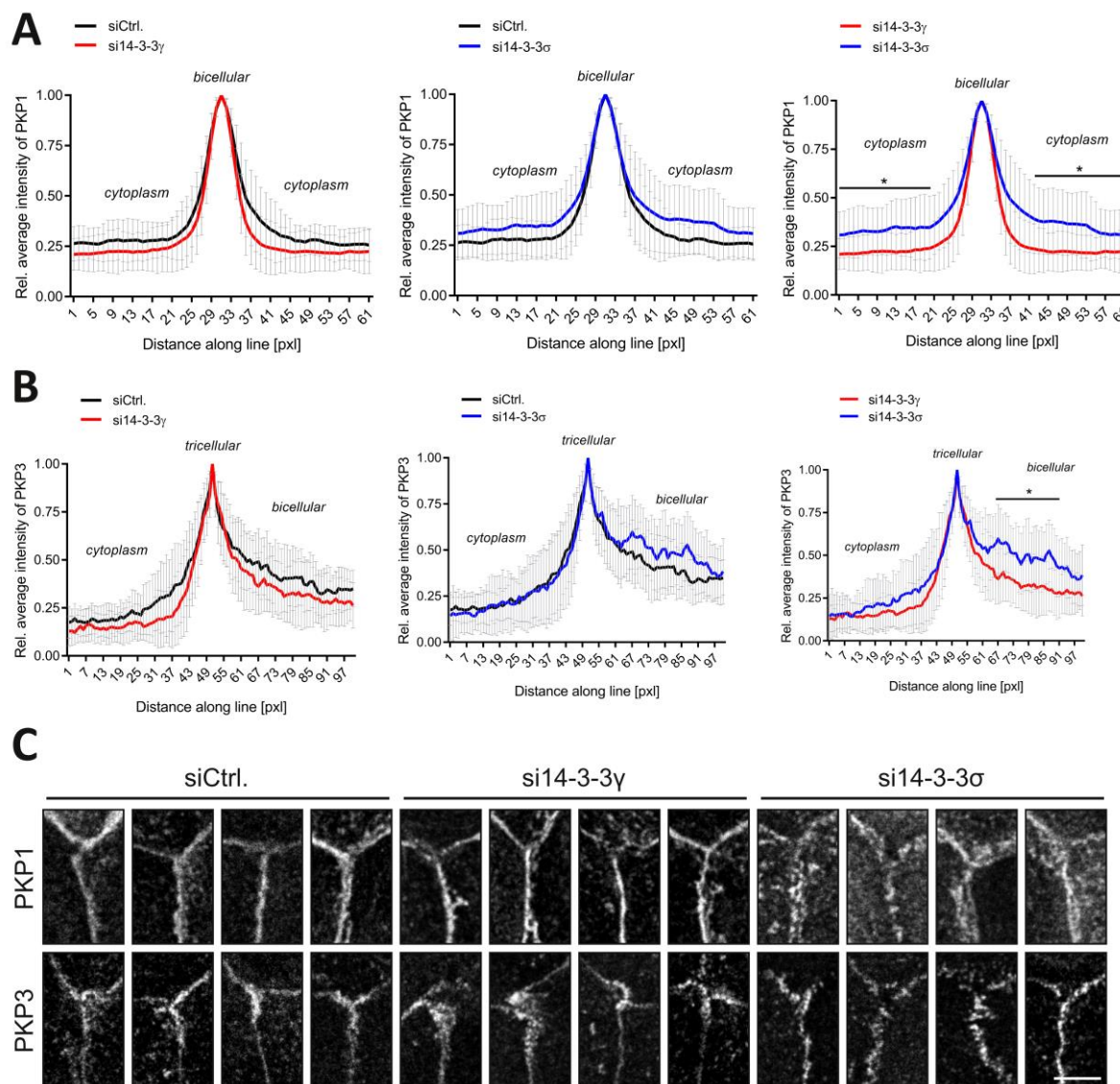
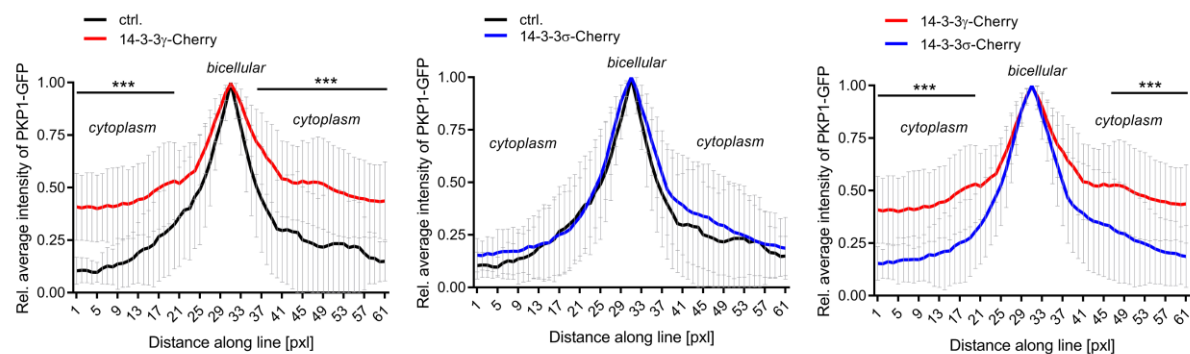
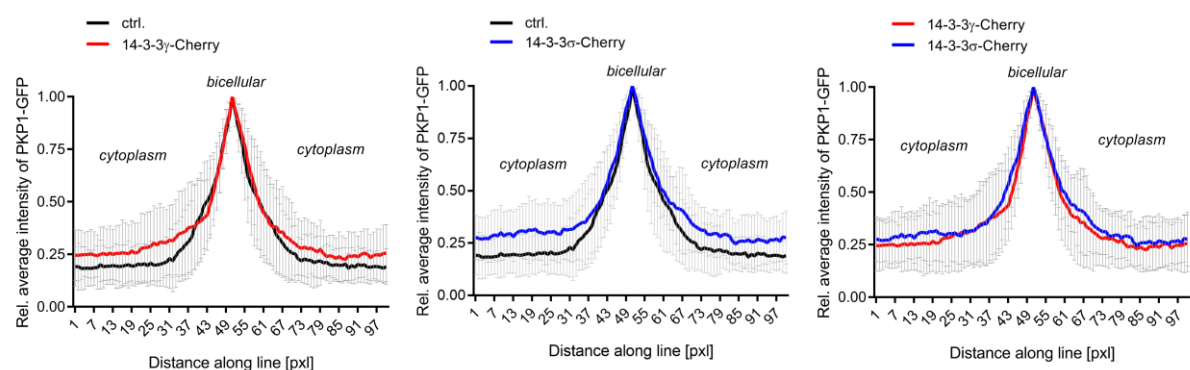


Fig. 57I Depletion of 14-3- σ primarily affects the localization of PKP3 at tricellular contacts.

Mouse keratinocytes were transfected with non-targeting (siCtrl.), 14-3-3 γ -, or 14-3-3 σ -directed siRNAs, grown for 24 hours in HCM, and co-immunostained for PKP1 and PKP3. Fluorescence intensities of PKP1 (A) and PKP3 (B) were determined using ImageJ by measuring a segment of equal length and width across 30 individual bicellular or tricellular contacts for each condition. The graphs depict the fluorescence intensities (mean \pm SD, n=30) relative to the value at the respective cell contact. Statistical significance was determined by 2-way ANOVA testing (Tukey's multiple comparison test). * $P \leq 0.05$. (C) Depicted are details from confocal images of single optical sections emphasizing the relocalization of PKP1 (upper row) and PKP3 (lower row) at bicellular and tricellular contacts dependent on the expression of 14-3-3 γ or 14-3-3 σ . To compare fluorescence intensities, images were collected with equal hardware settings. Scale bar: 10 μ m. ctrl., control; HCM, high calcium medium; PKP, plakophilin; pxl, pixel; Rel., relative.

A PKP1-GFP (cells in complete medium):**B** PKP1-GFP (serum-starved cells):**Fig. 58I Growth factor signaling regulates the PKP1-14-3-3γ interaction.**

PKP1-KO keratinocytes expressing PKP1-GFP were transfected with 14-3-3 γ -Cherry and 14-3-3 σ -Cherry, followed by serum-stimulation (A) or -starvation (B) + 1.2 mM CaCl₂ for 24 hours. Fluorescence intensities of PKP1-GFP in transfected cells were determined by measuring a segment of equal length and width across 30 individual bicellular contacts for each condition. The graphs depict the PKP1-GFP fluorescence intensities (mean \pm SD, n=30) relative to the value at the appropriate cellular contact sites. Statistical significance was determined by 2-way ANOVA testing (Tukey's multiple comparison test). *** $P \leq 0.0005$. ctrl., control; GFP, green fluorescent protein; PKP, plakophilin; pxl, pixel; Rel., relative.

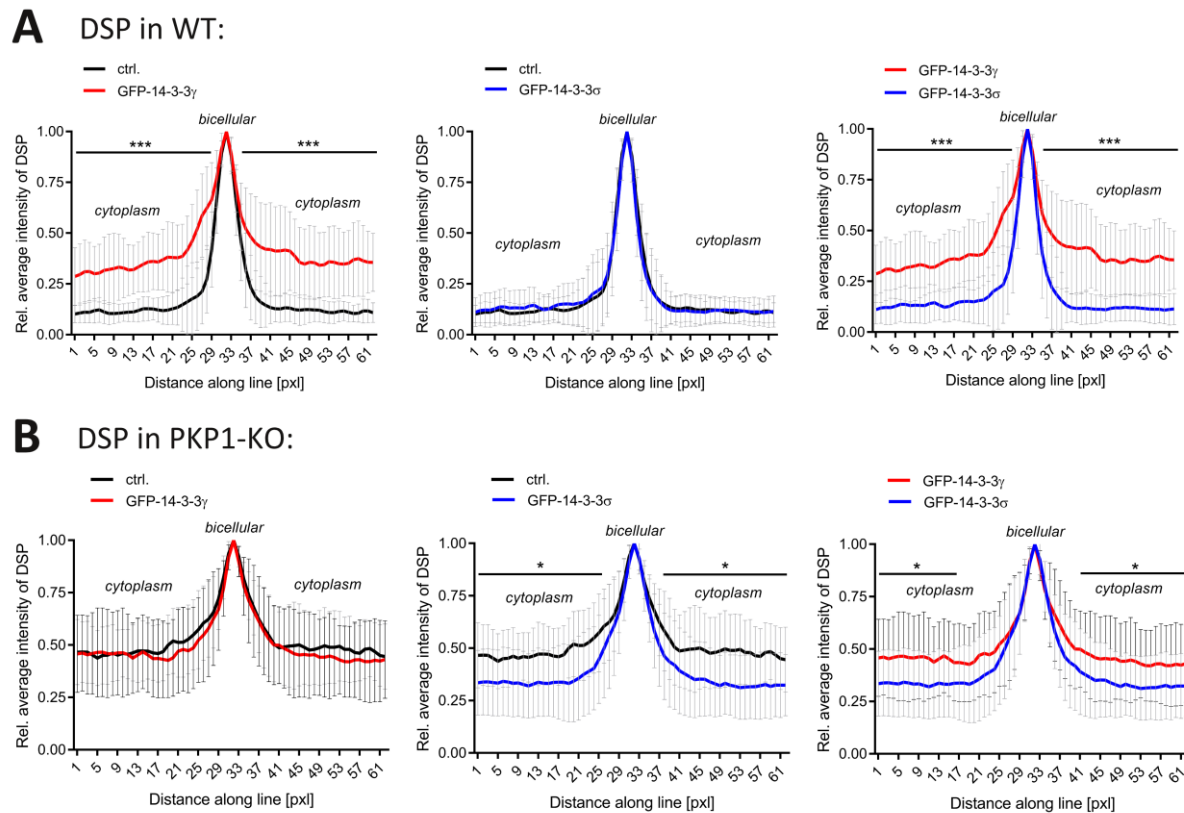


Fig. 59| PKP1 is important for the 14-3-3 γ -dependent regulation of intercellular cohesion.

WT (A) and PKP1-KO (B) keratinocytes were transfected with GFP-14-3-3 γ and GFP-14-3-3 σ , grown for 24 hours in HCM, and immunostained for DSP. Fluorescence intensities of DSP in transfected cells were determined by measuring a segment of equal length and width across 30 individual bicellular contacts for each condition. The graphs depict the fluorescence intensities (mean \pm SD, $n=30$) relative to the value at the appropriate cellular contact sites. Statistical significance was determined by 2-way ANOVA testing (Tukey's multiple comparison test). * $P \leq 0.05$, *** $P \leq 0.0005$. ctrl., control; DSP, desmoplakin; GFP, green fluorescent protein; HCM, high calcium medium; KO, knockout; PKP, plakophilin; pxl, pixel; Rel., relative; WT, wildtype.

7.3. Abbreviations

%	Percentage
°C	degree Celsius
μ	Micro
4E-BP	eIF4E-binding protein
A	alanine
A	Ampere
A	absorption
aa	amino acid
AGC	protein kinase A/G/C
AJ	adherens junction
Ala	alanine
APC	adenomatous polyposis coli
ARVCF	armadillo-repeat gene deleted in velo-cardio-facial syndrome
ATP	adenosine triphosphate
Axin	axis inhibition protein
BCA	bicinchoninic acid
BL	basal layer
BrdU	5-bromo-2'-deoxyuridine
BSA	bovine serum albumin
cad	cadherin
CAMK	Ca ²⁺ /calmodulin protein kinase
cat	catenin
cby	chibby
cDNA	complementary DNA
CDS	coding sequence
CK	casein kinase
CLDN	claudin
CLS	chemiluminescence solution
cm	Centimeter
CMV	cytomegalovirus
C-TAK1	Cdc25C-associated kinase 1
ctrl.	control
d	day
da	dominant active
DABCO	1,4-diazabicyclo[2.2.2]octane
ddDNA	double-stranded DNA
DEAE	diethylaminoethyl
desm.	desmosomal
DMEM	Dulbecco's Modified Eagle Medium
DMSO	dimethyl sulfoxide

dn	dominant negative
DNA	deoxyribonucleic acid
dNTP	deoxynucleotide triphosphate
DSC	desmocollin
DSG	desmoglein
DSH	dishevelled
DSP	desmoplakin
DTT	dithiothreitol
E	glutamate
ECM	extracellular matrix
<i>E. coli</i>	<i>Escherichia Coli</i>
EDSFS	ectodermal dysplasia-skin fragility syndrome
EDTA	ethylenediaminetetraacetic acid
EGF(R)	epidermal growth factor (receptor)
EGTA	ethylene glycol-bis(β -aminoethyl ether)-N,N',N'-tetraacetic acid
eIF	eukaryotic initiation factor
endog.	endogenous
Erk	extracellular signal-regulated kinase
EtOH	ethanol
FA	formaldehyde
FAD	flavin adenine dinucleotide
FCS	fetal calf serum
Fig.	figure
Fl	floxed
Flg	filaggrin
FLP1	site-specific recombinase Flp
for	forward
FRAP	fluorescence recovery after photobleaching
FXR1	fragile X mental retardation syndrome-related protein 1
g	Gram
g	times gravity
G3BP	Ras-GTPase activating protein SH3 domain binding protein
GEF	guanosine triphosphate exchange factor
GFP	green fluorescent protein
GL	<i>granular layer</i>
Glu	glutamate
GSK	glycogen synthase kinase
GST	glutathione S-transferase
h	hours
H&E	hematoxylin and eosin
HCM	high calcium medium

HEPES	4-(2-hydroxyethyl)-1-piperazineethanesulfonic acid
HPV	human papilloma virus
HRP	horse-radish peroxidase
IF	immunofluorescence
I_f	immobile fraction
IGF1(R)	insulin-like growth factor 1 (receptor)
IHC	immunohistochemistry
Inv	involucrin
IP	immunoprecipitation
IPTG	isopropyl- β -D-1-thiogalactopyranoside
IR	insulin receptor
JAM	junctional adhesion molecule
k	Kilo
KD	knockdown
KO	knockout
Krt(s)	keratin(s)
l	Liter
LB	Luria Bertani
LCM	low calcium medium
Lor	loricrin
LRP	LDL-receptor-related protein
m	Meter
m	Milli
M	Molar
M1-4	phosphorylation motif 1-4
m ⁷ GpppN	7-methylguanosine cap
mAb	monoclonal antibody
MAPK	mitogen-activated protein kinase
MEK	mitogen-activated protein kinase kinase
Met-tRNA _i ^{Met}	methionyl-initiator tRNA
M_f	mobile fraction
min	Minute
MKC	mouse keratinocytes
mRNA	messenger RNA
mRNP	messenger ribonucleoprotein
MS	mass spectrometry
MT	microtubule
mTORC1	mammalian target of rapamycin complex 1
n	Nano
n.s.	not significant
Neo	Neomycin

NLS	nuclear localization sequence
NPRAP	neural plakophilin-related armadillo protein
OCLN	occludin
OD	optical density
OE	overexpression
P	Pico
<i>P</i>	probability
p120ctn	p120-catenin
PAA	polyacrylamide
pAb	polyclonal antibody
PABPC	cytoplasmic poly(A)-binding protein
PAGE	polyacrylamide gel electrophoresis
PBS(E)	phosphate buffered saline (with EDTA)
PCR	polymerase chain reaction
PDK1	phosphoinositide-dependent kinase-1
PG	plakoglobin
pH	potential of hydrogen
PI3K	phosphatidylinositol-4,5-bisphosphate 3-kinase
PKC	protein kinase C
PKP	plakophilin
Pro-Flg	pro-filaggrin
pS/T	phospho-serine/threonine
PTM	post-translational modification
RBP	RNA-binding protein
Rel.	relative
rev	reverse
RNA	ribonucleic acid
ROI	region of interest
RSK	p90 ribosomal S6 kinase
RT	room temperature
S	serine
S6	ribosomal protein S6
p70S6K	p70 ribosomal S6 kinase
SBC	sodium cacodylate buffer
SC	<i>stratum corneum</i>
SCC	squamous cell carcinoma
SDS	sodium dodecyl sulfate
sec	Seconds
Ser	serine
SFM	serum-free medium
SG	stress granule

SG	<i>stratum granulosum</i>
siRNA	small interfering RNA
SL	<i>spinous layer</i>
T	threonine
T	thymidine
t _{1/2}	half-time
TBS(T)	Tris-buffered saline (with Tween20)
TCF	T-cell factor
TER	transepithelial electrical resistance
term.	terminus
TEWL	transepidermal water loss
Thr	threonine
TJ	tight junction
tRNA	transfer RNA
UPF1	up-frameshift factor 1
UTR	untranslated region
V	Volt
v/v	volume/volume
w/v	mass/volume
WB	western blot
WT	wildtype
Y2H	yeast two-hybrid
YT	yeast extract tryptone
ZO	zonula occludens
α-tub	α-tubulin

7.4. List of figures

Fig. 1 Intercellular junctions of the epidermis.....	4
Fig. 2 Heterogeneous expression of desmosomal proteins, keratins, and differentiation markers in the epidermis.....	7
Fig. 3 Structural details of PKP1.....	10
Fig. 4 PKP1: an important stabilizer of desmosomes.....	13
Fig. 5 Model of PKP1's subcellular localization and function.....	16
Fig. 6 Regulation of translation initiation by growth factors and PKP1.....	20
Fig. 7 Expression patterns of 14-3-3 proteins in human epidermis.....	23
Fig. 8 Regulation of PKP2 and PKP3 by 14-3-3 proteins.....	25
Fig. 9 Generation of the PKP1 knockout.....	28
Fig. 10 Validation of the PKP1 knockout.....	29
Fig. 11 PKP1-KO mice suffer from skin fragility and reduced birth weight.....	30
Fig. 12 PKP1-KO skin shows cell separation and a reduced adipocyte layer.....	31
Fig. 13 Analysis of corneocytes in WT and PKP1-KO dorsal skin.....	32
Fig. 14 Analysis of proliferation in WT and PKP1-KO dorsal skin.....	33
Fig. 15 Ultrastructure reveals sparse and smaller desmosomes in PKP1-null mice skin.....	34
Fig. 16 PKP1-KO mice reveal a defective epidermal barrier.....	35
Fig. 17 The inside-out liquid barrier is impaired in the epidermis of PKP1-KO mice.....	36
Fig. 18 PKP1 is essential for the localization of desmosomal proteins.....	38
Fig. 19 Keratin localization in WT and PKP1-KO epidermis.....	39
Fig. 20 Analysis of keratin expression in WT and PKP1-KO epidermis.....	40
Fig. 21 Differentiation is mildly altered in the PKP1-null epidermis.....	41
Fig. 22 Localization of AJ proteins in WT and PKP1-KO epidermis.....	42
Fig. 23 Expression of AJ proteins in WT and PKP1-KO epidermis.....	43
Fig. 24 PKP1-KO keratinocytes recapitulate the defects observed in PKP1-KO epidermis.....	44
Fig. 25 TJ function and recruitment to the plasma membrane is disturbed in PKP1 deficient keratinocytes.....	46
Fig. 26 PKP1 controls cell growth in a keratinocyte-intrinsic manner.....	47
Fig. 27 Schematic view, nomenclature, and amino acid sequence of PKP1 phosphosite mutants.....	50
Fig. 28 Intracellular localization of PKP1 depends on its phosphorylation.....	51
Fig. 29 Phospho-mimetic mutations cause PKP1 to accumulate in the cytoplasm.....	52
Fig. 30 Growth factor signaling regulates the localization of PKP1.....	54

Fig. 31 PKP1 phospho-mimetic mutant reduces intercellular adhesion.	55
Fig. 32 PKP1 phospho-mimetic mutant promotes wound healing of MCF-7 cells.	57
Fig. 33 PKP1 phospho-mimetic mutant increases proliferation.	58
Fig. 34 PKP1 phospho-mimetic mutant promotes anchorage-independent growth and car- cinogenesis in an Akt2-dependent manner.	59
Fig. 35 14-3-3 isoform expression in murine skin and keratinocytes.	62
Fig. 36 14-3-3 γ / σ have opposing effects on intercellular cohesion of murine keratinocytes.	63
Fig. 37 14-3-3 proteins affect the localization of PKP1 and PKP3.	65
Fig. 38 Quantification of knockdown efficiencies of 14-3-3 γ - and 14-3-3 σ -siPools.	66
Fig. 39 Depletion of 14-3-3 σ primarily affects the localization of PKP3 at tricellular contacts.	67
Fig. 40 Growth factor signaling affects the PKP1-14-3-3 association.	69
Fig. 41 Growth factor signaling affects the localization of PKP1 via 14-3-3 γ	70
Fig. 42 14-3-3 γ acts preferentially through PKP1 to regulate desmosomal adhesion.	71
Fig. 43 Distinct PKP-14-3-3 complexes regulate intercellular cohesion of keratinocytes.	72
Fig. 44 S155 phosphorylation is essential for 14-3-3 γ binding to PKP1.	73
Fig. 45 14-3-3 γ modulates the solubility of PKP1.	74
Fig. 46 14-3-3 proteins differentially modulate PKP dynamics.	76
Fig. 47 Model for PKP1 regulation by growth factor signaling.	87
Fig. 48 Model depicting the regulation of intercellular cohesion via 14-3-3 γ and - σ	92
Fig. 49 Schematic comparison of multifunctional PKP1 and β -catenin.	96
Fig. 50 Soft agar assay setup.	115
Fig. 51 PCR reaction and program for site-directed mutagenesis.	127
Fig. 52 DNA and protein standards.	IV
Fig. 53 PKP1 is phosphorylated by Akt2.	XV
Fig. 54 PKP1 phosphosite mutants reveal distinct localization patterns in HaCaT cells.	XVI
Fig. 55 Phosphorylation of PKP1 by Akt2 affects its solubility and stability.	XVII
Fig. 56 Overexpression of 14-3-3 γ or 14-3-3 σ affects the localization of PKP1 and PKP3.	XVIII
Fig. 57 Depletion of 14-3-3 σ primarily affects the localization of PKP3 at tricellular contacts.	XIX
Fig. 58 Growth factor signaling regulates the PKP1-14-3-3 γ interaction.	XX
Fig. 59 PKP1 is important for the 14-3-3 γ -dependent regulation of intercellular cohesion.	XXI

7.5. List of tables

Table 1 Solutions used for keratinocyte culture.....	106
Table 2 DNA transfection by CaPO ₄ precipitation.....	108
Table 3 DNA transfection by Xfect reagent.....	109
Table 4 siRNA transfection by Lipofectamine® RNAiMax reagent.....	110
Table 5 Preparation of diluted BSA standard.....	119
Table 6 Extraction of genomic DNA from mouse tail by KAPA Mouse Genotyping Kit.....	133
Table 7 KAPA2G Fast Genotyping PCR Protocol.....	133
Table 8 Lab equipment.....	I
Table 9 Kits and ready-to-use reagents.....	III
Table 10 Solutions and buffers.....	IV
Table 11 Oligonucleotides used for genotyping and probe amplification.....	VI
Table 12 Oligonucleotides used for site-directed mutagenesis.....	VI
Table 13 Oligonucleotides used for cloning.....	VIII
Table 14 Primary antibodies.....	VIII
Table 15 Secondary antibodies.....	X
Table 16 Cell lines.....	X
Table 17 Plasmids for bacterial expression.....	XI
Table 18 Plasmids for expression in cell lines.....	XI
Table 19 siRNAs.....	XII
Table 20 <i>E. coli</i> strains.....	XIII
Table 21 Mutations within PKP1 causing EDSFS and clinical features.....	XIII

Danksagung

Für die bedingungslose Unterstützung und den nötigen Rückhalt über die ganzen Jahre hinweg möchte ich mich bei meinen Eltern Ralf und Iris Rietscher bedanken. Sie ermöglichten mir nicht nur das Biochemie Studium, sondern haben mich auch in allem gefördert, was mir am Herzen lag.

Prof. Mechthild Hatzfeld danke ich für die mittlerweile langjährige wissenschaftliche Zusammenarbeit. Ihr Engagement, ihre Diskussionsbereitschaft sowie konstruktive Kritik haben meine Arbeitsweise und das Herangehen an wissenschaftliche Fragestellungen nachhaltig geprägt. Zudem half sie mir bei vielen Gelegenheiten, Manuskripte, Vorträge oder Ähnliches zum erfolgreichen Abschluss zu bringen. Nicht zuletzt danke ich ihr für die Möglichkeit, diese Dissertation in ihrer Arbeitsgruppe anfertigen zu dürfen und für ihren Beistand über die Jahre. Prof. Stefan Hüttelmaier sowie Prof. Carien Niessen danke ich für die Übernahme der Begutachtung dieser Dissertation.

Allen derzeitigen und ehemaligen Mitarbeitern des Hatzfeld-Labors danke ich für die gute Zusammenarbeit und die freundliche Atmosphäre. An besonders stressigen Tagen war Andrej Mun stets eine helfende Hand, vielen Dank dafür. Dr. Annika Wolf danke ich besonders für ihre Hilfsbereitschaft zu Beginn meiner Dissertation, ihr Engagement und ihre Freundschaft. Die gemeinsame Projektarbeit bleibt eine unvergessene Zeit in meinem Herzen. Dr. René Keil danke ich für die tatkräftige Unterstützung bei der Quantifizierung meiner mikroskopischen Aufnahmen. Beiden danke ich zudem für das Korrekturlesen dieser Arbeit. Für die Diskussionsbereitschaft und konstruktiven Ideen bzgl. des Maus-Projektes danke ich Prof. Thomas Magin sowie Prof. Carien Niessen. Mein besonderer Dank gilt außerdem: Prof. Sabine Werner für die Bereitstellung der SCC Proben, Dr. Dr. Gerd Hause für die Anfertigung und Annekathrin Rother für die Quantifizierung der EM-Bilder, Dr. Barbara Schreier für die TER-Einweisung, Annemarie Jordan für die gemeinsame Arbeit am 14-3-3 Projekt, den Mitarbeitern der Core Facility Imaging für die praktische Unterstützung, Conny Gottschalk für die herzliche Zusammenarbeit und ihre einfühlsame Arbeitsweise mit den Mäusen in der Tierhaltung sowie Anja Doering für die technische Unterstützung bei der Anfertigung der Paraffin-Gewebeproben.

Bei Maria bedanke ich mich für ihre Freundschaft und Diskussionsbereitschaft sowie den Spaß nach Feierabend. Meiner Familie und meinen Freunden danke ich, dass sie mich zu jeder Zeit und in jeder Form unterstützt und motiviert haben. Zuletzt danke ich Sebastian für seine Liebe und sein Verständnis, gerade gegen Ende der Dissertation.

Curriculum VitaePersonal Details

Name: Katrin Rietscher
 Date of birth, birthplace: 18.06.1985, Räckelwitz
 Citizenship: German
 Address: Bertramstrasse 16, 06110 Halle (Saale)

Professional praxis

since 12/2011

Research fellow

Martin-Luther-University Halle-Wittenberg
 Medical Faculty
 Institute of Molecular Medicine
 Section Pathobiochemistry
 Doctoral studies in the research group of Prof. Dr.
 Mechthild Hatzfeld

Scientific education

10/2005 – 11/2011

Study of Biochemistry

Martin-Luther-University Halle-Wittenberg
 Diploma thesis in the research group of Prof. Dr.
 Mechthild Hatzfeld; title: The regulation of plakophilin 1

08/2009 – 09/2009

Internship abroad

University of Copenhagen, Denmark
 Department of Neuroscience and Pharmacology

09/2008 – 01/2009

ERASMUS scholarship

Study program: student in Molecular & Cell Biology
 University Aberdeen, Scotland

School education

09/1996 – 07/2004

Gotthold-Ephraim-Lessing Grammar school in Kamenz,
 Abitur

Halle (Saale), 06.11.2017

Katrin Rietscher

Publications:

Rietscher K, Jordan A, Keil R, Hatzfeld M. (2017). 14-3-3 proteins regulate desmosomal adhesion via plakophilins. *submitted*.

Keil R, **Rietscher K**, Hatzfeld M. (2016). Antagonistic regulation of intercellular cohesion by plakophilins 1 and 3. *J Invest Dermatol.* 136, 2022-29.

Rietscher K, Wolf A, Hause G, Rother A, Keil R, Magin TM, Glass M, Niessen CM, Hatzfeld M. (2016). Growth retardation, loss of desmosomal adhesion, and impaired tight junction function identify a unique role of plakophilin 1 in vivo. *J Invest Dermatol.* 136, 1471-78.

Wolf A, **Rietscher K**, Glaß M, Hüttelmaier S, Schutkowski M, Ihling C, Sinz A, Wingenfeld A, Mun A, Hatzfeld M. (2013). Insulin signaling via Akt2 switches plakophilin 1 function from stabilizing cell adhesion to promoting cell proliferation. *J Cell Sci.* 126, 1832-44.

Presentations:

Rietscher K: "Regulation of plakophilin 3 by EGF signaling", SPP meeting, 12.10.2017, Aachen (Germany).

Rietscher K: "Growth retardation and loss of desmosomal adhesion identify a unique role of plakophilin 1 *in vivo*", 3th Congress for PhD students, 20.11.2015, Halle (Germany).

Rietscher K and Hatzfeld M: "Loss of plakophilin 1 in mice causes skin fragility and neonatal lethal phenotype", DGZ meeting, 25.03.2015, Cologne (Germany).

Abstracts & posters:

Rietscher K, Wolf A, Hatzfeld M: "Role of the multi-functional protein plakophilin 1 in growth control and carcinogenesis", EMBO conference, 27.-31.05.2016, Cavtat (Croatia).

Rietscher K, Wolf A, Hause G, Hatzfeld M.: „Plakophilin 1 is essential for desmosomal adhesion and survival“, 45th annual EDSR meeting, 11.09.2015, Rotterdam (Netherlands).

Rietscher K, Wolf A, Hatzfeld M.: „The regulation of cell-cell adhesion by 14-3-3 proteins“, DGZ meeting, 24.-27.03.2015, Cologne (Germany)

Wolf A, **Rietscher K**, Hatzfeld M.: „The dual functions of plakophilin 1 in adhesion and translation are regulated by growth factor signaling“, DFG meeting, Leipzig (Germany).

Eidesstattliche Erklärung

Hiermit erkläre ich, dass ich die vorliegende Arbeit selbstständig und ohne fremde Hilfe verfasst habe. Die verwendeten Quellen und Hilfsmittel wurden vollständig angegeben. Die aus den verwendeten Quellen wörtlich oder inhaltlich entnommenen Stellen wurden unter Angabe der Quelle kenntlich gemacht. Insbesondere wurden alle Personen genannt, die direkt an der Entstehung der vorliegenden Arbeit beteiligt waren. Diese Dissertation wurde an keiner anderen Einrichtung vorgelegt.

Halle (Saale), den 06.11.2017

Katrin Rietscher